UNIVERSITY OF BIRMINGHAM

COMBUSTION AND EMISSIONS PERFORMANCE OF OXYGENATED FUELS IN A MODERN SPARK IGNITION ENGINE

By

Ritchie Lewis Daniel

A thesis submitted to

The University of Birmingham

For the degree of

DOCTOR OF PHILOSOPHY

The University of Birmingham

School of Engineering

May 2012

ABSTRACT

The combustion and emissions performance of oxygenated fuels has been investigated in a modern direct-injection spark-ignition (DISI) engine. In particular, the new biofuel candidate, 2,5-dimethylfuran, otherwise known as DMF, has been assessed as a future automotive fuel against ethanol, the most commercially accepted spark-ignition (SI) biofuel.

When operating with DMF, the engine performance and emissions are less sensitive to changes in key control parameters than with gasoline. This allows a wider window for improving performance and/or reducing emissions. The relevance of modern injection strategies to increase performance or efficiency has also been assessed when using DMF. The use of split-injection at full load is shown to be less beneficial than with gasoline.

Novel fuel preparation techniques have been investigated by comparing externally supplied gasoline-biofuel blends (conventional method) to internally mixed, dual-injection blends. This new mode presents an avenue for optimising oxygenated fuels with a low heat of vaporization, such as DMF and *n*-butanol; low blends with gasoline ($\leq$25% by volume) are more efficiently utilised than in external blends. Furthermore, the particulate matter (PM) emissions can be reduced with dual-injection because gasoline is supplied through PFI.

The unlegislated emissions when using DMF have been benchmarked against gasoline and compared to other oxygenated fuels. In particular, the emissions of the major carbonyls are lower when using DMF compared to gasoline and even less so than ethanol, which heavily emits acetaldehyde and formaldehyde. The dual-injection mode further reduces the total carbonyl emissions when using DMF and ethanol blends compared to direct-injection (DI).

ACKNOWLEDGEMENTS

First and foremost, I would like to thank Professor Hongming Xu (Primary Supervisor) for his help and guidance during my PhD course. The support from Professor Mirosław L. Wyszyński (Secondary Supervisor) and Dr Athanasios Tsolakis is also greatly appreciated.

Great thanks go to the laboratory technicians - Peter Thornton, Carl Hingley, Simon Rowan and Lee Gauntlett - for their support with all test facility matters. I also appreciate the help from Graham Burns, Chi Tsang and Peter Ashton in the Chemistry department.

I am sincerely grateful for the conversations with all my colleagues at the Future Power Systems department. In particular, Dr Dale Turner, Dr Guohong Tian, Dr Xuesong Wu and Chongming Wang keenly offered advice and I wish them all the success with their future careers. I also thank Dr Lixia Wei for his support with the chemical reactions in Chapter 8.

My thanks go to Jaguar Land Rover (JLR) for helping to support the engine rebuilds and for providing advice on the experimental results. The support from Shell Global Solutions, UK in supplying the commercial fuels used in this study (gasoline and ethanol) is greatly appreciated. I would also like to thank the EPSRC for providing the funding for this project.

Thanks go to the industrial partners who supported this work and gave valuable advice. This includes: Paul Richards (Innospec), Dave Richardson (JLR), Colin Hygate (Green Fuels), Roger Cracknell, Bob Head (Shell Global Solutions, UK) and Prof. Francis Palmer (IQFC).

Finally, on a more personal level, I would like to thank my fiancée, Emma, for her patience and encouragement throughout this project and with all my other endeavours.

CONTENTS

LIST OF FIGURES

LIST OF TABLES

LIST OF ABBREVIATIONS

aTDC	After Top Dead Centre
AFR	Air-Fuel Ratio
$AFR_{stoich.}$	Stoichiometric Air-Fuel Ratio
bTDC	Before Top Dead Centre
BDI	*n*-Butanol in Direct-Injection
BUT	*n*-Butanol
CAD	Crank Angle Degrees
$CAD_{EOI-SPK}$	Crank Angle Degrees from End of Injection to Ignition
CAD_{SPK-90}	Crank Angle Degrees from Ignition to 90% Mass Fraction Burned
CAD_{10-50}	Crank Angle Degrees from 10 to 50% Mass Fraction Burned
CAD_{10-90}	Combustion Duration (Crank Angle Degrees from 10 to 90% MFB)
CAD_{50-90}	Crank Angle Degrees from 50 to 90% Mass Fraction Burned
CA50	Crank Angle at 50% Mass Fraction Burned
CLD	Chemiluminescence Detector
CO	Carbon Monoxide
CO_2	Carbon Dioxide
COV	Coefficient of Variation
DDI	DMF in Direct-Injection
DI	Direct-Injection
DISI	Direct-Injection Spark-Ignition
DME	Dimethyl Ether
DMF	2,5-Dimethylfuran
DNPH	2,4-Dinitrophenylhydrazine
EBS	Ethanol Boosting Systems LLC
EDI	Ethanol in Direct-Injection

EGR	Exhaust Gas Recirculation
EMF	2-Ethyl-5-Methylfuran
EOI	End of Injection
ETCS	Engine Timing Control System
ETH	Ethanol
EVC	Exhaust Valve Closing
GDI	Gasoline Direct-Injection
G-BDI	*n*-Butanol Dual-Injection (Gasoline in PFI and *n*-Butanol in DI)
G-DDI	DMF Dual-Injection (Gasoline in PFI and DMF in DI)
G-EDI	Ethanol Dual-Injection (Gasoline in PFI and Ethanol in DI)
G-MDI	Methanol Dual-Injection (Gasoline in PFI and Methanol in DI)
FID	Flame Ionisation Detector
FTIR	Fourier Transform Infrared Detector
GC/FID	Gas Chromatography Flame Ionisation Detector
GC/MS	Gas Chromatography Mass Spectrometry
HC	Hydrocarbons
HCCI	Homogeneous Charge Compression Ignition
HHV	Higher Heating Value
HMF	Hydroxymethylfurfural
HPLC	High Performance Liquid Chromatography
IARC	International Agency for Research on Cancer
IMEP	Indicated Mean Effective Pressure
IVC	Intake Valve Closing
IVO	Intake Valve Opening
KLSA	Knock-Limited Spark Advance
λ	Relative Air to Fuel Ratio

LHV	Lower Heating Value
MBT	Minimum Spark Advance for Best Torque
MDI	Methanol in Direct-Injection
MF	2-Methylfuran
MFB	Mass Fraction Burned
MTH	Methanol
NDIR	Non-Dispersive Infrared Detector
NO	Nitric Oxide
NO_x	Oxides of Nitrogen
NTP	National Toxicology Program
OEM	Original Equipment Manufacturer
PFI	Port Fuel Injection
Φ	Equivalence Ratio (Fuel-Air Ratio)
PM	Particulate Matter
P_{max}	Maximum In-Cylinder Pressure
PPM	Parts per Million
RON	Research Octane Number
RPM	Revolutions per Minute
RPR	Rate of Pressure Rise
SGDI	Spray-Guided Direct-Injection
SI	Spark-Ignition
SMPS	Scanning Mobility Particle Sizer
SOI	Start of Injection
SR	Spark Retard
SR5	5CAD Spark Retard from MBT or KLSA
SR10	10CAD Spark Retard from MBT or KLSA

TDC	Top Dead Centre
θP_{max}	CAD (aTDC) of Maximum In-Cylinder Pressure
T_{ign}	In-Cylinder Temperature at Ignition
T_{max}	Maximum In-Cylinder Temperature
t_R	Retention Time
TWC	Three-Way Catalyst
VAF	Volumetric Air Flow
VCT	Variable Cam Timing
VE	Volumetric Efficiency
WOT	Wide Open Throttle

LIST OF PUBLICATIONS

1. **Combustion and Emissions of 2,5-Dimethylfuran in a Direct-Injection Spark-Ignition Engine** Shaohua Zhong, Ritchie Daniel, Hongming Xu, Jun Zhang, Dale Turner, Miroslaw L. Wyszynski and Paul Richards. Energy and Fuels, 2010, 24(5), pp 2891-2899.

2. **Laminar Burning Velocities of 2,5-Dimethylfuran Compared with Ethanol and Gasoline** Guohong Tian, Ritchie Daniel, Haiying Li, Hongming Xu, Shijin Shuai and Paul Richards. Energy and Fuels, 2010, 24(7), pp 3898-3905.

3. **Spray Characteristics and Engine Adaptability of 2,5-Dimethylfuran** Guohong Tian, Hongming Xu, Ritchie Daniel, Haiying, Li and Yanfei Li. Journal of Automotive Safety and Energy, 2010, 1(2), pp 132-140.

4. **Effect of Spark Timing and Load on a DISI engine fuelled with 2,5-Dimethylfuran** Ritchie Daniel, Guohong Tian, Hongming Xu, Miroslaw L. Wyszynski, Xuesong Wu and Zuohua Huang. Fuel, 2011, 90(2), pp 449-458.

5. **Dual-Injection: the Flexible, Bi-Fuel Concept for Spark-Ignition Engines Fuelled with Various Gasoline and Biofuel Blends** Xuesong Wu, Ritchie Daniel, Guohong Tian, Hongming Xu, Zuohua Huang and Dave Richardson. Applied Energy, 2011, 88(7), pp 2305-2314.

6. **DMF - a New Biofuel Candidate** Guohong Tian, Ritchie Daniel and Hongming Xu. Biofuel Production – Recent Developments and Prospects, InTech, 2011, ISBN 978-953-307-478-8.

7. **Ignition Timing Sensitivities of Oxygenated Biofuels Compared to Gasoline in a Direct-Injection SI Engine** Ritchie Daniel, Guohong Tian, Hongming Xu and Shijin Shui. Fuel, 2012, 99, 72-82.

8. **Effects of Combustion Phasing, Injection Timing, Relative Air-Fuel Ratio and Variable Valve Timing on SI Engine Performance and Emissions using 2,5-Dimethylfuran*** Ritchie Daniel, Chongming Wang, Guohong Tian and Hongming Xu. SAE. 2012-01-1285, 2012.

9. **Dual-Injection as a Knock Mitigation Strategy using Ethanol and Methanol*** Ritchie Daniel, Chongming Wang, Guohong Tian, Hongming Xu and Dave Richardson. SAE. 2012-01-1152, 2012.

10. **Combustion Performance of 2,5-Dimethylfuran Blends using Dual-Injection compared to Direct-Injection in a SI Engine** Ritchie Daniel, Hongming Xu, Chongming Wang, Guohong Tian and Dave Richardson. Applied Energy, 2012, 98, 59-68.

11. **Gaseous and Particulate Matter Emissions of Oxygenated Fuel Blends using Dual-Injection compared to Direct-Injection in a SI Engine** Ritchie Daniel, Hongming Xu, Chongming Wang, Guohong Tian and Dave Richardson. Applied Energy. 2012. In Review.

12. **Split-Injection Strategies at Wide-Open Throttle using Gasoline, Ethanol and 2,5-Dimethylfuran in a Direct-Injection SI Engine** Ritchie Daniel, Chongming Wang, Guohong Tian and Hongming Xu. SAE. 2012-01-0403, 2012.

13. **Combustion and Emissions of 2-Methylfuran in a DISI Engine** Chongming Wang, Hongming Xu, Ritchie Daniel, Akbar Ghafouri, Jose Martin Herreros, Shijin Shuai and Xiao Ma. Fuel. 2012. In Review.

14. **Hydrocarbon and Carbonyl Emissions Speciation of 2,5-Dimethylfuran in a DISI Engine** Ritchie Daniel, Lixia Wei, Chongming Wang, Hongming Xu and Miroslaw L. Wyszynski. Energy and Fuels. 2012. In Review.

*Also published in: SAE International Journal of Fuels and Lubricants, January 2012.

Conference Contributions:

1. **Impact of DMF on Engine Performance and Emissions as a New Generation of Sustainable Biofuel** Ritchie Daniel, Xuesong Wu, Guohong Tian and Hongming Xu. UK-China Energy Conference (Poster Presentation), Beijing, China, 8/9 March 2011.

Awards:

1. **Austin Rover Prize (PG)** for the most worthwhile thesis.

Ritchie Daniel, School of Mechanical Engineering, University of Birmingham, December 2011.

2. **Hufton (PG) Scholarship** for outstanding academic performance.

Ritchie Daniel, School of Mechanical Engineering, University of Birmingham, March 2012.

CHAPTER 1

INTRODUCTION

Currently, there are two major issues facing the automotive industry. The first is the increasing need for energy security because traditional oil supply is becoming increasingly volatile. The world's oil reserves are also depleting and could be consumed in the next 40 years unless something is done to slow down the current trend (Shell, 2011). The second major concern is rising global temperatures. This is calling for restrictions on carbon dioxide (CO_2) production in an effort to protect the environment and search for a more carbon-neutral economy. In summary, these key areas present an opportunity for the automotive industry to search for alternative fuel sources and more advanced combustion technology.

Hydrogen is considered the most promising long term option in replacing fossil fuels due to its abundance, high energy density (surpassing gasoline by threefold) and low emissions. However, the safety issues over its storage and refuelling infrastructure are major barriers to its success. Although hydrogen fuel cell vehicles are being demonstrated and hydrogen SI engines extensively researched by Ford and BMW (Natkin, 2003, Berckmüller, 2003), it is unlikely that hydrogen solutions will suit the demands of the marketplace in the near term. Although the emergence of hybrid electric platforms is growing as most major automotive manufacturers now offer a hybrid option in their fleet, these full electric platforms are in their infancy.

Therefore, the most logical near term solution is to use liquid biofuels. This is due to their ease of implementation into existing combustion systems and infrastructure. This allows the simultaneous improvement of IC engines whilst developing a hydrogen economy.

1.1 Background

It is believed that biofuels can help to support the near term demands of energy security, whilst meeting the targets for continuous emissions reduction, including CO_2. Biofuels can be supplied in blends with traditional liquid fossil fuels or used in neat form. This versatility allows continual supply of energy despite the effect of volatile energy markets.

Although the use of biofuels in SI engines is not new, their use is being promoted because of the gradual move towards sustainable energy sources and shift from gasoline. The automotive industry is moving towards high efficiency engines through turbocharging and increased compression ratios. Biofuels are therefore being incorporated in these efforts. In particular, most oxygenated biofuels produce a twofold leap in knock reduction. The oxygen contained in the fuel helps to produce a high chemical resistance to autoignition whilst improving the charge-cooling effect.

In the search for sustainable energy sources, various novel biofuels are receiving attention. For example, algae-based fuels are being promoted for use in aviation and even animal fat (tallow) is being considered in CI engines. This shows the versatility and willingness of the research community to explore all types of alternatives to traditional fuel sources.

Currently, most biofuels are second generation biofuels. The feedstock for these biofuels is less contentious than the first generation counterparts. This is because second generation biofuels do not compete with land for food as the waste products are used. However, the lifecycle carbon footprint and costs remain the main barriers to widespread commercial adoption of biofuels. Nevertheless, the automotive industry has a socio-economic duty to explore the alternatives and propose the optimal use of biofuels in IC engines.

When used in low quantities oxygenated fuels, such as ethanol, are provided as additives to gasoline. However, their use in higher blends is increasing. Currently, high blends of ethanol (and even neat ethanol) are widely accepted in Latin and North America. Countries such as Brazil can benefit from ethanol because of the vast land available required for cultivating its feedstock. However, in regions where land available for crops is less abundant, the issue of energy security remains.

Therefore, it is becoming important to select biofuels that reliably produce high yields. When effective manufacture is coupled biofuels with high energy density, the chances of potential commercialisation dramatically increase. Amongst the oxygenated fuels, furan derivatives are beginning to fit this role and, along with butanol, are quickly becoming attractive potential energy carriers.

1.2 Research Outline

For biofuels to be commercialised, their combustion and emissions should be shown to be competitive with traditional fuels. Therefore, the research presented in this thesis presents a comparison between gasoline and oxygenated fuels in pure form or in blends with gasoline.

The sensitivity of these oxygenated fuels to key engine parameters is investigated. However, the combustion and emissions of 2,5-dimethylfuran has been particularly explored.

The performance of external blends has been compared with dual-injection. Dual-injection shows benefits in CI engines, as well as homogeneous charge compression ignition (HCCI) combustion because the two fuels produce a synergetic reaction with favourable output.

Finally, the level of emissions toxicity from oxygenated fuels has been compared.

1.3 Objectives and Approaches

The research presented in this thesis was conducted by the author at the *Future Engines and Fuels* research lab at the University of Birmingham. The experiments were conducted on a prototype single cylinder DISI research engine representative of a V8 production engine.

The main objective of this study is to investigate the combustion and emissions performance of oxygenated fuels in modern combustion systems. However, because the main financial support for this work was provided by the EPSRC (EP/F061692/1), priority is given to DMF, which is mainly compared to ethanol. The areas of investigation include:

i. The sensitivity of DMF and other oxygenated fuels to key DISI engine parameters;

ii. The suitability of DMF and ethanol to split-injection strategies at wide open throttle;

iii. The effectiveness of a dual-injection knock mitigation strategy using lower alcohols;

iv. The effectiveness of oxygenated fuel blends using dual-injection compared to DI;

v. The identification of HCs when fuelled with DMF using GC/FID and GC/MS;

vi. The quantification of carbonyls when using DMF and other oxygenated fuel blends;

vii. The effect of dual-injection on the carbonyl emissions of DMF and ethanol blends;

viii. The effect of spark retard and load on the PM emissions when using DMF in DI;

ix. The effect of dual-injection on the PM emissions when using ethanol blends.

1.4 Thesis Outline

This thesis is divided into nine chapters that cover the aspects of oxygenated fuel combustion in modern DISI engines. A brief summary of the contents of each of the following chapters is provided below.

Chapter 2 - Literature Review

This chapter includes the review of the literature relevant to this thesis. Firstly, a review of the modern SI engine technology is discussed including the efforts in downsizing and optimal modes of fuel injection. This is expanded in the next section by discussing the alternative gasoline replacement fuels including furan derivatives like DMF. Finally, the regulated and unregulated emissions studies from oxygenated fuels are discussed.

Chapter 3 - Experimental Setup

This chapter details the experimental test facilities and data acquisition systems used in this study. The thermal single-cylinder research engine is described in detail along with the analysis software and the key calculations used to meaningfully interpret the data.

Chapter 4 - Combustion Behaviour and Emissions of 2,5-Dimethylfuran

The main engine parameters affecting the performance and emissions are varied in order to examine the effect of DMF. The results are benchmarked against gasoline and compared to ethanol and other oxygenated fuels. The sensitivity to spark timing is analysed in detail.

Chapter 5 - Modern GDI Combustion Modes using DMF and Ethanol

The effectiveness of split-injection strategies when fuelled with DMF and ethanol are compared to gasoline. The gains in performance and emissions are examined whilst varying the second injection timing at wide open throttle.

Chapter 6 - Dual-Injection as a Knock Mitigation Method

The minimum injection of ethanol and methanol in dual-injection to suppress knock is examined. The change in performance and emissions from PFI gasoline is evaluated.

Chapter 7 - Dual-Injection Blends compared to DI Blends

Various blends of DMF are compared between DI and dual-injection. The performance and emissions are compared to the individual constituents. This is followed by the effectiveness with other oxygenated fuels such as ethanol, methanol and *n*-butanol.

Chapter 8 - HC Speciation and PM Emissions of 2,5-Dimethylfuran

The individual HC emissions when fuelled with DMF are identified using GC/MS and GC/FID. The effect of DI and dual-injection on the carbonyl emissions is explored. The PM emissions are examined using DMF in DI by varying the spark timing and load. Finally, the PM emissions are compared between dual-injection and DI using ethanol blends.

Chapter 9 - Summary, Conclusions and Further Work

This chapter summarises the main findings of this thesis and provides recommendations for further work. The conclusions are drawn from each section in order to give an overview of the author's progress and novelty of the research.

CHAPTER 2

LITERATURE REVIEW

The aim of this chapter is to review the literature relevant to this thesis. The areas of discussion include the major developments in SI combustion, fuels and emissions.

2.1 Introduction

Firstly, this chapter explores the advent of current SI engine technology and the main modern control variables that affect the performance and emissions. The phenomenon of engine knock is discussed, as well as the attempts to avoid it to raise engine efficiency. This is followed by a discussion of the advances in injection technology and finally the growing emphasis on engine 'downsizing'.

Secondly, the potential of various competitive gasoline replacement fuels are discussed. This includes a discussion of the advantageous and disadvantageous fuel properties compared with gasoline and the effect of these replacement fuels on engine optimisation. This section concludes with a focus on furanic biofuels and the early stage results achieved by others prior to the publication of this thesis.

Finally, an overview of the emissions related to SI combustion is presented. Firstly, the US and European emissions legislations are discussed because this strongly influences the research and development of automotive engines regardless of the fuel used. The effect of individual emissions species is then made on both the environment and on human health. This is then followed by a discussion of the development in fuel specific emissions tools.

2.2 Spark-Ignition Combustion

The majority of today's internal combustion (IC) engines are derived from the successful application by Nikolaus Otto (Otto, 1887). Principally, the aptly named Otto cycle converts liquid energy into mechanical work through the initiation of spark energy. Nevertheless, compared to compression ignition (CI) engines, named after Rudolf Diesel (Diesel, 1895), SI engines suffer from inherent limitations. Apart from the principal ignition differences, SI engines have decreased thermal efficiency compared to CI counterparts. SI engines suffer from knock, which limits the maximum compression ratio, and pumping losses, which occur due to throttling. However, SI engines emit very little soot or particulate matter (PM). This is due to fuel type and early injection homogeneous mixtures promoting mixture quality.

Since the inception of the SI engine more than a century ago, the incremental developments in fuelling, ignition and emissions control technology have resulted in sophisticated modern engines. The Otto cycle is also applicable to a range of high volatility fuels, largely liquid fuels, but also natural gas and hydrogen. Early carburettor type injectors have long been replaced by high pressure injectors which are capable of multiple injections per cycle. The main goal is high efficiency whilst meeting emissions legislations. This has led to increased compression ratios and a shift towards GDI (Heywood, 2009).

2.2.1 Spark Timing

In SI engines, one of the main control parameters is the spark timing; it significantly affects the combustion process and determines the fuel economy, torque output and emissions (Heywood, 1988). The spark timing is usually optimised using sophisticated mathematical approaches, including polynomial regression techniques (Holliday, 1998, Suzuki, 2009),

radial basis functions and neural networks (Morton, 2002, Beham, 2004) as well as advanced Design of Experiment (DoE) methodologies (Roepke, 2002, Stuhler, 2002, Guerrier, 2004). Each technique requires extensive model tuning in order to find the optimum, or minimum advance for best torque (MBT) timing. Minimal advance or retard about this point gives modest variation in power and fuel consumption but can lead to large changes in NO_x and HC emissions. Therefore, in order to minimise emissions or counteract knock, a spark retard or knock margin is used when operating under high load and low speed conditions and when protecting the catalyst from excessively high temperatures (Heywood, 1988, Stone, 1999).

2.2.2 Knocking Phenomena

As mentioned, the onset of knock ultimately limits the maximum allowable spark advance and prevents the use of MBT timing. Engine exposure to spark-knock can lead to damage to the surface of in-cylinder engine components, such as the piston, liner, head and gasket. Therefore, it is critical to detect knock and avoid damage.

In the early 20^{th} century there was a focus towards chemical control of detonation. This was led by Harry Ricardo in the UK and Thomas Midgley in the US (Hancock, 1985). It became clear that the knocking tendency of fuels depend on the physicochemical properties. This led to the development of the research and motor octane numbers: RON and MON, respectively and the Octane (Antiknock) Index (OI = [RON+MON]/2) (Heywood, 1988, Kalghatgi, 2001a). However, the shift to DI and the drive for increased compression ratios has meant that the effect of charge-cooling also influences knock suppression. For instance, an increase of 2-8kJ/kg_{air} in 'cooling power' ($\Delta H_{vap}/AFR_{stoich}$) is equivalent to a unity increase in RON (Milpied, 2009). This is also important when using biofuels with high 'cooling power'.

Currently there are few publications disclosing the RON or MON of DMF. What is known, however, is that DMF has been used as an octane enhancer for gasoline (Barlow, 1982, Nisbet, 1946). Nevertheless, in comparison to pure ethanol, the increased knock suppression of DMF has been shown to be less significant (Daniel, 2011).

2.2.3 Port Fuel Injection

Traditionally, carburettors were used to inject the fuel for each cycle. The fuel quantity was governed by the varying air flow requirement. However, tightening emissions legislations led to the use of manifold or port fuel injection (PFI). PFI offered flexibility over the carburettor as the fuel injection was electronically controlled by measuring the exhaust O_2 content. The early injection of PFI promotes fuel mixture quality with a cost-effective, low pressure fuel injector. However, the technology of PFI was incapable of controlling the air-fuel ratio (AFR). Therefore, in the drive for lower pumping losses through stratification, PFI injectors were replaced by in-cylinder alternatives. The use of direct-injection (DI) was born.

2.2.4 Direct-Injection

The shift from PFI to DI was elicited by the ability to influence combustion behaviour by adjusting the injection timing. Fuel consumption at low and part-loads can be improved through stratification as the pumping losses are reduced (Alkidas, 2003). High-load torque is also increased due to knock suppression through charge-cooling. The much higher injection pressures of DI also allows greater control of the injection quantity and improves the vaporization rate and thus stability (Zhao, 2002). Although DI avoids fuel impingement on

the intake wall, it can lead to impingement (wetting) on the piston crown or cylinder wall. Therefore, wetting is avoided when using advanced injectors which guide the fuel away.

The DI injector is the most critical element in DISI engines (Zhao, 2002). An effective injector should deliver a highly repeatable spray geometry with high fuel atomization in a much smaller period than with PFI. Therefore, several high-precision multi-hole injectors have evolved: wall-, air- or spray-guided injectors (Figure 2.1).

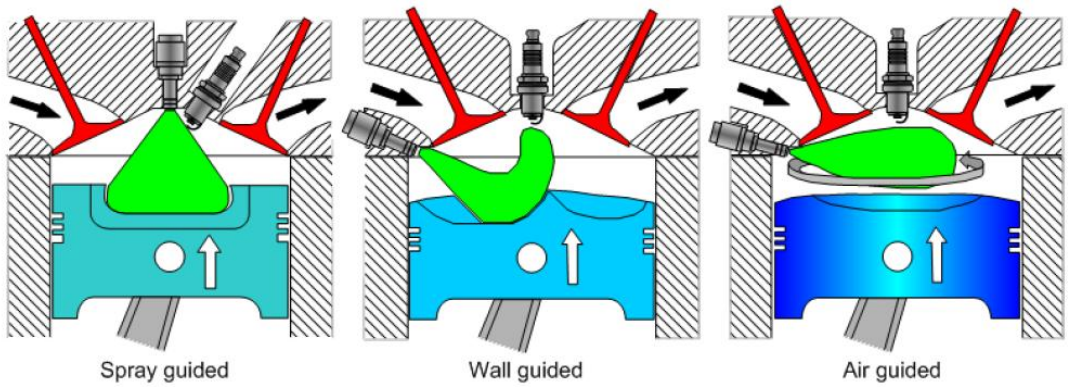

Figure 2.1 Direct-Injection Systems (Celik, 2010)

Wall-guided injectors (sometimes referred to as piston-in-bowl injectors) rely on the spray to be redirected from the piston crown towards the spark plug. Although stratification is easier to control using this method, the intentional piston wetting results in high PM, carbon monoxide (CO) and unburned HC emissions (Yang, 2002). Although air-guided injectors avoid piston wetting, they rely on tumble or swirl motion through specific intake tumble valves and piston crowns which require complex and expensive calibration. Alternatively, spray-guided direct-injection (SGDI) is usually located centrally, which helps to reduce surface impingement (Bosch, 2006, Honda, 2004). However, this makes SGDI more sensitive to stratification. Nevertheless, its use can lead to fuel consumption improvements (Brehob, 1998) and reductions to PM emissions over wall-guided counterparts (Price, 2006).

As such, there is pre-eminent focus from the automotive industry towards SGDI technology.

2.2.4.1 Homogeneous Combustion

Modern GDI engine management systems use a mixture of homogeneous and stratified combustion depending on the speed/load demand. A typical map is shown in Figure 2.2.

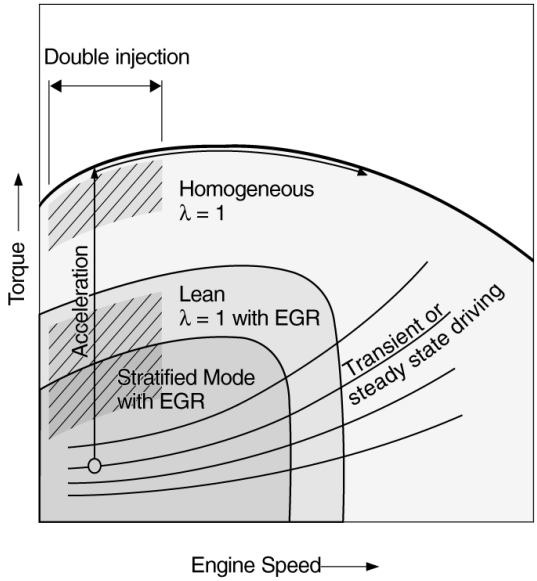

Figure 2.2 Engine Operating-Mode Map (Küsell, 1999)

At low speed and load, the engine is operated under stratified conditions, whereby exhaust gas recirculation (EGR) is used to help reduce NO_x emissions. As such, the fuel consumption is reduced by almost 20% over homogeneous stoichiometric operation because the pumping losses are dramatically reduced (AFR ≈ 40:1) (Brehob, 1998). With increasing speed and load, the benefits of EGR and lean combustion reduce. At the highest speed and load the engine is operated in homogeneous stoichiometric mode.

At the load transitions between stratified and homogeneous operation (shown by the dashed area in Figure 2.2), the use of double or split-injection offers constant torque with minimised

NO_x (Küsell, 1999) and PM emissions (Bosch, 2006). At WOT, split-injection is also used to extend the knock limit and increase torque by up to 5%. Early attempts to raise the torque at WOT employed fuel enrichment ($\lambda<1$) approaches (Yang, 1998, Fry, 1999) despite knock occurring most greatly slightly rich of stoichiometry. Although the richer mixture is effective in suppressing knock, the fuel economy and efficiency of the three-way catalyst (TWC) is compromised. Therefore at full load, a global stoichiometric mixture is commonly used with split-injection (Bai, 2010) or a rich mixture is used when at high engine speeds in order to lower the temperature of the TWC and prevent thermal damage.

2.2.4.2 Stratified Combustion

Although stratified combustion was proposed by Otto, the successful operation was not achieved in practice (Heywood, 1988). Stratification involves creating a very rich local mixture around the spark plug late in the compression stroke whilst maintaining a very lean global AFR ($\lambda >> 1$; WOT). The load is controlled by the fuel quantity and the start of injection (SOI) timing. However, stable combustion with stratification has always been difficult to achieve. That was, until the development of novel high precision injectors.

Stratification is not possible with a carburettor or PFI as the charge is well mixed before entering the cylinder. However, DI stratification is produced by igniting the mixture cloud as late as possible (Bosch, 2006). The difference between homogeneous and stratified combustion is shown in Figure 2.3. This late ignition requires careful optimisation of the end of injection (EOI) timing relative to spark timing, where small variations in flow structure can lead to misfires (Adomeit, 2007). However, the development of high energy ignition systems are helping to increase durability (Piock, 2010, Toulson, 2010). The late injection

with stratification can lead to significant fuel impingement on the piston crown. If the fuel is not vaporised prior to the onset of combustion the unburned HCs and PM emissions are significantly increased. This limits the use of stratification at higher loads, together with high NO_x emissions due to the high combustion temperatures. Although the NOx emissions could be reduced using EGR, stratification is limited to low load and speed conditions which are usually steady-state. At high load, the highly rich, stratified mixture produces high PM emissions and at high speed, the in-cylinder turbulence prohibits the effective use of stratification (Celik, 2010).

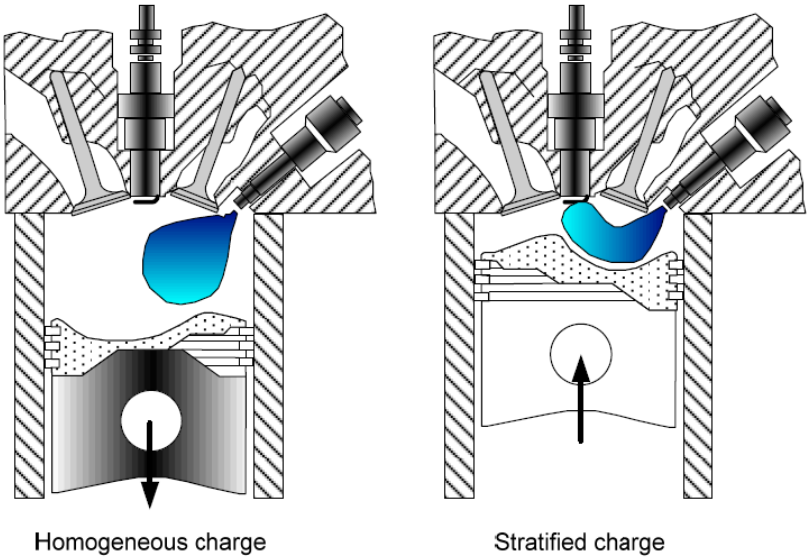

Figure 2.3 Homogeneous and Stratified Charge Combustion Modes (Celik, 2010)

Another concern with stratification is that traditional TWCs are not effective at reducing NO_x. Therefore, more complex and expensive systems, associated with CI engines are being used, such as NO_x traps and selective catalytic reduction (SCR) systems. However, this increases the exhaust back pressure and increases the exhaust stroke work. Despite this, the overall process produces a net fuel saving due to reduced throttling and lean combustion.

The sensitivity of EOI timing relative to spark timing leads to difficulties in the stratified to homogeneous mode transitions. However, this is overcome using split-injection.

2.2.4.3 Split-Injection

Split-injection strategies are used in load transitions (between low-load stratified combustion and high-load homogeneous combustion) and to improve cold engine starts (Serras-Pereira, 2007b). The use of multiple injections improves charge preparation, reduces PM emissions (Serras-Pereira, 2007a, Schmidt, 2011) and reduces part-load ISFC (Szekely, 2005).

The stratified mode is very sensitive to the EOI-to-ignition window even when using highly volatile fuels like gasoline. However alcohol fuels have been shown to tolerate stratification. The use of ethanol and *n*-butanol in low-load stratification produces similar combustion stability to iso-octane (gasoline reference) despite the lower vaporization rates (Smith, 2007).

However, little is known about the effectiveness of using biofuels with partial stratification (split-injection) at full load. The research with high ethanol blends (E85 and E50) has shown the reduction in piston and wall impingement compared to gasoline (Mittal, 2010). Once again, this is surprising because ethanol has a lower rate of vaporization.

2.2.5 Dual-Injection

The rising blend content of biofuels, such as ethanol, has led to the development of flex-fuel vehicles (FFVs). However, other optimisation methods are currently under development such as dual-injection (McAulay, 2010). Dual-injection is the combination of PFI and DI to supply gasoline-biofuel blends (Figure 2.4). Using both injection systems simultaneously, allows instantaneous blend ratios to be supplied to the engine to best suit the duty cycle.

Traditionally, the method of fuel injection of blends has mirrored that with gasoline; the blend is either injected using PFI or DI. This is true for ethanol FFVs used ubiquitously in Brazil; a variable blend of ethanol and gasoline (mixed in the fuel tank) is permitted, as the actual blend ratio can be detected by the diagnostic system (Nakajima, 2007). However as the blend ratio is measured it cannot be varied in real-time using the engine control unit. Therefore, dual-injection maximizes the properties of each fuel by optimising the fuel supply. Ultimately, this method combines the advantages of bi-fuel and flex-fuel engines.

Figure 2.4 Dual-Injection Concept as used in the 2GR-FSE Engine developed by Toyota

The potential of dual-injection inspired the creation of Ethanol Boosting Systems (EBS) in 2006, a spin-out from Massachusetts Institute of Technology. With modest hardware modifications, EBS examined the use of ethanol (hydrous and anhydrous) boosted dual-injection engines, to help cool the charge and suppress knock (Bromberg et al., 2010, Cohn et al., 2010, Cohn et al., 2005). In addition, Ford adopted the dual-injection technology into

their ‘Ecoboost’ gasoline turbo-charged direct-injection (GTDI) engines. Here, PFI gasoline and DI E85 was used to improve efficiency and suppress high-load knock (Stein, 2009).

Other automotive original equipment manufacturers (OEMs) that have investigated the combination of PFI and DI fuelling (albeit with gasoline in both injectors) include Toyota and more recently, Audi. The work by Toyota in 2006 demonstrated improved engine performance (fuel economy and torque) and reduced emissions at full load using a 3.5L V6 gasoline engine (2GR-FSE) (Ikoma, 2006). For Audi, the dual-injection technique is being used in a turbocharged 1.8L gasoline engine. As with the 2GR-FSE engine, this combustion mode contributes to higher fuel efficiencies compared to conventional single injection, albeit at part-load only (Wurms, 2011).

Dual-injection has been seen to produce a synergetic reaction for CI engines (Reitz, 2011, Leermakers, 2011). Reitz and colleagues claim that PFI gasoline aids the combustion of stratified DI diesel. The lower-reactivity gasoline charge helps to advance the start of combustion of the higher-reactivity diesel charge, so that combustion occurs in a smaller volume and results in increased efficiency. This effect on combustion chemistry is also supported through the research at the author’s institution on ‘Dieseline’; external splash blends of gasoline and diesel have been shown to produce competitive engine performance (Zhang, 2011).

With recent industry focus on engine downsizing, it is more important to mitigate knock. Dual-injection with ethanol in DI effectively meets this demand. However, methanol also has the potential to increase charge-cooling and therefore greatly suppress the knock with PFI gasoline. Therefore, EBS has conducted modelling studies of alcohol fuels in a GTDI engine which could be used in heavy-duty long haul applications (Bromberg, 2010). They suggested

that turbo-charged DI alcohol engines could be as, or more efficient than CI engines. The team have also produced simulation results comparing E85 and methanol in collaboration with Volvo (Blumberg, 2008). Their results show how methanol is potentially more effective than E85 because half the amount of fuel is required for similar knock suppression. However, the comparison has not yet been made experimentally.

2.2.6 Downsizing

The terms ‘downsizing’ and ‘downspeeding’ are being used synonymously with increased efficiency. However, engine providers believe that the need to improve fuel economy should not compromise performance by negatively altering the driving experience (Morris, 2010). As such, high power-to-weight ratio engines have been demonstrated (Fraser, 2011).

Although hybrid technology is providing an option to increased efficiency, its success is determined by battery technology. Therefore, the liquid fuel option is believed to provide the sanctuary for automobiles in the short- to mid-term and leading authorities are exploring the potential of downsizing (Fraser, 2011, Turner, 2011b, King, 2011). Other approaches for increased efficiency and power from smaller power units include lean and Miller cycle boosting (Lake, 2004, Taylor, 2011). Although turbochargers increase the exhaust back pressure, this penalty is overcome by harvesting the exhaust energy and increasing the mechanical and thermal efficiency by the higher effective compression ratio. Nevertheless, when the compression ratio is dramatically increased, there is a threat of ‘super-knock’ causing catastrophic engine damage due to the high in-cylinder pressures (Bradley, 2011). However, some researchers believe that the knock propensity of downsizing can be partially overcome by increasing intake tumble flow (Berntsson, 2011).

Other efforts to raise efficiency have been made by combining super- and turbochargers. The supercharger helps to overcome the low exhaust mass flow rate at low engine loads and the turbocharger maximises the recovery of waste heat at higher flow rates and loads (VanDyne, 2008, Meier, 2007, Szengel, 2007). Experimental and simulation results show that up to 8% BSFC gains are possible at low speeds (Chadwell, 2010, VanDyne, 2008). These efforts help to overcome the technical barriers to engine downsizing such as steady-state low speed torque and rapid transient response (Fraser, 2009).

2.3 Spark-Ignition Fuels

SI engines were initially developed to exploit the properties of the fuels available. However, the anti-knock property of early SI fuels was poor and the compression ratio was limited by their chemical properties. Therefore, the effort to improve efficiency has seen the evolution of SI fuels. Modern SI fuels have been derived to meet the demands of advanced DISI engines. This includes, but is not limited to, the ease of starting, fast warm-up, good transient response, tolerance of high engine speeds, avoidance of vapour lock, knock and hot/cold stability (Hancock, 1985).

These engine demands require an understanding of the physicochemical fuel properties. Specifically, SI fuels should have high OI (knock avoidance), Reid vapour pressure (cold start tolerance) and heat of vaporization (charge-cooling) as well as a low boiling and flash point (improved ignitability). These characteristics help to maximise and maintain efficiency under hot/cold weather conditions. Other fuel properties for IC engines in general, include good lubrication and low corrosiveness to reduce component wear, low solubility in water to avoid contamination and a high energy density to produce high fuel economy.

2.3.1 Gasoline

In the early years gasoline (known as Standard Petrol) referred to the light fractions distilled from crude oil, and was mainly formed from pentanes and hexanes (Hancock, 1985). Since then, gasoline has become a complex mix of aliphatic, aromatic, olefinic and paraffinic HCs that boil in the range of 40 to 190°C. The composition of gasoline can be tailored to best suit the varying engine demands (outlined in Section 2.3).

Improving the knock resistance is a main driver in gasoline development. Modern SI engines equipped with knock detection sensors allow the spark timing to reach borderline knock regardless of the fuel (Bosch, 2006). Several additives have been used to suppress knock. Lead based additives raise efficiency, but since 1986 have been mostly discontinued (still used in aviation fuels) following EU and US legislation (Directive(78/611/EC), 1978, EPA, 1970). This has led to the search for equally proficient knock-resistant additives. Other gasoline octane enhancers include ethyl tert-butyl ether (ETBE) and methyl tert-butyl ether (MTBE). Nowadays however, the use of ETBE and MTBE is limited because the products used in their synthesis are as attractive (ethanol and methanol, respectively). The need for sustainable energy sources is seeing an increasing use of renewable oxygenated additives in commercial gasoline. It is believed that this will help to address the regional energy security and global CO_2 issues. The world's carbon is believed to be depleted within the next 40 years (Allen, 2009, Shell, 2011) and so there is a need to confront the ballooning energy demand and alleviate environmental stress.

2.3.2 Oxygenated Alternatives

The idea of IC engines fuelled by biofuels is not new (White, 1902). In the early 1900s, Harry Ricardo noted that an engine running on ethanol was:

"*noticeably sweeter and smoother than on petrol"* (Hancock, 1985).

Today, liquid biomass is at the forefront of engine and fuel development. Biomass offers a high energy density option that is compatible with existing combustion systems.

In the UK, biofuels offer the most viable mid-term supplement to or substitute for gasoline, compared to technologies which are in their infancy (hydrogen fuel cells and full electric platforms) (Brevitt, 2002). In Europe, the promotion of biofuels has led to a legislative approach; by 2020, all EU member states must conform to a 10% minimum target on the use of alternative fuels (biofuels or other renewable fuels) in transportation, as based on EU Directives (Directive(2009/28/EC), 2009). In the US, tax incentives have been used to promote the use of ethanol blends (Curtis, 2008), in an effort to replicate the success seen in Brazil (Goldemberg, 2008).

Government policy on energy use is also changing in emerging nations (Wang, 2011). For large energy consuming nations, such as China and India, which have an increasing gap between energy demand and supply, the biofuel route offers improved energy security and reduced dependency on imported oil. Therefore, more emphasis is being placed on the automotive sector to, not only design compatible systems with these alternative fuels, but to also optimise their use in neat form and in blends with gasoline.

Currently, ethanol is the most widely adopted biofuel (Demirbas, 2007, Demirbas, 2011). In 2007, ethanol accounted for 80% of the world's total biofuel production (OECD, 2008).

However, engines using ethanol suffer from poor cold starts and high fuel consumption. Therefore countries with a hot climate such as Brazil can affordably use ethanol in neat form or in various blends to reduce gasoline dependency (Agarwal, 2007, Fatih Demirbas, 2009).

Although researchers have explored many different alcohol based gasoline alternatives (Gautam, 2000, Zhang, 2009, Pourkhesalian, 2009) current focus hinges on the effect of ethanol blends (Cooney, 2009, Kar, 2009b, Koc, 2009, Kumar, 2009). Ethanol's high knock tolerance can improve the thermal efficiency and torque output (Nakama, 2008). However, to address the shortcomings of its poor fuel economy caused by the low calorific value, higher compression ratios and boosted technologies are now being used (Yoon, 2009).

Alternatively, China has focused on the use of methanol and leads the world as a producer and consumer (Dolan, 2008). This is largely due to the lack of grain and abundance of coal, as opposed to favouring its performance over ethanol. Nevertheless, low methanol blends have been shown to require only minor engine modifications (Kowalewicz, 1993) but yet yield similar performance to gasoline (Liu, 2007, Wei, 2008). However, the low energy densities of methanol and ethanol (high oxygen content) hinder their use in high blends.

On the other hand, *n*-butanol has a high volumetric energy density (only 17% less than gasoline) and a reduced solubility in water. British Petroleum (BP) and DuPont have recognized this and have invested in its large-scale production (AIChE, 2007, Guzman, 2010). Similarly, to ethanol and methanol, *n*-butanol can be blended at low concentrations without compromising fuel performance (Bryner, 2008). In SI engines, *n*-butanol is comparable to gasoline (Merola, 2011, Wigg, 2011), as well as 2- and *t*-butanol (Niass, 2011). Nevertheless, new candidate biofuels are emerging, such as furan based fuels.

2.3.3 Furanic Alternatives

Furan derivatives, or 'furanics' as they have become known (Jong, 2009), have been noted for their explosive ability (Ayers, 1951) and improved vapour lock protection (Christensen, 2011). However, it is their anti-knock qualities that have seen the development of several patents (Mottlau, 1943, Lloyd, 1956, Barlow, 1981). In a rapid compression machine, the use of low furanic blends (<20%) were as effective at resisting auto-ignition as ethanol (Ohtomo, 2011). Therefore, there is a growing focus on improving their production techniques (Gruter, 2009, Mascal, 2009) and even the potential use in CI engines (Jong, 2009).

2.3.3.1 2,5-Dimethylfuran

The particular furanic analysed in this work is 2,5-dimethylfuran: (C_6H_8O) (see Figure 2.5).

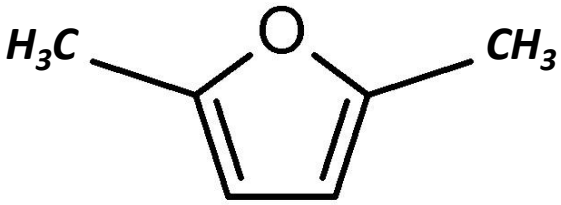

Figure 2.5 Chemical Structure of 2,5-Dimethylfuran

This furan derivative is a heterocyclic compound, sharing an oxygen atom with 4 double-bonded carbon atoms in a 5-point ring structure. Two methyl (CH_3) groups extend from the furan ring to produce a molecular mass of 96. Recently, significant breakthroughs in the production of 2,5-dimethylfuran were reported (Roman-Leshkov, 2007). Dumesic and his team, who then coined the term DMF, demonstrated advances in the biomass-to-liquid conversion of fructose into DMF (Roman-Leshkov, 2007, Dumesic, 2007). Their method produces higher efficiency and yield (due to the catalytic pathways) than biological methods

for biofuels like ethanol helping to reduce cost (Kazi, 2011). This concept was improved by Zhao and his team, who observed high yields of 5-hydroxymethylfurfural, or HMF (the intermediate for DMF), without the need for acid catalysts used by Dumesic (Zhao, 2007). Not only does Zhao's method dramatically reduce the production costs, but it now includes glucose as a potential feedstock for HMF. Furthermore, Mascal reported that cellulose can itself be converted into furanics (Mascal, 2008). This has led to the production development of DMF (Thananatthanachon, 2010, Tong, 2010, Gorski, 2011, Hu, 2011) and attracted attention towards its use as a SI fuel, and potential alternative to gasoline (Luque, 2008).

DMF's physicochemical properties are competitive to ethanol. Firstly, its energy density (31.5MJ/L) is 40% higher (23MJ/L) and much closer to gasoline (35MJ/L) (Binder, 2009). Secondly, it has a higher boiling point (92°C) than ethanol (78°C), which makes it less volatile and more practical as a liquid fuel for transportation (Binder, 2009). Thirdly, unlike ethanol, DMF is insoluble in water, which makes it stable in storage and unlikely to contaminate underground supplies or be contaminated by water in transportation pipelines (Roman-Leshkov, 2007). Finally, DMF offers competitive anti-knock qualities (Mousdale, 2008), which will allow the use of high compression ratios or forced induction technology to maximize the thermal efficiency and power (Nakata, 2007). In addition, DMF has favourable lubrication properties, so would help to reduce engine component wear (Felix-Moore, 2009). Together with the aforementioned production improvements, these physicochemical properties make DMF a potentially viable competitor to ethanol.

Currently, few publications can be found on pure DMF as a gasoline alternative fuel (DMF blends have been briefly investigated (Turner, 2010)). The bench testing work by Wu et al. was the first to be reported. This included the combustion intermediates of DMF (Wu,

2009b) and extensive laminar burning velocity studies (Wu, 2009a, Wu, 2011b, Wu, 2011c, Wu, 2012).

Recently, the author of this thesis contributed to the first report of neat DMF combustion (Zhong, 2010). This was followed by the comparison of the laminar burning velocities (Tian, 2010a) and spray properties (Tian, 2010b). Since then, several publications have been produced by the author of this thesis (Daniel, 2011, Daniel, 2012a, Daniel, 2012b, Daniel, 2012c, Daniel, 2012e, Daniel, 2012f, Daniel, 2012g). The results are discussed herein.

2.3.3.2 2-Methylfuran

Similarly to DMF, 2-methylfuran (herein denoted MF) is a heterocyclic compound with the chemical formula C_5H_6O. MF is formed by the removal of the second methyl group (CH_3) branched on the 5th carbon in the ring of DMF (Figure 2.6). Until the publications in *Science* and *Nature* in 2007 (Zhao, 2007, Roman-Leshkov, 2007), little was known about the combustion and emissions of MF. Experimental results have shown that MF is more tolerant to cold engine starts than ethanol due to its higher rate of vaporization (Thewes, 2011a, Thewes, 2011b). However, the high combustion pressures of MF lead to high NO_x emissions due to a high adiabatic flame temperature.

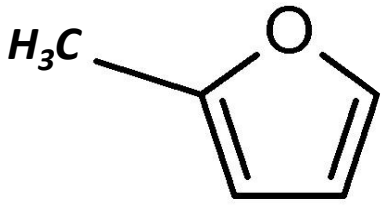

Figure 2.6 Chemical Structure of 2-Methylfuran

Investigations on MF have been performed by the author's group (Wang, 2012). This study confirms the high combustion pressures, rates and NO_x emissions of MF. It also presents the low formaldehyde and acetaldehyde emissions compared to gasoline and ethanol.

2.4 Regulated Engine-out Emissions

In the early 1960s, emissions controls were imposed on automobiles due to the serious air pollution effects (Hancock, 1985). Since then, the developments in engine technology have largely been driven by emissions restrictions. For instance, the shift in fuel delivery from the carburettor, towards PFI and finally DI stratification has dramatically reduced the regulated emissions. However, for SI engines, the majority of emissions are controlled by TWC. Once activated (warmed-up) a TWC effectively oxidises/reduces the harmful combustion products.

2.4.1 HC, CO and NO_x Emissions

The regulated emissions include the major pollutants from IC engines: HC, CO and NO_x. The HC and CO emissions are products of incomplete combustion and increase with poor fuel vaporization, mixture quality and burn rate. The main source of HC emissions is from combustion chamber crevices, which can constitute half the total HCs emitted (Cheng, 1993, Alkidas, 1995). Split-injection strategies have been used to reduce CO and unburned HCs by reducing the fuel impingement on the piston and wall (Serras-Pereira, 2007a, Serras-Pereira, 2007b, Serras-Pereira, 2008). However at low and part-loads the HCs from wall wetting are negligible with a warm engine (Kaiser, 1996) due to improved fuel droplet vaporisation, subsequent dispersion and increased combustion efficiency.

The CO emissions are sensitive to AFR. With insufficient oxygen present to oxidise the carbon atoms, the CO emissions will increase. Conversely CO emissions decrease in the presence of abundant oxygen and are typically removed when using stratified lean combustion (Dunn-Rankin, 2007). Furthermore, the use of oxygenated fuels and/or higher H/C ratios are known to reduce HC and CO emissions (Owen, 1995, Harrington, 1973).

The NO_x emissions include nitrogen dioxide (NO_2) and nitric oxide (NO). These emissions increase very strongly with combustion temperature and residency time (Stone, 1999). In SI engines, the NO_2/NO ratio is negligible and the NO_x emissions consist of mainly NO (Heywood, 1988). Also, compared to CI engines, the NO_x emissions are very high in SI engines due to the stoichiometric mixture which is required for efficient use of the TWC.

Reductions in engine-out NO_x emissions are achieved by reducing combustion temperature. For instance, the charge-cooling effect from DI helps to lower the temperature on ignition and hence the peak combustion temperature. Spark retard also reduces the peak combustion temperature and helps to activate the TWC, which in itself is very effective at reducing NO_x. Furthermore, the dilution effect of EGR and lean combustion leads to lower combustion temperatures. However, the latter requires NO_x reduction strategies as used in CI engines.

2.4.2 Particulate Matter Emissions

The high PM emission from CI engines has resulted in strict regulations. As a result, the effect of different CI fuels on PM is well-known (Andersson, 2004). However, PM formation is very complex and includes many components such as solid carbonaceous and liquid matter (Rounce, 2011). The identification of PM modes has been made (Kittelson, 1998) but is still

debated (Peckham, 2011). In addition, the measurement techniques are contentious and efforts are being made to standardise them (Giechaskiel, 2009).

Compared to CI engines, SI engines produce very little PM emissions. However, the smaller particles which are not visible (unlike soot) have been shown to be more harmful (Kittelson, 1998). Therefore, the PM emissions from SI engines are becoming increasingly regulated.

It is believed that the PM emissions from DISI engines exceed those from PFI engines (Graskow, 1999). This is due to reduced fuel preparation time and increased wall wetting. In fact, the PM number and mass emissions from PFI engines have been shown to be similar to CI engines using a diesel particulate filter (DPF) due to the improved homogeneity (Price, 2006, Braisher, 2010). Stratified combustion also results in fuel rich areas and high PM emissions due to the susceptibility to variations in in-cylinder flow. Therefore, the growing use of stratification is leading to advanced after treatment systems (Xu, 2011).

In SI engines, PM emissions can be reduced through spark timing retard. Although this compromises performance, it helps to increase the mixing time and subsequent exhaust temperature. Furthermore, the use of high oxygenated fuels like ethanol can contribute to reduced PM emissions, especially soot particles (Chen, 2010). However, the consequence is an increase in the nucleation mode (Price, 2007).

2.4.3 Legislation

The most stringent emissions limits in the US (shown in Table.1) are set by the state of California, largely due to the pollution of Los Angeles in the 1940s (Bosch, 2006). These

emissions standards are set over the Federal Test Procedure (FTP) drive cycle, developed to mirror actual highway driving conditions.

Table.1 US Emissions Limits for Light Duty SI Vehicles <80,000km (Delphi, 2012)

Emissions	Unit	Tier I 1994	Tier II 2004
NMHC	mg/km	160	65
NO_x		250	90
CO		2100	1050
PM (mass)		50	15 (120k)
PM (number)	Nb/km	-	-

In Europe, the emissions limits were defined in 1970 (Directive(70/156/EC), 1970) and are also set over a drive cycle: the New European Drive Cycle (NEDC). The limits are shown in Table.2 for vehicles with a mass less than 2,610kg:

Table.2 EU Emissions Limits for Light Duty SI Vehicles (Delphi, 2012)

Emissions	Unit	Euro III 2000	Euro IV 2005	Euro V(a) 2011	Euro V(b/b+) 2013	Euro VI 2015
HC	mg/km	200	100	100	100	100
NO_x		150	80	60	60	60
CO		2300	1000	1000	1000	1000
PM (mass)		-	-	5	4.5	4.5
PM (number)	Nb/km	-	-	-	-	TBD

The PM mass (and number) emissions limits are being implemented in the US and Europe to develop low emissions vehicles. The PM levels will be aligned with that for CI engines which will encourage major developments in combustion and/or emissions after treatment, such as DPFs used in CI engines.

The introduction of on-board diagnostics (OBD) in 1988 saw a further restriction on emissions. The fault detection of emissions-related components is now required within a prescribed time (Bosch, 2006) demanding an understanding of real-world use (Daniel, 2009).

2.4.4 CO_2 Emissions

Although CO_2 is a non-toxic gas, which is not classified as an engine pollutant, it is one of the substances responsible for global temperature rises through the greenhouse effect. Therefore, there is an increasing political drive to reduce CO_2 emissions from automobiles (Johnson, 2010). Improved combustion efficiency and fuel consumption result in lower CO_2. However, oxygenated fuels typically produce high engine-out CO_2 emissions (Owen, 1995) because their lower low heating value (LHV) increases the fuel consumption. However, 'downsized' vehicles help to reduce fuel consumption and directly support CO_2 reduction.

2.5 Unregulated Engine-out Emissions

Currently, with the exception of formaldehyde in the US, the individual HCs are not regulated in the US or Europe. However, it is anticipated that the more harmful HC emissions will become regulated as emissions legislations are tightened. In California, the regulation for low emissions light-duty vehicles stipulates that the formaldehyde emissions limit during the FTP cycle is <9.4g/km for low mileage vehicles (Delphi, 2012). This move is likely to be followed by other organizations, as the strict limits imposed in California are historically exemplary. There is a need to understand the individual HC emissions.

The level of toxicity and photochemical reaction rate of each HC is important in scrutinizing the allowable emission. The various levels of carcinogenicity of HCs are determined by the

International Agency for Research on Cancer (IARC) and the National Toxicology Program (NTP). Certain HCs present respiratory, ophthalmic or dermatological irritation symptoms (Richardson, 1994). Known carcinogens include 1,3-butadiene, formaldehyde and benzene, whereby acetaldehyde and furan are possible carcinogens (IARC, 2011, NTP, 2011) as shown in Appendix A. However, the long term effect of increased ambient levels of the major aldehydes (formaldehyde and acetaldehyde) is not well known.

Environmental impact of HCs is measured by the photochemical reactivity (ozone forming potential), which is given by the maximum incremental reactivity (MIR) scale (Carter, 2010). For the aforementioned carcinogenic HCs, the MIR values are 12.61g ozone/gHC (1,3-butadiene), 9.46g ozone/gHC (formaldehyde) and 0.72g ozone/gHC (benzene) and for acetaldehyde, the MIR value is 6.54g ozone/gHC (CARB, 2010). Although, believed to be non-carcinogenic, furan derivatives also have high MIR values (furan, MF and DMF are 9.15, 8.3 and 7.88g ozone/gHC, respectively (CARB, 2010)). The remaining MIR values for the worst offending HCs and those present in this work are shown in Table A.2 (the fuels used in this work are highlighted). The level of toxicity of DMF and other furan derivatives is ongoing and more work is anticipated as the focus on DMF increases (Fromowitz, 2010). Therefore, it is essential to understand the magnitude of these emissions, firstly on the engine-out emissions and secondly, after the TWC.

2.5.1 Speciation of Hydrocarbons

The industry standard total HC measurement method is with a flame ionization detector (FID). However, the inherent reduced sensitivity of FID analyzers to oxygenated fuels (Cheng, 1998, Wallner, 2008) suggests that the total HC emissions is different and dependant

on the individual HC (Grob, 1985). For instance, the FID response to acetaldehyde (C_2H_4O) is approximately half that of a non-oxygenated HC (Chung, 2003). To overcome this insensitivity, some researchers use a response factor (Magnusson, 2002), which is found by comparing the signal of known concentrations. Corrections can then be made to compensate for the oxygenated HCs in the exhaust. For improved accuracy, response factors should be applied to each oxygenated HC.

A method of HC speciation is to use gas chromatography (GC). However, the method of engine sampling and sample transportation is critical to the accuracy. Any loss or change in the concentration of the HCs will dramatically affect the results. The most accurate sampling method is an inline measurement using a heated line directly from the engine to the emissions analyser. However, in some instances this is not possible. Therefore, collection of exhaust gas in bags or flasks is a preferred alternative. In this case, studies have shown that the stability of certain gases, such as 1,3-butadiene may be compromised (Jemma, 1995, Kaiser, 1994). Furthermore, when using bag sampling, dilution air must be used to avoid water condensation. In the case of flasks, reduced pressures can be used (Kar, 2009).

Another method used for HC speciation is GC coupled with mass spectrometry (MS). The GC/MS is a powerful analytical tool and is widely used to identify HCs (Grob, 1985). Each compound emitted has a characteristic mass spectrum. Usually, the largest peak represents the unfragmented molecule and is the largest mass detected. This is referred to as the 'parent mass' (Grob, 1985) and usually leads to the determination of the molecular mass, M_w.

Some researchers have simultaneously measured the exhaust using GC/FID and GC/MS to analyse the light and mid-range HCs when fuelled with gasoline (Jemma, 1995) and methanol (Hoekman, 1993). However, the complexity of gasoline makes it difficult to detect

all HCs although changes in speed and load are pronounced (Elghawi, 2009). Therefore, the use of single component fuels produces a clear output with less variation as the HC emissions mainly comprise unburned fuel (Sodré, 2003). The results using ethanol have shown that less 1,3-butadiene is emitted than using gasoline (Kelly, 1996) and that benzene and toluene emissions are reduced as more ethanol is added to gasoline (Poulopoulos, 2001).

2.5.2 Carbonyls

The carbonyl (aldehydes and ketones) emissions of ethanol are shown to be dominated by the emissions of acetaldehyde and then formaldehyde (Magnusson, 2011). However, investigations using a TWC have shown that acetaldehyde is not easily reduced. In his investigations, Elghawi showed that formaldehyde is eradicated using a TWC, but acetaldehyde is only reduced between 5-15% (Elghawi, 2009). The low conversion efficiency of the TWC for acetaldehyde is known (Stepanek, 2010, Poulopoulos, 2001). Therefore, this knowledge helps to develop more effective conversion methods and develop alternative catalysts, especially with the rise in high blends of ethanol in light-duty vehicles (Lupescu, 2009). This is also important during cold engine starts, as the emissions of acetaldehyde in high ethanol content blends will rise (Wallner, 2010).

As the combustion of oxygenated fuels has a profound influence on the total HC emissions, it is important to compare individual HC emissions species between fuels like ethanol, methanol and *n*-butanol. However, very little literature compares all pure fuels together and, as yet, nothing has included DMF. The carbonyl emissions of methanol have been compared to other oxygenates like MTBE and ETBE on a 2-stroke engine (Magnusson, 2011).

However, the data was not collected in the same period so the comparison lacked sufficiency.

Increasing blends of ethanol in gasoline dramatically increases acetaldehyde (CH_3CHO) emissions but reduces formaldehyde and benzaldehyde (Storey, 2010). Formaldehyde formation is a product of combustion temperature (Zhang, 2010), which is a characteristic of the fuel's combustion behaviour. Similarly, low blends of methanol (≤30%, by volume) has a large influence on the formaldehyde emissions (Zhang, 2010). However, the emissions were shown to dramatically reduce with the use of a TWC. The formaldehyde emissions when using *n*-butanol are lower than when using methanol but higher than ethanol (Wallner, 2010).

The emissions of formaldehyde and methanol have been detected using GC coupled with a pulsed discharge helium ionization detector (Wei, 2009). The emissions are detected within several minutes and are much quicker than traditional methods. However, the use of Fourier Transform Infrared (IR) Spectroscopy (FTIR) provides a very fast response (1Hz) and continuous analysis of all the carbonyl emissions in the exhaust stream (Zhang, 2010). Nevertheless, the FTIR method requires the capture of all the individual emissions in order to accurately interpret the IR spectrum. Therefore, the initial task when exploring new fuels is to detect all HC emissions present. In this work, the commonly employed California Air Resources Board (CARB) Method 1004 is used to quantify the carbonyls.

Understanding the variation of individual HCs emitted allows the most effective exhaust after treatment devices to be designed. This is especially true when using new fuels. If the use of DMF is to increase, an understanding of the individual HC emissions will help to safeguard human health and the environment.

2.5.3 Fourier Transform Infrared Spectroscopy

As mentioned, FTIR is another speciation technique which is growing in acceptance due to its fast response (1Hz sample time). It is well-known that FTIR is more effective than liquid impingers (e.g. CARB Method 1004) and is likely to produce more reliable measurements than with an FID (Wallner, 2010) as the varying sensitivity of an FID is eliminated (Cheng, 1998, Kar, 2009). Furthermore, the FTIR does not require daily gas calibration like an FID, so reduces the complexity and cost of setup.

However, the IR spectrum must be completely identified in order to accurately quantify the HCs (Gasmet, 2009). Nevertheless, once setup, the FTIR method is proven to reliably predict the HC emissions from oxygenated fuels (Spartz, 2008).

2.6 Summary

In summary, the literature review discusses the development of modern GDI technology and the associated fuels. The major areas include the discussion of stratification and split-injection strategies to reduce piston impingement, the effect of knock on engine performance and the progression towards downsized engines to improve fuel economy and reduce CO_2.

The effect of new alternative oxygenated fuels suitable in SI engines is also discussed. The main focus is on DMF, a furanic biofuel. Advances in the biomass-to-liquid conversion of fructose into DMF have spurred the research into the potential use of DMF as a supplement for, or alternative to gasoline. In addition, investigations from other institutions have recently disclosed the favourable anti-knock qualities of DMF and MF. Together, with the advance of manufacturing techniques, this highlights the pre-eminence of DMF as an automotive fuel. Nevertheless, little is known about the combustion performance and emissions of DMF in modern DISI engines, which reflects the early stage of development of this 'new' fuel.

The optimal combustion of oxygenated fuel blends with gasoline is discussed using the dual-injection technology. Using gasoline alone, dual-injection improves part-load fuel economy. However, when using ethanol in DI – the only biofuel to be utilised in dual-injection – the knock associated with PFI (gasoline) is suppressed dramatically, improving high-load torque.

This literature review acknowledges that the development of IC engines and associated fuels are largely driven by the imposed emissions regulations. Restrictions on PM emissions from SI engines are now being imposed and this is leading to the monitoring of individual HCs.

Ultimately, the literature review introduces the main motivation of this thesis, which is to examine, in detail, the combustion and emissions behaviour of DMF in a modern SI engine.

CHAPTER 3

EXPERIMENTAL SETUP AND TECHNIQUES

The aim of this chapter is to present the experimental test facilities and data acquisition systems used in this study.

3.1 Introduction

The equipment used throughout this study is described in this chapter. This includes the details of the single cylinder test hardware and instrumentation, as well as the emissions equipment. The engine control methodology, data collection process and analysis software are all described in turn.

The test facility was upgraded by Jaguar, the laboratory technicians and previous doctoral researchers prior to the author commencing his study. However, throughout the test period the author was responsible for maintaining the facility. This included minor component replacement (e.g. injectors, pumps, accumulator seals and hoses) and two engine rebuilds.

The two engine rebuilds were required during the test period due to component failure. Each rebuild was managed by the author and the engine overhaul process was supported by two research students, Chongming Wang and Daniel Fennell. This work included sourcing new components and the reinstallation. Other minor work included the replacement, installation and calibration of various sensors, an air intake damper and the dual-injection system.

Nevertheless, this chapter provides a brief overview of the current test facility. A further detailed description can be found in (Turner, 2010).

3.2 Single Cylinder Thermal Engine

The 4-stroke single cylinder engine used in the investigation is shown in Figure 3.1.

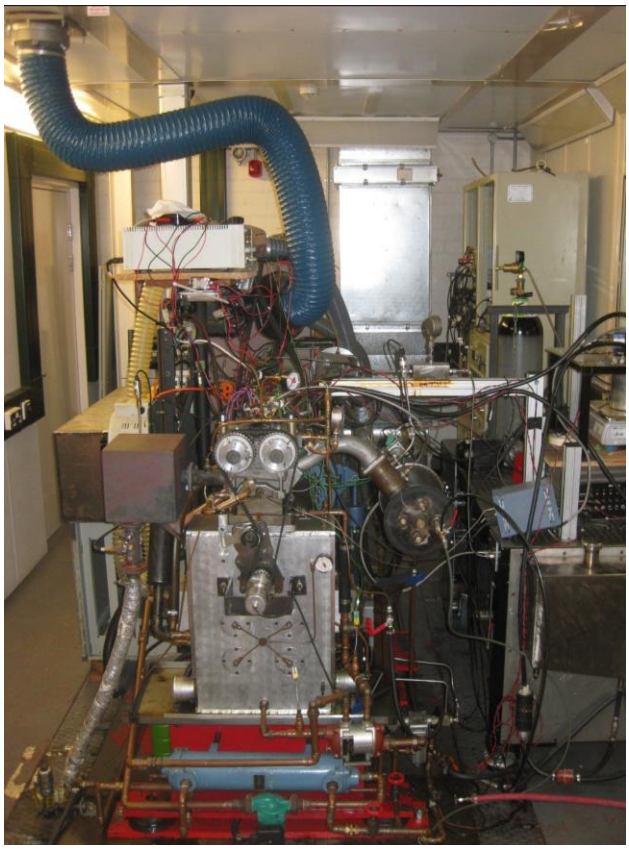

Figure 3.1 Single Cylinder Engine

The balancing unit is based on a Ricardo Hydra engine. It was re-designed by the Internal Combustion Engines (ICE) Group at the University of Oxford and now features a Jaguar V8 production engine cylinder head (AJ133) (Sandford, 2009). This gives the engine a four-valve SGDI cylinder head, representative of modern DISI engines. The engine is also fitted with a variable cam timing system, which will be described in more detail.

As shown in Table 3.1, the over-square engine configuration has a high compression ratio and swept volume. This helps to maximise efficiency and output power.

Table 3.1 Specification of the Single Cylinder Engine

Engine Geometry	
Swept Volume	565.6 cm^3
Bore x Stroke	90 x 88.9 mm
Connecting Rod Length	160 mm
Compression Ratio	11.5:1

The engine is provided on a test bed and the ancillary equipment will be equally discussed.

3.2.1 Overview of Test Facility

The schematic of the test facility is shown in Figure 3.2.

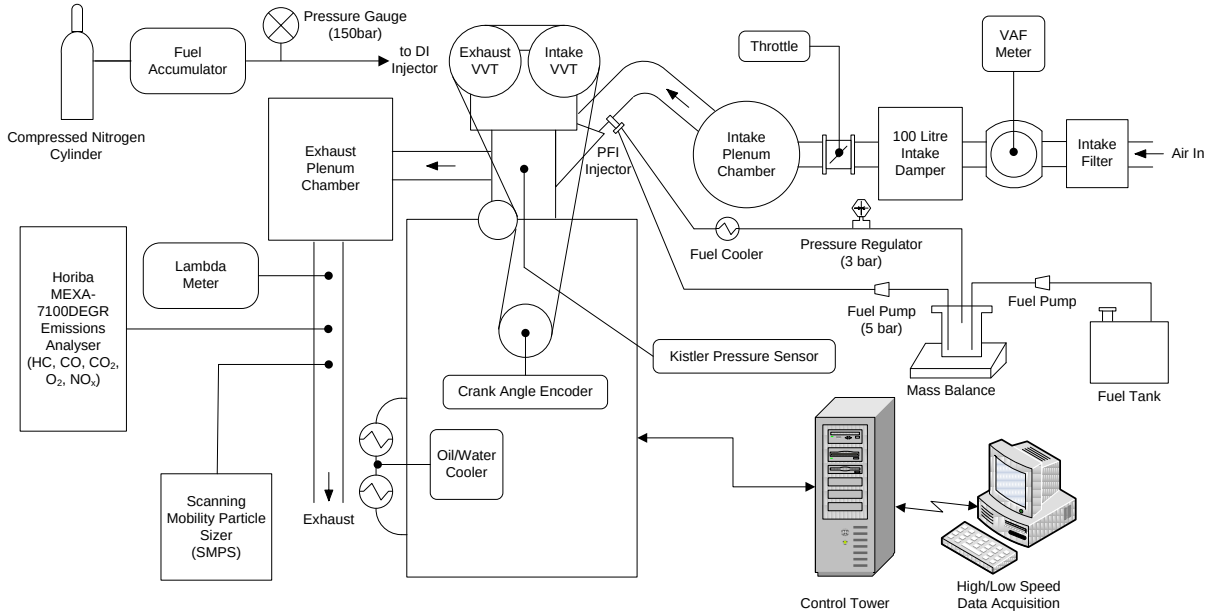

Figure 3.2 Schematic of Engine, Instrumentation and Acquisition Systems

The intake and exhaust pressure fluctuations are reduced using external bespoke plenums, which are approximately 200 and 10 times the size of the swept engine volume respectively.

Each group of parts is discussed in turn in the proceeding sections.

3.2.2 Intake and Exhaust System

As shown in Figure 3.2, three chambers help to stabilize the gas flow through the engine. On the intake side, this includes an intake damper (airbox) and intake plenum either side of the throttle. On the exhaust side, an exhaust plenum is used.

The purpose of the intake airbox and plenum is to stabilise the air flow through the air flow meter and after the throttle disturbance, respectively. The exhaust plenum equally helps to stabilise the emissions flow measurements.

A 100L intake airbox is used to operate the engine at WOT with sufficient air flow. This satisfies commonly used sizing criteria (>86L), as detailed in Equation 3.1 (Kastner, 1947):

$$V_b = \frac{417 \times 10^6 \times K^2 d^4}{N_c V_s n_{min}^2}$$

Equation 3.1 Minimum Airbox Volume

In Equation 3.1, K represents half the number of strokes per cycle, d is the bore diameter, N_c is the number of cylinders, V_s is the swept volume and n_{min} is the minimum engine speed at which accurate measurements are required.

3.2.3 Heating and Cooling Circuits

The test facility incorporates a heating and cooling circuit for the engine coolant and oil. Each circuit is independently pumped and heated. During the experiments, the engine coolant and oil temperatures were controlled at 85±5°C, and 95±3°C, respectively, using a Proportional Integral Differential (PID) controller. The PID controller releases a solenoid

valve that controls the flow of mains water. When opened, the mains water cools the hot engine coolant through a heat exchanger. The engine coolant then acts to cool the oil through another heat exchanger. Both heat exchangers were supplied by Bowman and an oil paper filter is used to remove impurities (and is replaced when necessary).

As the long-term oil degradation behaviour is otherwise unknown when testing new fuels, the author took precaution and closely observed the oil level and quality. Therefore, throughout the testing, the engine coolant and oil levels were routinely checked and replenished/replaced when required.

The engine water cooling and lubricating oil circuits are shown in Appendix A.1.

3.2.4 Fuel Supply Systems

As well as firing under high pressure (150bar) SGDI conditions, a low pressure (3bar) PFI system is available. The two fuelling modes can be used independently or simultaneously, where the latter is herein coined dual-injection.

3.2.4.1 Port Fuel Injection (PFI)

The low pressure (3bar) PFI system was primarily used for warming up the engine prior to DI testing. However, during the dual-injection testing, the PFI system is used to incorporate gasoline. Although the fuel temperature was not controlled, the fuel level in the PFI tank remained high during testing in order to avoid overheating of the pump and excessive fuel vapour loss.

3.2.4.2 Direct Fuel Injection (DI)

The high pressure (150bar) DI combustion system consists of a centrally mounted, six-hole injector with the spray orientation shown in Figure 3.3. The nozzle pattern consists of two groups of 3 holes, symmetrical about the crankshaft axis. Spray plumes 1 and 6 are directed towards and around the spark plug in order to promote ignition during stratified combustion. The spark plug is mounted at an angle of 18° from the cylinder axis in order to best receive the vaporized fuel droplets from these plumes.

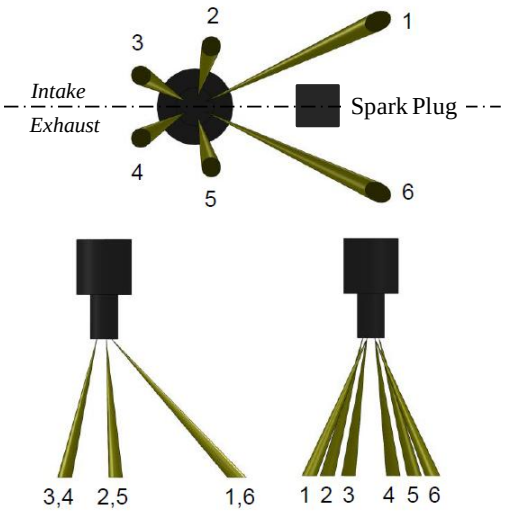

Figure 3.3 Orientation of 6-Hole Injector Spray Plume

The DI fuel system uses a free piston accumulator in order to maintain a constant pressure of 150bar. The fuel required for the test is pumped from a day-tank using an electric pump to the top of the accumulator cylinder and through to the DI injector using a variety of rigid and flexible tubing and stainless steel compression fittings. The other side of the accumulator piston is then pressurized using oxygen-free nitrogen from a compressed gas cylinder supplied by British Oxygen Company (BOC) and a high pressure gas regulator. The system contains various manually operated valves which can be used to return unused fuel back to

the tank at the end of the test. When changing fuels, the system was purged with nitrogen. At the end of a test day, the system was then cleaned with gasoline in order to avoid damage to the injector and accumulator seals.

3.2.4.3 Dual-Injection (PFI + DI)

The two fuelling modes (PFI and DI) can be used simultaneously in order to operate the dual-injection mode. When in this mode, the DI injection timing becomes the first injection in the operating software at 280°bTDC$_{comb}$ and the PFI injection timing is the second injection at 50°bTDC$_{comb}$. Although this results in a very early PFI injection for the next cycle, 76CAD after IVC (126°bTDC$_{comb}$), it allows the current LabVIEW software to be used whilst only changing the electrical connections in the National Instruments (NI) breakout box.

3.3 Control System

The engine timing control system (ETCS) controls the SOI injection and injection pulse width, together with the ignition timing and coil charge time. The ETCS software is written using LABVIEW (NI card 6602) and was originally developed by the ICE Group but was then modified by a previous researcher at this institution (Luszcz, 2009). Each ETCS parameter can be changed in real-time, whilst the engine is running. Two injections per cycle (independent pulse widths) are allowed with either PFI or DI. This is sometimes referred to as double pulse injection, but is herein termed split-injection. When operating the engine in dual-injection mode, the PFI and DI injectors can be run simultaneously. This is achieved by

changing the terminal connections on the control panel and the use of an external DI injector controller. When running in this mode, split-injection is disabled.

The control of air flow whilst at constant engine speed is achieved through the adjustment of a butterfly throttle valve. The mixture strength is then controlled by adjusting the injector pulse width using the ETCS software.

3.3.1 Crankshaft Encoder Setup

During the second engine rebuild, the crankshaft encoder was accurately setup. This signal determines the location of the piston relative to top dead centre (TDC) and is used by the ETCS software to control the injection, ignition and variable valve timings. The encoder timing was obtained by inputting a spark timing of 0°bTDC_{comb} (TDC) using the control software and observing the stroboscopic response at the flywheel when motoring the engine at low speed. The difference in response was determined using the crank angle degree (CAD) markings, which were verified by a previous researcher (Turner, 2010). This was then entered into the ETCS software so that there was no disagreement between the control software and the stroboscope pick-up. The TDC location of the flywheel was verified before the engine installation by measuring the dead zone of a dial gauge.

3.3.2 Variable Cam Timing System

As mentioned previously, the engine is fitted with a fixed phase variable cam timing (VCT) system. The VCT system uses the crankcase oil pressure (approximately 3.5bar), to control the offset of the camshaft relative to the timing of the camshaft pulley (±25CAD). A custom LABVIEW script, developed by a previous student (Luszcz, 2009), controls the VCT system

using an NI card (6202). In brief, the software measures the pick-up from a hall-effect type sensor, which is triggered when a disc attached to the rotating camshaft is detected. This denotes the cycle position (one camshaft revolution; two crankshaft revolutions). Adjustments are then made to the cam timing by varying the pulse width to the hydraulic solenoids (mounted on the cylinder head). The software then automatically regulates the cam position so that, in stable operation, the timing is maintained to ±0.1CAD.

The geometry of the intake and exhaust camshafts is shown in Table 3.2.

Table 3.2 Spark-Ignition Camshaft Geometry

Camshaft Geometry	
Intake Valve Lift	10.5 mm
Exhaust Valve Lift	9.3 mm
Intake Valve Duration	250 CAD
Exhaust Valve Duration	250 CAD

The baseline valve timings used in the experiments are shown in Figure 3.4.

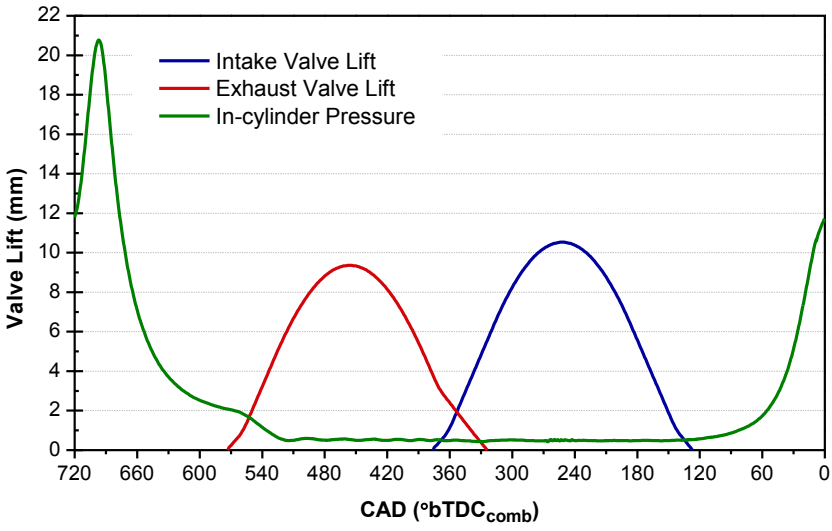

Figure 3.4 Intake and Exhaust Camshaft Profiles

This camshaft is typical for a high lift profile as used in production engines of this cylinder size. The intake valve opening (IVO) timing is 16°bTDC$_{intake}$ and the exhaust valve closing (EVC) timing is 36°aTDC$_{intake}$. This timing was optimised for low load conditions (3.5bar IMEP) as used by others (Turner, 2010).

3.3.2.1 Variable Cam Timing Setup

During the engine rebuilds the timing of the intake and exhaust cams relative to the crankshaft was setup. The procedure requires the user to manually rotate the flywheel in order to vertically align the cam lobes, with the use of timing pegs, at 255°bTDC and 70°bTDC for the exhaust and intake cams, respectively.

First, the exhaust camshaft is correctly timed and then, using the timing belt, the flywheel is rotated clockwise until 70°bTDC, whereby the belt is removed in order to correctly align the intake camshaft. At this timing location, both camshafts are in the reset position.

3.4 Instrumentation

The test facility is fitted with various fixed instrumentation in order to provide the data to interpret the combustion performance of the engine. This largely includes speed, pressure, temperature and flow rate measurements. Each is briefly discussed.

3.4.1 Engine Torque and Speed

The engine was coupled to a DC dynamometer to maintain a constant speed of 1500rpm (±1rpm) regardless of the engine torque output. This represents a frequent mode in an emissions test duty cycle and is commonly used by engine researchers.

In addition to the speed, the instantaneous (at any CAD, θ) indicated torque (T_i) can be calculated using Equation 3.2:

$$T_i = p_g(\theta) A_p \frac{ds}{d\theta}$$

Equation 3.2 Instantaneous Indicated Torque (Kiencke, 2000)

Here, p_g is the in-cylinder gas pressure, A_p is the piston area and $ds/d\theta$ is the rate of change of piston displacement with CAD.

3.4.2 Pressure and Temperature Measurements

The in-cylinder pressure is measured with a Kistler 6041A water-cooled piezoelectric pressure transducer fitted flush to the cylinder head. The signal is then passed to a Kistler 5011B charge amplifier and finally to the data acquisition system.

The temperatures in the engine test facility were all measured using K-type thermocouples.

3.4.2.1 Air Flow Meter

The positive displacement rotary flow meter or 'roots blower', as supplied by Romet, is designed to admit a fixed volume with each rotation. However, in this study the volumetric air flow (VAF) rate was not measured in this way. The flow meter was instead calibrated using the period for 30 revolutions (calculated by LabVIEW) at various throttle angles correlating to the VAF rate. The results of the calibration are shown in Figure 3.5.

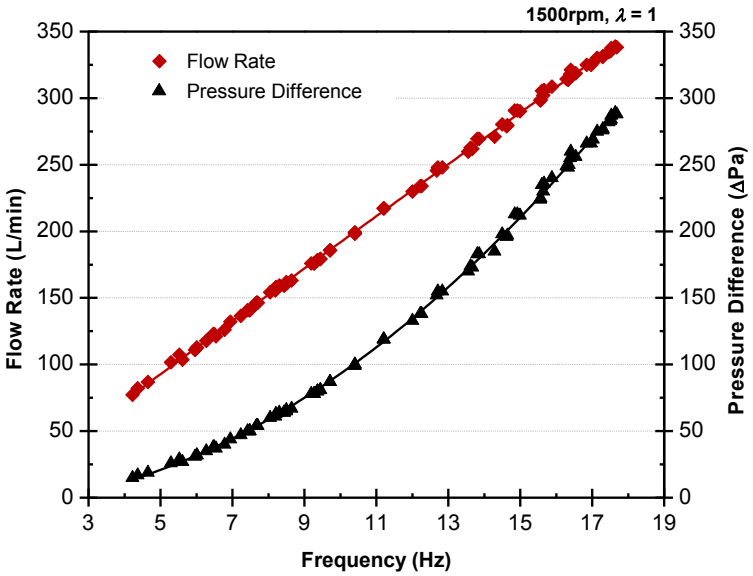

Figure 3.5 Calibration Results of the VAF Meter

The engine was motored and fired at several throttle positions in order to produce different VAF rates. An inclined manometer was used to detect the upstream and downstream air pressures (P_1 and P_2, respectively) across an orifice plate which was placed downstream of the VAF meter but upstream of the throttle. Due to the unsteady flow through the orifice plate an average of the recorded pressure drops were calculated as are shown in Figure 3.5 and were then used in Equation 3.3 to find the average VAF rate.

$$Q = C_d A_2 \sqrt{\frac{1}{1-\beta^4}} \sqrt{\frac{2(P_1 - P_2)}{\rho}}$$

Equation 3.3 Volumetric Flow Rate through an Orifice (Eastop, 1993)

Here, β and C_d are dimensionless numbers representing the ratio of the orifice plate diameters (d_2/d_1) and coefficient of discharge due to the orifice restriction, respectively.

The minimum and maximum VAF rates measured during this study were 120 and 325L/min, respectively, which is within the calibration range shown in Figure 3.5.

3.4.2.2 Lambda Meter

Wherever possible, the actual lambda value was measured using an ETAS LA4 lambda meter and a Bosch heated LSU wideband oxygen sensor. The LA4 lambda meter uses fuel-specific curves to interpret the actual AFR using the oxygen content in the exhaust. Before each test, the user inputs the fuel's hydrogen-to-carbon (H/C) and oxygen-to-carbon (O/C) ratios, as well as the stoichiometric AFR (AFR_{stoich}), so that the fuel composition can be used to characterize the fuel curves. Lambda is then manually controlled in an open loop; the engine operator adjusts the throttle or injection pulse width as required.

3.5 Emissions Measurement

In this study both the currently legislated and unlegislated European and US emissions are analysed and are referred to as the regulated and unregulated emissions, respectively. The regulated emissions include the HC, CO, NO_x and PM emissions. The devices used to measure these emissions in this work are described in the following sub-sections.

3.5.1 Gaseous Emissions

The emissions are sampled downstream of the exhaust plenum, 0.3m from the exhaust valve. The sample is then pumped through a pre-filter and along a heated line, both maintained to 191°C. This is finally analysed by a Horiba MEXA-7100DEGER, as detailed in Table 3.3.

Before each test schedule, the Horiba analyser was purged and calibrated using suitable span and zero calibration gases. Also, when not measuring, the analyser was purged with nitrogen to avoid contamination build-up from a stagnant sampling zone.

Table 3.3 Exhaust Emissions Measurement with Horiba MEXA-7100DEGR

Emissions Methods	
Total Hydrocarbon, *HC*	FID (hot-wet)
Carbon Monoxide, *CO*	NDIR (dry)
Carbon Dioxide, CO_2	NDIR (dry)
Nitrogen Oxides, NO_x	CLD (dry)

3.5.2 Particulate Matter Emissions

The PM emissions are measured using a Scanning Mobility Particle Sizer, or SMPS (Model: 3936) as manufactured by TSI. This measures the size and number distribution of the particles in the exhaust stream. The SMPS comprises three units: a particle classifier (Model: 3080), a Differential Mobility Analyser, or DMA (model 3081) and a Condensing Particle Counter, or CPC (Model: 3775). The settings used in this study are shown in Table 3.4.

Table 3.4 SMPS Measurement Settings

SMPS Settings	
Sample Flow Rate (L/min)	1
Sheath Flow Rate (L/min)	10
Scan Time (s)	120
Minimum Particle Diameter (nm)	7.23
Maximum Particle Diameter (nm)	294.3

Exhaust samples were taken from the same position as the Horiba analyser but measured asynchronously. The sample was pumped into a heated (150°C) rotating disc diluter (Model:

379020A, also supplied by TSI) before being sent to the SMPS for PM sizing. A thermo-denuder was not used. The dilution ratios used in this study are 30:1 and 67:1 (each instance is specified in the results). The high dilution ratio was chosen specifically for DI combustion. However, for PFI, the separation between modes was better defined with a low dilution ratio.

3.5.3 Unregulated Emissions Measurement

The methods used to perform the qualitative and quantitative investigations of the unburned HCs are given in this section.

Firstly, a qualitative analysis is performed using GC/FID and GC/MS to detect the light and mid-range HCs. This is followed by a quantitative analysis of the carbonyls using CARB Method 1006 through HPLC analysis. The chromatographic methods are summarised in Table 3.5 and in the proceeding sections.

Table 3.5 Chromatography Equipment Setup and Procedure

	GC/FID	GC/MS	HPLC
Separation	Shimadzu GC-2010	Perkin-Elmer Clarus600	Shimadzu LC20
Detection	FID	Perkin-Elmer Clarus600T	Shimadzu SPD-M20A
Column	PlotQ: 30m x 0.32mm x 10µm	Elite-1: 30m x 0.32mm x 3µm	Luna: 250 x 4.6mm x 5µm
Sample	Tedlar Bag (10-15:1)	Tedlar Bag (10-15:1)	DNPH (20ml)
Injection Size	5ml	1ml	25µl
Split Ratio	Splitless	20:1	-
Flow Rate	1mL/min	2mL/min	1mL/min
Test Conditions	60°C, 5mins; 10°C/min; 110°C, 6mins; 10°C/min; 200°C, 10mins; 10°C/min; 250°C, 10mins	50°C, 1min; 12°C/min; 200°C, 1min	10:90 to 70:30 v/v MeCN/water, 120mins; UV λ = 360nm
Test Duration	50mins	14.5mins	130mins

The unregulated emissions setup is shown in Figure 3.6. The engine-out exhaust emissions are either directed towards the diluter to be analysed by GC/FID or GC/MS, or towards the ice bath bubbler for HPLC analysis. The path direction is determined by a three-way valve.

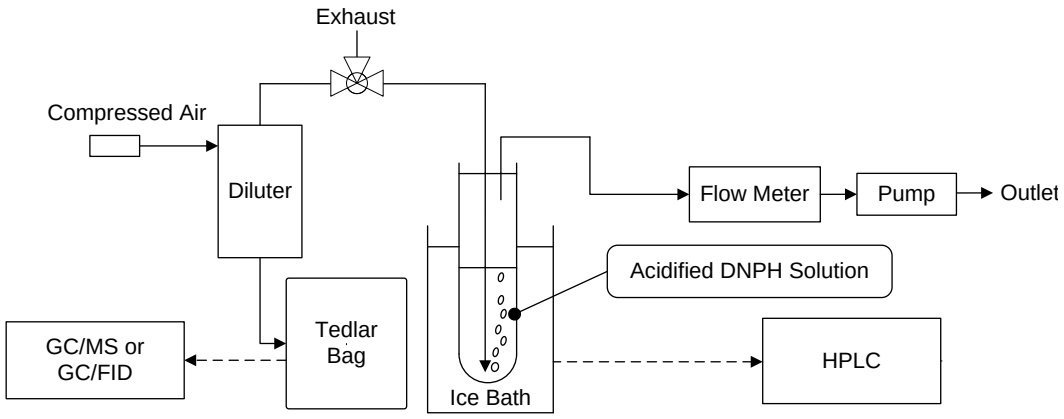

Figure 3.6 Schematic Setup of Emissions Sampling for GC/FID, GC/MS and HPLC

3.5.3.1 Light-Range Hydrocarbons (GC/FID)

The identification of light-range HCs (C_1-C_7) in the emissions of DMF was performed using GC/FID. Principally, the GC/FID consumes the eluted gases in a small oxy-hydrogen flame. The ions produced during this process generate a small current, the signal strength of which is approximated by the carbon content (McNair, 1997). However, the signal strength, or response factor decreases in the presence of oxygen. Therefore, response factors are required from each instrument and test procedure for accurate quantitative analysis.

Ideally, a direct connection from the exhaust pipe to the GC/FID or GC/MS should be made. This reduces any post combustion reactions and avoids possible contamination. However, both analytical devices were off-line and so a transportation solution was required. This was overcome using an impermeable container such as a Tedlar bag. Although other containers exist (e.g., evacuated flasks and gas syringes), Tedlar bags provide the most cost-effective

transportation means. The 2mL thick polyvinyl fluoride (PVF) Tedlar film is considered chemically inert to a wide-range of compounds. Despite this, some species, such as 1,3-butadiene have shown instability in Tedlar bags during long-term storage (Jemma, 1995, Kaiser, 1992, Kaiser, 1994). Therefore, exhaust samples were analysed immediately and transferred in an opaque container to prevent photochemical reactions (McCarrick, 2000).

Nevertheless, the prevention of HC condensation becomes a critical factor when collecting and transporting samples. To overcome this, all samples were diluted with compressed (and filtered) workshop air using a venturi dilution tunnel by drawing the sample though a heated sample line from the engine exhaust. Although the dilution ratio varies between 10 to 15:1, depending on the exhaust temperature, a qualitative analysis was only required and so is insignificant. This method has been used successfully by previous researchers (Elghawi, 2009, Rounce, 2011). After each test, the bags were purged 5 times with nitrogen (oxygen free) in order to eliminate any trapped residual gas from previous tests. Samples were then extracted through the septum in the polypropylene valve fitting using a 10ml gas syringe with needle (supplied by PerkinElmer); 5ml of gas was subsequently injected in the GC/FID. For all the tests, the Shimadzu GC-2010 GC/FID was used along with a PlotQ column (30m length, 0.32mm internal diameter) supplied by Restek (Rt-QPLOT). A splitless injection and a flow rate of 1mL/min (helium carrier gas) supplied the sample to the FID , whilst operating with the temperature profile shown in Table 3.5.

In order to identify the light-HCs, a 10L calibration cylinder, as supplied by Air Liquide was used. This contained 15 gases at concentrations of 50ppm (±2%) and at 180bar. The GC/FID output of these species is shown in Figure 3.7 and the order of elution, or retention time (t_R)

is shown in Table 3.6. The t_R is directly related to the boiling point or vapour pressure of each HC (McNair, 1997) and matches the calibration compounds to the exhaust samples.

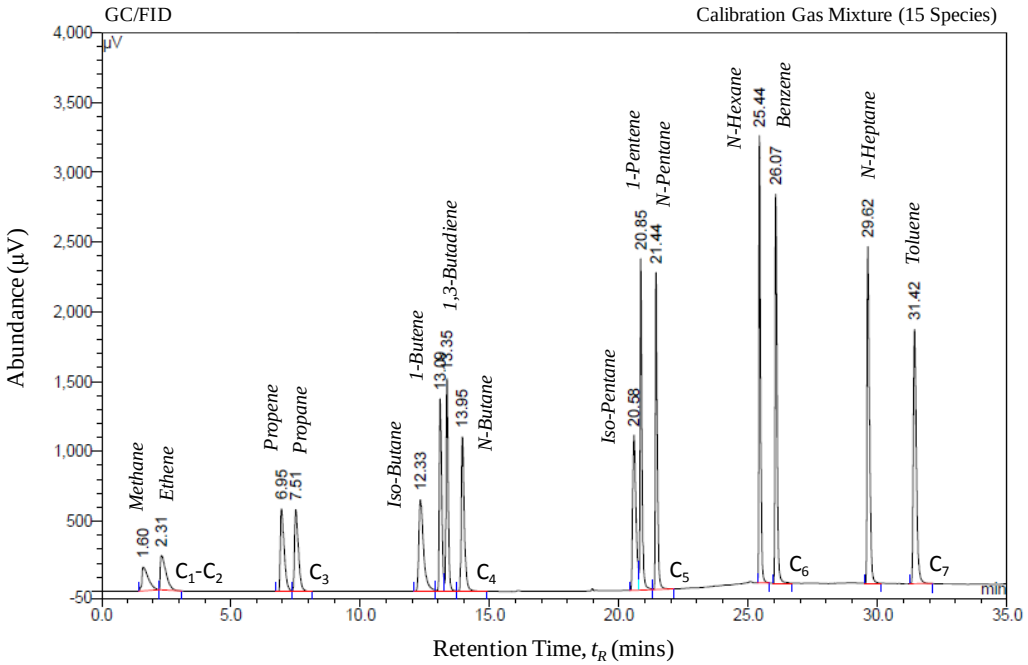

Figure 3.7 GC/FID Output using Calibration Gas Mixture

Table 3.6 Calibration Gases as supplied by Air Liquide

Alkanes		**Boiling Pt. (°C)**	**Retention Time, t_R (mins)**
Methane	CH_4	-162	1.6
Propane	C_3H_8	-42	7.51
iso-Butane	C_4H_{10}	-12	12.33
n-Butane	C_4H_{10}	-0.5	13.95
iso-Pentane	C_5H_{12}	28	20.58
n-Pentane	C_5H_{12}	36	21.44
n-Hexane	C_6H_{14}	69	25.44
n-Heptane	C_7H_{16}	98	29.62
Alkenes			
Ethene/Ethylene	C_2H_4	-104	2.31
Propene/Propylene	C_3H_6	-48	6.95
1-Butene	C_4H_8	-6	13.09
1-Pentene	C_5H_{10}	30	20.85
Allenes			
1,3-Butadiene	C_4H_6	-4	13.35
Aromatics			
Benzene	C_6H_6	80	26.07
Toluene	C_7H_8	111	31.42

Due to the low repeatability of gas syringe injection and the uncertainty of the Tedlar bag samples, the HC species have only been identified in this study.

3.5.3.2 Medium-Range Hydrocarbons (GC/MS)

In addition to the identification of light-range HCs, the use of MS enabled the identification of the heavier or medium-range HCs (C_6-C_{12}). The mass spectrum was identified for each peak at the mass-to-charge (m/z) ratio using a NIST (National Institute of Standards and Technology) library. The percentage match is discussed in Section 8.2.2.

The GC/MS used in this work is the Clarus600 (GC) and Clarus600T (MS) as supplied by Perkin-Elmer. A thick film non-polar phase capillary column was used. This column, which was supplied and recommended by product specialists at PerkinElmer with the following specification: Elite-1 (N931-6025), 30m length x 0.32mm ID x 3.0μm film.

The GC/MS signal was calibrated before each test using heptacosa reference gas as is commonly employed (Grob, 1985). In order to measure a clear signal, the masses above 35g/mol (and below 200g/mol) were only detected. This suppresses the effect of the background gases (helium carrier gas (4g/mol), water (18g/mol), nitrogen (28g/mol) and oxygen (32g/mol)), so that the mass spectra of the DMF exhaust compounds could be clearly identified.

3.5.3.3 Carbonyl Emissions (HPLC)

In this study, the emissions of carbonyls were investigated through the wet chemistry analysis of 2,4-dinitrophenylhydrazine (DNPH) solution using HPLC. This method is based on the techniques outlined by Lipari and Swarin (Lipari, 1982) and is being used extensively

in the automotive industry (Wagner, 1996, Yacoub, 1999) and partially at this institution (Elghawi, 2009, Rounce, 2011). DNPH cartridges have not been used as they have been shown to be less stable in storage, especially for acrolein (Akiyama, 2005).

The emissions collection method involves the bubbling of exhaust gas (1L/min) into acidified hydrochloric DNPH reagent (20ml). The DNPH is maintained at 0°C using an ice bath for a fixed period (20mins), as shown in Figure 3.6. The interaction of carbonyls in the exhaust gas with the DNPH reagent produces DNPH-carbonyl derivatives, which can be analysed through reverse phase HPLC. Once collected, the samples were stored below 4°C and analysed within 24hrs. The gas bubbler was fitted with a sinter in order to increase the bubble surface area and thus the reaction rate. A long tube and exit trap was also used to help to contain the DNPH reagent during the test.

The DNPH-derivative samples (25μL injection) were then analysed by HPLC (Shimadzu LC20). This was performed by an external laboratory (Chemistry Department, University of Birmingham), specialising in analytical chemistry. A Luna tubular column supplied by Phenomenex (part number: 00G-4252-E0) was used (size 250 x 4.6mm in length and diameter). An ultra-violet (UV) wavelength detector was used at a (λ=360nm) to detect the relative abundance of each compound. The mobile phase solvent included HPLC grade water (deionised) and acetonitrile at a fixed flow rate of 1mL/min. The mixing ratio was then varied linearly from 10:90 to 70:30v/v of acetonitrile to deionised water at 120mins and then held constant until the end of the test run.

The total analysis time was 130mins. After each test, the mixing ratio was then linearly reduced to 10:90v/v of acetonitrile to deionised water for 10mins ready for the next sample.

The peak area of each carbonyl was compared to that of the standard in order to quantify the concentration. This standard contained 13 different carbonyls in acetonitrile (supplied by Sigma Aldrich) and is shown in Figure 3.8.

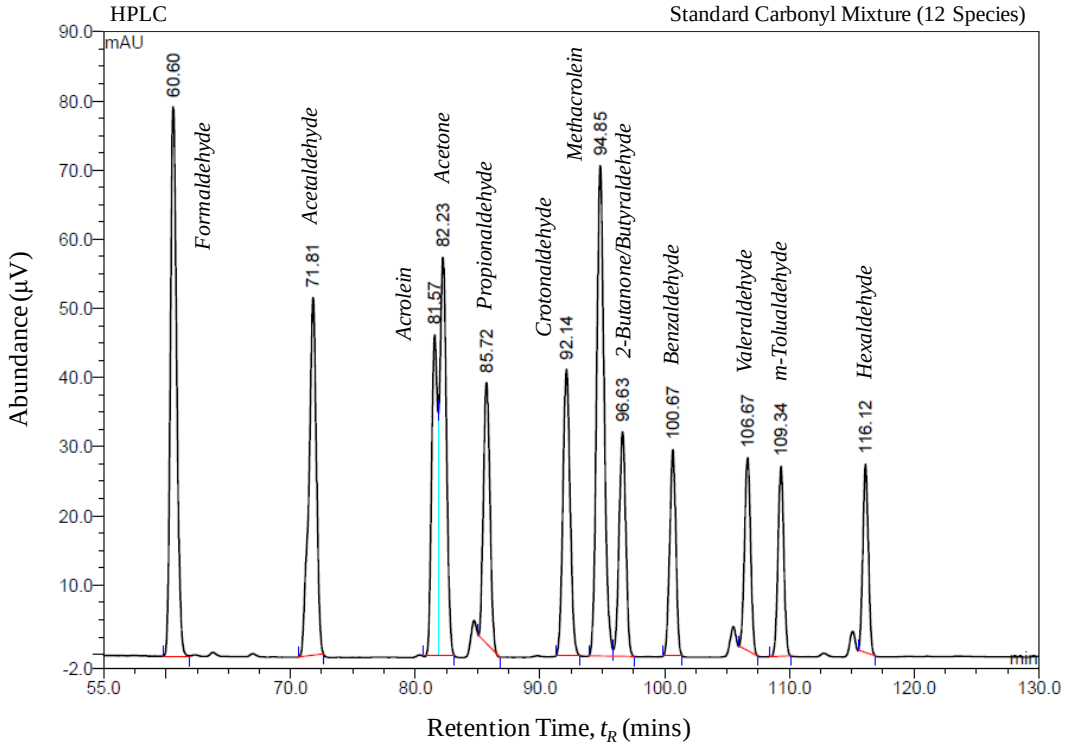

Figure 3.8 Carbonyl Standard using HPLC

In this study, 11 compounds are independently quantified. Although the separation of C_3 carbonyls is known to be very difficult (Coutrim, 1993), an adequate separation is shown in Figure 3.8. However, the separation of 2-butanone and butyraldehyde was inadequate as found by others (Lipari, 1982), so the combined emission is reported. Therefore, instead of independent quantification, the combination of 2-butanone and butyraldehyde is reported.

The t_R of the standard are summarised in Table 3.7.

Table 3.7 Carbonyls Detected (average of 6 runs) using DNPH CARB Method 1004

Saturated Aldehydes		**Retention Time (mins)**
Formaldehyde (CH_2O)	30.03g/mol	60.68
Acetaldehyde (C_2H_4O)	44.05g/mol	71.93
Propionaldehyde (C_3H_6O)	58.08g/mol	86.02
Butyraldehyde (C_4H_8O)	72.11g/mol	n/a
Valeraldehyde ($C_5H_{10}O$)	86.13g/mol	106.97
Hexaldehyde ($C_6H_{12}O$)	100.16g/mol	116.38
Unsaturated Aldehydes		
Acrolein (C_3H_4O)	56.06g/mol	81.83
Crotonaldehyde (C_4H_6O)	70.09g/mol	92.48
Methacrolein (C_4H_6O)	70.09g/mol	95.19
Aromatic Aldehydes		
Benzaldehyde (C_7H_6O)	106.12g/mol	101.01
m-Tolualdehyde (C_8H_8O)	120.15g/mol	109.64
Ketones		
Acetone (C_3H_6O)	58.08g/mol	82.50
2-Butanone (C_4H_8O)	72.11g/mol	n/a

3.6 Data Acquisition and Processing

The raw engine data is recorded using two NI cards. The first (model 6251), enables the acquisition of high speed, crank-angle-resolved data and the second (model 6220), enables low speed, time-resolved data acquisition. Both high and low speed systems are recorded using separate LabVIEW scripts.

3.6.1 High Speed Acquisition

The in-cylinder pressure data is recorded at high speed, at a resolution of 0.5CAD for 300 consecutive cycles. This captures the in-cylinder pressure changes in detail during each engine cycle, which completes every 80ms (12.5Hz) when operating at 1500rpm. The intake

pressure is recorded so that the in-cylinder pressure data can be 'pegged' (referenced) at the correct CAD (Section 3.6.4). The data from the intake and exhaust cam position sensors is also acquired in order to analyse the stability of the VCT system.

3.6.2 Low Speed Acquisition

The low speed data acquisition is time-resolved rather than crank-angle-resolved and records the low variation signals under steady-state conditions. This includes engine temperatures (intake, cylinder wall, exhaust, coolant and oil), ambient conditions (pressure, temperature, and relative humidity), VAF rate, throttle position, λ and the emissions measurements from Horiba (CO, HC, NO_x and O_2). The rate of VAF sampling is based on the completion of 30 revolutions and the frequency comparison to the calibration (Figure 3.5). This method was created by the author to capture VAFs at WOT without the use of a pitot tube and liquid manometer system as used previously (Turner, 2010).

However, other low speed measurements are recorded at 1Hz and averaged over 30s.

3.6.3 Data Processing

The data from the high and low speed data acquisition systems is processed using a custom MATLAB script written by the ICE group in Oxford and a previous researcher (Turner, 2010). This was further developed by the author in order to process dual-injection data and output the results in MS Excel. The net IMEP is calculated for each cycle using the method described by Stone (Stone, 1999) and then averaged over 300 consecutive cycles. Other averaged parameters include: the heat release rate, rate of pressure rise (RPR) and P_{max}, for example.

3.6.4 In-Cylinder Pressure Interpretation

The in-cylinder pressure measurements are made using a piezoelectric transducer (Section 3.4.2). Although piezoelectric transducers are susceptible to drift and are unsuitable for steady-state measurements, they are effective under transient in-cylinder conditions (Plint, 1999). Therefore, the absolute in-cylinder pressure signal needs to be 'pegged' to the intake manifold pressure at the same CAD. The commonly used position is BDC_{intake} because the in-cylinder and intake pressures are equal. This position has been used in this work to help overcome the effects of drift.

3.6.4.1 Heat Release Analysis

The in-cylinder pressure can be used to analyse the first law combustion behaviour. This is accomplished through the manipulation of the heat release rate in order to calculate the mass fraction burned (MFB). In this study, the net heat release rate ($dQ/d\theta$) is calculated using the method described in popular engine fundamental textbooks (Ferguson, 2001, Stone, 1999).

$$\frac{dQ}{d\theta} = \frac{\gamma}{\gamma - 1} P \frac{dV}{d\theta} + \frac{1}{\gamma - 1} V \frac{dP}{d\theta} + \frac{dQ_w}{d\theta}$$

Equation 3.4 Net Heat Release Rate

The heat capacity ratio (γ) is the ratio of specific heats (c_p/c_v) and is approximated depending on the respective parts of the engine cycle.

The MFB is the normalised integral of the heat release rate, as shown in Equation 3.5.

$$MFB = \frac{\int_{\theta_s}^{\theta_i} \frac{dQ}{d\theta} d\theta}{\int_{\theta_s}^{\theta_e} \frac{dQ}{d\theta} d\theta}$$

Equation 3.5 Mass Fraction Burned

The MFB profile is then used to interpret key aspects of combustion: combustion initiation duration, or CID, 50% MFB location, or CA50 and combustion duration, or $CAD_{10\text{-}90}$, as shown in Figure 3.9. In this study, the CID is defined as the CAD from ignition to 5% MFB.

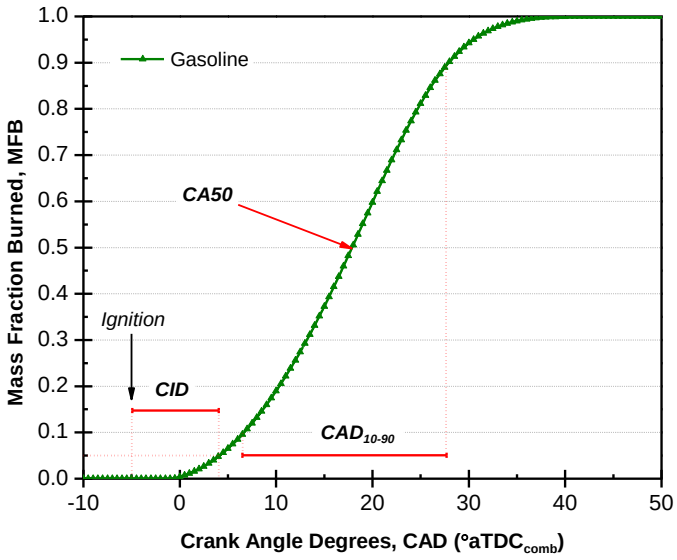

Figure 3.9 Typical MFB Profile Showing Key Parameters

3.6.5 Fuel Consumption

When operating with a known fuel (or blend), in either PFI or DI, the fuel consumption rate was calculated using the VAF rate and lambda value. However, when using dual-injection, the fuel consumption calculation is more involved.

3.6.5.1 Injector Calibration Curves

In order to assist the dual-injection fuel consumption calculations, the DI injector calibration curves were measured for all the fuels used in this study (at 150bar). The mass of 1000 injections was measured using a laboratory balance (±0.1g). The average gravimetric and inferred volumetric injection rates for ethanol, DMF and gasoline are shown in Figure 3.10.

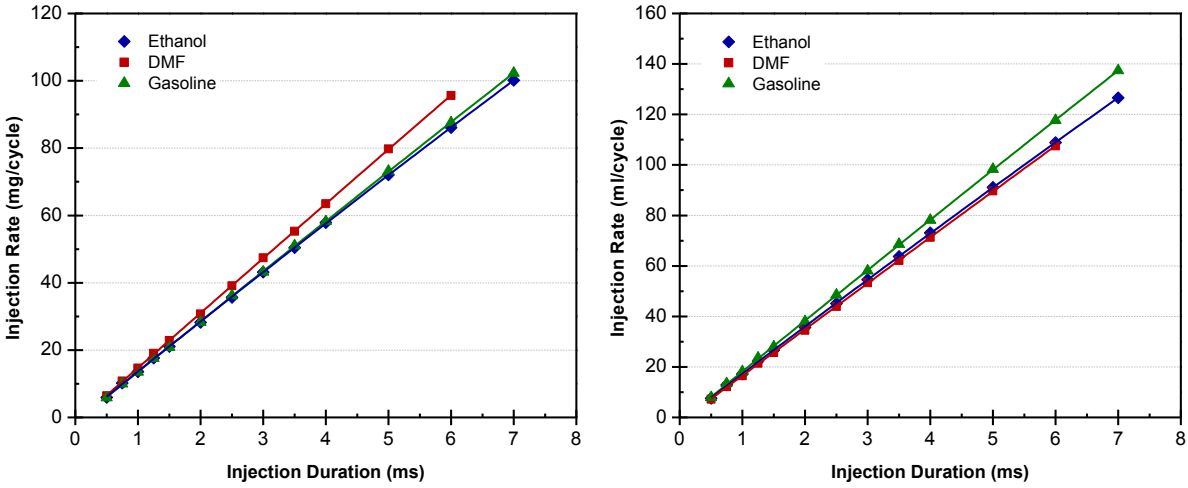

Figure 3.10 Gravimetric (a) and Volumetric (b) Calibration of SGDI Injector

The higher density of DMF results in a higher injection mass (Figure 3.10a). However, the inferred volume for ethanol and DMF are lower than for gasoline (Figure 3.10b). The minimum DI injection duration in this study was 4.1ms (methanol at WOT) and so the calibration range is sufficient.

Although some researchers have found the linearity to decay at injection durations below 0.4ms (Gandhi, 2009), Figure 3.11 shows linearity to 0.5ms, with some variation at 0.3ms. However, the marginal non-linearity for gasoline and methanol at 0.3ms is at the limit of the injector. In this work, very few points required injection durations below 0.5ms (only for low load dual-injection). Ethanol and DMF are not affected by this non-linearity behaviour.

However, to minimise the non-linearity and improve the accuracy, the author has used a line of best fit through all of the data points for each fuel.

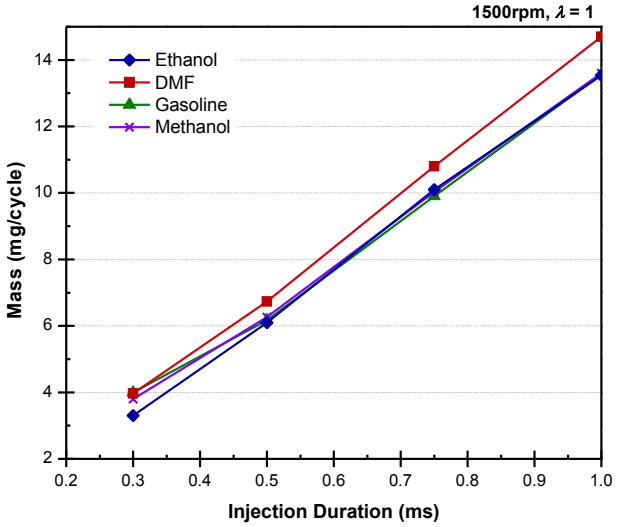

Figure 3.11 DI Injector Low Flow Rates using Gasoline, Ethanol and Methanol

3.6.5.2 Dual-Injection

In dual-injection, the exact in-cylinder blend ratio of the two fuels from PFI and DI varies as required and the overall composition is therefore unknown. To control lambda the authors have used the cross-over theory of the O_2 and CO emissions concentrations, instead of the lambda meter and oxygen sensor combination. This cross-over theory is the match of O_2 and CO emissions concentrations close to stoichiometry, as described in engine textbooks (Stone, 1999, Heywood, 1988). When the mixture is lean, excess air oxidizes the CO. Conversely, as the mixture becomes rich in fuel, the O_2 content decreases and the CO production increases inversely. The cross-over of the O_2 and CO emissions concentrations are easily obtained with an AFR sweep around λ=1. However, there is no published work that confirms this phenomenon using oxygenated fuels like ethanol or DMF in pure form or blends with gasoline. Therefore AFR sweeps (constant throttle) were performed at an arbitrary medium

load (6.5bar IMEP, at λ =1) using four fuels (gasoline, DMF, ethanol and toluene) and two blends (D50 and E50). Each sweep verifies the cross-over theory, as shown in Figure 3.12.

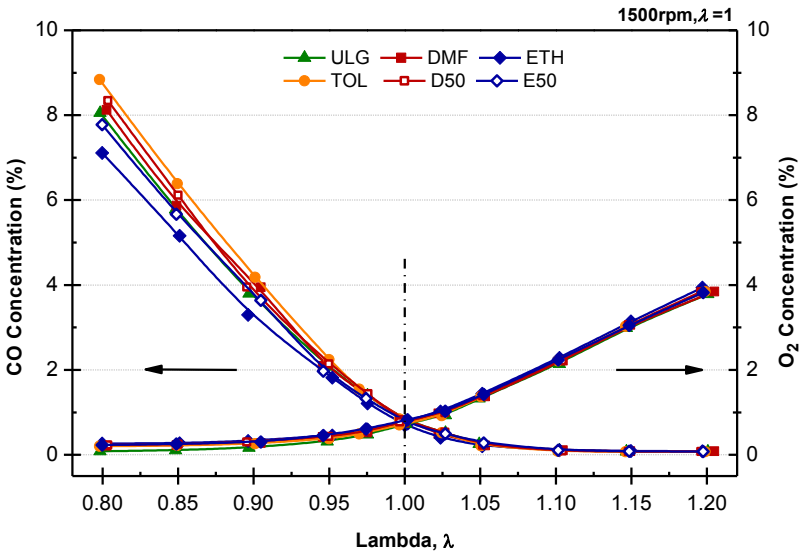

Figure 3.12 Oxygen and CO Concentrations with varying Lambda at 6.5bar IMEP

This verification was then checked at various loads. The engine was again run at the O_2 and CO cross-over and the corresponding lambda values were measured (Figure 3.13).

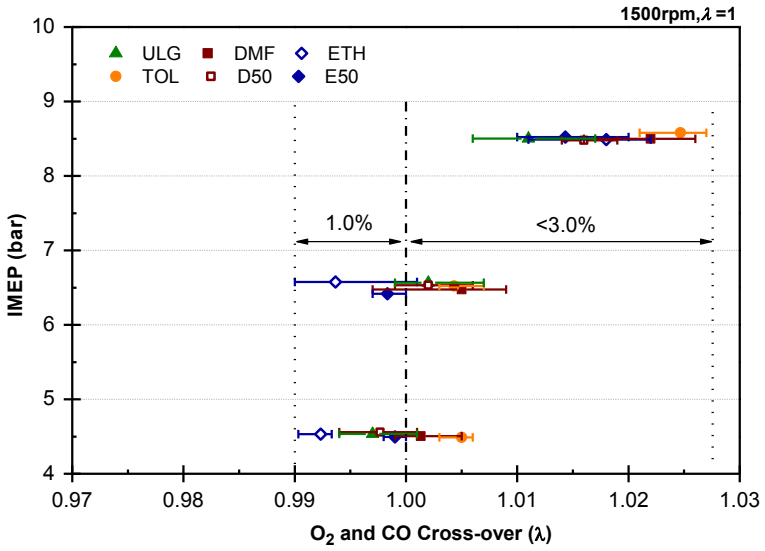

Figure 3.13 Oxygen and CO Cross-over Excess Air Ratio with varying Load

For the six fuels, the deviation from stoichiometry is less than 1% at 4.5bar and 6.5bar IMEP and less than 3% at 8.5bar IMEP. This is within experimental uncertainty (95% confidence level) and proves the cross-over theory can be used to accurately control stoichiometry during the in-cylinder mixing of different fuels.

The dual-injection blend ratios can be inferred and controlled during the test or calculated afterwards. This is achieved using a MATLAB script written by the author. In order to calculate the blend ratio, the fuel flow rates for the PFI and DI injections are needed, which requires two assumptions. Firstly, the blending AFR_{stoich} and LHV were assumed linear. Secondly, the DI injector calibration mass flow rates were assumed using an offset. In an experimental situation, the local temperatures and pressures affect the fuel spray distribution and differ from the calibration. Therefore an offset is required to the 100% DI case in order to accurately estimate the flow, as explained in Figure 3.14. For instance, when comparing the actual DI flow rate of ethanol during combustion to the calibration, an offset exists. If this offset is applied to the lower flow rates, then the DI flow rate can be accurately assumed.

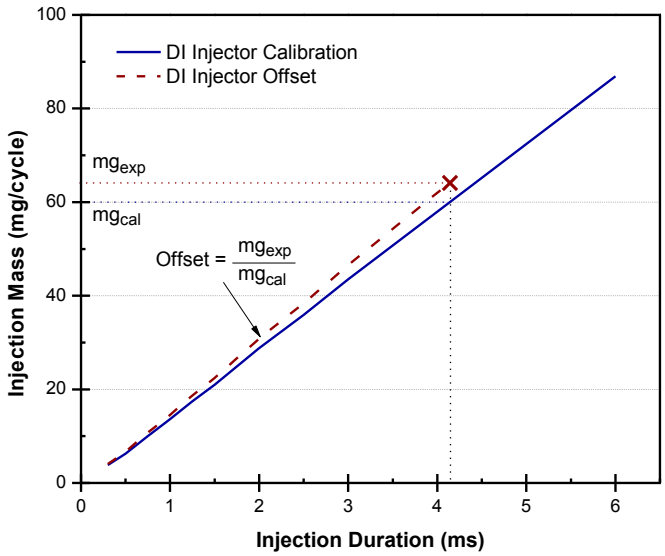

Figure 3.14 SGDI Injector Calibration Curve Offset

Using the estimated DI flow rate, along with the VAF rate and λ, the gasoline fuel mass in PFI can be inferred using the relative AFR:

$$\lambda = \frac{AFR_{actual}}{AFR_{stoichiometric}}$$

Equation 3.6 Lambda calculation

For a given gasoline-oxygenated fuel blend in DI, this equation becomes:

$$\frac{\left(\frac{m_a}{m_{f,DI} + m_{f,PFI}}\right)}{\left[\left(\frac{m_{f,DI}}{m_{f,DI} + m_{f,PFI}}\right) AFR_{s,DI} + \left(\frac{m_{f,PFI}}{m_{f,DI} + m_{f,PFI}}\right) AFR_{s,PFI}\right]}$$

$$\therefore \ \lambda = \frac{m_a}{(m_{f,DI}) AFR_{s,DI} + (m_{f,PFI}) AFR_{s,PFI}}$$

Equation 3.7 Substiution of PFI and DI components into lambda calculation

In Equation 3.7, m_a and m_f denote the mass of air and fuel (in PFI and DI), respectively. Equation 3.7 can then be simplified and re-arranged to make the mass of gasoline in PFI ($m_{f,PFI}$) the subject, as shown in Equation 3.8:

$$m_{f,PFI} = \frac{m_a - (m_{f,DI}) AFR_{s,DI}}{AFR_{s,PFI}}$$

Equation 3.8 Gasoline fuel mass calculation in PFI

It is now possible to calculate the fuel blend, as both PFI and DI components are known.

3.6.6 In-Cylinder Gas Temperature Calculation

The combustion temperature is affected by the rate of chemical reaction and influences the emissions production, especially NO_x (Stone, 1999). Also, when developing new fuels, it is important to study the heat loss and temperature behaviour because this is related to the onset of knock. Therefore, the in-cylinder gas temperature was simulated for parts of this work. An engine model was created using Ricardo WAVE and is described in the next section.

3.6.6.1 Ricardo WAVE Combustion Model

Ricardo WAVE is a one-dimensional (1D) engine and gas dynamics simulation tool supplied by Ricardo Consulting Engineers PLC, and is used globally by the automotive industry.

1D simulation codes like WAVE do not use detailed chemical kinetics because the reaction mechanisms are very complex. Instead, WAVE uses the ideal gas law combined with the prediction of trapped residuals and fuel vaporisation behaviour to estimate the in-cylinder gas temperature. This reduces the calculation time. Therefore, the results presented in this thesis represent an insight into the global averaged gas temperatures. Until the detailed chemical kinetics of the combustion of DMF is better understood, these results help to show the differences to ethanol and gasoline. The model is shown in Figure 3.15.

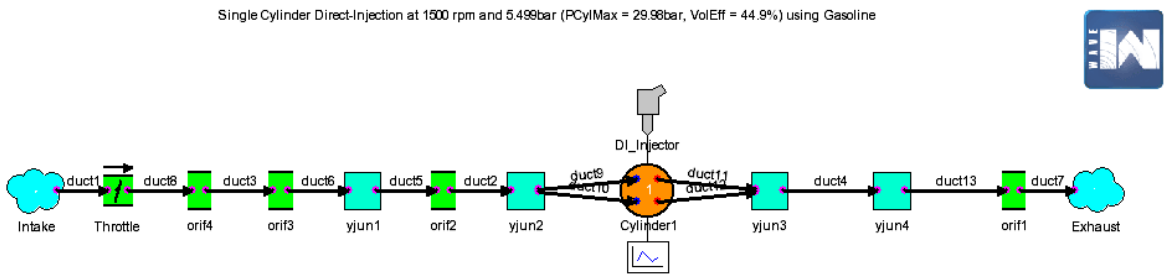

Figure 3.15 Ricardo WAVE Simulation Model for Direct-Injection Mode

When simulating the combustion of gasoline, the fluid properties of indolene were used. However, DMF is not present in the WAVE fuel library, so its fuel properties were inputted. Unknown properties, such as the viscosity-temperature behaviour, were taken from indolene.

The simulation of gasoline in PFI was performed using WAVE to help predict the gas temperatures of dual-injection. In this instance, a PFI injector was positioned between 'orif2' and 'yjun2'. Unfortunately, the use of two fuels simultaneously (mixed in-cylinder) is not possible in WAVE, so the 100% gasoline case was only simulated.

The WAVE models were validated using known combustion performance data to maintain the volumetric efficiencies (VE) to within 5% at all engine loads. The SI Wiebe combustion sub-model was also used. This required the input of CA50 and $CAD_{10\text{-}90}$, in order to match P_{max} and IMEP to within 99.5%.

3.6.7 Gravimetric Emissions Analysis

The indicated specific emissions are defined as the mass flow rate of pollutant for each unit of power output (Heywood, 1988). In this study, the indicated specific emissions are calculated from the gaseous measurements using Horiba, in parts per million (ppm). Firstly, the mass of each emissions component (NO_x, CO, HC and CO_2) is calculated by comparing its mole fraction to the molar mass of the exhaust using the fuel and air consumption rates. Then, the indicated specific emissions are calculated (in terms of g/kWh) by dividing by the mean indicated power (P_i), as shown for unburned HCs in Equation 3.9.

$$isHC = \frac{\dot{m}_{HC}}{P_i}$$

Equation 3.9 Indicated Specific HC Emissions Calculation

3.6.8 Combustion Efficiency

Although the indicated efficiency describes the effectiveness of the fuel energy conversion into indicated work, it does not explain the completeness of combustion. This requires an analysis of the incomplete combustion products (e.g. HCs and CO) and is represented by the combustion inefficiency.

The fraction of chemical energy that is burned, compared to that which is supplied, is expressed by the combustion efficiency (Heywood, 1988). This is shown in Equation 3.10 (Christensen, 2000) where x_i and Q_{LHVi} represent the mass fractions and LHV of HC, CO, NO and hydrogen (H_2), respectively.

$$\eta_c = 1 - \frac{\sum x_i Q_{LHV_i}}{[\dot{m}_{fuel}/(\dot{m}_{air} + \dot{m}_{fuel})]Q_{LHV_{fuel}}}$$

Equation 3.10 Combustion Efficiency

For this work, Q_{LHVHC} has been treated equal to $Q_{LHVfuel}$. In reality, the total HCs contain different species with different Q_{LHV}. However in this work the HC species are not quantified and so the assumption is made to approximate the combustion efficiency.

3.7 Fuel Properties

The properties of the fuels discussed in this thesis are shown in Table 3.8. The commercial gasoline and ethanol was supplied by Shell Global Solutions, UK, whereas the *n*-butanol and methanol was supplied by Fisher Scientific, UK (99.5 and 99% purity respectively). Two Chinese suppliers were used to supply DMF (Shijiazhuang Lida Chemical Co. Ltd. and Beijing LYS Chemicals Co. Ltd), due to its high production cost in Europe.

Table 3.8 Test Fuel Properties

	Gasoline	DMF	MF	*n*-Butanol	Ethanol	Methanol
Chemical Formula	C_2-C_{14}	C_6H_8O	C_5H_6O	$C_4H_{10}O$	C_2H_6O	CH_4O
H/C Ratio	1.795	1.333	1.2	2.5	3	4
O/C Ratio	0	0.167	0.2	0.25	0.5	1
Gravimetric Oxygen Content (%)	0	16.67	19.51	21.6	34.78	50
Density @ 20ºC (kg/m^3)	744.6	889.7*	913.2	811	790.9*	792
Research Octane Number (RON)	96.8	101.3†	102.5†	98	107‡	106‡
Motor Octane Number (MON)	85.7	88.1†	86.1†	84	89‡	92‡
Octane Index, ([RON + MON]/2)	91.25	94.7	94.3	91	98	99
Stoichiometric AFR	14.46	10.72	10.04	11.2	8.95	6.47
LHV_{mass} (MJ/kg)	42.9	32.89*	31.2	32.71*	26.9*	19.83*
LHV_{vol} (MJ/L)	31.9	29.26*	28.5	26.5*	21.3*	15.7*
Carbon Intensity (gCO_2/MJ)	74.4	83.6	86	72.7	71	69.4
Flash Point (ºC)	-40	1	-22	36	13	12
Heat of Vaporization, ΔH_{vap} (kJ/kg)	373	332	358	430	840‡	1103‡
Stoichiometric Heat of Vaporization (kJ/kg_{air})	25.8	31	35.5	38.4	93.9	170.5
Initial Boiling Point (ºC)	32.8	92	63	118	78.4	65
Reid Vapour Pressure (kPa)	70.6	3.45	18.5	0.3	5.83	32

*Measured at the University of Birmingham: ASTM D240

† API Research Project 45 (1956) and Phillips data.

‡ Heywood, J.B., *Internal Combustion Engine Fundamentals*. 1988: McGraw-Hill

Although the DMF is not produced from biomass, it is representative of the bio-derived fuel as the purity is >99%.

The high octane gasoline represents the most competitive option offered by the market and provides the benchmark to the oxygenated fuels. Although gasoline variations were supplied during the testing, the majority of work was completed using that shown in Table 3.8 (GC analysis shown in Table 3.9). During each test, a gasoline benchmark was always recorded so that old data was never required.

Table 3.9 Gasoline GC Analysis

Hydrocarbon Group	% volume
Paraffins	11.6
iso-Paraffins	34.5
Olefins	14.2
Dienes	0.2
Napthenes	4
Aromatics (Benzene)	35 (1.3)
Oxygenates	0
Unknowns	0.5

The calorific values outlined in Table 3.8 were determined using a IKA C200 Calorimeter according to ASTM D240. In brief, this measures the increase in temperature due to the combustion of the sample, which is used to determine the higher heating value (HHV). The LHV was then calculated by subtracting the ΔH_{vap} of the water vapour produced during combustion from the HHV.

3.7.1 Experimental Test Procedures

As noted by a previous user of the test facility (Turner, 2010), there are various levels of inevitable uncertainty within the collection of data. Therefore, wherever possible, error bars have been used to highlight the repeatability of the data collection.

Prior to each test, a gasoline (PFI or DI) baseline was recorded so that erroneous behaviour would be diagnosed early. Detrimental behaviour was then rectified so that the results were accurate. When reliable, the engine tests were repeated twice for each batch in order to minimise any experimental uncertainty. Whenever possible, the tests were performed over 3 consecutive days, in varying order, in order to minimise the effect of ambient conditions and engine drift, as recommended by leading researchers (Beck, 2006).

3.8 Summary

In summary, this chapter highlights the experimental test facility used in this work. All tests were carried out on a 4-stroke single cylinder engine with a compression ratio (11.5:1) and variable valve timing (intake and exhaust) system that is reflective of modern gasoline DISI engines. Different fuel compositions can be used in DI and can be examined separately or with gasoline in PFI as in the dual-injection system.

Although the author was fortunate to benefit from the engine setup by the previous operator (Turner, 2010), the facility benefitted from two engine rebuilds and improvements to the intake air flow measurement system (airbox installation and VAF meter improvement). In addition, the author implemented a dual-injection system which was effectively used to minimise the measurement error. This included the calibration of injectors, validation of the cross-over of the O_2 and CO exhaust concentrations at stoichiometry and the development of a MATLAB script to analyse the blend ratios or predict the current blend ratio in use. Clearly, a fuel flow meter on both PFI and DI injection systems is the most accurate but this was not available during the course of the work.

The unregulated emissions test setup was based on known methods. The analysis was also performed by an external laboratory which involved the setup of the temperature-time profile for the best separation of compounds. The carbonyl emissions analysis using HPLC required the bubbling of exhaust gases in DNPH solution. This did, however, require the bespoke design of a gas bubbler in order to maximise the surface area for exhaust gas absorption.

Finally, the data collection procedure is briefly discussed. The test order was designed to minimise errors encountered through engine drift and fuel contamination during changes.

CHAPTER 4

COMBUSTION BEHAVIOUR AND EMISSIONS OF 2,5-DIMETHYLFURAN

This chapter explores the effect of various engine parameters on the combustion behaviour and emissions of DMF in order to understand its potential as an SI engine biofuel.

4.1 Introduction

This chapter examines the sensitivity of DMF to various engine parameters. Wide parameter windows increase the calibration flexibility. This allows the performance and emissions to be optimised. In particular, the effect of spark timing, engine load, injection timing, relative AFR and valve timing (intake and exhaust) are examined.

The spark timing strongly influences the combustion event. Therefore, the sensitivity of the oxygenated fuels to spark timing is a major focus of this chapter. The term spark retard (SR) has been used and the combustion and emissions behaviour is observed at 10CAD SR, or SR10. The effect of varying engine load is examined at gasoline MBT timing and fuel-specific MBT/KLSA timing. The increase in oxygen content of each fuel is shown to give rise to more favourable performance and emissions. However, the disadvantage is increased fuel consumption. Furthermore, the injection timing, relative AFR and valve timing (intake and exhaust) show varying sensitivities between the fuels. Ethanol is the least sensitive to valve timing in terms of maximum indicated efficiency and reduced emissions.

The sensitivity results are compared primarily to ethanol and gasoline and secondly to *n*-butanol and methanol.

4.2 Effect of Spark Timing

In this work, the MBT timing is defined as the spark timing to produce the maximum IMEP for a fixed throttle position (λ=1). If audible knock occurs, the MBT timing is retarded by 2CAD, an arbitrarily safe margin, as is advised (Heywood, 1988, Stone, 1999). At this point, the spark timing is then referred to as the knock-limited spark advance (KLSA). Retarding the spark timing further for emissions preservation was not used, in order to better isolate its effect and minimise subjectivity.

The spark timing sweep shown in Figure 4.1a at 8.5bar IMEP demonstrates the effect on IMEP using DMF, ethanol and gasoline (the data for methanol and *n*-butanol is omitted to present the methodology). At this load, there is a clear difference between the three fuels. Ethanol combustion, which is uninhibited by knock at this compression ratio, permits a wide spark sweep and allows the IMEP to be analysed either side of the MBT timing (21°bTDC). DMF and gasoline on the other hand, are much more sensitive to spark knock and only retarded timing can be observed.

There appears to be a relationship between the MBT/KLSA location and rate of change of IMEP. It is evident that the more retarded the MBT/KLSA timing, the higher the rate of IMEP decay becomes with spark retard. This rate of decay can be used as an indicator of the fuel's spark timing sensitivity.

When normalizing the IMEP and spark timing data (by their respective MBT/KLSA values) from Figure 4.1a, these sensitivities become clearer. This is shown in Figure 4.1b, using the term spark retard, which represents the number of retarded CAD from MBT/KLSA. As the term suggests, a positive value represents retarded timing from MBT/KLSA, whereas a

negative value is advanced. This term was previously used by Ayala et al. to help develop their combustion retard parameter (Ayala, 2006).

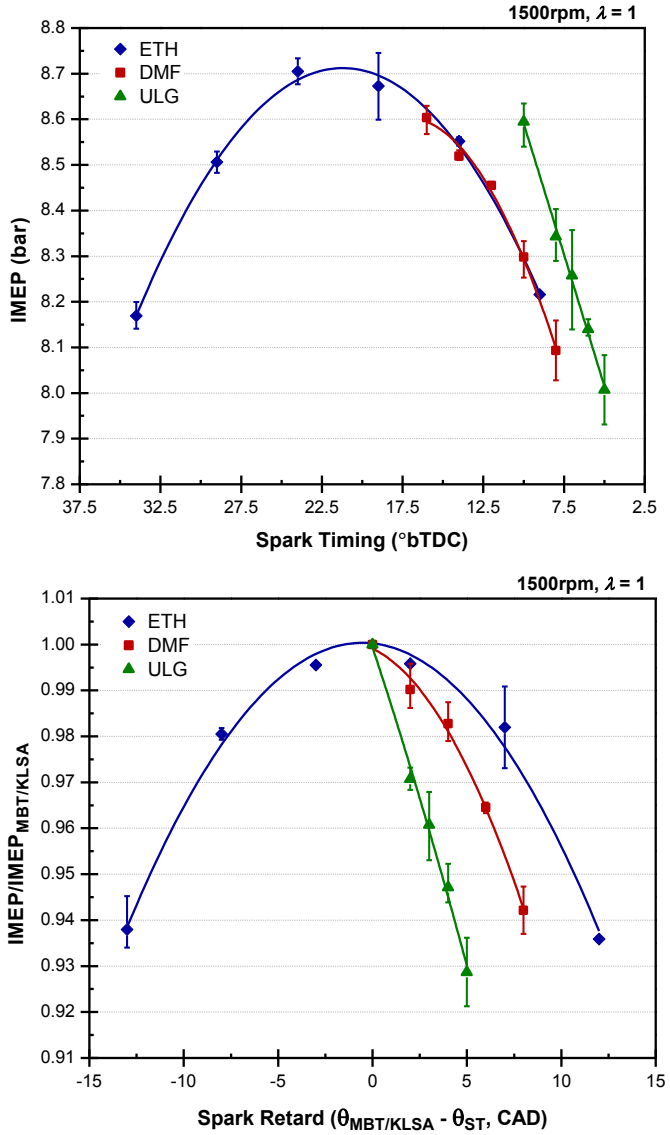

Figure 4.1 Effect of Spark Retard on Absolute (a) and Normalized IMEP (b)

When using ethanol, the rate of decay is symmetrical about MBT and decreases at a lower rate than DMF or gasoline. This is largely explained by the knock suppression superiority of ethanol.

The initial rate of decay also indicates how far the KLSA timing is from MBT. For instance, the initial rate of decay using DMF is less than with gasoline, which suggests the KLSA timing for DMF is much closer to its theoretical MBT timing. Within the range of IMEP decay, ethanol is the least sensitive to spark timing variations. This is clearly shown in Figure 4.1b at the arbitrary 5CAD spark retard location, or SR5 (most retarded point for gasoline). Here, when using ethanol, there is a loss in IMEP of approximately 1% from MBT. However, when using DMF and gasoline this loss is 2.5% and 7% from the KLSA timings, respectively. Evidently, it is gasoline which is the most sensitive to spark timing at this load, which is largely a function of its relatively low OI (Table 3.8).

4.2.1 Optimum Spark Timing

For this work, the MBT/KLSA timings were also determined for loads between 3.5bar and 8.5bar IMEP, in 1bar IMEP intervals (fixed engine speed of 1500rpm). At each load, the spark timing was advanced to find KLSA or until a significant drop in performance or stability was seen (IMEP decrease >5% or COV of IMEP increase >3%). Similarly, the spark timing was retarded until a similar drop in performance was seen. While performing each sweep, the fuel and air flow rates were kept constant for each fuel once the required load and AFR_{stoich} was achieved at the anticipated MBT point (estimated from the previous load). Firstly, the throttle position was fixed and then the fuel injection pulse width was adjusted finely (±1μs) to find stoichiometry.

The MBT/KLSA timings for each fuel are shown in Figure 4.2. Individual data points, observed experimentally are linked using polynomial trend lines to show the relationship with increasing load.

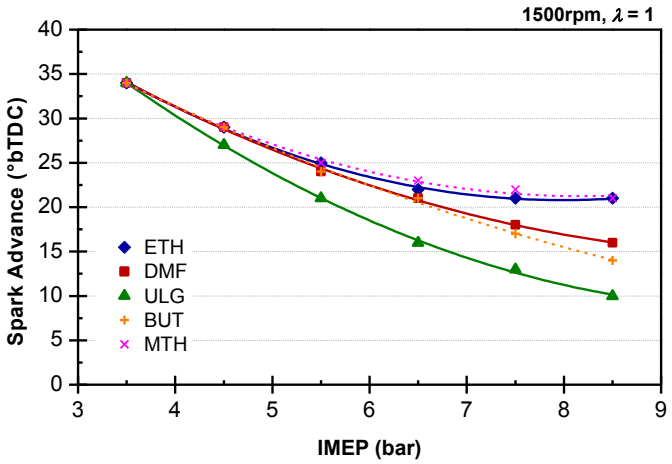

Figure 4.2 MBT/KLSA Timings at Various Loads

At 3.5bar IMEP, the MBT timings are equal for all fuels: the spark sweeps were relatively flat IMEP around MBT (34°bTDC). However, as the load increases the most advanced spark timings are obtained with methanol and ethanol due to their high OI and burning velocities. These lower alcohols also generate greater charge-cooling due to higher ΔH_{vap} (Table 3.8), which lowers the ignition temperature and discourages pre-ignition. At 8.5bar IMEP, both lower alcohols are 11CAD more advanced than gasoline and 5CAD more than DMF. Until 6.5bar IMEP, the oxygenated fuels are separated by less than 1CAD. Despite this, the maximum IMEP when using DMF and *n*-butanol are limited by audible knock and MBT is not achieved. However, the KLSA timings for DMF are within 5CAD of ethanol MBT. When using gasoline and *n*-butanol, a knock margin was enforced as early as 4.5bar IMEP due to their low OI and ΔH_{vap}, especially when compared to the lower alcohols (Table 3.8). The similarity of gasoline and *n*-butanol suggests that the higher ΔH_{vap} and thus cooling effect of *n*-butanol offsets its lower OI to have comparable knock suppression. The OI, as defined in the Co-operative Fuel Research engine (CFR) tests, is not the only knock mitigation factor.

For gasoline, the OI is largely governed by the aromatic content (fractions of benzene, toluene, etc). However, for pure, oxygenated fuels the knock suppression capability is related to the oxygen content (Gautam, 2000). For DMF, a non-benzene ring aromatic, the oxygen content is lower than the other oxygenated compounds (Table 3.8). This could explain why the knocking tendency of DMF occurs at low loads. For ethanol and methanol, fuels with relatively high oxygen content, no knock margin was required at any load. In addition, these fuels burn with high velocity and produce a greater charge-cooling effect (Table 3.8). This helps to lower the combustion temperature and discourage end-gas pre-ignition.

4.2.2 Spark Timing Sensitivity

Although the RON provides an insight into the sensitivity to spark timing, it does not include the effect of charge-cooling with modern DI. Furthermore, the RON values for fuels which outperform iso-octane (100RON) are extrapolated. As such, the CFR tests, developed in the 1930s, have received criticism for their relevance to modern engines (Kalghatgi, 2001b, Kalghatgi, 2001a, Mittal, 2009, Mittal, 2008).

In an effort to examine the antiknock performance of DMF, the authors have proposed a modern alternative. By analysing the spark timing sweeps at various loads (at 1500rpm), it is possible to determine the spark sensitivity of each fuel.

This method is applied to ethanol, DMF and gasoline in Figure 4.3. Low spark sensitivity gives a wide spark window and provides a greater opportunity to reduce emissions.

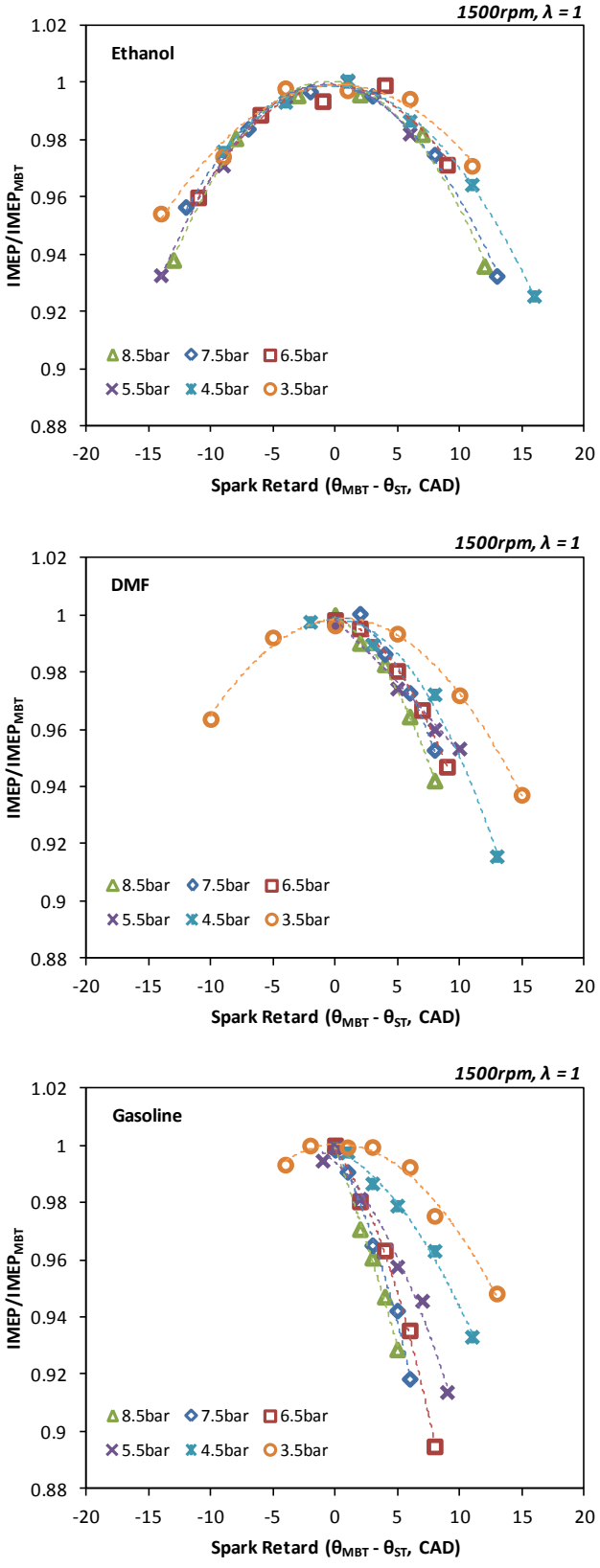

Figure 4.3 Effect of SR on IMEP for (a) Ethanol, (b) DMF and (c) Gasoline

There are clear spark sensitivities with load, which is best shown with gasoline (Figure 4.3c). As the load increases, the rate of decay of IMEP from the maximum (or spark sensitivity) increases. At 3.5bar IMEP, the decay at SR5 is <1%. However, with each 1bar increment in load, the decay in performance rapidly increases to a maximum of 7.2% at 8.5bar IMEP. This increased sensitivity with respect to load is also evident for DMF and ethanol but in an increasingly subtle manner.

The spark sensitivity of ethanol is also symmetric either side of MBT due to the benefit of a higher OI and ΔH_{vap} (Table 3.8). It appears that the spark timing sensitivity for DMF is closer to ethanol than gasoline because the spread between the loads is lower. However, this is subjective and requires quantification.

Typically, once the MBT timing is found, engineers employ a SR for emissions preservation. This is commonly the spark retard that produces an IMEP of 2% less than that from MBT and is shown by the dashed lines in Figure 4.4 (Heywood, 1988).

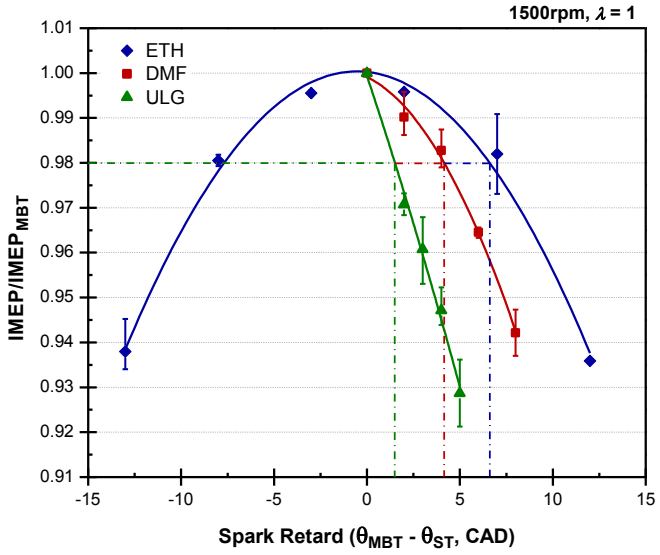

Figure 4.4 SR at 2% IMEP Decay when using Ethanol, DMF and Gasoline

This highlights the window of acceptable SR between the three fuels and helps to quantify the sensitivity. The near equal separation between the three fuels mirrors the relationship with OI shown in Table 3.8.

The relationship between OI and SR is clear when examining all loads by interpolating the spark sweeps. Figure 4.5a presents the permissible SR for a 2% drop in IMEP from MBT (3.5-8.5bar IMEP) for gasoline, ethanol and DMF. Here, greater SR gives a wider spark window (greater opportunity for emissions optimisation). For all fuels, the spark window is the widest at the lowest load and generally decreases with load. The low spark sensitivity of ethanol is consistent with load and generates a gap to gasoline of ≈5CAD when ≥5.5bar IMEP. DMF resides between gasoline and ethanol.

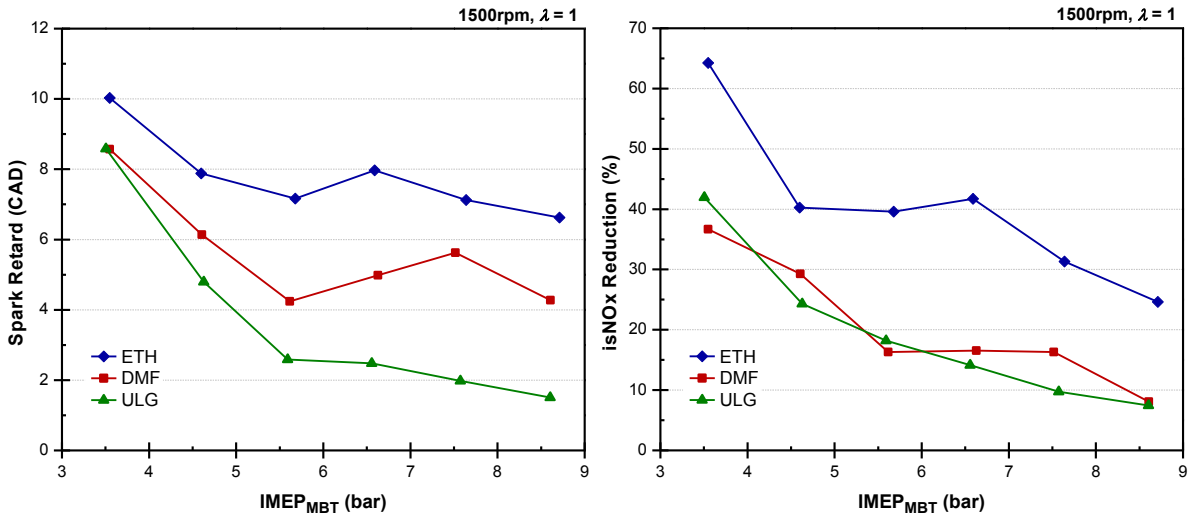

Figure 4.5 SR (a) and isNO$_x$ Reduction (b) at 2% IMEP Decay at all Engine Loads

An example of the benefits of widened spark timing windows is shown in Figure 4.5b. Here, the effect of SR on indicated specific NO$_x$ (isNO$_x$) emissions is shown for all loads. It is clear that the isNO$_x$ reduction is more effective with ethanol than with gasoline and DMF. At 3.5bar IMEP, this reduction with ethanol is up to 64% and steadily decreases with load to

25% at 8.5bar IMEP. With DMF, the isNO_x reduction is consistently similar to gasoline despite the greater spark timing window. From 3.5bar to 8.5bar IMEP, the isNO_x reduction with DMF reduces from 37% to 8%. In later work, DMF will be shown to produce higher isNO_x emissions than ethanol and gasoline, possibly due to higher combustion temperatures (Daniel, 2011), which might explain the lower decrease in isNO_x emissions despite higher SR.

Another method to quantify the spark sensitivity is to examine the change in performance and emissions at an arbitrary location. In this instance, the SR10 location has been chosen because it best emphasizes the trend at the lower loads (difficult with SR5).

4.2.3 Combustion Performance and Emissions at SR10

In this section the spark sensitivity between the fuels is examined specifically at SR10. The aim is twofold: (1) to position the knock mitigation ability of DMF with other oxygenated fuels by taking the ΔH_{vap} in account and (2) to study the effect of SR with such fuels on modern engine performance and emissions.

Error bars are shown where applicable for the primary fuels (ethanol, DMF and gasoline) but have been omitted for the secondary fuels (*n*-butanol and methanol) to maintain clarity. Similarly, solid lines are use for the primary fuels, whereas dashed lines are used for the secondary fuels.

Firstly, the effect of spark sensitivity at SR10 is quantified for each load and fuel. As can be surmised from Figure 4.3, the loss of IMEP at SR10 with increasing initial load, quantifiably decreases from gasoline, to DMF and finally to ethanol. This is clearly shown in Figure 4.6.

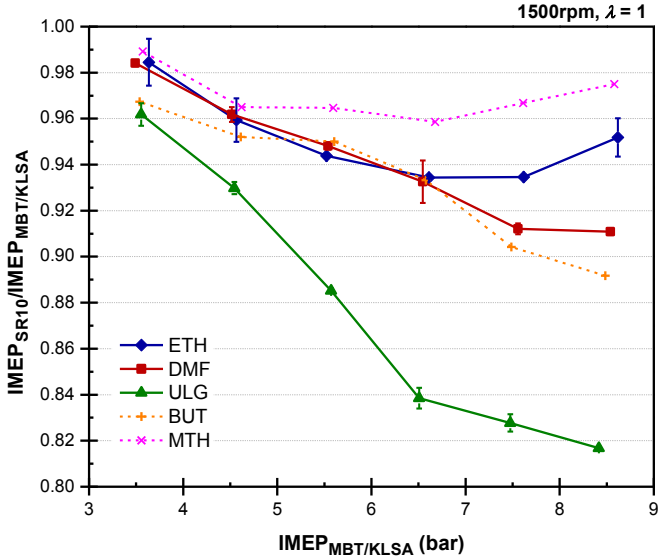

Figure 4.6 Effect of SR10 on Normalised IMEP

When fuelled with ethanol, the decay of IMEP at SR10 is ≤7% (≤0.5bar IMEP) across the load range, suggesting that the exact MBT timing for ethanol is less critical than the other two primary fuels. For DMF, the decay of IMEP at SR10 is much closer to ethanol than for gasoline. Up to 6.5bar IMEP, the decay is almost identical to that seen with ethanol. Above this load, the sensitivity increases and ethanol outperforms DMF. In comparison to gasoline, this loss is less significant.

At 8.5bar IMEP, the decay of IMEP at SR10 when using DMF is only 9% (0.8bar IMEP). However, for gasoline this loss increases to 18.3% (1.5bar IMEP). Evidently, gasoline is much more sensitive to SR in terms of IMEP, than both ethanol and DMF, which is largely a function of its relatively low OI (Table 3.8). The SR10 performance of *n*-butanol and methanol is below DMF and above ethanol, respectively. When using methanol, the fuel with the highest OI (Table 3.8), the loss is ≤4% at all loads and is superior to ethanol. Although the difference in OI between ethanol and methanol is marginal, the greater cooling effect of methanol plays a key role in further knock suppression. This is true for *n*-butanol.

Despite a similar OI to gasoline, the spark sensitivity of *n*-butanol is far superior due to the greater ΔH_{vap} (Table 3.8). This observation helps us to explain the performance of DMF. DMF has a relatively high OI because its low ΔH_{vap} is not taken into account in the CFR tests, which is proven to dramatically affect actual knock resistance (Milpied, 2009). In reality, the low charge-cooling effect when using DMF counterbalances the benefit of the increased OI to suppress knock. Therefore, as observed by other researchers, it is important to consider the charge-cooling effect and not only the OI, when selecting a fuel to improve knock suppression (Nishino, 2004).

The indicated efficiency is a measure of the fuel conversion efficiency and compares the total work done to the theoretical energy available. Figure 4.7 shows the loss of indicated efficiency for the three fuels at SR10, which demonstrates a similar trend between the fuels in Figure 4.6. Once again, the low decay in indicated efficiency of ethanol (and methanol) reiterates the low sensitivity to SR.

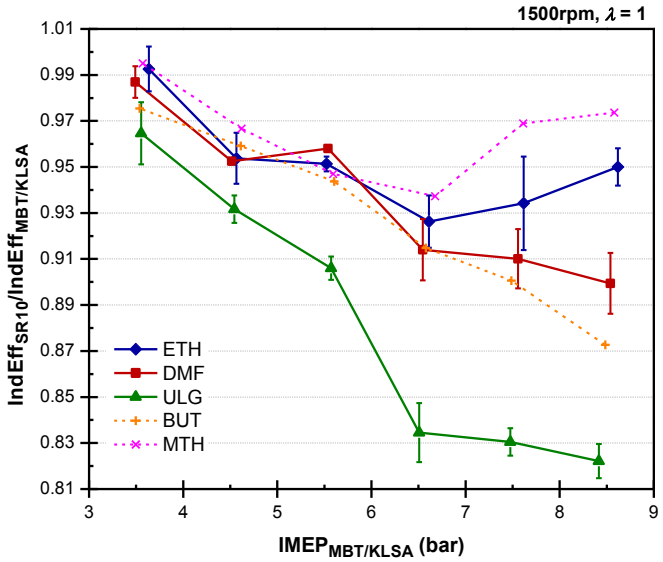

Figure 4.7 Effect of SR10 on Normalized Indicated Efficiency

When using gasoline at 8.5bar IMEP, the normalized indicated efficiency drops by 18%, almost double the loss experienced with DMF (10%) and 3.6 times more than with ethanol (5%). The low sensitive fuels benefit from an earlier optimum, where the effect of SR is lower. Nevertheless, there is a clear difference in sensitivity between ethanol and methanol, despite a similar MBT. This could be explained by the faster burning rate of methanol, which enables the energy from the air-fuel mixture to be more fully utilized earlier in the expansion stroke. Clearly, the varying efficiency losses due to SR have a detrimental impact on fuel consumption.

The indicated specific CO_2 ($isCO_2$) emissions with spark retard are shown in Figure 4.8.

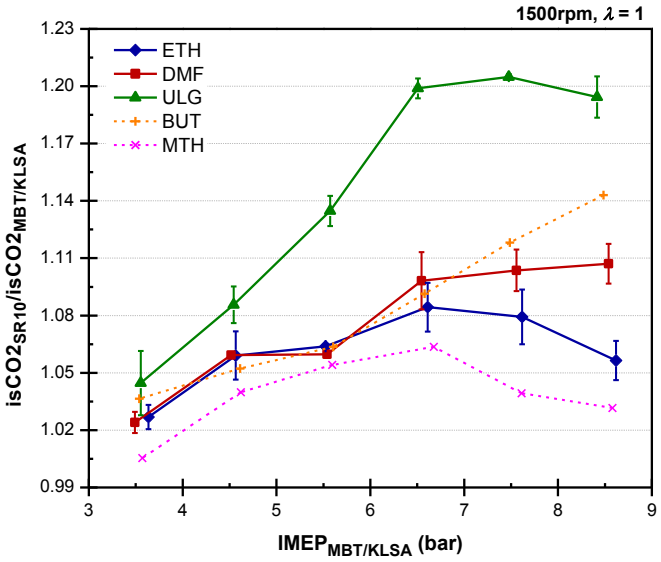

Figure 4.8 Effect of SR10 on Normalized $isCO_2$

The $isCO_2$ emissions increase at SR10 and with increasing load. This emissions penalty is due to the increase in fuel consumption and reduction in indicated efficiency shown in Figure 4.7. In fact, the inverse of the CO_2 emissions almost equals the trend in indicated efficiency at SR10. As discovered with indicated efficiency, SR with gasoline results in the highest

change in isCO_2 emissions, while ethanol produces the least and DMF produces only slightly more than with ethanol. At 8.5bar IMEP, the isCO_2 increase with gasoline is 19.4%, whereas with ethanol and DMF it is 5.6% and 10.7%, respectively. However, the low spark sensitivity of methanol results in the lowest change in isCO_2 emissions amongst the fuels (3.2% at 8.5bar IMEP).

The differences in performance and efficiency can be better explained when analysing the in-cylinder pressure data, in particular, P_{max} (Figure 4.9) and the resulting heat release data. In this instance, the CID has been selected, in order to best highlight the detrimental impact at SR10 (Figure 4.10).

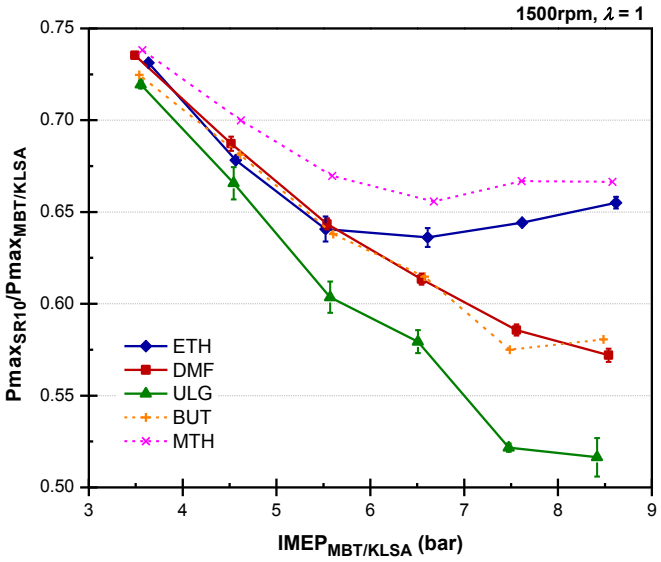

Figure 4.9 Effect of SR10 on P_{max}

In general, the effect at SR10 with load is a dramatic reduction in P_{max} and increase in the change in normalized CID. At low load, the decay in P_{max} is similar between fuels; the range at 3.5bar IMEP is <2%. However, as the load increases, the differences become self-evident, whereby gasoline exhibits the greatest changes at SR10. At 8.5bar IMEP, the spark timing at

SR10 for gasoline is TDC. This delays the combustion phasing towards the expansion stroke and produces a 48% reduction in P_{max}. Amongst the oxygenated fuels, *n*-butanol and DMF follow similar reductions in P_{max} mainly due to the similar knock suppression abilities. Ethanol behaves similarly up to 5.5bar IMEP, but is less affected at higher loads. Methanol, which has the greatest OI, is least affected at SR10.

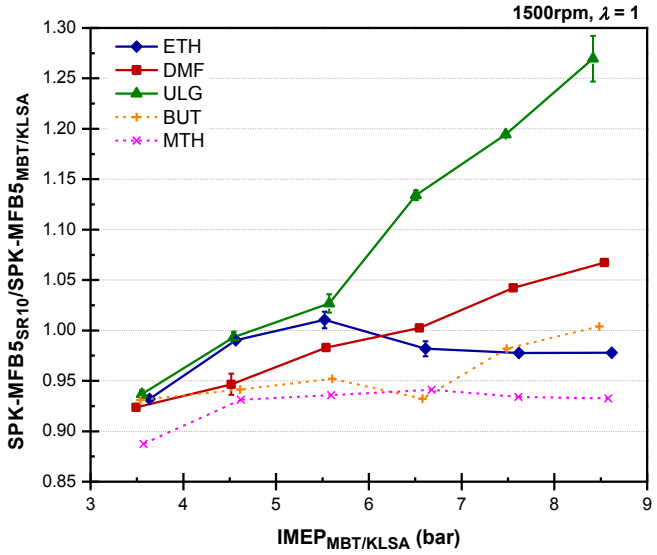

Figure 4.10 Effect of SR10 on CID

Clearly, this change in pressure impacts the CID. At low loads for gasoline (≤4.5bar IMEP) and DMF (≤6.5bar IMEP), and almost all loads for ethanol, *n*-butanol and methanol, the CID actually reduces at SR10. This is due to greater in-cylinder pressures at the point of ignition as it approaches TDC. However, because gasoline requires the most retarded MBT/KLSA timings, this benefit is rapidly lost above 5.5bar IMEP. With methanol, however, the most retarded SR10 spark timing is 11°bTDC (at 8.5bar IMEP). Therefore, combustion originates later in the compression stroke when the piston is closer to TDC and the in-cylinder pressure is higher (compared to MBT). For DMF, the CID is more affected than the other oxygenated biofuels at 8.5bar IMEP, but this effect is still less so than with gasoline. Here, the increase

in CID when using DMF is 6.7% (0.96CAD), whereas for gasoline the effect is much worse (27% increase, or 3.93CAD).

The effect of spark sensitivity on combustion stability is shown in Figure 4.11. The absolute and normalized units are shown in order to highlight the effects at SR10.

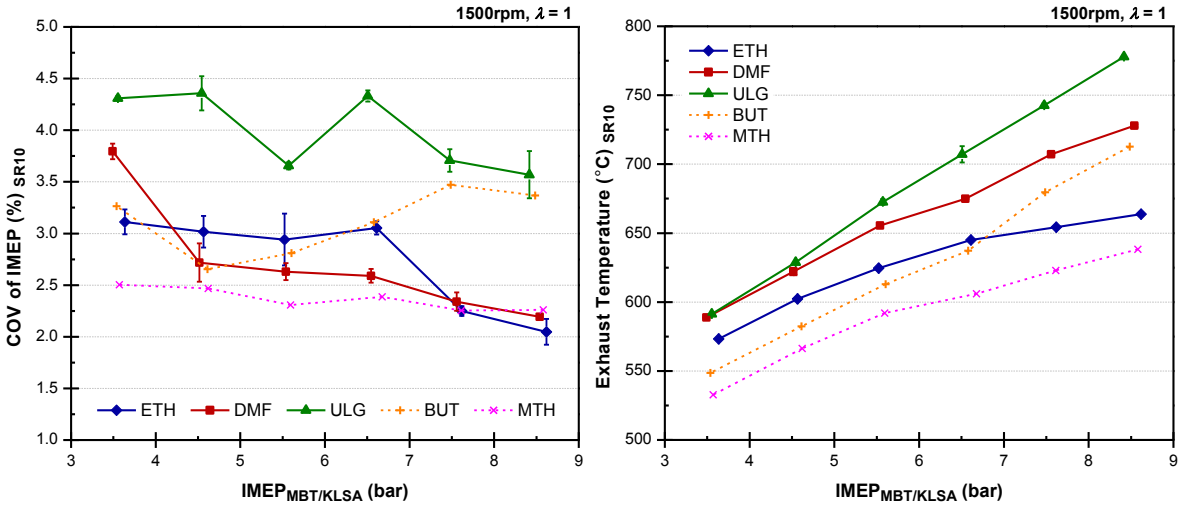

Figure 4.11 Effect of SR10 on COV of IMEP (a) and Exhaust Gas Temperature (b)

Figure 4.11a highlights the advantage of the oxygenated fuels on combustion stability over gasoline. Although the effect of spark sensitivity for all fuels decreases with load (except *n*-butanol), the instability of gasoline remains the highest. This is due to reduced $CAD_{10\text{-}90}$ as the O/C increases and the spark timing becoming more advanced (at SR10).

In general, it is methanol that offers the highest stability (lowest COV of IMEP) through SR. For gasoline and DMF, the MBT/KLSA timing is more retarded and closer to TDC. At this point, the in-cylinder turbulence is reduced which subsequently compromises the burning rate (Stone, 1999). For ethanol, the MBT timing is more advanced, so the combustion at SR10 occurs during higher turbulence intensity, which enhances the burning rate. Despite this, during the mid-loads (4.5-7.5bar IMEP), DMF offers improved combustion stability

over ethanol. This is possibly due to the offset of improved fuel droplet vaporization because of the lower ΔH_{vap} of DMF (Table 3.8). In fact, DMF is known to produce smaller fuel droplets than ethanol at 150bar injection pressure and with increasing distance from the injector nozzle (Tian, 2010b). Furthermore, the lower charge-cooling effect of DMF results in higher initial temperatures and helps to promote mixture homogenization prior to ignition.

Similarly to combustion stability, the exhaust temperature should be low enough for component protection, but high enough to improve cold-start performance (for TWC light-off) and enable rapid boost pressure build-up through SR. Although these tests have been performed in a warm condition, the trends may be correlated to a cold engine. The high exhaust temperatures when using DMF (Figure 4.11b) demonstrate its ability to warm-up the engine during combustion and to provide a high exhaust flow rate for boosting whilst maintaining high combustion stability. At the lowest load, the exhaust temperature at SR10 matches that with gasoline (the most favourable fuel to meet the aforementioned demands) and, with increasing load, remains close to gasoline and higher than all oxygenated fuels. Methanol, on the other hand, despite offering high combustion stability with low spark sensitivity, produces the lowest exhaust temperature and demonstrates its unsuitability as a engine warm-up fuel.

4.3 Effect of Engine Load

In this section, the performance and emissions of DMF are compared to gasoline and ethanol using gasoline and fuel-specific spark timings between 3.5-8.5bar IMEP. The fuel-specific timings are indicated by solid lines, whereas gasoline timings are shown using broken lines.

4.3.1 Fuel Consumption and Combustion Efficiency

Figure 4.12a shows the gravimetric indicated specific fuel consumption (ISFC).

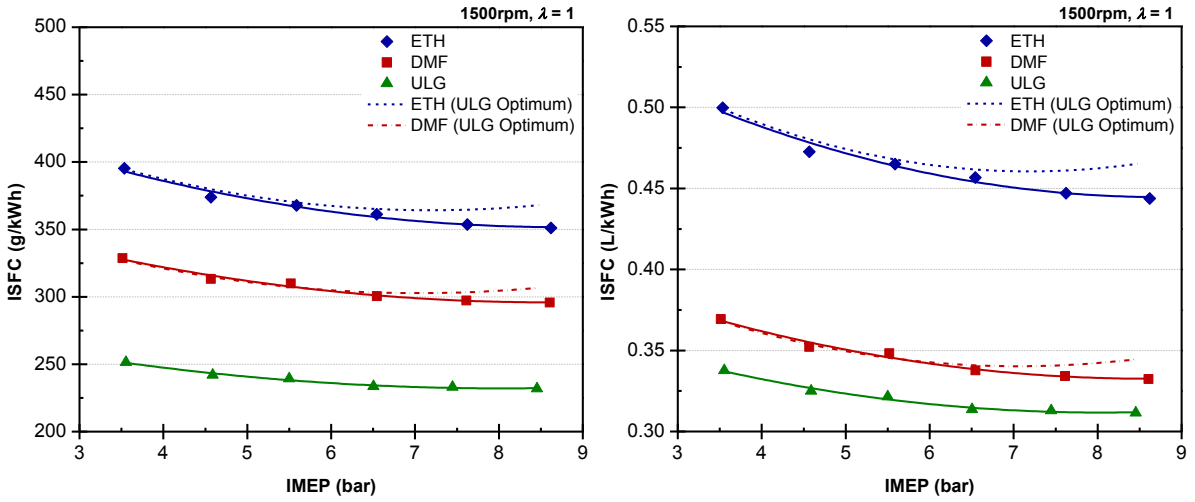

Figure 4.12 Gravimetric (a) and Volumetric (b) ISFC using Gasoline, ethanol and DMF

The effect of gasoline's superior energy density is clear; relative to gasoline, DMF and ethanol require more fuel for the same load. Here, small gains are shown above 5.5bar IMEP when optimising spark timing. However, gasoline offers lower gravimetric ISFC across the load range. Compared to ethanol, DMF consumes less fuel, largely because the gravimetric LHV of DMF is 25% (6.8MJ/kg) higher than ethanol (Table 3.8). However, the volumetric ISFC is normally the benchmark for fuel economy. This is shown in Figure 4.12b. Here, the performance of both fuels is improved relative to gasoline due to higher densities (Table 3.8). However, the ISFC using DMF is much closer to gasoline, due to a higher density than ethanol and closer volumetric LHV to gasoline.

Another method of interpreting the fuel conversion efficiency is through the gasoline equivalent fuel consumption rate (ISFCE), using Equation 4.1. This eliminates the effect of LHV on ISFC and provides an insight into the efficiency of combustion.

$$ISFCE_x = \frac{ISFC_x \times LHV_x}{LHV_{ULG}}$$

Equation 4.1 Gasoline Equivalent ISFC

Similarly, the indicated efficiency can be used to assess the relative performance. The comparable results of ISFCE (by mass) and indicated efficiency are shown in Figure 4.13.

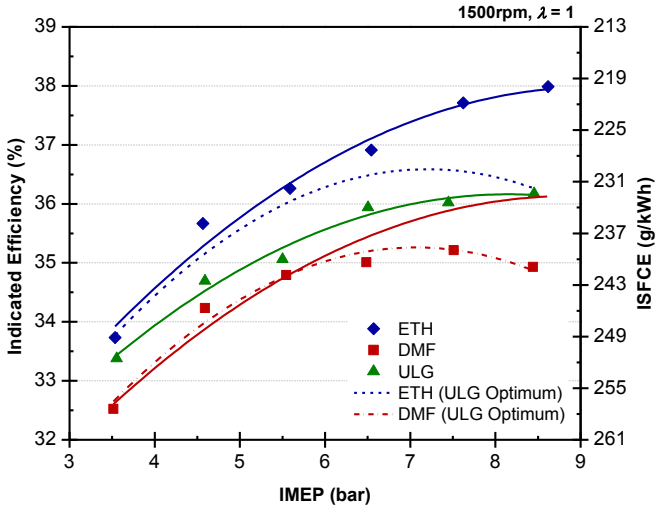

Figure 4.13 Indicated Efficiency and ISFCE using Gasoline, ethanol and DMF

Under gasoline MBT/KLSA timing, the fuels peak between 7-7.5bar IMEP. Previous modelling investigations have shown how the temperature of DMF combustion is the highest (Zhong, 2010), which helps to explain why the indicated efficiency is the lowest (Section 5.3.2). Higher combustion temperatures generate greater heat loss through the cylinder walls reducing the conversion of fuel energy into useful work. The greater temperature rise is mainly due to DMF's lower ΔH_{vap} (Table 3.8); despite requiring less energy to change phase, more energy is lost through higher combustion temperatures. The result is lower indicated efficiency. This is also reflected in the ISFCE. When using fuel-specific MBT/KLSA timing, however, DMF becomes competitive to gasoline above 8bar IMEP. Furthermore, the

limitations of the higher AFR_{stoich} of gasoline (Table 3.8) suggest that higher efficiencies can be found using the biofuels at even higher loads (and throttle positions) than were tested, based on the current trend. This could theoretically increase the maximum efficiency of DMF beyond that of gasoline.

The indicated efficiency, however, does not explain the completeness of combustion. This is shown by the combustion efficiency using Equation 3.10. Typical combustion efficiencies for SI engines operating under lean conditions, are between 95-98% (Heywood, 1988).

The results for this investigation are shown in Figure 4.14.

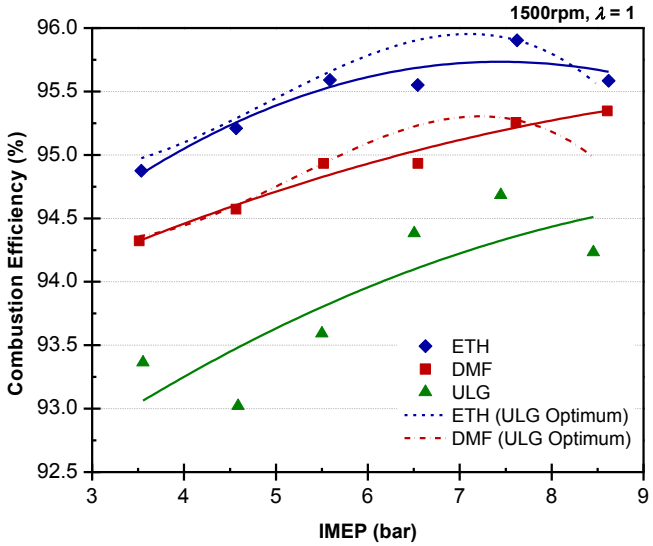

Figure 4.14 Combustion Efficiency using Gasoline, ethanol and DMF

Between the three fuels, ethanol consistently offers the highest combustion efficiency, closely followed by DMF and then gasoline. This is due to the higher oxygen content. The oxygen that hinders the fuel consumption performance because it offers no additional energy, paradoxically improves the completeness of combustion.

Using gasoline MBT/KLSA timing, the peak combustion efficiency coincides with the peak indicated efficiency (Figure 4.13), similarly decaying after 7-7.5bar IMEP. The cross-over using DMF and ethanol around 8bar IMEP is caused by the over-retarded combustion when using gasoline MBT/KLSA timing, which delays combustion.

4.3.2 In-Cylinder Pressure and Temperature

The P_{max} and maximum theoretical in-cylinder temperatures (T_{max}) are shown in Figure 4.15.

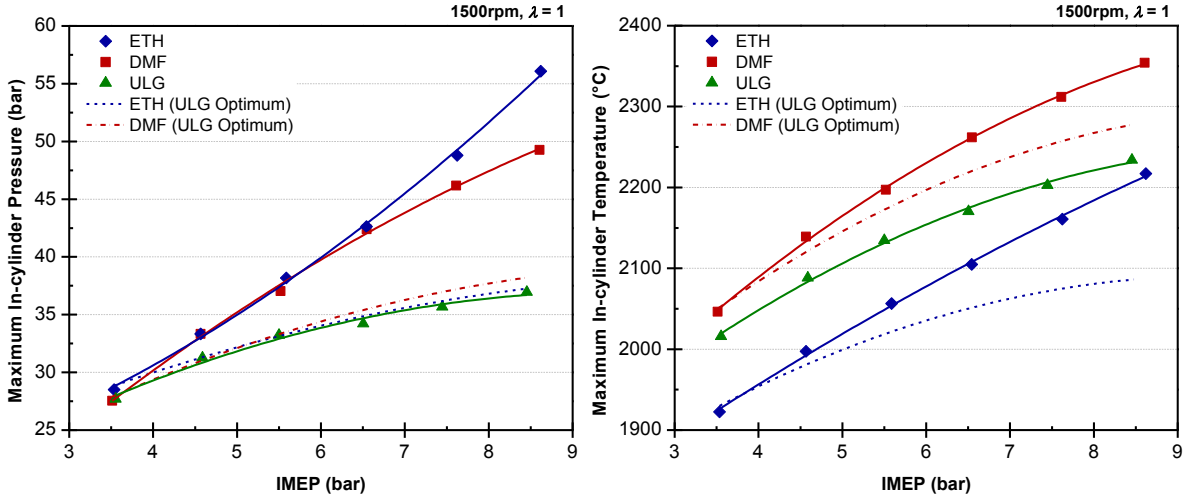

Figure 4.15 P_{max} (a) and Theoretical T_{max} (b) using Gasoline, ethanol and DMF

For gasoline MBT/KLSA timing, there are clear differences between the fuels at all loads. At low loads, ethanol produces the highest $P_{max.}$ At 3.5bar IMEP, P_{max} is 1bar higher than for DMF and gasoline. However, at high load, P_{max} using DMF then exceeds ethanol and gasoline by a similar amount. This effect is similar to that seen with CID (Figure 4.18). At low loads, the ethanol-air mixture reacts quicker than with DMF. However, at high loads, this trend is reversed and the lower CID for DMF results in a higher P_{max}. This might also be

due to higher combustion temperatures compared to ethanol and gasoline. When using fuel-specific spark timing, P_{max} for ethanol exceeds DMF due to more advanced timing.

The theoretical T_{max} is calculated using the WAVE model described in Section 3.6.6.1. Here, the experimental and simulated IMEP and P_{max} agree to within 99.7% at all test conditions. The higher ΔH_{vap} of ethanol (Table 3.8) encourages greater charge-cooling than with gasoline and DMF, which reduces the T_{max} and P_{max} for the same spark timing. More thermal energy is absorbed to evaporate the liquid ethanol in the combustion chamber, whereas less energy is required for gasoline and DMF to change phase, producing more net heat. Previous investigations show the similarity in T_{max} between gasoline and DMF (Zhong, 2010). However, when using fuel-specific MBT/KLSA timing, T_{max} when using DMF is higher than with gasoline due to the lower ΔH_{vap} of DMF. At 8.5bar IMEP, T_{max} when using DMF is 120°C greater than with gasoline, significantly impacting the NO_x emissions (Figure 4.20a). The increase in T_{max}, when using fuel-specific spark timing is also seen with ethanol. For example, at 8.5bar IMEP, T_{max} when using ethanol is ≈17°C lower than gasoline. This is a significant increase compared to the difference of ≈290°C, when using gasoline MBT/KLSA timing, which again significantly affects the NO_x emissions (Section 4.3.5).

4.3.3 VE and Pumping Loss

The difference in pumping loss and the consequential effect on fuel economy between DMF and ethanol is due to the difference in physicochemical properties. By weight, ethanol contains more oxygen, which results in lower AFR_{stoich} (Table 3.8). This reduces the throttle demand, which increases the net pumping losses and ISFC. This behaviour explains the trend of VE in Figure 4.16.

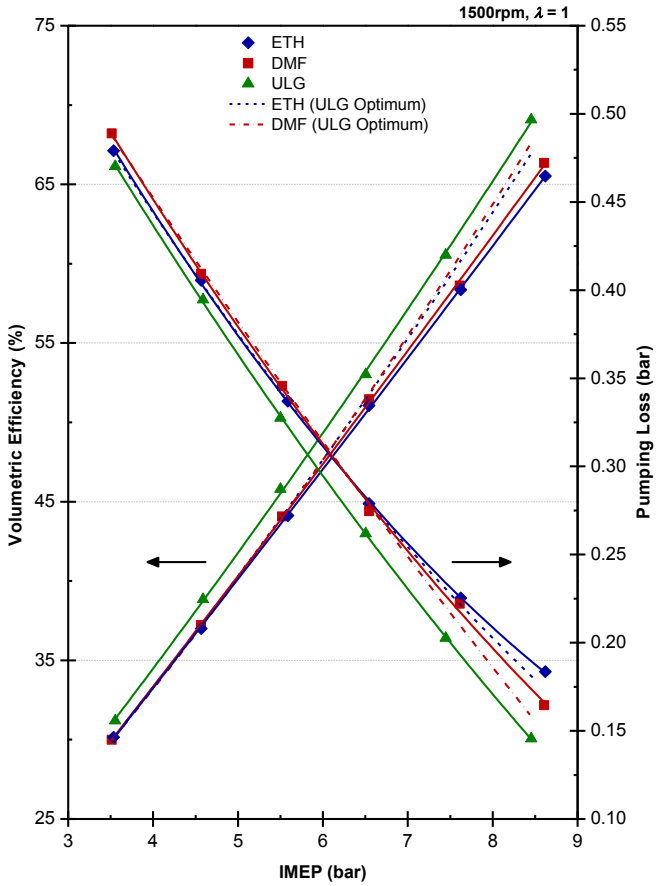

Figure 4.16 VE and Pumping Losses using Gasoline, ethanol and DMF

Although, at lower loads (<6bar IMEP), there is little difference between the oxygenated fuels, at higher loads (≥6bar IMEP) the separation is more evident due to ethanol's lower AFR_{stoich}. For gasoline, whose AFR_{stoich} is much higher (Table 3.8), the VE is superior because more air is required to compensate for no oxygen in the fuel. However, with closer inspection of the pumping losses below 6bar IMEP, ethanol offsets the higher throttling requirement by the higher charge-cooling effect. At 3.5bar IMEP, the pumping loss of ethanol is 1kPa lower than with DMF due to the impact of its higher ΔH_{vap}. However, at 8.5bar IMEP, this difference shifts in favour of DMF (by 2.1kPa) due to the lower AFR_{stoich} of ethanol and thus greater throttling. The charge-cooling effect on VE in a DISI engine is well documented (Wyszynski, 2002, Engler-Pinto, 2008, Heywood, 1988, Stone, 1999) and

counteracts the throttling losses. The turning point is 6bar IMEP. Above this, the higher throttling required with ethanol outweighs the benefits of cooling.

4.3.4 Combustion Phasing

Figure 4.17 shows the variation in CID between the three fuels. The MFB is calculated from the heat release analysis using the standard method described by Stone (Stone, 1999).

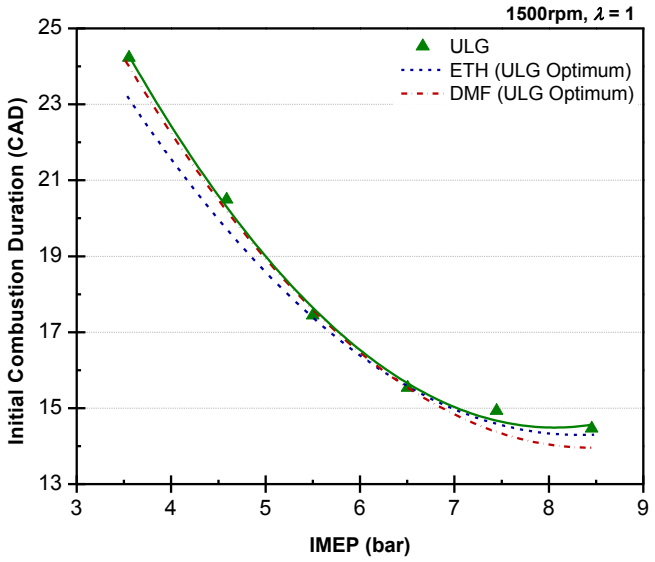

Figure 4.17 CID using Gasoline, ethanol and DMF at Gasoline MBT/KLSA Timing

The fuel-specific MBT/KLSA data has been removed so that a comparison can be made under the same spark timings. This variation in CID helps to explain the P_{max}; lower CIDs result in higher P_{max} as the pressure rise occurs earlier in the expansion stroke. The faster burning rate of ethanol compared to gasoline is reported by others (Aleiferis, 2008, Cairns, 2009, Yeliana, 2008, Gautam, 2000). At 3.5bar IMEP, the CID using ethanol was 0.9CAD lower than DMF, possibly due to the higher laminar flame speed (Tian, 2010a). However, at 8.5bar IMEP, the CID using DMF is 0.3CAD lower than ethanol. This is due to higher T_{max}

when using DMF (Figure 4.15b), which increases the burning speed, as shown from the laminar flame speed research (Tian, 2010a).

This low CAD_{10-90} of the biofuels compared to gasoline is shown in Figure 4.18. At gasoline timings, DMF has the lowest CAD_{10-90} (apart from 3.5bar IMEP). At 8.5bar IMEP, the CAD_{10-90} with DMF is 1CAD lower than ethanol and 1.3CAD lower than gasoline. Using fuel-specific timings, the CAD_{10-90} reduces further. At 8.5bar IMEP, the CAD_{10-90} of the biofuels is 4CAD less than gasoline. Once again, except the extremity of loads, the CAD_{10-90} is marginally lower when using DMF, than for ethanol (at least 0.35CAD).

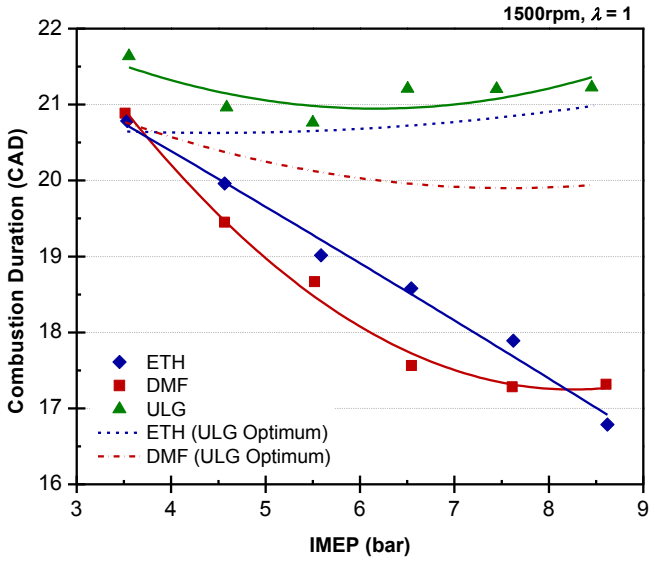

Figure 4.18 CAD_{10-90} using Gasoline, ethanol and DMF

Figure 4.19 shows the combustion durations either side of CA50, using gasoline MBT/KLSA timing at 8.5bar IMEP. For all three fuels, the duration before CA50 (CAD_{10-50}), is slightly higher than afterwards (CAD_{50-90}). For DMF, the combustion durations are lower than ethanol; CAD_{10-50} is 0.12CAD lower than ethanol and CAD_{50-90} is 0.83CAD lower. The reduction in CAD_{50-90} using DMF is also 3% and 7% higher than for gasoline and ethanol, respectively, highlighting the particularly high burning speed of DMF combustion.

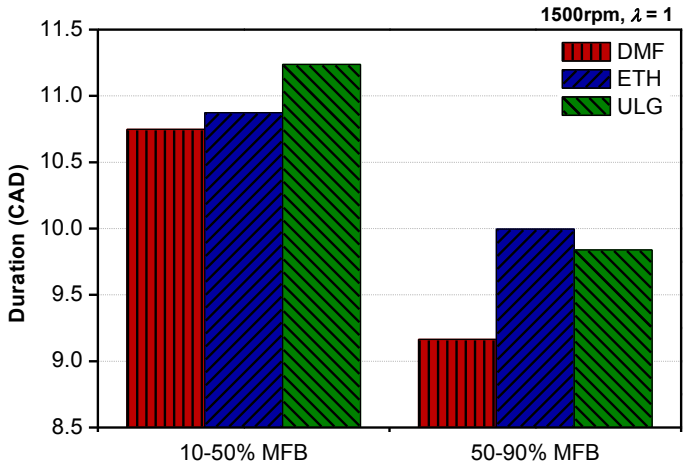

Figure 4.19 Combustion Durations at 8.5bar IMEP using Gasoline KLSA Timing

These results highlight the advantage of the burning speed when using DMF compared to ethanol despite DMF having a lower measured laminar flame speed (Tian, 2010a). However, under these test conditions, both oxygenated fuels have lower $CAD_{10\text{-}90}$ than gasoline.

4.3.5 Gaseous Emissions

The engine-out emissions are compared between the three fuels at the various loads and spark timings. Firstly, the regulated emissions are evaluated (HC, CO and NO_x), followed by an analysis of the CO_2 emissions. Figure 4.20a shows the $isNO_x$ emissions for all tests.

It is clear in Figure 4.20a that the $isNO_x$ emissions increase with load. This is because the formation of NO_x increases very strongly with combustion temperature (Stone, 1999). When using gasoline MBT/KLSA timing, ethanol produces much lower $isNO_x$ emissions compared to gasoline. This is because ethanol burns at a relatively higher rate (Figure 4.18) and lower temperature (Figure 4.15b). Although DMF appears to have a lower $CAD_{10\text{-}90}$ than ethanol, the $isNO_x$ emissions of DMF are more similar to gasoline because T_{max} is higher (Figure 4.15b). The $isNO_x$ emissions increase for fuel-specific timing, especially for DMF. With

ethanol, the increase with load is comparable to gasoline above 7.5bar IMEP. The fuel-specific timing with ethanol is 11CAD more advanced than the gasoline timing. However, T_{max} with ethanol is below that with gasoline (Figure 4.15b) due to the higher charge-cooling effect. Therefore, the tendency to produce $isNO_x$ emissions is lower.

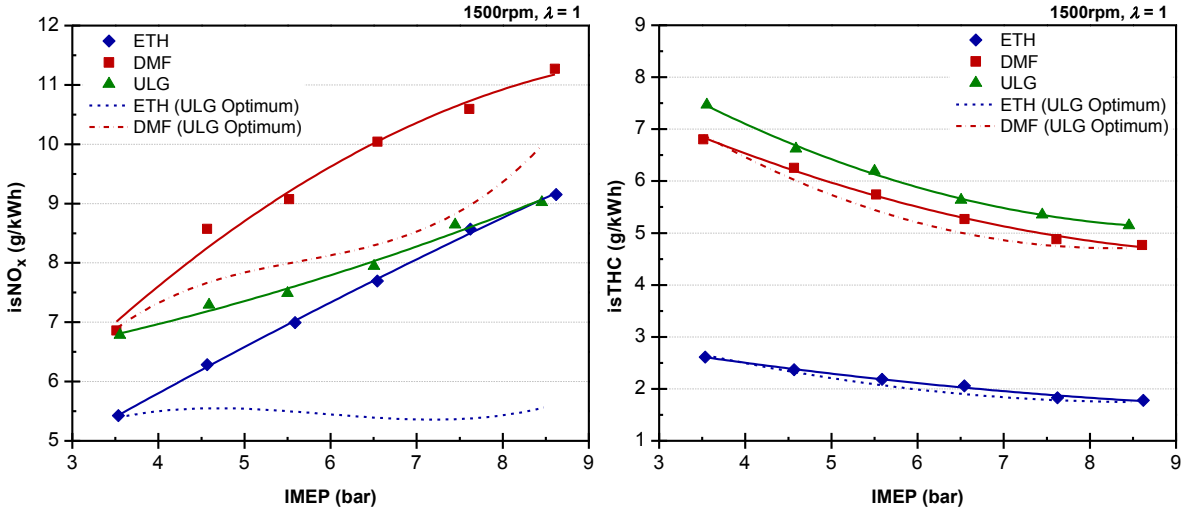

Figure 4.20 Effect of $isNO_x$ (a) and isHC (b) when using Gasoline, Ethanol and DMF

The relative $isNO_x$ emissions can also be attributed to the H/C ratio. Ethanol, which produces the lowest $isNO_x$ emissions, has the highest H/C ratio, whereas DMF produces the highest $isNO_x$ emissions and has the lowest H/C ratio (Table 3.8). Therefore, the $isNO_x$ emissions have an inverse relationship to H/C, a trend reported by Harrington (Harrington, 1973).

As shown in Figure 4.20b, the indicated specific HC emissions (isHC) for DMF are similar to gasoline. However, the isHC emissions are much lower for ethanol. It must be noted that these isHC emissions are uncorrected. The sensitivity of the FID analyser to oxygenated compounds has not been taken into account. Nevetheless, ethanol does have a higher oxygen content compared to DMF (Table 3.8), so together with its higher combustion efficiency (Figure 4.14) the oxidation of unburned HCs may be improved, as oxygen is more readily

available. As the load increases from 3.5-8.5bar IMEP, the isHC emissions decrease by approximately 30% for all fuels. This is due to increased T_{max} (Figure 4.15b) and thus combustion efficiencies (Figure 4.14) because of greater oxidation of the hydrogen and carbon molecules. As mentioned, the reduced sensitivity of the FID analyser to oxygenated fuels suggests that the total isHC emissions for ethanol and DMF are higher (Cheng, 1998, Wallner, 2008) necessitating detailed HC emissions speciation for reliable analysis.

The isCO comparison is made in Figure 4.21a.

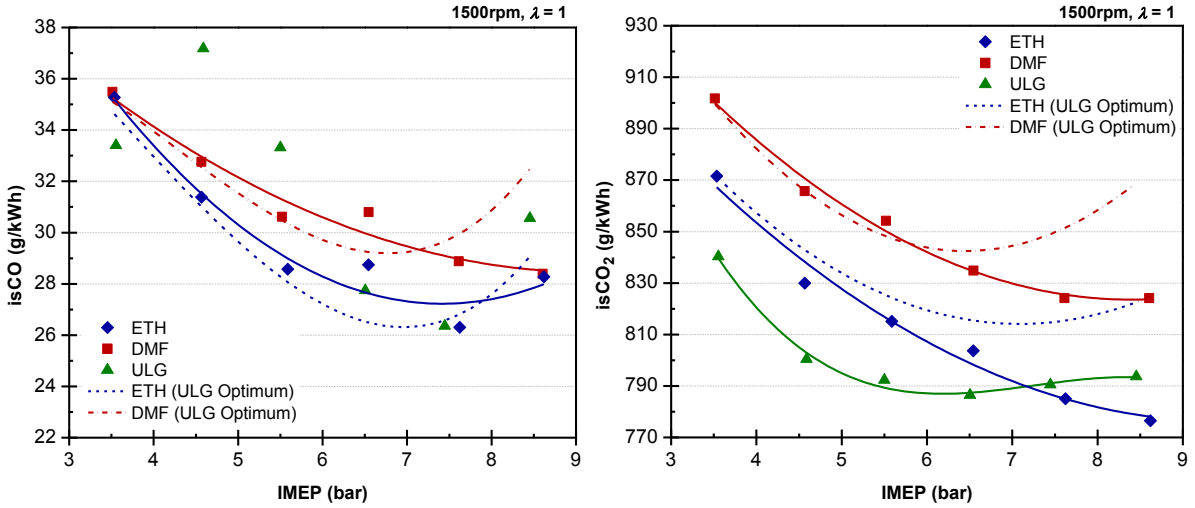

Figure 4.21 Effect of isCO (a) and $isCO_2$ (b) when using Gasoline, Ethanol and DMF

Similarly to the isHC emissions (Figure 4.20b), the isCO emissions generally decrease as load increases. The trend is similar to the ISFCE (Figure 4.13b), where the lowest isCO emissions arise at the highest ISFCE. Between the two oxygenated fuels, ethanol consistently produces the lowest isCO emissions. This is due to the higher oxygen content and combustion efficiency. Under gasoline timing, the difference increases with load. At 3.5bar IMEP, ethanol is 1g/kWh lower, whereas at 8.5bar IMEP this increases to 3g/kWh. Under fuel-specific MBT timing, the largest difference is seen at medium loads. For gasoline, the

relationship with load is less predictable. The peak at 4.5bar IMEP could be explained by the lower combustion efficiency at this point (Figure 4.14). Here, the mixture may be inhomogeneous, resulting in localized pockets of fuel-rich mixture and incomplete combustion. However, the remaining isCO emissions fluctuate within a similar range to the two biofuels, which decrease to a minimum between 7-7.5bar IMEP.

The isCO_2 production is shown between the three fuels in Figure 4.21b. The isCO_2 emissions decrease with increasing load and spark timing advance towards MBT/KLSA. The isCO_2 emissions are an indication of the completeness of combustion. Therefore, as the load is increased, the combustion is more complete, which is shown by the increase in combustion efficiency (Figure 4.14) and decrease in isCO_2 due to the reduction in pumping losses. Under gasoline timing, DMF and ethanol combustion produce a minimum in isCO_2 (thus a peak in combustion efficiency) between 6-7bar IMEP. Although both fuels produce higher isCO_2 emissions than gasoline, their lifecycle CO_2 emissions may be lower. This is due to the consumption of CO_2 during production.

4.4 Effect of Injection Timing

A calibration parameter that dramatically influences the combustion behaviour in modern DISI engines is the start of injection (SOI) timing. The SOI can be optimised to reduce the fuel consumption at low and part-loads through stratification as the pumping losses are removed (Roepke, 2002, Stuhler, 2002, Guerrier, 2004). Alternatively, at high-load, the engine torque can be increased due to charge-cooling as the knock is suppressed and the spark is advanced. The higher injection pressures of DI encourages rapid fuel atomization and an increased vaporization rate, which aids combustion stability (Alkidas, 2003).

However, this can lead to fuel impingement on the piston crown or cylinder wall (Zhao, 2002).

Therefore, as with spark timing, it is essential to understand the effect of SOI timing on engine behaviour when introducing new fuels. Each fuel has a different charge-cooling impact and the droplet size distribution will affect the extent of vaporization and wall wetting. Ethanol is known to be highly sensitive to SOI timing due to the high ΔH_{vap} (Hennessey, 2001, Chen, 2010, Kapus, 2007). Although this can help to increase maximum IMEP, it does narrow the window for emissions optimisation.

SOI timing sweeps were conducted either side of 270°bTDC$_{comb}$. Although this is not the reference condition, when using intervals of 30CAD, the behaviour at TDC and BDC is included as used by Yang (Yang, 1998). Firstly, SOI timing was advanced to 360°bTDC$_{comb}$ (TDC) and then retarded to 180°bTDC$_{comb}$ (BDC) with two records of 270°bTDC$_{comb}$. This allows the effect of any engine drift during the sweeps to be observed and accounted for.

4.4.1 VE and Pumping Losses

The effect of SOI timing on IMEP and VE using the three fuels is shown in Figure 4.22a. The data from 8.5bar IMEP is shown as this presents the greatest differences between the fuels. As previously discussed, the SOI timing window of 360-180°bTDC$_{comb}$ (in 30CAD increments) was chosen in order to highlight the positive impact of charge-cooling during the intake stroke (IVO/IVC = 376/126°bTDC$_{comb}$). As shown using ethanol in Figure 4.22a, the peak VE occurs mid-way through the stroke when the piston speed is close to its peak. This is due to the spray ‘chasing’ the piston, which minimises fuel impingement on the piston crown and increases charge density. The loss of VE (and reduced IMEP) with early SOI

(360°bTDC$_{comb}$) is due to the high penetration rate causing piston impingement and loss of cooling (Fry, 1999). With later SOI timings, the VE for ethanol decays. However, for gasoline and DMF, the VE increases when the SOI timing is very late (210°bTDC$_{comb}$). This is because of reduced charge-cooling as there is less time for the fuel to evaporate.

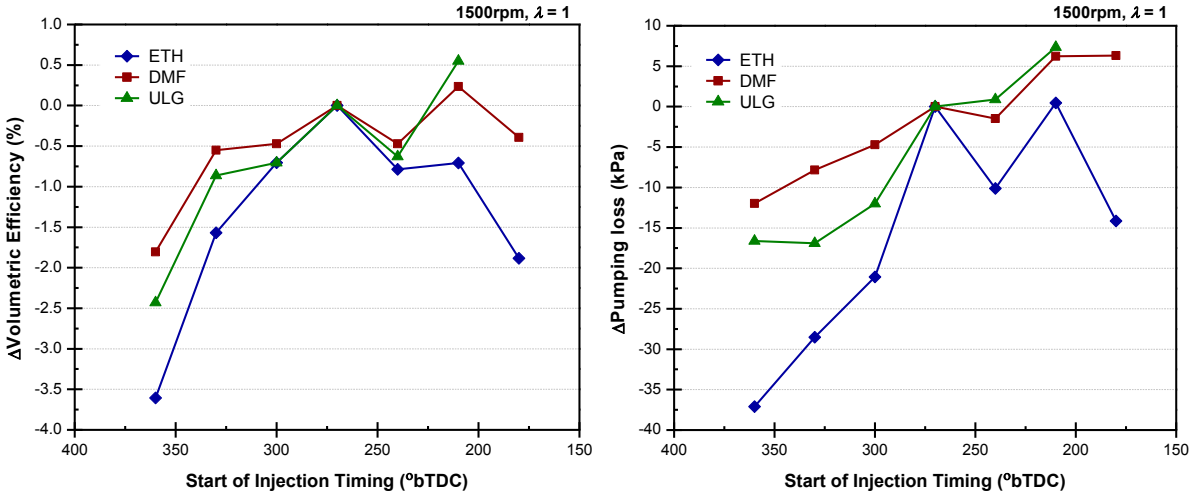

Figure 4.22 Effect of SOI timing on Change in VE (a) and Pumping Loss (b)

The change in pumping loss shown in Figure 4.22b counteracts the benefits of VE. This has a negative effect on the ISFC and IMEP during the SOI timing sweep. As SOI is advanced, so the pumping loss is reduced. As with VE, the highest rate of decrease is with gasoline and then DMF. The lower sensitivity to changes in SOI using DMF is because DMF has a low ΔH_{vap} (Table 3.8) which reduces the charge-cooling effect.

A more detailed discussion of the effect of SOI timing using DMF is found in Chapter 5.

4.5 Effect of AFR

The use of stratification (lean-burn) is commonly applied to modern DISI engines (Dunn-Rankin, 2007). This simultaneously increases efficiency and reduces emissions but is very

complex to control (Shayler, 2001a). At part-load operation, greater throttle openings reduce the pumping losses associated with stoichiometric operation. In terms of emissions, lean-burn strategies can dramatically reduce NO_x emissions (when using efficient lean-burn NO_x traps (Iwachido, 2009)) as the combustion temperature is reduced. Nevertheless, as the mixture is leaned, there is a limit of stable combustion called the 'lean limit'. At this point, ignition becomes unreliable and the combustion is less complete leading to engine misfire (Shayler, 2001b). The lean limit is also fuel dependant because the vaporization rates and combustion speeds vary between fuels. Therefore, a fuel which produces a very lean combustion limit will enable a wide window for optimisation to greatly reduce NO_x emissions.

The CO and NO_x emissions are reduced with stratification as the combustion efficiency is increased. However, as the mixture becomes leaner, the combustion stability decreases. Therefore, instead of using the IMEP as a marker to sensitivity, the lean limit has been used, which is defined as 5% COV of IMEP. Each AFR sweep was determined using the injector pulse-width, once the desired load was found at stoichiometry. Firstly, the AFR was enriched ($\lambda<1$) until $\lambda=0.8$ and then leaned until the lean limit was reached.

4.5.1 Combustion Stability

The AFR sensitivities are shown in Figure 4.23. In some cases, when the AFR at 5% COV of IMEP was not directly achieved, the trend is interpolated or extrapolated as in the case for ethanol at 5.5bar and 8.5bar IMEP (the lowest COV of IMEP requiring extrapolation was 4.5%). Even though AFR sweeps are shown at 5.5bar IMEP (Figure 4.23a), the differences between the fuels is more apparent at 8.5bar IMEP (Figure 4.23b). Here, the biofuels show

lower AFR sensitivities than gasoline. This is because single component oxygenated fuels burn more quickly (Daniel, 2011). Ethanol, which has more oxygen than DMF and a lower number of molecules, produces the lowest instabilities. Consequently, the AFR window is much wider. When using gasoline, the COV of IMEP rises quickly above 3% when $\lambda \geq 0.95$.

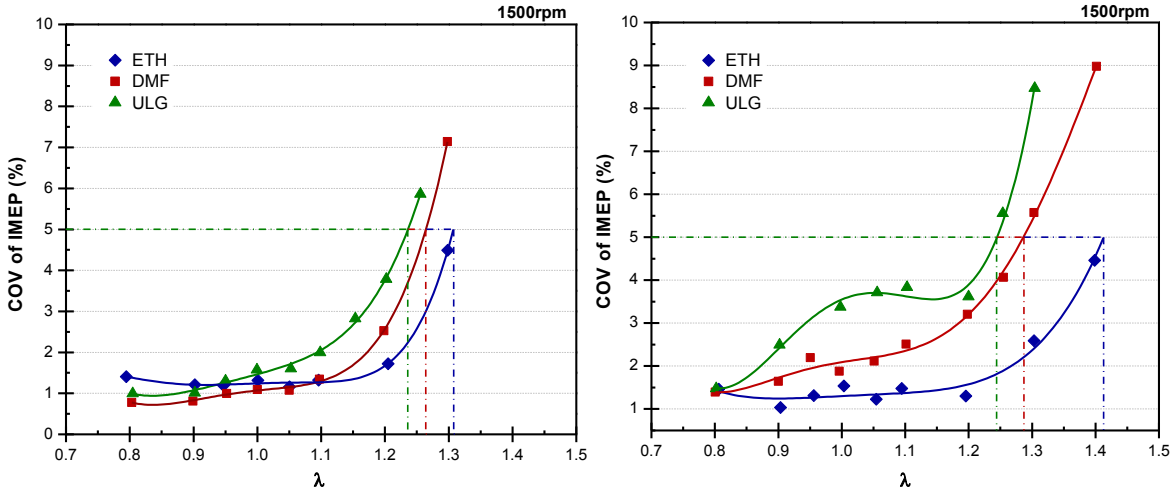

Figure 4.23 Effect of AFR on Combustion Stability at Part (a) and High (b) Load

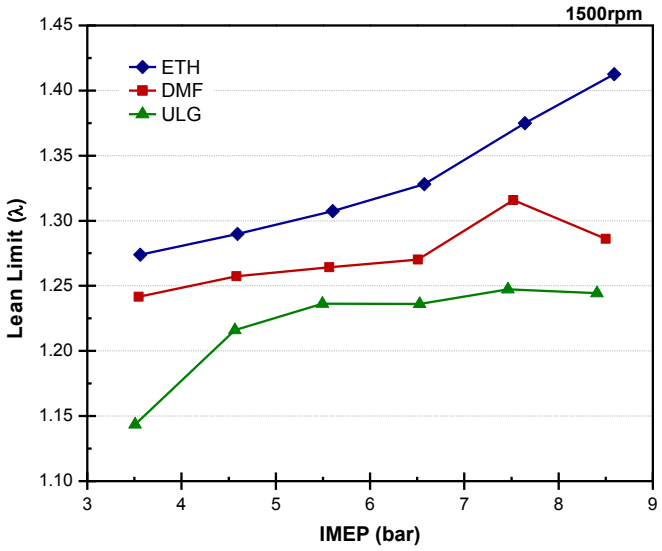

Figure 4.24 Lean Limit of Combustion at Each Load

In Figure 4.24 the lean limit with ethanol is consistently higher than with DMF and gasoline, which increases with load for all fuels. When the load exceeds 6.5bar IMEP, the lean limit

with ethanol is much higher than with DMF. The benefit of this increased lean limit becomes apparent when analysing key performance parameters and emissions.

4.5.2 Engine Efficiency

Figure 4.25a shows the effect on indicated efficiency (relative to stoichiometry).

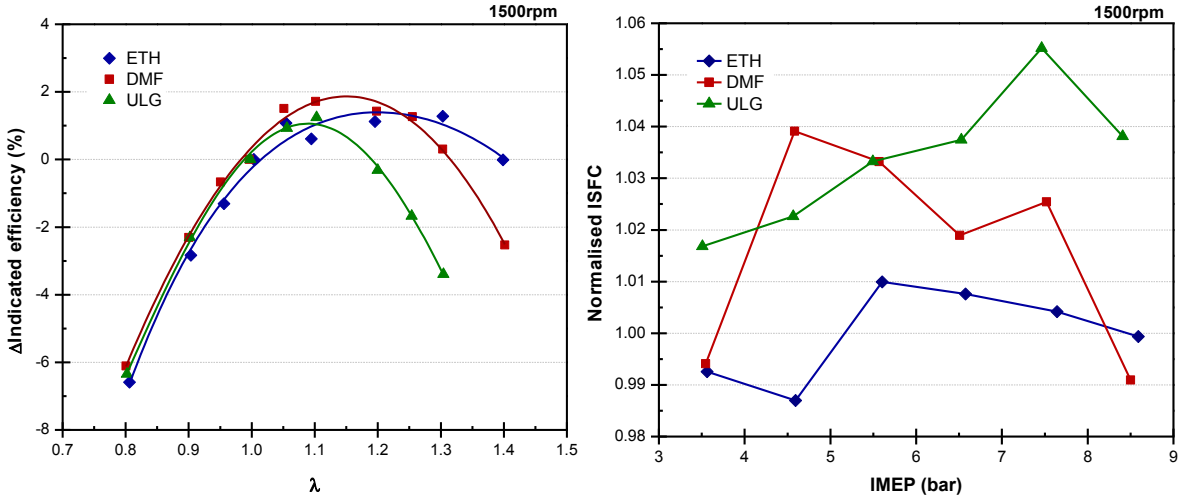

Figure 4.25 Effect of AFR on Indicated Efficiency (a) and ISFC at the Lean Limit (b)

The indicated efficiency at the lean limit is lower than the maximum. For gasoline, the maximum efficiency is at λ≈1.1, whereas at the lean limit (λ≈1.25), the indicated efficiency drops by 1.7%. However, for DMF and ethanol, the effect on indicated efficiency around their respective lean limits is minimal (when using DMF, the indicated efficiency actually increases by 0.3%). Therefore, as the lean limit increases, the sensitivity of the indicated efficiency reduces, which reduces the window for optimisation.

Figure 4.25b shows the effect of the lean limit on ISFC. Clearly, the ISFC increases at the lean limit with load. However, this increase in ISFC is linked to the sensitivity of the fuel to AFR, whereby ethanol is the least affected and gasoline, on the whole, is affected the most.

4.5.3 NO_x Emissions

The effect of AFR sensitivity on $isNO_x$ emissions is shown in Figure 4.26a.

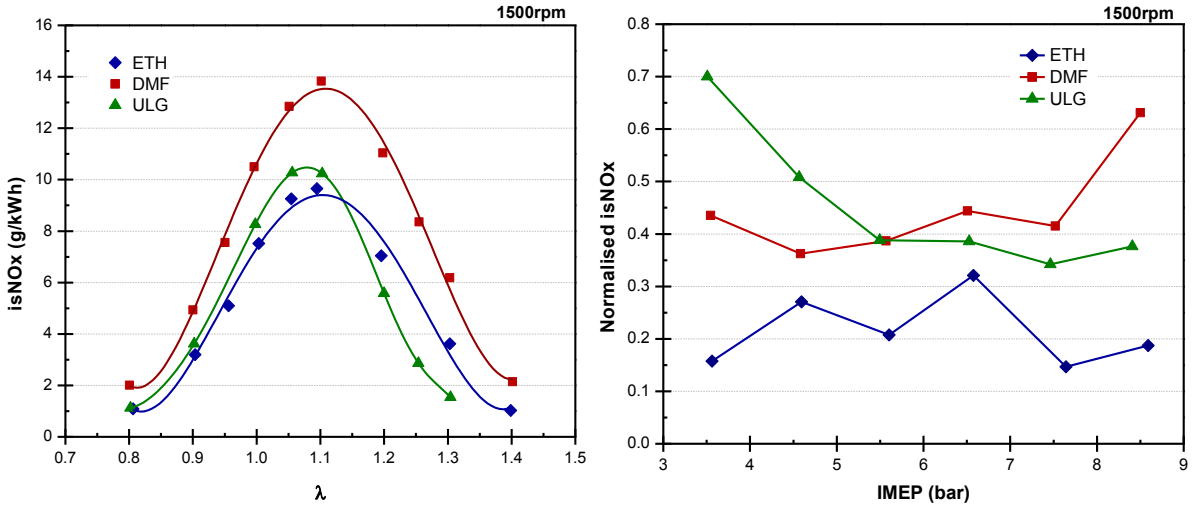

Figure 4.26 Effect of AFR on $isNO_x$ (a) and ISFC at the Lean Limit (b)

The $isNO_x$ emissions are more sensitive to AFR when using DMF than with gasoline and ethanol. This was found with spark timing sensitivity (Figure 4.5b). Nevertheless, the lowest $isNO_x$ emissions are found at leaner AFRs and the emissions are much lower at the lean limit than at stoichiometry. For ethanol, this decrease is 80%, whereas for DMF this is only 35%, (63% with gasoline). Although the AFR window is widened when using DMF compared to gasoline, the reduction in $isNO_x$ emissions is less beneficial.

The normalised $isNO_x$ emissions for ethanol (Figure 4.26b) are more greatly reduced at the lean limit. Below 5.5bar IMEP, DMF produces greater decreases in $isNO_x$ than with gasoline but the reverse is true at higher loads. Clearly, the lower sensitivity when using DMF inhibits the reduction of $isNO_x$ emissions. This is due to higher T_{max} when using DMF.

4.6 Effect of Valve Timing

Finally, the valve timing sensitivities are examined. Timing sweeps were made either side of the mid-points (0°aTDC, IVO and 20°aTDC, EVC) in 5CAD intervals (40CAD range).

4.6.1 Intake Valve Timing

Most modern engines are equipped with variable valve timing systems. Varying the intake valve opening (IVO) timing, or more importantly the intake valve closing (IVC) timing, can help to optimise the charge air flow at each engine speed and load. The analysis focuses on the effect of IVO timing at high load (8.5bar IMEP) because at this load, the trends are magnified (the IVC timing is also shown). The IVO timing directly influences VE, as shown in Figure 4.27a. Here, the change in VE either side of the maximum shows a clear separation between the fuels. At the 2% drop in VE, gasoline presents the narrowest window of IVO variation, whereas ethanol and DMF produce a wide window in which to optimise for efficiency. Between DMF and ethanol, there is little separation in VE variation although ethanol is marginally less sensitive.

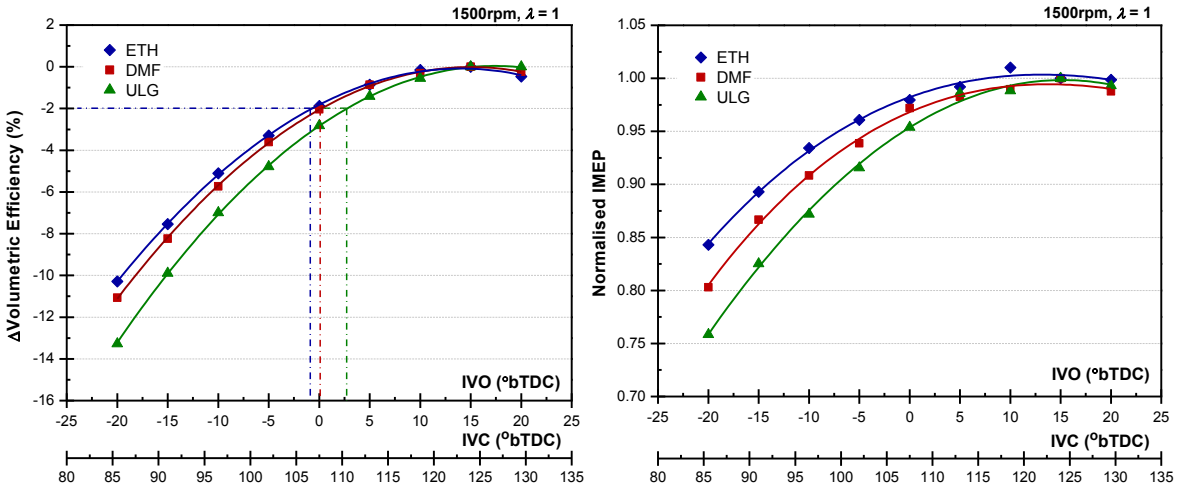

Figure 4.27 Effect of IVO on Change in VE (a) and Normalised IMEP (b)

The effect of VE on IMEP is shown in Figure 4.27b. Here, the IVO timing at the maximum IMEP coincides with that at the maximum VE. At the most advanced IVO, the IMEP, when using gasoline, drops by 24% from the IVO at maximum VE. For DMF and ethanol, this decrease is 20% and 16% respectively, as the sensitivity is lower.

When examining the effect on indicated efficiency (Figure 4.28a), which is the inverse of ISFC, the benefits of the wider IVO window are more apparent. This is because, the maximum indicated efficiency is found marginally later than the maximum IMEP or VE. This IVO timing is also related to the sensitivity and is found later as the sensitivity reduces. For the three fuels, the maximum indicated efficiencies are obtained because these points are within the IVO windows. The location of maximum indicated efficiency is determined by the location of the lowest $CAD_{10\text{-}90}$, as shown in Figure 4.28b. Here, ethanol shows little variation but a clear minimum $CAD_{10\text{-}90}$ with IVO timing at TDC. For DMF and gasoline, the minimum $CAD_{10\text{-}90}$ is increasingly more advanced.

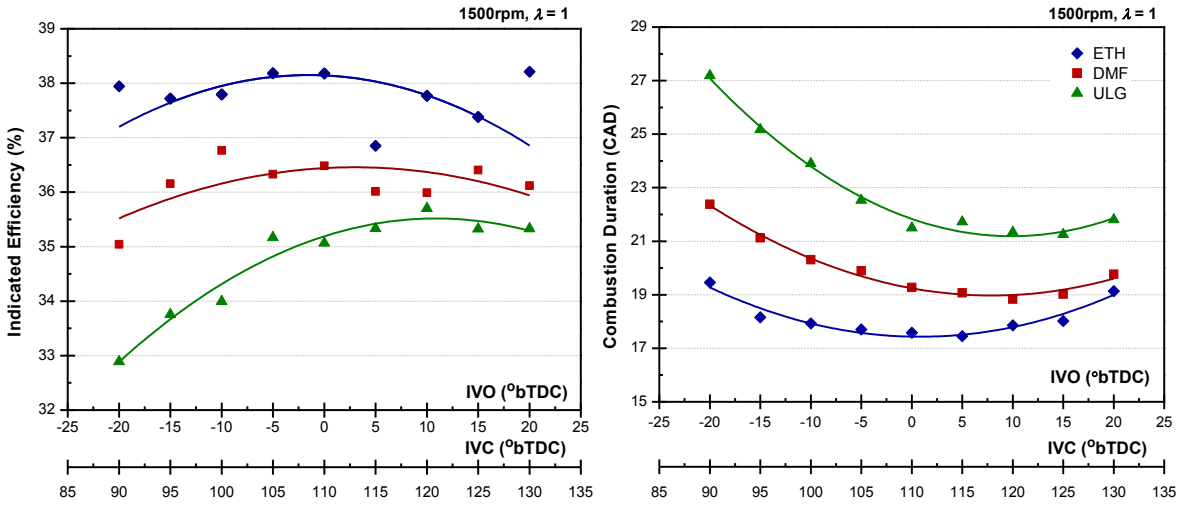

Figure 4.28 Effect of IVO on Indicated Efficiency (a) and $CAD_{10\text{-}90}$ (b)

4.6.2 Exhaust Valve Timing

The exhaust valve timing helps to control the trapped exhaust residual gas, which has a direct impact on the emissions rather than performance. In this analysis, the sensitivity of each fuel to exhaust valve closing (EVC) timing is also quantified at the 2% drop in IMEP.

The effect of EVC on load and VE are shown in Figure 4.29. The separation between fuels is less evident on VE (Figure 4.29b), so the effect on IMEP (Figure 4.29b) is discussed.

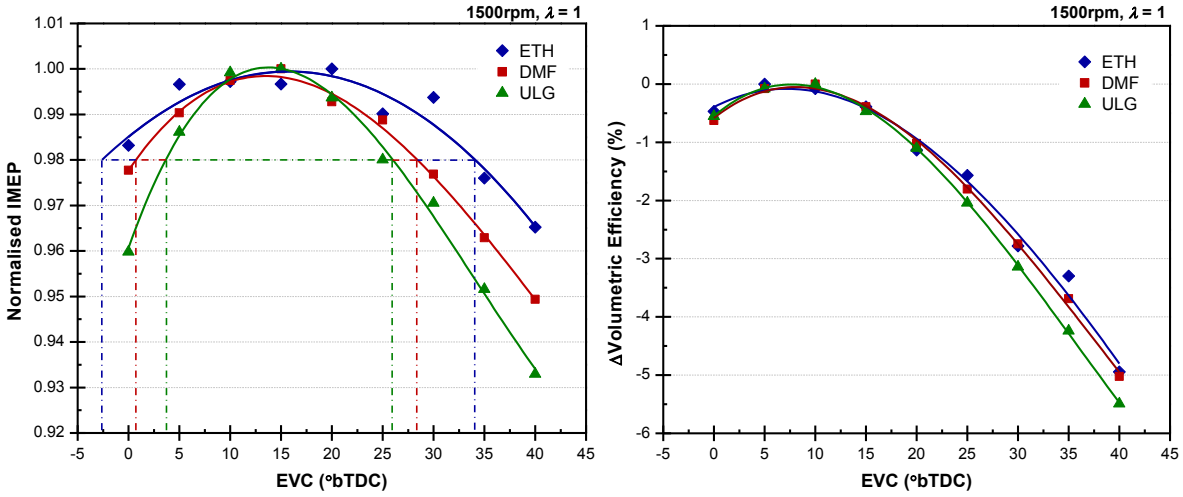

Figure 4.29 Effect of EVC on Normalised IMEP (a) and Change in VE (b)

The maximum IMEP is close to the middle of the AFR sweeps and the 2% drop in IMEP encloses a wide EVC range. Similarly to previous parameters, ethanol generates the widest EVC window, and gasoline, the least (see dashed lines). The window for ethanol is 9.5CAD more than with DMF, which, in turn, is 4CAD more than with gasoline. At the latest EVC timing the IMEP with ethanol reduces by 3.5%. However with gasoline this is almost double.

The effect of EVC timing on isHC emissions is shown in Figure 4.30a. Clearly, EVC retard reduces the isHC emissions. The most retarded EVC timings for DMF and ethanol within the

permissible EVC range produce 25% and 30% reductions in isHC emissions, respectively. For gasoline however the EVC sensitivity is higher, so the reduction in isHC is only 15%.

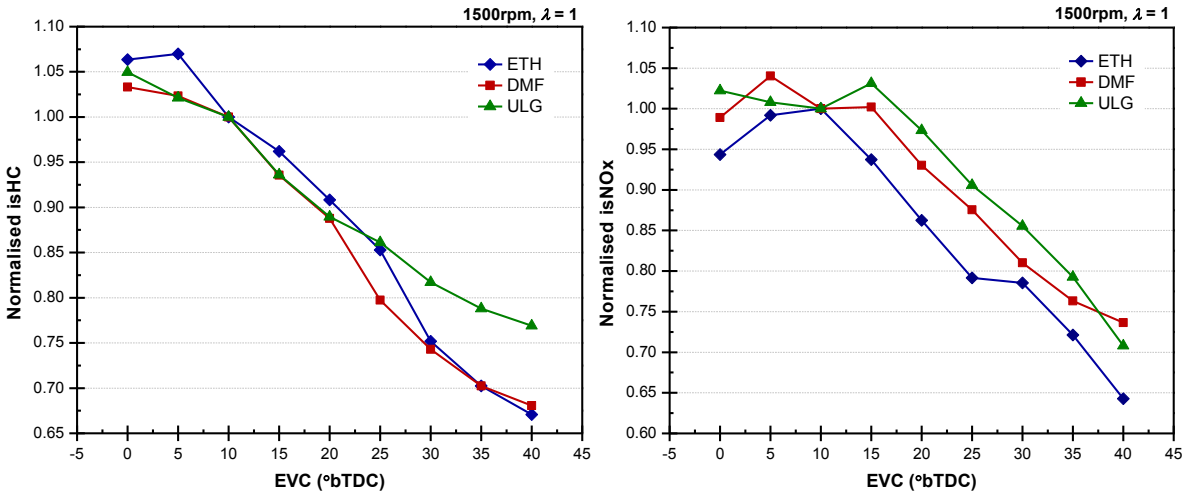

Figure 4.30 Effect of EVC on Normalized isHC (a) and isNOx (b)

This trend is magnified with isNO_x emissions because the fuels have a varying sensitivity to EVC timing (Figure 4.30b). This is due to more residual exhaust gas being trapped with earlier EVC timings. For the three fuels, the isNO_x emissions reductions increase in the order of gasoline, DMF and then ethanol with reductions of approximately 10%, 18% and 28%, respectively. Clearly, the biggest reductions are found with ethanol, which benefit from reduced sensitivity to IMEP as well as to the individual emissions.

4.7 Summary

This chapter examines the sensitivity of DMF to various engine parameters. The results are compared to gasoline and other oxygenated fuels.

In summary, both biofuels have lower CID and $CAD_{10\text{-}90}$ than gasoline, especially with spark advance. The volumetric ISFC of DMF is similar to gasoline. For an end-user, DMF could show similar mileage to gasoline. Due to the oxygen content, the combustion efficiency of DMF is higher than gasoline. However, the indicated efficiency is lower due to greater energy loss, possibly due to higher T_{max} values. The engine-out emissions of DMF are similar to gasoline (except isNO_x).

The fuels show varying spark sensitivity that increases with load. In terms of IMEP and indicated efficiency, the order of ascending sensitivity is: methanol < ethanol < DMF < *n*-butanol < gasoline. These sensitivities are due to the combination of chemical (OI) and physical (ΔH_{vap}) properties. Both isNO_x and isHC decrease for all fuels at SR10. The isCO emissions are largely reduced for all oxygenated fuels, but not for gasoline, which increased to 76%. The trend in isCO_2 is inversely proportional to that seen with efficiency.

Ethanol showed the highest sensitivity to variations in SOI timing. When examining VE, DMF showed the least sensitivity, allowing a wider window for emissions optimisation. In terms of AFR, the limit of lean combustion for ethanol was greater than with DMF and gasoline. However, the isNOx emissions reductions were lower for DMF than for gasoline.

Overall, these experiments highlight the benefit of biofuels over commercial gasoline, in terms of parameter sensitivity. This is due to the greater knock resistance of biofuels. DMF has reduced sensitivity compared to gasoline and allows a wider optimisation window.

CHAPTER 5

MODERN GDI COMBUSTION MODES USING DMF AND ETHANOL

This chapter examines the effect of SOI timing at full-load on DMF and ethanol compared to gasoline. The benefits of split-injection strategies to suppress knock are also investigated.

5.1 Introduction

It is well known that DI is an enabler for stratification in SI engines. However, little is known about the benefits of this strategy with DMF. Therefore, the effect of SOI timing on a DISI engine fuelled with DMF and ethanol has been examined.

Firstly, single-pulse SOI timing sweeps were conducted at full-load with each fuel to find the highest VE (360-180°bTDC$_{comb}$ every 30CAD). The optimum SOI timing for gasoline was then used for the first SOI timing with each fuel and second SOI timing sweeps were made. All tests are carried out at stoichiometric conditions at 1500rpm.

Secondly, the benefits of two-stage injection strategies are examined when using ethanol and DMF. At full-load or wide-open throttle (WOT), partial charge stratification can suppress knock, enabling greater spark advance and increased torque. Such split-injection strategies are employed when using gasoline.

However, this section analyses if such techniques are transferable to biofuels. The effect of an equal split-ratio (1:1) is compared to one which favours the first injection (2:1). Gasoline is used as a benchmark and the second SOI timing is swept between 240-90°bTDC$_{comb}$, in 30CAD intervals.

5.2 Effect of Single-Pulse Injection Timing at Full Load

In order to study the effect of SOI timing on engine performance and emissions between gasoline, ethanol and DMF, sweeps were performed at WOT (λ=1, 1500rpm). For each condition, the MBT timing was determined for each fuel and KLSA timing is used in the case of knock. The test procedure shown in Table 5.1 was followed for each sweep.

Table 5.1 Test Procedure

Step	Test
1	Baseline single-pulse PFI
2	Baseline single-pulse DI
3	Incremental injection timing retard
4	Baseline single-pulse DI (repeat)
5	Incremental injection timing advance

Firstly, baseline points were taken at the single-pulse PFI and DI (270°bTDC$_{comb}$) conditions. Using DI, the SOI timing was swept either side of the single-pulse baseline in 30CAD steps. The timing was first retarded towards BDC (180°bTDC$_{comb}$) and then advanced to TDC (360°bTDC$_{comb}$) so that the entire intake stroke could be examined (Figure 5.1).

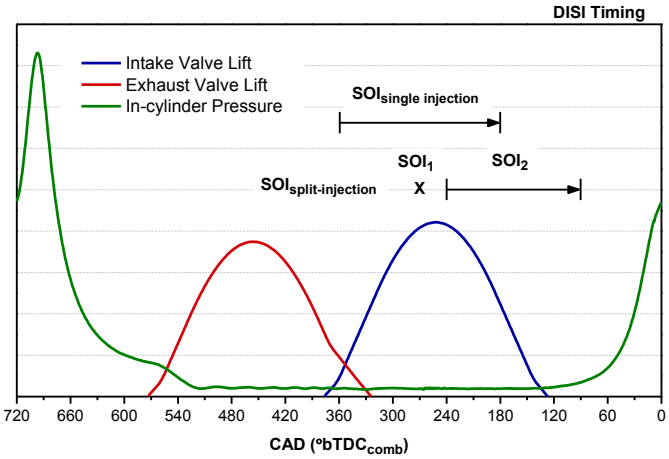

Figure 5.1 Engine Timing Setup showing Single and Split-injection Strategies

This procedure was repeated twice with each fuel to produce an average (error bars show repeatability). This back-to-back procedure reduces experimental uncertainty and is used by Ford (Yang, 1998). While performing each SOI timing sweep, the pulse-width was adjusted finely (±1μs) to maintain stoichiometry, once MBT or KLSA was found.

5.2.1 Gasoline

Firstly, the effect of single SOI timing is briefly examined using gasoline only. This helps to understand the fundamental combustion behaviour and effect of charge-cooling on engine performance at WOT. Following this, the behaviour of ethanol and DMF is compared to the gasoline benchmark. Finally, the SOI timing that provides the greatest improvement in IMEP, with minimal effect on fuel consumption is chosen using gasoline and defines SOI_1 for the proceeding split-injection tests.

5.2.1.1 Effect on Engine Performance and Efficiency

The effect of varying the single-pulse SOI timing on IMEP and VE is shown using gasoline in Figure 5.2. The SOI timing window of 360-180°$bTDC_{comb}$ was chosen in order to highlight the positive impact of charge-cooling during the intake stroke (IVO/IVC = 376/126°$bTDC_{comb}$ shown in Figure 5.1). The record of SOI at 30CAD intervals allows the inclusion of TDC, BDC and mid-way through the stroke when the piston speed is close to its greatest, as used by Yang (Yang, 1998). As shown in Figure 5.2a, the peak IMEP occurs around the point of maximum piston speed. Here, the IMEP reaches 9.36bar, which is 5.8% more than the baseline PFI result (8.85bar IMEP). This increase is due to the spray ‘chasing’ the piston, which minimises fuel impingement on the piston crown and increases the fuel

conversion efficiency. This might be coupled with increased in-cylinder tumble flow, which is believed to contribute to reduced piston impingement (Serras-Pereira, 2007a).

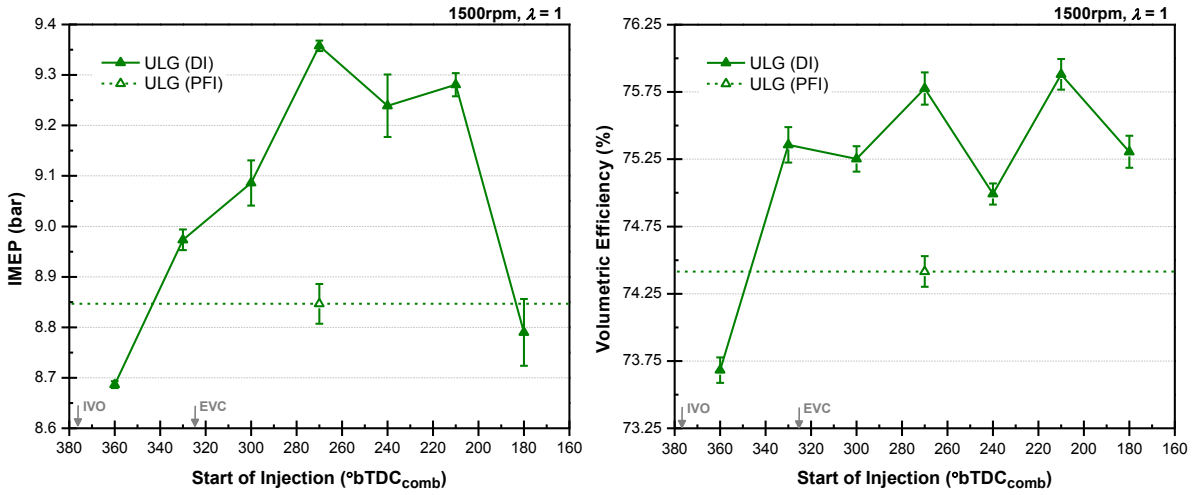

Figure 5.2 Effect of SOI on IMEP (a) and VE (b) using GDI and PFI at WOT

The effect of SOI timing on VE is shown in Figure 5.2b. Here, the VE is relatively low despite being at WOT. This is due to the low engine speed (1500rpm), flow loses in the throttle (which still contribute even when fully open) and the sub-optimal IVO timing. Nevertheless, the peak VE using DI is higher than PFI due to the cooling effect (raising the charge density) and the higher partial pressures because the air is not replaced with fuel. The loss of VE (and reduced IMEP) with early injection (360°bTDC$_{comb}$) is believed to be more likely attributed to the high penetration rate causing piston impingement and loss of cooling (Fry, 1999), rather than earlier heat transfer from the walls to the cooled charge (Yang, 1998). With later SOI timings, the VE fluctuates within 75.4±0.45%, with peaks at 270 and 210°bTDC$_{comb}$. Although there is a marginal loss in VE with SOI timing at 270°bTDC$_{comb}$ compared to 210°bTDC$_{comb}$ (0.1%), the IMEP is 0.8% higher. When considering the fuel consumption in Figure 5.13a (which is directly related to CO_2 emissions), it will be proven that 270°bTDC$_{comb}$ offers the most favourable overall performance.

5.2.1.2 Effect on Knock-Limited Spark Advance

The increased KLSA timing using PFI (6°bTDC$_{comb}$) is shown in Figure 5.3 along with the duration from EOI to KLSA timing (CAD$_{EOI-SPK}$).

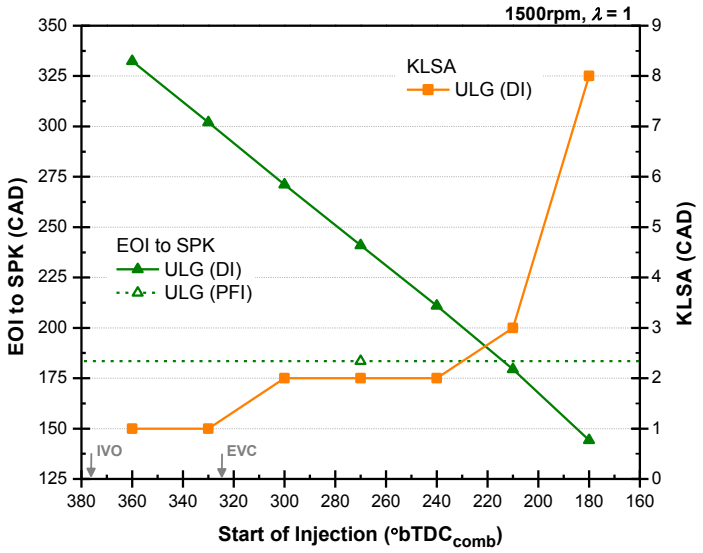

Figure 5.3 Effect of SOI on KLSA and CAD$_{EOI-SPK}$ using GDI and PFI at WOT

KLSA increases with delayed SOI timings due increased charge-cooling. This reduces the ignition temperature (T_{ign}) and suppresses knock (Figure 5.4).

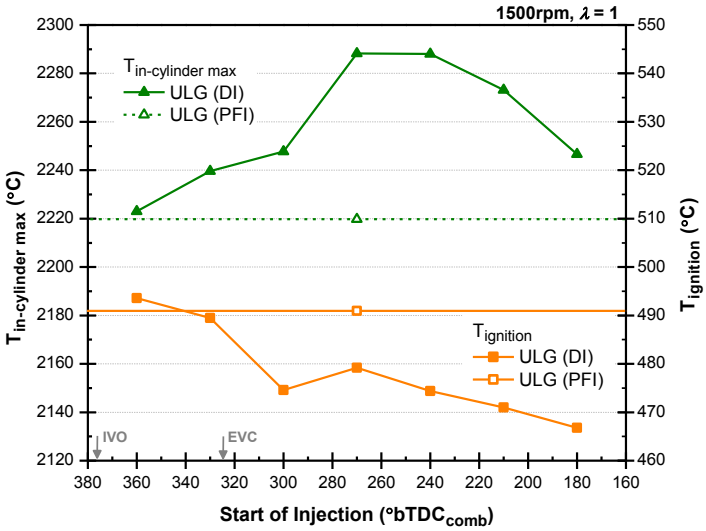

Figure 5.4 Effect of SOI on T_{max} and T_{ign} using GDI and PFI at WOT

Earlier SOI timings reduce the charge-cooling but increase wall heat transfer. This raises T_{ign} (Figure 5.4), limiting the KLSA (Yang, 1998) but increasing T_{max}.

5.2.1.3 Effect on In-Cylinder Pressure

This varying knock suppression tendency affects P_{max} and its location (θP_{max}) (Figure 5.5).

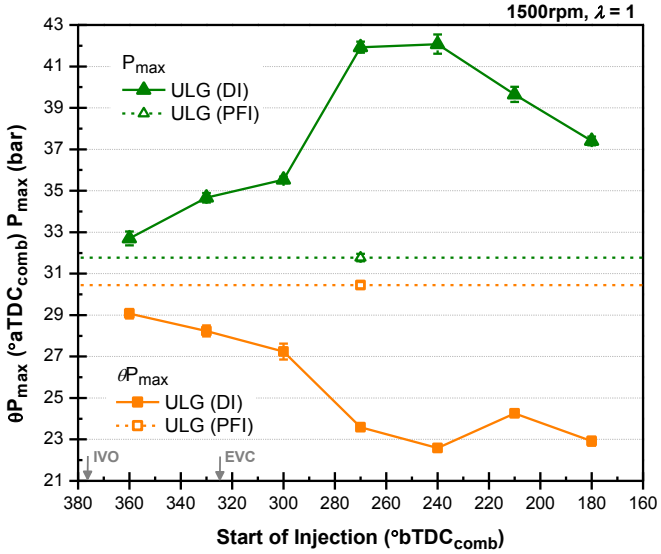

Figure 5.5 Effect of SOI on P_{max} and θP_{max} using GDI and PFI at WOT

In general, θP_{max} decreases with delayed SOI timings because the combustion phasing is advanced (increased KLSA). However, the effect of KLSA on P_{max} is only proportional until 240°bTDC$_{comb}$. After this, P_{max} begins to decrease because CAD$_{EOI\text{-}SPK}$ decreases (Figure 5.3). This effect is also reflected in the increase in combustion initiation duration, or CID, and CAD$_{10\text{-}90}$, as shown in Figure 5.6. The CAD$_{EOI\text{-}SPK}$ reduction, coupled with the cooler charge (Figure 5.4) compromises the quality of the mixture preparation and therefore the combustion performance (Figure 5.2a). However, once again, the best performance (lowest durations) is seen at SOI timings of 270 and 240°bTDC$_{comb}$.

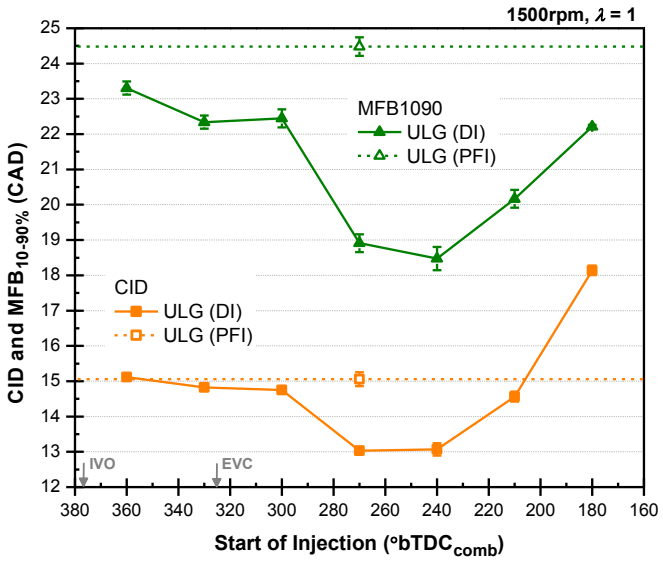

Figure 5.6 Effect of SOI on CID and $CAD_{10\text{-}90}$ using GDI and PFI at WOT

In summary, the optimum injection timing occurs close to the lowest CID and $CAD_{10\text{-}90}$, and highest P_{max}. This is because the KLSA increases due to charge-cooling, which increases VE. Earlier or later SOI timings result in reduced KLSA or $CAD_{EOI\text{-}SPK}$ respectively, which compromises IMEP. This behaviour can be correlated to the results with ethanol and DMF.

5.2.2 Ethanol and DMF

In this section, the effect of the single-pulse SOI timings on the performance of ethanol and DMF is compared to the previous gasoline results in Section 5.2. As with gasoline, these effects were observed at WOT using optimum spark timings at stoichiometry (λ=1). Firstly, the effects of SOI on IMEP and VE are examined.

5.2.2.1 Effect on Engine Performance and Efficiency

The variation of IMEP with SOI timing is shown in absolute and relative terms in Figure 5.7.

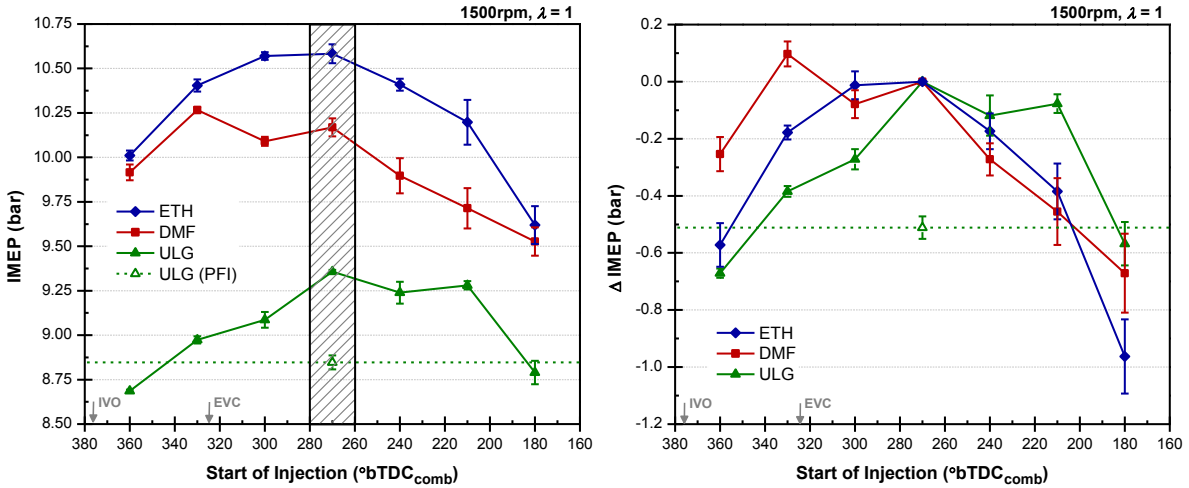

Figure 5.7 Effect of SOI on Absolute (a) and Normalised (b) IMEP at WOT

The difference in maximum IMEP between the fuels in Figure 5.7a is due to the varying AFR_{stoich}, OI and ΔH_{vap} (Table 3.8). Ethanol and DMF contain an oxygen molecule, so have a lower AFR_{stoich} compared to gasoline. This also helps to increase the OI and ΔH_{vap}. The lower AFR_{stoich} demands more mass specific fuel for a similar VAF rate at λ=1. This, coupled with greater KLSA results in increased IMEP over gasoline at WOT.

The effect on IMEP with delayed SOI is also different between fuels. This is clearly shown in Figure 5.7b, using the change in IMEP (ΔIMEP) either side of 270°$bTDC_{comb}$.

When using ethanol, the ΔIMEP with SOI timing is symmetrical either side of the maximum (10.58bar) between 300°$bTDC_{comb}$ and 270°$bTDC_{comb.}$ However, for DMF and gasoline the trend is asymmetric about the respective peaks (10.27bar and 9.36bar, respectively) with opposing locations. For DMF, the peak IMEP location tends towards an earlier SOI timing (330°$bTDC_{comb}$) than with gasoline and the peak for ethanol resides between the two. Earlier SOI timings increase the mixture preparation time before combustion, which improves the vaporization. This is essential in order to combat the lower vapour pressures of DMF and

ethanol compared to gasoline (Table 3.8). Gasoline fuel droplets vaporize more easily and so later SOI timings are sufficient. This is highlighted by the ΔIMEP between the fuels at 210°bTDC$_{comb}$. When using DMF and ethanol the IMEP drops by 0.5 and 0.4bar respectively (compared to the maximum), which is at least 0.3bar more than with gasoline. Conversely, the greater IMEP decrease at early SOI for gasoline is due to retarded spark timings.

As with gasoline in Section 5.2, DI gives charge-cooling benefits over PFI which can greatly affect VE. This advantage depends on the fuel properties, as shown in Figure 5.8.

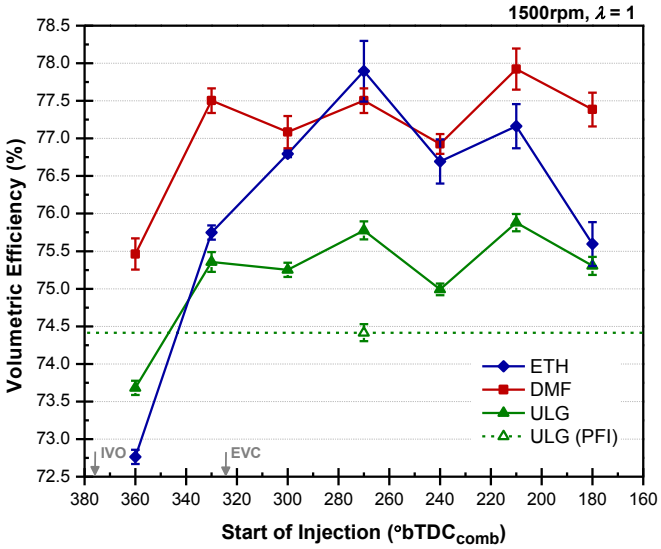

Figure 5.8 Effect of SOI on VE at WOT

For gasoline, the maximum VE (75.9%, SOI: 210°bTDC$_{comb}$) is lower than for ethanol (77.9%, SOI: 210°bTDC$_{comb}$) and DMF (77.9%, SOI: 270°bTDC$_{comb}$) due to the lower ΔH_{vap} and reduced charge-cooling effect (Table 3.8). Ethanol has the greatest sensitivity of VE to SOI timing. The VE range across the SOI window for DMF and gasoline is 2.5% and 2.2% respectively, whereas for ethanol this is 5.1%. The greater influence of charge-cooling when using ethanol implies the SOI timing is a more critical parameter.

The lower VE with all fuels at early SOI timing (360°bTDC$_{comb}$) is due to fuel impingement on the piston crown and poor optimisation due to sub-optimal valve timing. Interestingly, the maximum VE and IMEP do not always occur at the same SOI timing (Yang, 1998). This is clear with DMF, where the peak IMEP and VE are 120CAD apart. However, unlike ethanol, between 330 and 180°bTDC$_{comb}$, the VE is stable when using DMF and gasoline, which suggests that the different SOI timings for maximum IMEP and VE is less critical.

As with gasoline (Section 5.2), delayed SOI timings allow the spark timing to be advanced with ethanol and DMF (Figure 5.9), although DMF was hindered by knock.

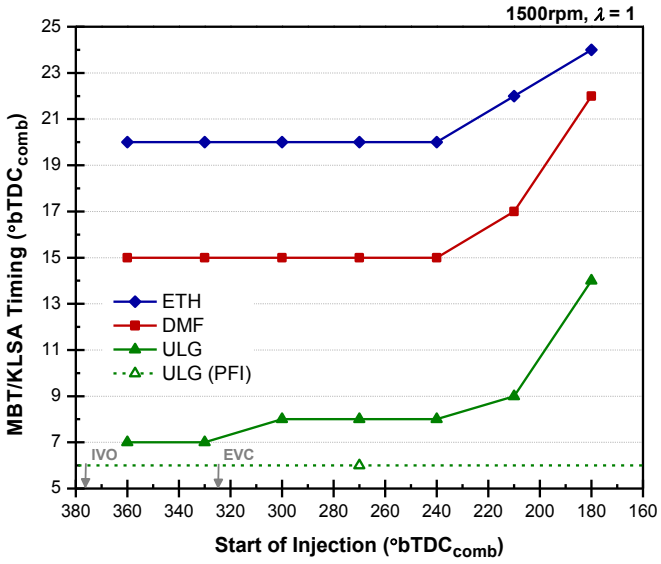

Figure 5.9 Effect of SOI on Ignition timing at WOT

When using ethanol, no knock occurs so the MBT timing is always found. Later SOI timings improve the knock resistance, albeit with no IMEP improvement. Earlier SOI timings have no effect on spark timing with ethanol and DMF. However, with gasoline the spark is retarded. The maintained spark advance when using DMF and ethanol with early SOI timings (due to their higher OI) explains why the IMEP remains high compared to gasoline.

5.2.2.2 Effect on In-Cylinder Pressure and Temperature

These variations in spark timing are largely due to the effects of charge-cooling, which are best shown in Figure 5.10a using T_{ign} as calculated in WAVE (Section 3.6.6.1). With all three fuels, T_{ign} decreases as SOI is delayed which helps to reduce the onset of knock and advance spark timing (due to ΔH_{vap}). The order of T_{ign} between fuels directly correlates to the order of their spark advance (Figure 5.9). In turn, this spark advance lowers the CID until the SOI timings are delayed to 240°bTDC$_{comb}$, shown in Figure 5.10b. After 240°bTDC, the spark timing is over-advanced, which produces an increase in CID and no benefits in IMEP (except with gasoline at 210°bTDC).

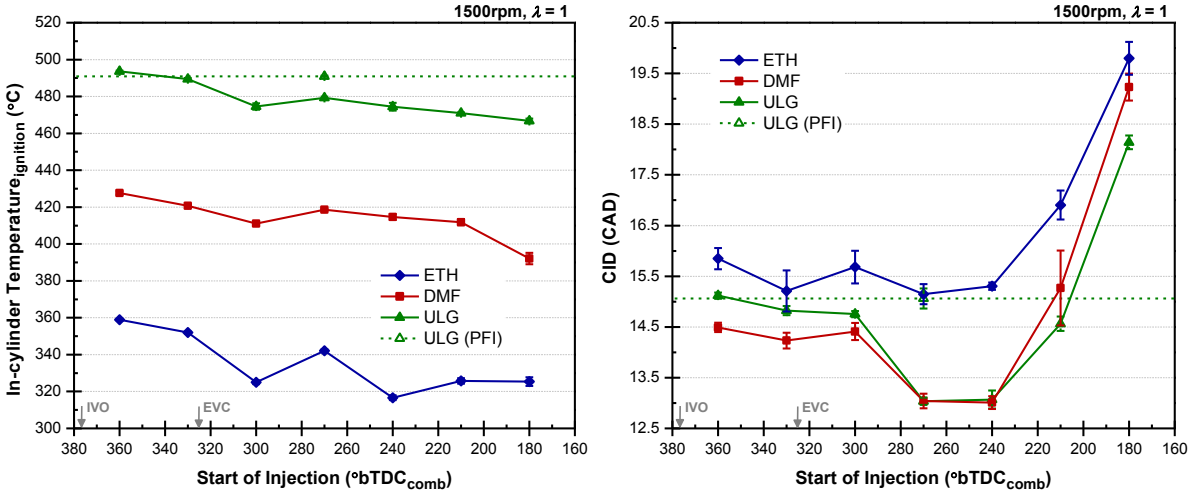

Figure 5.10 Effect of SOI on T_{ign} (a) and CID (b) at WOT

The high T_{ign} when using DMF and gasoline results in the lowest CID of 13CAD at an SOI of 270°bTDC$_{comb}$. For ethanol, the CID is at least 2CAD higher and similar to gasoline in PFI due to the low T_{ign} seen in Figure 5.10a. Nevertheless, T_{max} when using ethanol increases towards that with gasoline, as shown in Figure 5.11a. This, together with its high burning velocity, lowers the CAD$_{10\text{-}90}$ of ethanol to that seen with DMF (Figure 5.11b).

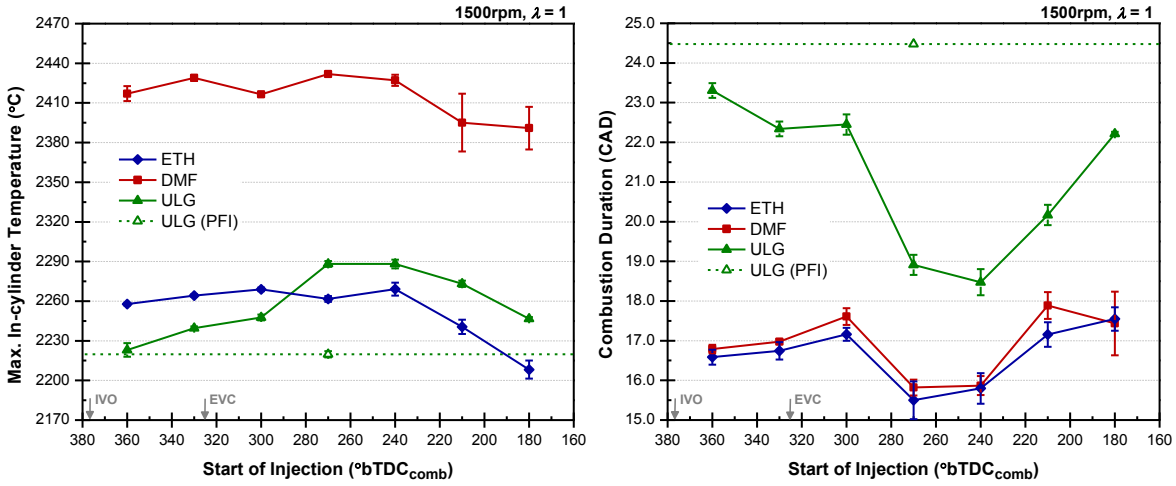

Figure 5.11 Effect of SOI on T_{max} (a) and $CAD_{10\text{-}90}$ (b) at WOT

For all fuels, the lowest $CAD_{10\text{-}90}$ exists between an SOI of 270 and 240°bTDC$_{comb}$. Unlike with gasoline, the $CAD_{10\text{-}90}$ when using ethanol and DMF is less affected by variations in SOI timing. This may be a result of the more readily available oxygen molecules.

The combustion speed of DMF is reinforced in Figure 5.12a.

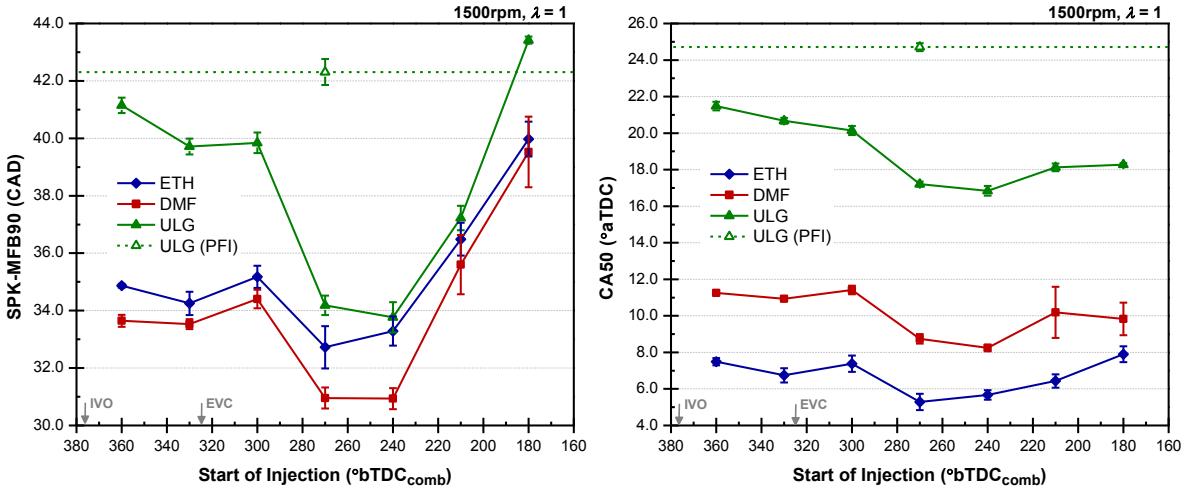

Figure 5.12 Effect of SOI on $CAD_{SPK\text{-}90}$ (a) and CA50 (b) at WOT

With varying SOI timing, the total combustion duration (CAD from ignition to 90% MFB, or $CAD_{SPK\text{-}90}$) with DMF is lower than with ethanol, which is in turn lower than gasoline. This

is highlighted by CA50 for DMF in Figure 5.12b. From 360 to 240°bTDC$_{comb}$, the difference in spark timing between DMF and ethanol is 5CAD (Figure 5.9). However, the CA50 varies between 2.5 and 4.2CAD. This highlights the low duration of spark timing to CA50 with DMF compared to ethanol. However, CAD$_{50\text{-}90}$ with ethanol is then similar if not lower, which helps to produce similar CAD$_{SPK\text{-}90}$ to DMF (Figure 5.12a). Therefore, it seems that T_{ign} slows the combustion with ethanol, but as the temperature rises, the combustion speed of ethanol increases. As mentioned, ethanol is unhindered by knock and so the MBT timing is used. This results in CA50 values around 8°aTDC, a recognized value of MBT (Zhu, 2007).

5.2.2.3 Effect on Fuel and Combustion Efficiency

The effect of SOI timing on the volumetric ISFC and combustion efficiency between the fuels is shown in Figure 5.13.

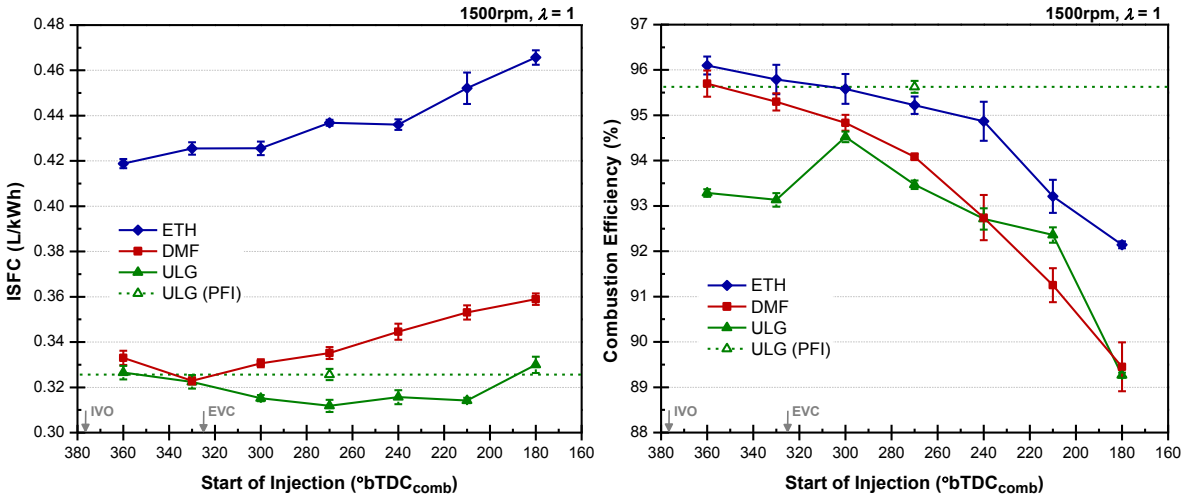

Figure 5.13 Effect of SOI on ISFC (a) and Combustion Efficiency (b) at WOT

In both instances, the optimum for ethanol and DMF are obtained at early SOI, between 330 and 360°bTDC$_{comb}$, for ISFC and combustion efficiency, respectively. However, for gasoline

this is 60CAD later, between 270 and 300°bTDC$_{comb}$. This is largely due to the improved mixture preparation, as earlier SOI allows more time for vaporization, helping to combat the low vapour pressure of ethanol and DMF (Table 3.8). This effect is very prominent when using DMF at 330°bTDC$_{comb}$. Here, the ISFC is similar to that with gasoline in DI and PFI and represents the benefits in fuel rate over ethanol. At this point, DMF is almost 25% more fuel efficient than ethanol, whilst maintaining similar combustion efficiency (Figure 5.13b).

Clearly, the variation of SOI timing during the inlet valve opening period strongly affects the IMEP. For ethanol, the effect of charge-cooling plays the greatest role in this variation, whereas for DMF it is the mixture preparation and vaporization time. The optimum SOI timing in terms of fuel efficiency and IMEP for DMF (270°bTDCcomb) and arguably ethanol (300°bTDCcomb) are slightly earlier than with gasoline. Nevertheless, in the WOT split-injection work, the first SOI timing is fixed at the optimum for gasoline (270°bTDCcomb) so that the effect of the second SOI timing on the performance and emissions can be isolated.

5.3 Effect of Split-Injection at Full Load

Once the single-pulse SOI timing sweeps were performed for each fuel, the increase of IMEP was analysed. The optimum SOI timing (highest IMEP) when using gasoline was then chosen as the first SOI timing (SOI_1) for the split-injection work. The second SOI timing (SOI_2) was then varied from 240°bTDC$_{comb}$ (induction stroke) to 90°bTDC$_{comb}$ (compression stroke) in 30CAD intervals (Figure 5.1). The majority of SOI_2 timings were during the IVO phase, apart from 120 and 90°bTDC$_{comb}$ (IVC: 126°bTDC$_{comb}$). Two split-injection pulse-width ratios, 1:1 and 2:1 (SOI_1:SOI_2) were employed. Similarly, to the single-pulse SOI

sweeps, PFI and DI baseline points were recorded for comparison. Once again, the tests were performed at λ=1 and 1500rpm, where the spark timing was advanced to find the respective MBT or KLSA timings. The tests for both the single-pulse and split-injection timing tests were performed over three consecutive days in order to minimise the effect of ambient conditions and engine drift, as recommended by leading engine researchers (Beck, 2006).

Split-injection strategies have long been used to increase high-load torque output above that of equivalent single-pulse injections (Yang, 1998). This mode also improves air entrainment, fuel evaporation and vapour diffusion, and reduces the fuel impingement on in-cylinder surfaces (Serras-Pereira, 2007a, Li, 2005). Some studies have shown the behaviour with gasoline can be correlated to ethanol (Mittal, 2010), but little is known about the behaviour with DMF. Therefore, this section compares the performance and emissions of DMF to gasoline and ethanol using two split-ratios with varying SOI_2 timing (240 to 90°bTDC$_{comb}$).

In the following plots, the 1:1 (SOI_1:SOI_2) split-ratio results are shown using filled markers whereas the 2:1 results use unfilled ones. The single-pulse SOI (270°bTDC$_{comb}$) results using each fuel in DI are shown using dash-dot lines. Once again, the same colour scheme is used for each fuel. Error bars are omitted for clarity.

Firstly, a discussion of the effect on IMEP and VE is made.

5.3.1 Engine Performance and Efficiency

The effect of the split-injection strategies on IMEP when using the fuels is shown in Figure 5.14. The behaviour with gasoline helps to explain that with DMF. Clearly, with gasoline, the 2:1 split-ratio produces the most consistent increase in IMEP across the entire SOI_2

timing sweep. This increase is, on average, 1.2% (≈0.11bar) higher than the single-pulse SOI timing case. The 1:1 ratio only achieves an IMEP increase over single-pulse SOI at 240 and 210°bTDC$_{comb}$, which is similar to the 2:1 ratio. This widened SOI_2 window under the 2:1 ratio presents options for output tuning (e.g. ISFC, CO_2) whilst maintaining superior IMEP. The IMEP increase could be attributed to the reduced fuel impingement with SOI_2 which improves fuel droplet evaporation and mixture preparation. This effect is reduced (piston impingement is more likely) as SOI_2 enters the compression stroke, especially at 90°bTDC$_{comb}$. Nevertheless, the in-cylinder pressure will increase at this point, helping to reduce the spray penetration.

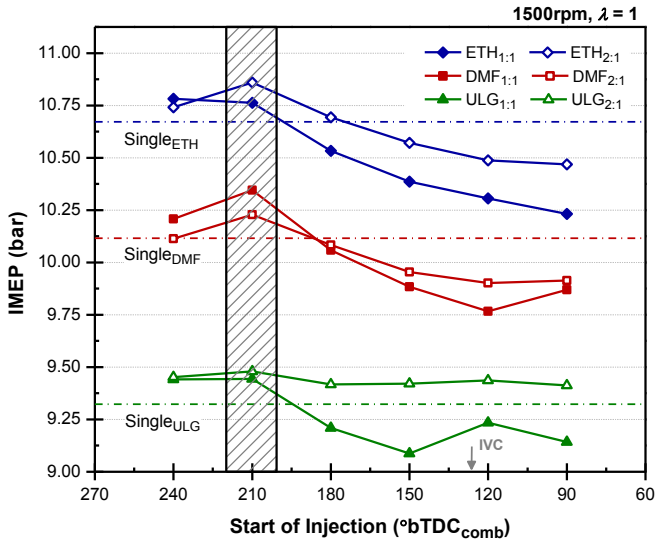

Figure 5.14 Effect of SOI_2 with Split Ratio on IMEP

For the two biofuels, the advantage of split-injection is less consistent with SOI_2. Despite increases in IMEP for both ratios and fuels at earlier SOI_2 (240 and 210°bTDC$_{comb}$), later SOI_2 is detrimental to performance. These reductions could be explained by the reduced fuel vaporization time, which is more necessary for fuels with lower vapour pressures and high boiling points (Table 3.8). For ethanol, it is clear that the 2:1 ratio produces higher IMEP

with SOI_2. However, for DMF the advantage of 2:1 is lost at 240 and 210°$bTDC_{comb}$. In spray characteristic studies, DMF is shown to have a higher penetration length (under quiescent and atmospheric initial conditions) than ethanol and gasoline (Tian, 2010b). Reducing the SOI_1 pulse-width using a 1:1 split-ratio reduces the piston impingement on the SOI_1 timing with DMF. However, as experienced with ethanol and gasoline, the 1:1 ratio results in increased piston impingement with SOI_2 because the pulse-width increases relative to 2:1. Nevertheless, the largest increase in IMEP between all fuels is seen with DMF (2.3%, or 0.23bar) using the 1:1 ratio and SOI_2 at 210°$bTDC_{comb}$. In fact, this early SOI_2 homogeneous split-injection strategy is the most effective means to raise IMEP for gasoline (IMEP increases by 1.7%) and ethanol (IMEP increases by 1.8%) albeit with a 2:1 split-ratio.

The comprehensive studies by Serras-Pereira et al. show how the split-injection strategy reduces piston crown and wall impingement (Serras-Pereira, 2007a, Serras-Pereira, 2007b, Serras-Pereira, 2008). During cold engine operation, the effect of split-injection (20°C) was as effective as raising the engine temperature to 90°C for the single-pulse strategy (Serras-Pereira, 2007b). This reduced impingement affects the air entrainment and is shown in Figure 5.15 using VE.

For all fuels, the 2:1 ratio generally produces higher VEs than 1:1, which is sometimes higher than the baseline single-pulse SOI. This is due to the charge-cooling effect of DI. The increase in VE with 2:1 over 1:1 is due to more heat transfer with the intake air, whereby the 1:1 ratio is compounded by lower fuel impingement. For DMF (and partially for gasoline and ethanol when SOI_2 is between 240-180°$bTDC_{comb}$), the 2:1 strategy consistently raises VE above that with the single-pulse case (average: 0.2%). The spray droplet size with DMF is also lower than with ethanol and gasoline (Tian, 2010b). Therefore, the lower amount of

fuel injected in SOI_1 produces more optimum charge-cooling as more heat can be transferred to the intake charge rather than metal surfaces. Also, when using DMF, VE is less sensitive to variations in SOI (Figure 5.8).

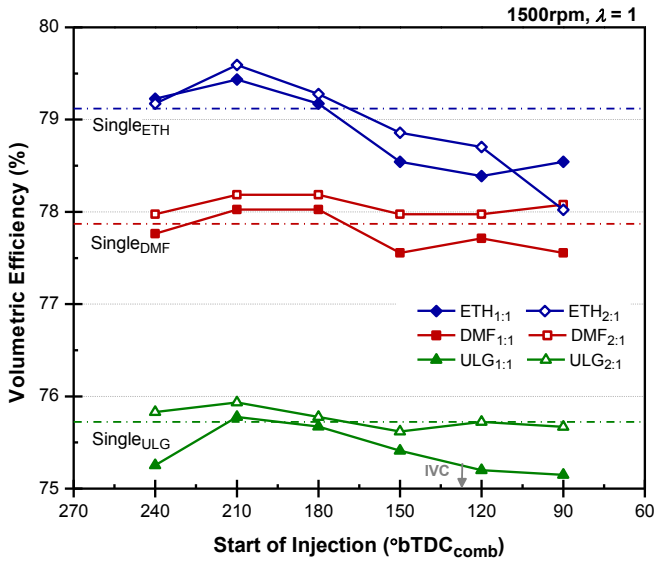

Figure 5.15 Effect of SOI_2 with Split Ratio on VE

5.3.2 Mass Fraction Burned

Although the split-injection strategy increases VE, and therefore induces more charge-air, the IMEP increase is not consistent. In order to understand this irregularity, the MFB is investigated. This is achieved using scatter plots showing the change in $CAD_{10\text{-}90}$ (from single-pulse SOI), or $\Delta CAD_{10\text{-}90}$ (total and both halves), and ΔCID with respect to ΔIMEP, for each fuel. The SOI_2 timings are not shown, but can be linked to ΔIMEP with Figure 5.14.

The $\Delta CAD_{10\text{-}90}$ and ΔIMEP show an inversely proportional relationship in Figure 5.16, irrespective of the fuel or split-injection strategy; as $\Delta CAD_{10\text{-}90}$ decreases, ΔIMEP increases. This explains the decrease in IMEP for the 2:1 strategy using DMF, despite the increase in VE over the single-pulse case. Although there is more charge air (therefore more potential

energy), the $CAD_{10\text{-}90}$ increases due to shortened mixing time. Conversely, with gasoline the mixture preparation is improved and $CAD_{10\text{-}90}$ reduces, which increases the IMEP. It is also clear that the 1:1 ratio increases $\Delta CAD_{10\text{-}90}$, which subsequently inhibits performance.

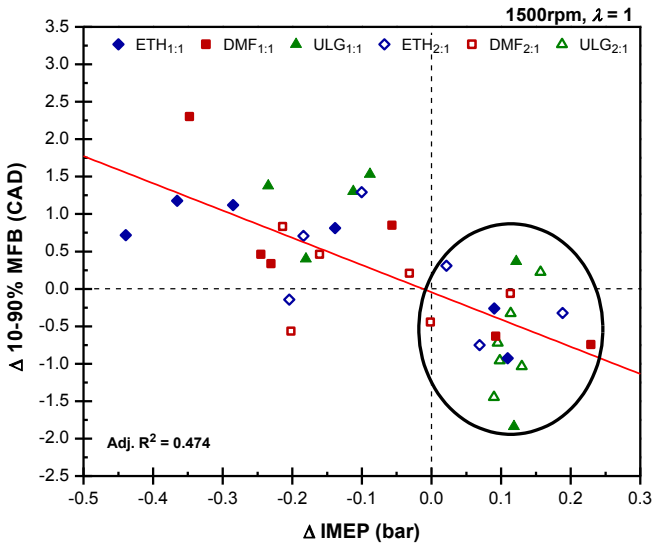

Figure 5.16 Effect of SOI_2 with Split Ratio on $\Delta CAD_{10\text{-}90}$ and ΔIMEP

When analysing the two halves of $CAD_{10\text{-}90}$, the effect of the combustion process on ΔIMEP can be better explained, as shown in Figure 5.17 and Figure 5.18.

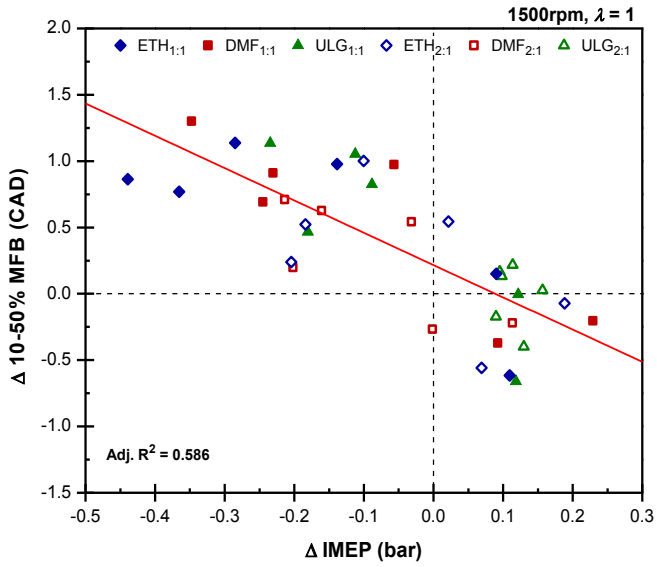

Figure 5.17 Effect of SOI_2 with Split Ratio on $\Delta CAD_{10\text{-}50}$ and ΔIMEP

It appears that there is a more consistent link between ΔIMEP and $\Delta CAD_{10\text{-}50}$ than with the $\Delta CAD_{50\text{-}90}$. As with $\Delta CAD_{10\text{-}90}$, increases in IMEP are seen when $\Delta CAD_{10\text{-}50}$ is negative. However, this is not the case for $\Delta CAD_{50\text{-}90}$ in Figure 5.18.

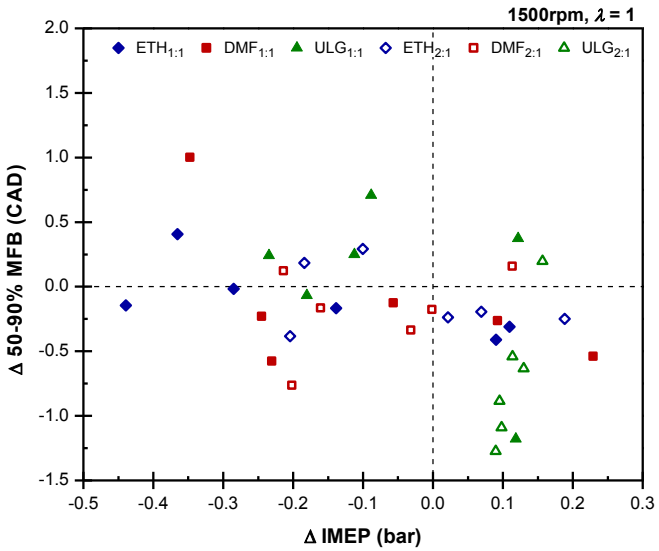

Figure 5.18 Effect of SOI_2 with Split Ratio on $\Delta CAD_{50\text{-}90}$ and ΔIMEP

More often than not, split-injection produces negative $\Delta CAD_{50\text{-}90}$ even when the IMEP is reduced, so the relationship is less clear. The reduced $CAD_{10\text{-}50}$ and $CAD_{10\text{-}90}$ with split-injection is due to increased vapour diffusion compared to single-pulse SOI, which improves the mixture preparation and results in faster burn rates. This creates a greater fluctuation of $\Delta CAD_{10\text{-}90}$ with ΔIMEP and shows that the relationship between $\Delta CAD_{10\text{-}50}$ and ΔIMEP is stronger (also shown by the higher adjusted R^2 value).

As observed with the single-pulse injections (Figure 5.10b), a decrease in ΔCID tends to increase ΔIMEP with split-injection, shown in Figure 5.19. The difference in ΔCID between the ratios is due to increased knock resistance of the 1:1 split-ratio, shown in Figure 5.20.

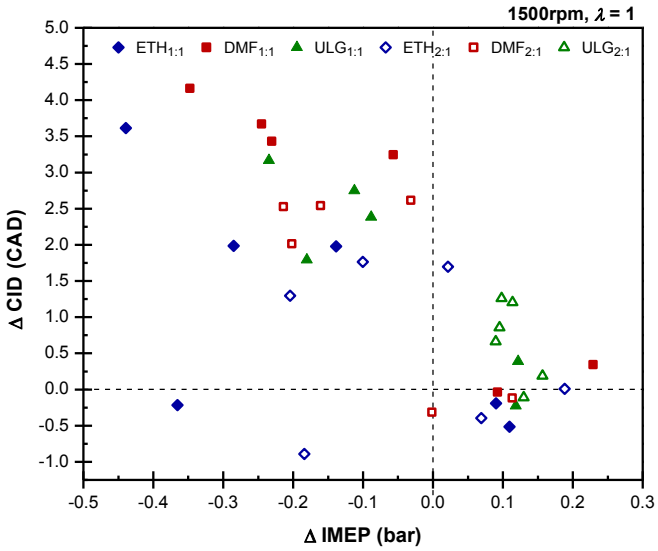

Figure 5.19 Effect of SOI_2 with Split Ratio on ΔCID and ΔIMEP

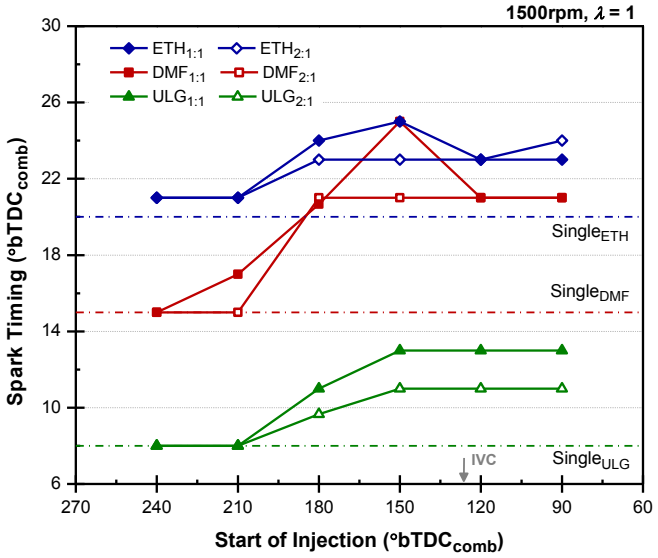

Figure 5.20 Effect of SOI_2 with Split Ratio on Spark Timing

For gasoline, the 1:1 ratio results in 2CAD KLSA compared to 2:1 when SOI_2 is between 150-90°$bTDC_{comb}$. This advances the combustion event towards a period of larger cylinder volume (lower pressure and temperature), which compromises CID and so $\Delta CAD_{10\text{-}90}$ increases. Although there is a divide between the two ratios with ethanol and DMF, the 1:1 ratio lowers KLSA compared to gasoline. The biofuels require more mixing time than

gasoline and so partial stratification is less beneficial. Nevertheless, it is important to assess these differences on consumer-related parameters like combustion stability and ISFC.

5.3.3 Combustion Stability and Efficiency

The combustion stabilities and ISFCs are shown in Figure 5.21 and Figure 5.22, respectively.

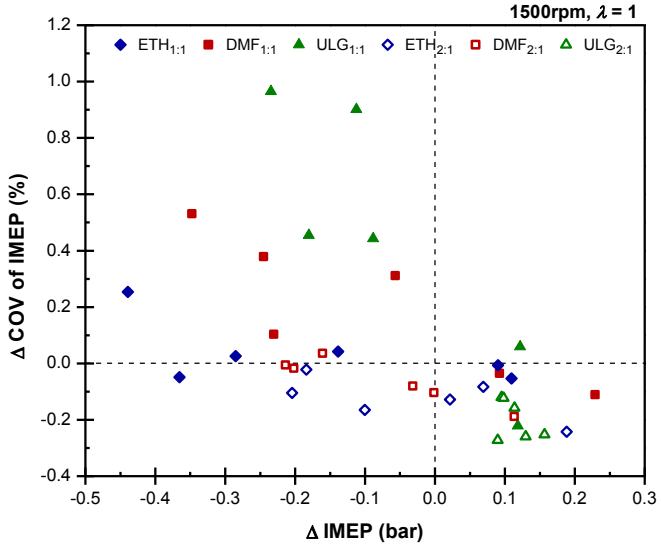

Figure 5.21 Effect of SOI_2 with Split Ratio on ΔCOV of IMEP and ΔIMEP

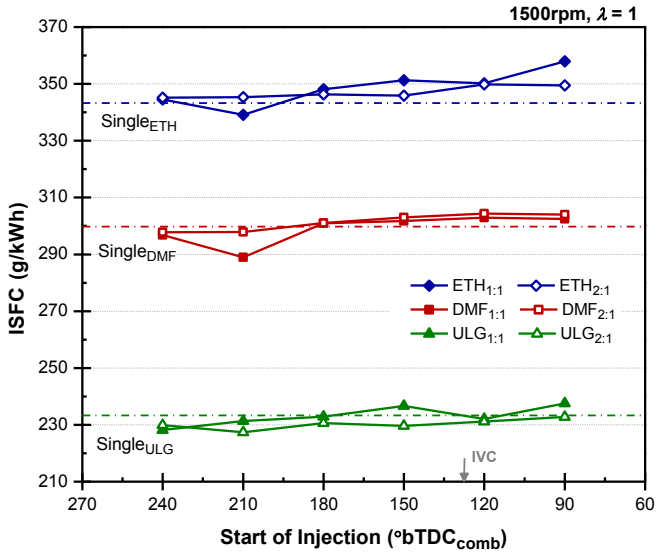

Figure 5.22 Effect of SOI_2 with Split Ratio on Volumetric ISFC

There are clear benefits in stability with the 2:1 ratio (COV of IMEP decreases). Also, ISFC decreases below the equivalent WOT single-pulse case. However, for ethanol and DMF, split-injection is less effective at converting fuel energy into useful work and reducing ISFC. With the exception of 210°bTDC$_{comb}$, SOI$_2$ timings result in an increase in ISFC. The later SOI$_2$ becomes, the greater the ISFC increase. The reduced mixing time allows less fuel droplets to vaporize and then diffuse, so the completeness of combustion is compromised.

This behaviour is reinforced in Figure 5.23 using the combustion efficiencies.

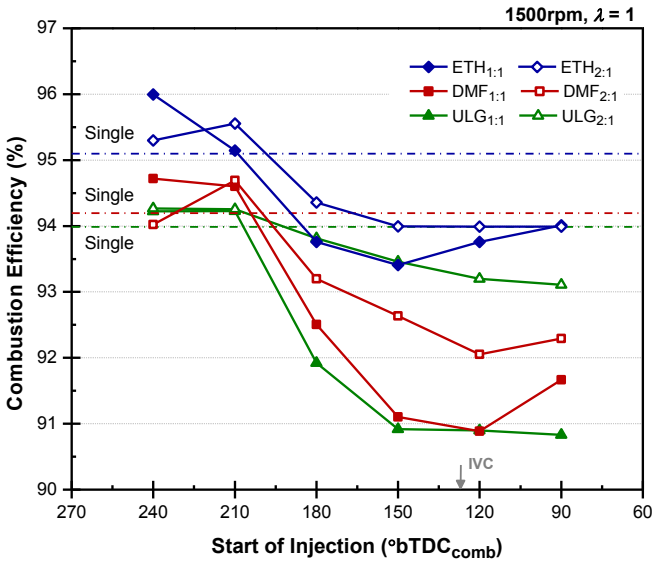

Figure 5.23 Effect of SOI$_2$ with Split Ratio on Combustion Efficiency

With SOI$_2$ timings at 180°bTDC$_{comb}$ or later, the combustion efficiency is reduced. Between the two ratios, a lower compromise is seen using 2:1. This is clearer with gasoline as the combustion efficiency at 90°bTDC$_{comb}$ (SOI$_2$) is 2.3% higher than with 1:1. However the difference is lower with ethanol and DMF at the same SOI$_2$ timing. This suggests that when using the biofuels in split-injection, a greater split-ratio (favouring SOI$_2$), or more injections would help to improve vaporization and avoid piston wetting as such high loads.

5.3.4 Gaseous Emissions

The engine-out emissions are compared between the fuels at the two split-ratios and various SOI_2 timings. Firstly, the traditional legislated emissions are evaluated (NO_x, HC and CO), which is followed by the CO_2 analysis.

5.3.4.1 Nitrous Oxide Emissions

Figure 5.24 shows the production of $isNO_x$ for all test conditions.

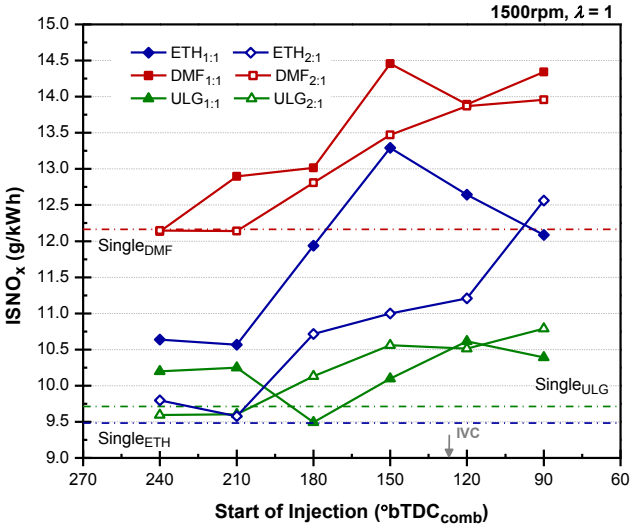

Figure 5.24 Effect of SOI_2 with Split Ratio $isNO_x$ Emissions

Compared to the single-pulse cases, the only competitive SOI_2 timings are at earlier timings (240°$bTDC_{comb}$ and 210°$bTDC_{comb}$). Later SOI_2 timings result in dramatic increases in $isNO_x$ emissions, because the charge-cooling effect is reduced and so the in-cylinder temperature is likely to rise (Stone, 1999). This is coupled by the advance in spark timing, which increases P_{max}. Between the split-ratios, it is the 2:1 ratio that produces the lowest $isNO_x$ emissions for the biofuels (there is little difference with gasoline). For ethanol and DMF, the largest difference between the two split-injections occurs at an SOI_2 timing of 150°$bTDC_{comb}$. This

rise is due to the increase in spark advance at this point, as shown in Figure 5.20 and highlights the sensitivity of isNO_x to spark timing. As a result, the decrease in combustion efficiency (Figure 5.23) when using ethanol and DMF is also very high (compared to the 1:1 split-ratio case).

5.3.4.2 Hydrocarbon Emissions

The isHC are shown in Figure 5.24. Despite the reduced sensitivity of the FID analyser to oxygenated fuels (Cheng, 1998, Wallner, 2008), suggesting the HC emissions are higher for ethanol and DMF, the data in this work is used to see trends in isHC emissions. As shown in Figure 5.25, the isHC emission rise with later SOI_2, as seen with isNO_x (Figure 5.24).

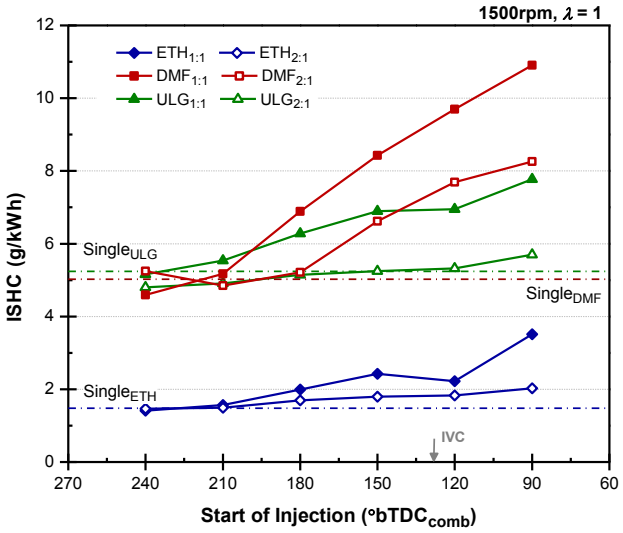

Figure 5.25 Effect of SOI_2 with Split Ratio on isHC Emissions

However, this time the increase is consistently lower with the 2:1 split-ratios for all fuels (exception 240°bTDC_{comb} for ethanol and DMF). At 210°bTDC_{comb}, the isHC emissions are competitive with the single-pulse SOI. Nevertheless, it appears that DMF is more sensitive to later SOI_2 timings as the rise is higher. For instance, at the least favourable SOI_2 timing

(90°bTDC$_{comb}$), the increase in isHC from single-pulse SOI is ≤0.5g/kWh with ethanol and gasoline when using the more favourable 2:1 split-ratio. However, when using DMF, this increases to 3.2g/kWh. This is due to the poor fuel droplet vaporization, which leads to localized pockets of fuel-rich mixtures and more incomplete combustion. The higher oxygen content of ethanol compared to DMF (Table 3.8), together with its higher combustion efficiency (Figure 5.23) aids the oxidation of unburned HCs, as oxygen is more readily available.

5.3.4.3 Carbon Monoxide Emissions

The isCO emissions are shown in Figure 5.26.

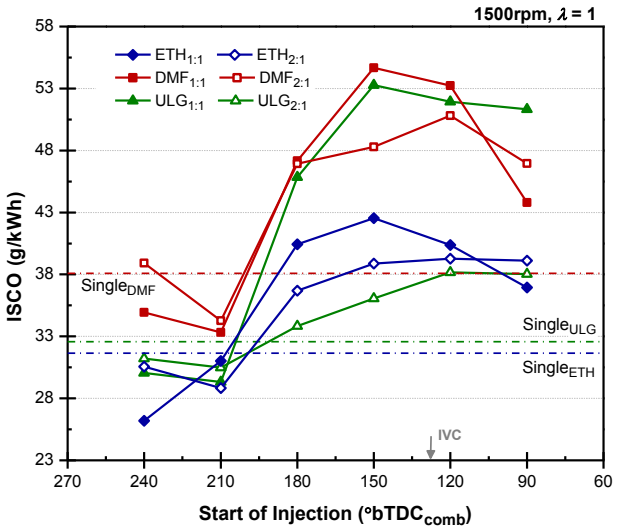

Figure 5.26 Effect of SOI$_2$ with Split Ratio on isCO Emissions

Once again, an SOI$_2$ of 210°bTDC$_{comb}$ provides the greatest reductions in isCO emissions due to improved vaporization and reduced wetting. The 1:1 split-ratio is less beneficial, especially for gasoline, possibly due to higher piston impingement as shown with the later SOI$_2$ timings. Between the two oxygenated fuels, ethanol consistently produces the lowest

isCO emissions due to higher combustion efficiencies (Figure 5.23). For DMF, the mixture may be more inhomogeneous, resulting in localized pockets of fuel-rich mixture (due to fuel impingement) and more incomplete combustion.

5.3.4.4 Carbon Dioxide Emissions

Similarly, to the results with isNO_x, isHC and isCO, the isCO_2 production using the 1:1 split-ratio is the most sensitive to variations in SOI_2 (Figure 5.27).

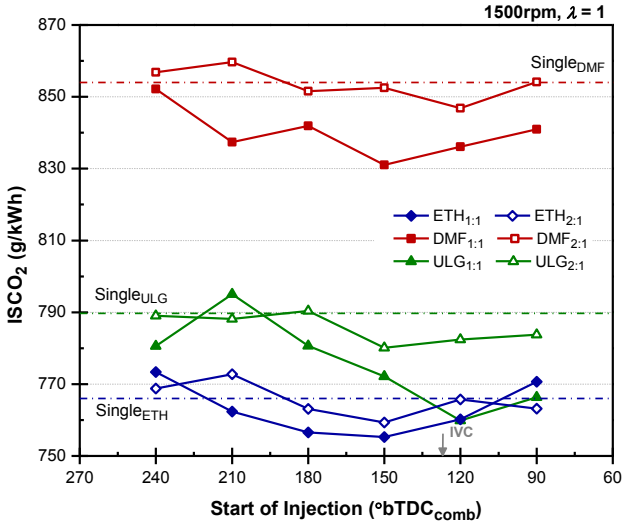

Figure 5.27 Effect of SOI_2 with Split Ratio isCO_2 Emissions

However, in contrast, this sensitivity has a positive effect. The lower charge-cooling effect with the 1:1 split-ratio reduces VE, shown in Figure 5.15. This reduces the amount of oxygen available for combustion and so reduces the total available to be converted into CO_2.

The isCO_2 production is an indicator of the completeness of combustion. Therefore, as the 1:1 split-ratio produces lower combustion efficiencies than 2:1 (Figure 5.23), the isCO_2 production decreases. Nevertheless, isCO_2 for ethanol and DMF are competitive to gasoline. Although DMF produces more isCO_2 than when using gasoline, it does have the added

benefit of consuming CO_2 during its production (similarly to ethanol). Therefore, it is possibly fairer to compare the relative lifecycle CO_2 emissions.

5.3.4.5 Combined Emissions

A summary of the change in total regulated emissions ($isNO_x$, isHC and isCO) for the different operating cases is shown in Figure 5.28. In general, when ΔIMEP is positive, the total emissions compared to the single-pulse SOI decreases with each fuel. The exception occurs with gasoline when using SOI_2 timings later than 210°$bTDC_{comb}$, due to poorer vaporization.

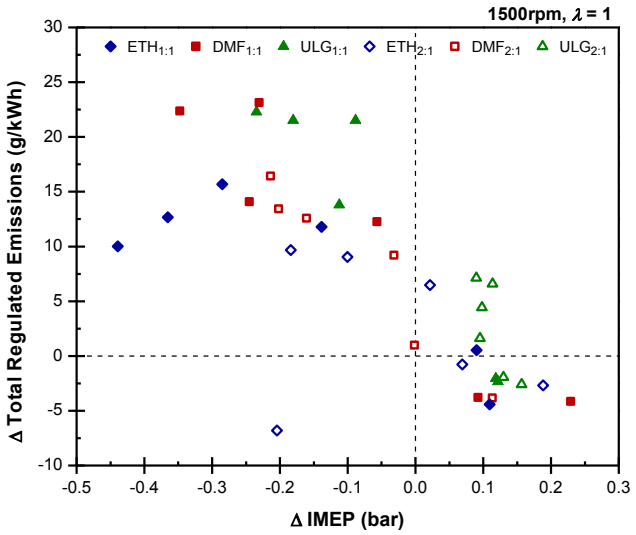

Figure 5.28 Effect of SOI_2 with Split Ratio on Total Emissions ($isNO_x$ + isHC + isCO)

5.4 Summary

This study investigates the split-injection technique for improving full-load torque with ethanol and DMF. Overall, these experiments suggest that split-injection can improve the combustion performance when using DMF and ethanol. However, maximum gains are found with multiple pulses or greater ratios (favouring SOI_1) by improving vaporization.

For the fuels, the ascending order of maximum IMEP with varying single-pulse SOI was: PFI gasoline (8.9bar), DI gasoline (9.4bar), DMF (10.3bar) and ethanol (10.6bar). Between the fuels, this order reflects the increase in OI and decrease in AFR_{stoich} due to increased oxygen content. The maximum with ethanol is due to optimal ignition timing as knock is avoided. In addition, the effect of charge-cooling helps to raise the maximum IMEP because VE and KLSA increase.

Early single-pulse SOI timing produces the highest IMEP when fuelled with DMF and, to a lesser extent, ethanol (maximum IMEP at 330 and 270°$bTDC_{comb,}$ respectively). However, later injections give rise to greater IMEPs when using gasoline.

Improvements with split-injection are lower with the biofuels and are sensitive to SOI_2 timing. IMEP increases up to 2.3% however, were found when using SOI_2 timings of 240 and 210°$bTDC_{comb}$ due to improved vaporisation and reduced wetting. The increase in IMEP with split-injection compared to single-pulse SOI is due to the decrease in $CAD_{10\text{-}50}$, which helps to lower $CAD_{10\text{-}90}$.

Compared to single-pulse SOI, there are NO_x, HC and CO emissions benefits with split-injection. This is typical at early SOI_2 timings and a 2:1 split-ratio when using ethanol and DMF. For CO_2 reduction, the 1:1 split-ratio is more effective.

CHAPTER 6

DUAL-INJECTION AS A KNOCK MITIGATION METHOD

This chapter examines the effect of the novel dual-injection strategy as a knock-mitigation technique for PFI gasoline using ethanol and methanol.

6.1 Introduction

As well as advanced injection modes using DI, this work examines the suitability of injection concepts such as dual-injection. This concept explores the combination of two injection modes (PFI and DI), whilst allowing the flexibility of on-line blending with little hardware modification. The use of dual-injection has been explored by Toyota, Ford and Audi, and the synergistic combustion has also been seen in CI engines (Section 2.2.5).

Dual-injection can be used as a knock mitigation tool. However, it is important to first understand the differences in combustion between PFI and homogeneous DI (DI_{hom}). This understanding is gained using gasoline only. However, when using ethanol and methanol, the knock with gasoline in PFI is mitigated due to the higher ΔH_{vap} and OI of the lower alcohols.

On an energy basis, methanol is more effective than ethanol; lower methanol fractions are required for the same load as a consequence of the higher ΔH_{vap}. However, the higher energy density of ethanol results in lower ISFC and CO_2 emissions. These results are contrary to the simulations by EBS, who predicted that half the amount of methanol is required compared to E85 to reach borderline knock, despite the 30% energy density deficiency (Blumberg, 2008). This is due to the higher OI and ΔH_{vap} of methanol.

6.2 Effect of PFI compared to DI

In his detailed technical review, Zhao emphasized the growing presence of DI in modern engines due to the influence of SOI timing (Zhao, 2002). However, when employing early SOI timing (DI_{hom}), PFI retains some clear advantages. The differences in performance between PFI and DI_{hom} are shown using gasoline in Figure 6.1 and Figure 6.2.

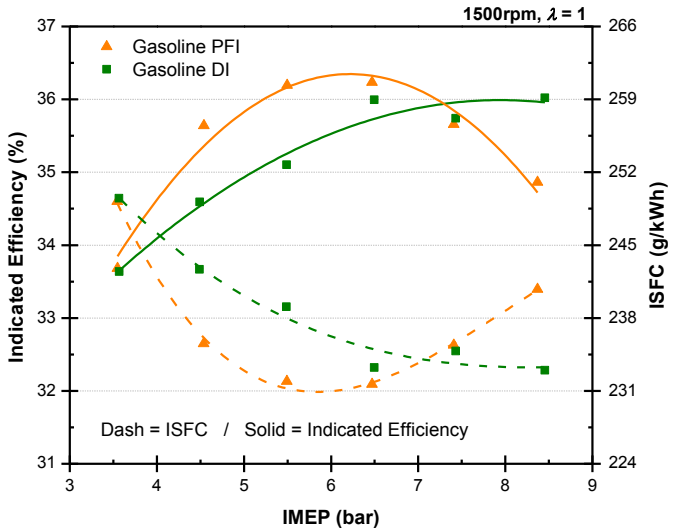

Figure 6.1 Indicated Efficiency and Gravimetric ISFC using PFI and GDI

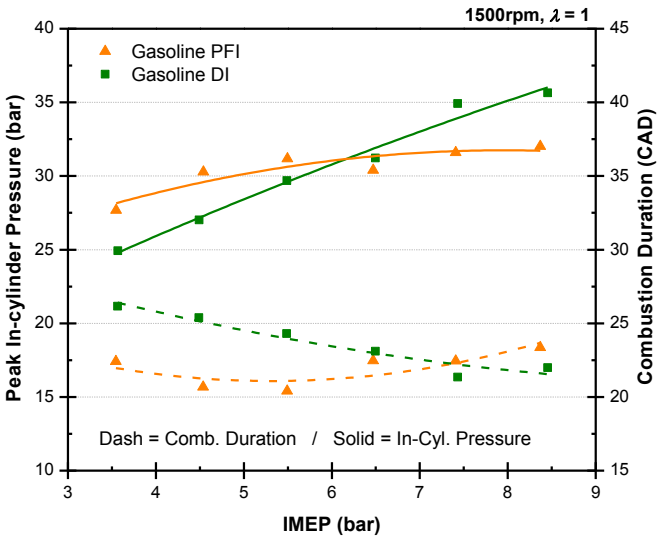

Figure 6.2 P_{max} and $CAD_{10\text{-}90}$ using PFI and GDI

At 3.5bar IMEP, the differences in efficiency between PFI and DI_{hom} are negligible (Figure 6.1). However, the efficiencies separate with increasing load. Although part-load efficiency benefits of PFI are greater than DI_{hom}, stratification of DI (late SOI timing) would increase efficiency by eliminating pumping work. Nevertheless, DI_{hom} is used as a baseline in this study due to its simplicity to control over DI stratification.

At 7bar IMEP, the two modes cross and PFI is superseded by DI_{hom}. Until this point, PFI generates greater indicated efficiencies and lower ISFC due to higher P_{max}. This lowers the $CAD_{10\text{-}90}$ (Figure 6.2). Above 7bar IMEP, the benefits of charge-cooling are apparent with DI_{hom}. The spark timing can be advanced due to greater knock suppression, which results in higher P_{max} and lower $CAD_{10\text{-}90}$ (as seen with PFI below 7bar IMEP). For PFI at high load, the benefits of lower throttling losses are offset by the increased knocking susceptibility. The advantage in indicated efficiency for PFI and DI_{hom} at their peaks (6bar and 8.5bar respectively) is 1%. Although the efficiency for DI_{hom} increases with load, PFI rises and falls with a higher gradient almost symmetrically about 6bar IMEP. The decrease in indicated efficiency from 6.5bar to 8.4bar IMEP is 1.3% and, in terms of ISFC, is 9.9g/kWh.

In summary, the difference in efficiency with load is primarily due to charge-cooling with DI_{hom}. When using PFI, the fuel evaporation event is much earlier (increasing homogeneity) and is caused by intake manifold wall and valve wetting. This reduces the cooling on the intake air as the heat is transferred elsewhere thus generating higher P_{max} and T_{max} than an equivalent DI_{hom} system. This increased physical intensity reduces the $CAD_{10\text{-}90}$ and thus increases efficiency. Although when using DI_{hom}, the charge-cooling is detrimental at low loads, at higher loads, it helps to suppress knock and allows the spark timing to be advanced. This in turn increases the combustion pressure and resulting efficiency.

Clearly, each mode is mutually exclusive. However, the theory of dual-injection allows the benefits of the two injection modes to be combined to maintain a high efficiency across a wide load range.

Firstly, the behaviour of dual-injection is briefly analysed with gasoline. This highlights the fundamental operation of dual-injection and serves as preliminary work to the analysis using ethanol and methanol in Section 6.4.

6.3 Effect of Dual-Injection using Gasoline

Indicated efficiency improvements have been shown with gasoline dual-injection over PFI and DI_{hom} by up to 1.5% at medium intake manifold pressure, or 0.8bar (≈ 6.5bar IMEP), when the DI mass fraction was between 20-60% (Wu, 2011a). However, in these tests, the spark timing was not optimised and only 3 load points were taken. Therefore, this work uses MBT/KLSA timings and various loads to directly compare dual-injection to PFI and DI_{hom} using gasoline.

In this work, dual-injection is defined at all times as the combination of PFI and DI. This approach allows the DI component to be introduced into the premixed PFI mixture in order to suppress the knock with PFI and attempt to reach the MBT/KLSA timing of 100% DI. This technique has been used by Toyota (Ikoma, 2006), Ford (Stein, 2009) and recently Audi (Wurms, 2011).

The spark timings achieved with DI knock mitigation are shown in Figure 6.3 between 4.5-8.5bar IMEP. The KLSA of dual-injection at high loads (7.5bar and 8.5bar IMEP) is 1CAD retarded from DI. Nevertheless, when using dual-injection for the lower loads (4.5-6.5bar

IMEP) the KLSA of DI was achieved. As the load increases, DI is more beneficial than PFI and dual-injection because of greater charge-cooling with DI alone.

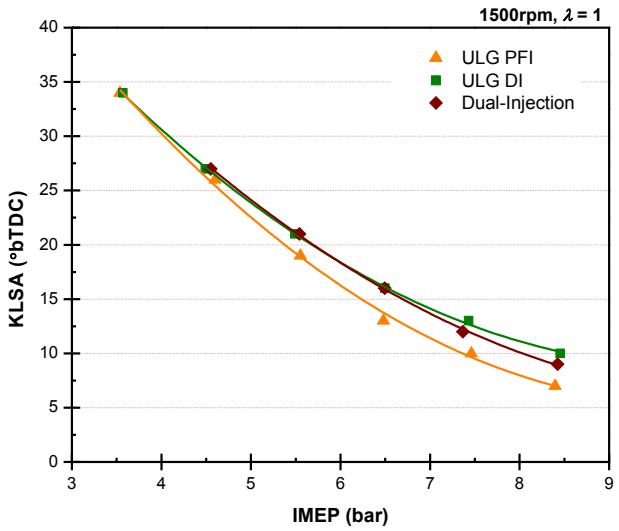

Figure 6.3 MBT/KLSA Timings for PFI, GDI and Gasoline Dual-Injection

The required mass fractions of DI in dual-injection are shown in Figure 6.4.

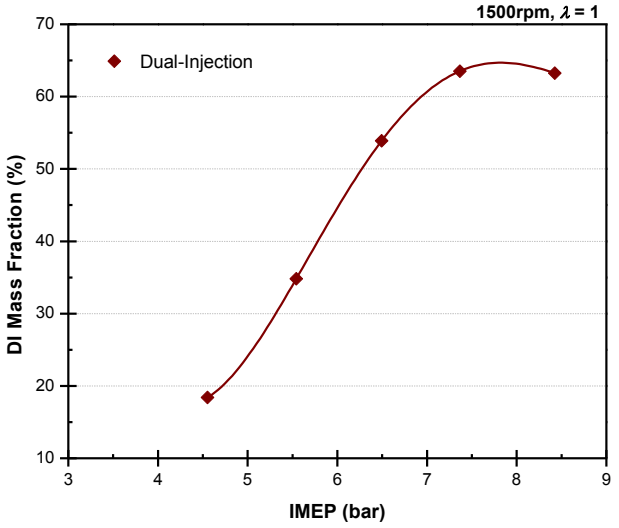

Figure 6.4 Mass fraction of GDI using Dual-Injection

The plateau around 63% between 7.5-8.5bar IMEP is due to the minimum PFI injector duration (2ms, 9.5mg/cycle). Higher DI fuel fractions were required at 7.5bar IMEP and

above, the PFI injector was unable to deliver less fuel. Therefore, the highest DI mass fraction was 63%. However, at 4.5bar IMEP, the minimum DI injector is also limited and the minimum fraction is 18%. This results in potentially more DI fuel than is required to raise KLSA by 1CAD. The knock suppression superiority of DI is due to the charge–cooling effect. This helps to reduce T_{ign} and increases KLSA. At 5.5bar IMEP, only a low DI fraction (35%) is needed to raise KLSA by 3CAD, which is the same increase as for 6.5bar IMEP (however, 54% is required in this case). This highlights the effectiveness of DI knock mitigation for PFI.

The effect of increasing KLSA with dual-injection over PFI is the increase in P_{max} and T_{max}, as shown in Figure 6.5a.

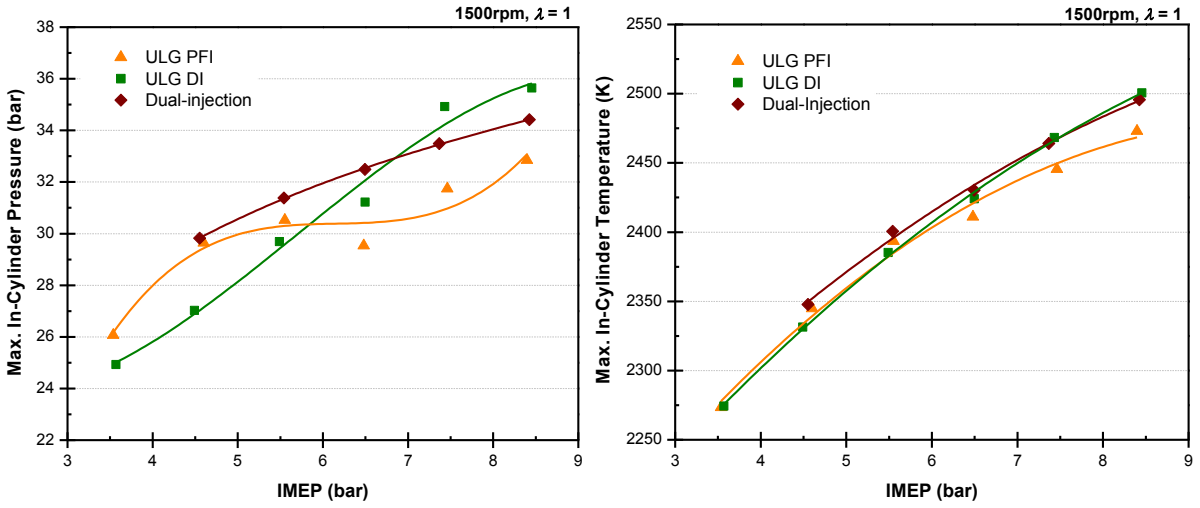

Figure 6.5 P_{max} (a) and T_{max} (b) for PFI, GDI and Gasoline Dual-Injection

Therefore, earlier spark timings contribute to higher P_{max}. PFI combustion consistently generates higher intake temperatures than DI due to little or no charge-cooling. Therefore, at lower loads the P_{max} with dual-injection is higher than DI, despite similar KLSA timings. This is due to the increase in T_{ign} because the PFI component is more dominant below 6.5bar

IMEP (Figure 6.4b). With increasing load (>6.5bar IMEP), the KLSA decreases with dual-injection below that with DI, which decreases the P_{max}. However, between 4.5-6.5bar IMEP, the P_{max} with dual-injection is higher than both PFI and DI. This is due to the combination of increased T_{ign} due to the PFI component and increased KLSA due to the DI component.

These high pressures have a direct impact on T_{max}, as shown in Figure 6.5b. Here, for each condition, the experimental and simulated IMEP and P_{max} (and hence heat release) agree to within 99%. At 3.5bar IMEP (and marginally at 4.5bar IMEP), T_{max} for gasoline in DI is lower than that in PFI. This highlights the effect of charge-cooling on T_{max}, as well as that seen with P_{max} (Figure 6.5a). Above 5.5bar IMEP, T_{max} for DI then increases above PFI, due to the more advanced spark timing. For dual-injection, the T_{max} values reflect the trend with P_{max} (Figure 6.5a) throughout the entire load range. Again, this is due to the combination of more advanced spark timing, due to the DI component and the lowered charge-cooling effect, due to the PFI component.

The CAD_{10-90} is very closely related to the P_{max} and T_{max} and is shown in Figure 6.6.

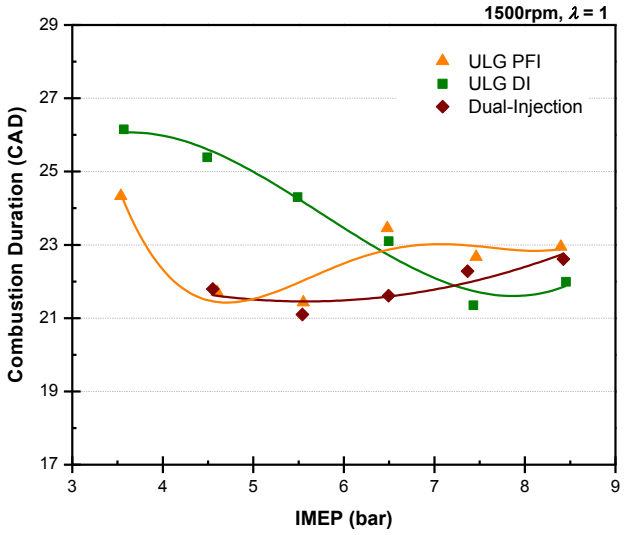

Figure 6.6 CAD_{10-90} for PFI, GDI and Gasoline Dual-Injection

In general, lower $CAD_{10\text{-}90}$ leads to higher P_{max}. Between 5-7bar IMEP, dual-injection produces lower $CAD_{10\text{-}90}$ (and thus higher P_{max}), compared to PFI and DI. For dual-injection, the PFI component helps to improve the homogeneity of the mixture, whereas the DI component cools the charge and allows the KLSA to increase. As such, dual-injection helps to overcome the reduced efficiencies of PFI and DI seen at medium loads (5.5-6.5bar IMEP).

In summary, gasoline dual-injection provides benefits in load specific regions. However, when combining this 'hybrid' injection strategy with two different fuels, greater benefits are obtained. Therefore, one of the main topics of this thesis is the effect of alcohols with high ΔH_{vap} such as ethanol and methanol in dual-injection. When injected in DI, these fuels greatly impact charge-cooling. However, their effectiveness as dual-injection fuels has hitherto been compared.

6.4 Effect of Dual-Injection using Ethanol and Methanol

For SI engines, the optimum spark timing is crucial for maximum efficiency. However, as the spark is advanced, so the propensity to knock increases, which compromises efficiency. One method to suppress knock, is to use high octane fuel additives. However, the blend ratio of these additives cannot be varied on demand. In conjunction with the advent of aggressive downsizing, new knock mitigation techniques are required.

Fortuitously, there are two well-known biofuels which exhibit attractive knock mitigation properties: ethanol and methanol. Both of these alcohols, not only have high OI, but also encourage greater charge-cooling than with gasoline. These attractive properties have been exploited in this work through the use of the dual-injection, or dual-fuel concept (gasoline

PFI and fuel additive in DI) using pure ethanol and methanol. The notation used to indicate the fuelling techniques is shown in Table 6.1.

Table 6.1 Test Notation for Alcohol Knock Mitigation

PFI Fuel	DI Fuel	MBT/KLSA	Notation
Gasoline		PFI	PFI
	Gasoline	GDI	GDI
	Ethanol	EDI	EDI
	Methanol	MDI	MDI
Dual-Injection			
Gasoline	Ethanol	EDI	G-EDI
Gasoline	Methanol	MDI	G-MDI

The MBT timings for the dual-injection cases are that for the DI fuel. Therefore, one aim of this work to compare the minimum DI fractions required to mitigate PFI and reach MBT.

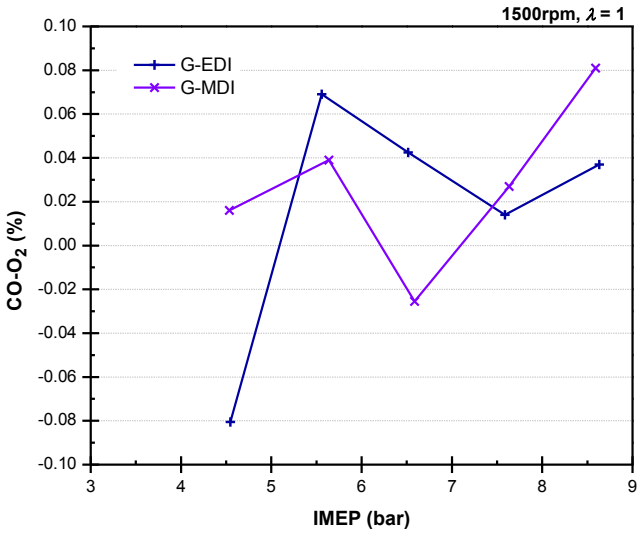

Figure 6.7 Differences between CO and O_2 Concentrations for G-EDI and G-MDI

Single component fuels with high ΔH_{vap}, like ethanol and methanol, can suppress the knock with PFI when using dual-injection. However, without knowing the exact blend composition, the cross-over of CO and O_2 is used to maintain λ=1. Previous investigations show how

stoichiometry can be controlled within 1% error (λ=1±0.01) when the difference between the CO and O_2 concentrations was within ±0.1% (Wu, 2011a). For this work, the CO and O_2 cross-over points for G-EDI and G-MDI are within this error, as disclosed in Figure 6.7.

Having accurately located stoichiometry, the minimum DI volume fractions of G-EDI and G-MDI (in order to reach MBT timing of EDI and MDI, respectively) are then calculated (Section 3.6.5.2). The results are shown in Figure 6.8a.

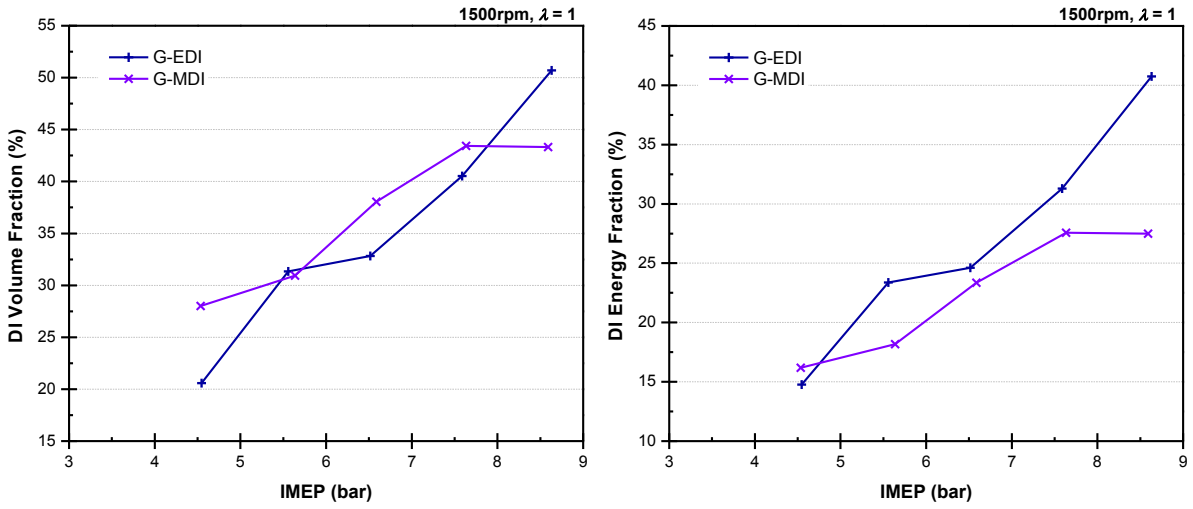

Figure 6.8 Volume (a) and Energy (b) Fractions for G-EDI and G-MDI

The DI volume fractions increase with increasing load because the need to suppress knock is greater as the spark advance from PFI increases. Both lower alcohols are very effective at suppressing knock. For instance, at 7.5bar IMEP, the minimum DI volume fractions with G-EDI and G-MDI are only 41% and 43%, respectively, whereas for gasoline dual-injection, this increased to 63% (Figure 6.4). This is compounded by greater spark advance (≥9CAD) required to reach MBT with ethanol and methanol (MBT for EDI and MDI are 21°bTDC and 22°bTDC compared to 12°bTDC with GDI; Figure 4.2). The reason why G-MDI requires greater DI volume fractions than with G-EDI at 6.5bar and 7.5bar IMEP, despite having a

greater charge-cooling effect (Table 3.8), is because the MBT timing is 1CAD earlier. However, in terms of LHV the DI volume fraction for G-EDI and G-MDI correspond to 32% and 27% of the overall alcohol-gasoline blend LHV, respectively (Figure 6.8b).

At the highest load (8.5 bar IMEP) this difference increases further; the energy fraction of G-EDI increases to 41%, whereas it remains at 27% with G-MDI. On this basis, a lower energy fraction is provided by methanol in G-MDI than is required by ethanol in G-EDI, which is a consequence of the greater ΔH_{vap} of methanol compared to ethanol (Table 3.8). At 4.5bar IMEP, the DI volume fraction with G-MDI is also higher than with G-EDI. This is because methanol has a lower LHV and so more fuel is required for the same energy input (Table 3.8). Nevertheless, the overall trend with G-EDI and G-MDI is comparable.

In addition to the control of stoichiometry, the minimum amount of lower alcohol in DI was used to reach the MBT timing of the 100% alcohol in DI, as shown in Figure 6.9a.

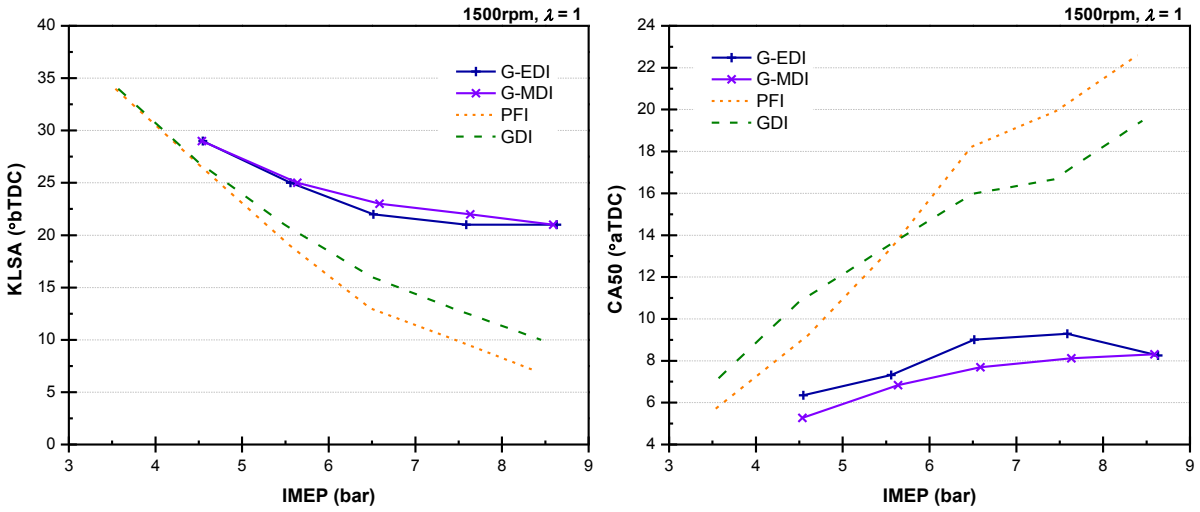

Figure 6.9 MBT/KLSA Timings (a) and CA50 (b) for G-EDI, G-MDI, PFI and GDI

This knock suppression is possible because of the improved chemical reactions (higher OI) and higher ΔH_{vap} of the alcohols (Table 3.8). At low load (3.5 bar IMEP), PFI is not limited

by knock. Therefore, G-EDI and G-MDI is not required. However, the remaining loads (4.5-8.5bar IMEP) are limited by knock when using PFI but not when using G-EDI and G-MDI.

Typically, at MBT, CA50 is between 8-10°aTDC (Zhu, 2007). These CA50 points are shown for G-EDI and G-MDI in Figure 6.9b, and are compared to PFI and GDI. The MBT timing is knock limited from 4.5bar IMEP using PFI and GDI. However, when using minimum DI volume fractions of ethanol and methanol (Figure 6.8a), the spark timings can be optimised to EDI and MDI, greatly advancing CA50. However, CA50 for G-MDI is always earlier than for G-EDI (Figure 6.9b) despite the MBT timings being similar (Figure 6.9a). This is due to the higher oxygen content of methanol (Gülder, 1982, Beeckmann, 2009, Vancoillie, 2011).

6.4.1 In-Cylinder Behaviour

As shown with gasoline dual-injection, advances in spark timing cause P_{max} to increase. For G-EDI and G-MDI, the P_{max} is shown in Figure 6.10.

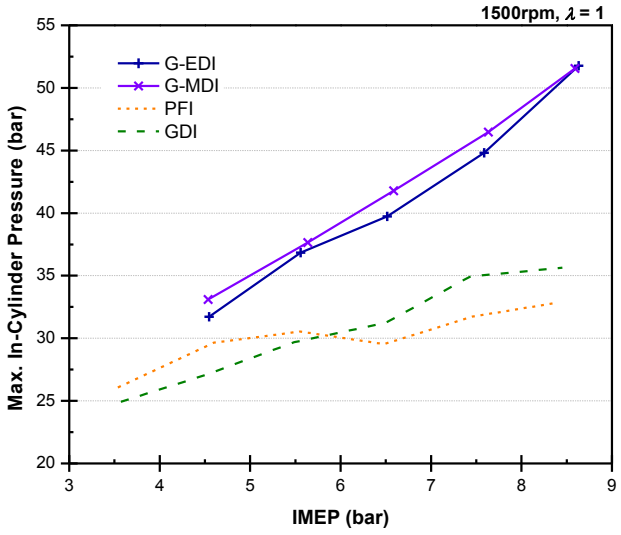

Figure 6.10 P_{max} for G-EDI, G-MDI, PFI and GDI

For each load, P_{max} is higher for G-EDI and G-MDI, than PFI and GDI. This is due to the advanced MBT timing because of greater charge-cooling when using ethanol and methanol as DI anti-knock supplements. At 8.5bar IMEP, P_{max} increases to 52bar with both lower alcohols, which is 16bar higher than GDI. As the spark is advanced from PFI the combustion process initiates (5% MFB, or CA5) before TDC (Figure 6.11a). Therefore, more of the combustion process occurs at a lower in-cylinder volume and generates higher combustion pressures. This improves the combustion rate and increases the expansion of the combustion products into useful energy. Furthermore, throughout the load range, P_{max} with G-MDI is marginally higher than G-EDI. This is due to higher combustion rates, and at some points, more advanced MBT timing (Figure 6.9a), which helps to advance CA5 (Figure 6.11a).

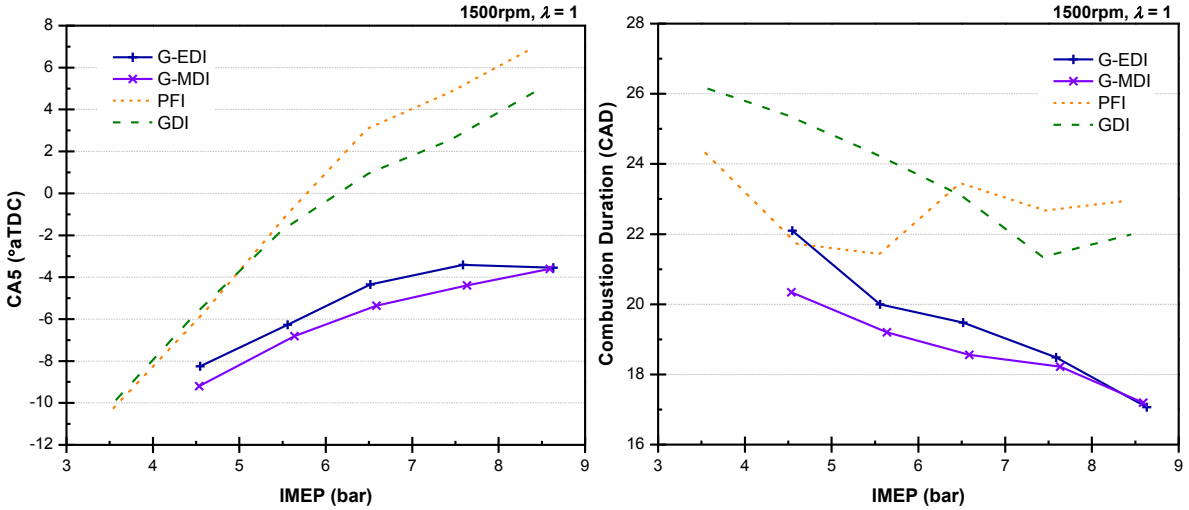

Figure 6.11 CA5 (a) and $CAD_{10\text{-}90}$ (b) for G-EDI, G-MDI, PFI and GDI

The $CAD_{10\text{-}90}$ for G-EDI and G-MDI is compared to PFI and GDI in Figure 6.11b. Clearly, the addition of these alcohols dramatically reduces $CAD_{10\text{-}90}$, which explains the increase in P_{max}. At 4.5bar IMEP, only 20% ethanol is required in G-EDI to match $CAD_{10\text{-}90}$ of PFI. As the load increases, $CAD_{10\text{-}90}$ reduces further compared to PFI and GDI. At 7.5bar IMEP, despite injecting less than 45% of the total fuel volume, the lower alcohols reduce $CAD_{10\text{-}90}$

by 3CAD over the lowest for gasoline (GDI). At 8.5bar IMEP, CAD_{10-90} when using G-EDI and G-MDI decreases by another 1CAD. This increases the separation with GDI to almost 5CAD. With G-MDI, CAD_{10-90} is lower than with G-EDI (up to 1.8CAD). This is because of the higher burning rate of methanol due to the higher oxygen content, as found by others (Gülder, 1982, Beeckmann, 2009, Vancoillie, 2011). The combustion phase of G-MDI is also more advanced than G-EDI, as shown by CA50 in Figure 6.9b. Therefore, the fuel is burned during a period of lower in-cylinder volume, which results in a higher increase in pressure (Stone, 1999, Heywood, 1988), as seen in Figure 6.10.

An explanation for this difference in effectiveness can be found by comparing CAD_{10-90} at the dual-injection with its 100% DI case, as shown in Figure 6.12.

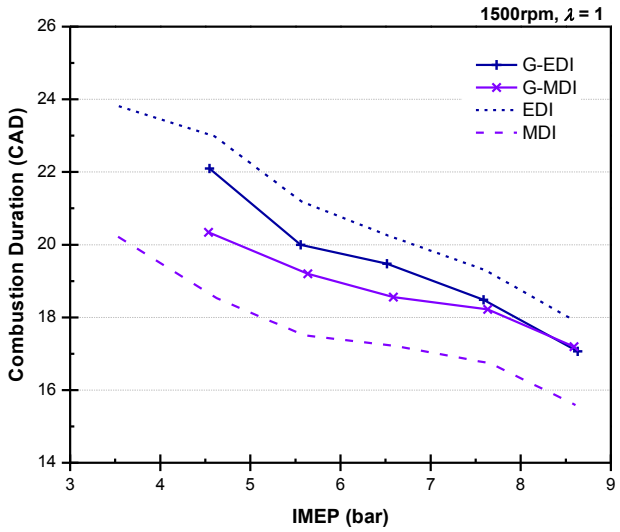

Figure 6.12 CAD_{10-90} for G-EDI, G-MDI, EDI and MDI

Here, CAD_{10-90} decreases when using G-EDI compared to EDI, whereas with G-MDI the effect is detrimental (CAD_{10-90} increases). This is possibly due to poorer in-cylinder mixing between the MDI component and PFI, especially around the spark plug region.

6.4.2 Indicated and Fuel Efficiency

The indicated efficiency and volumetric ISFC show the overall benefits of G-EDI and G-MDI in Figure 6.13 and Figure 6.14, respectively.

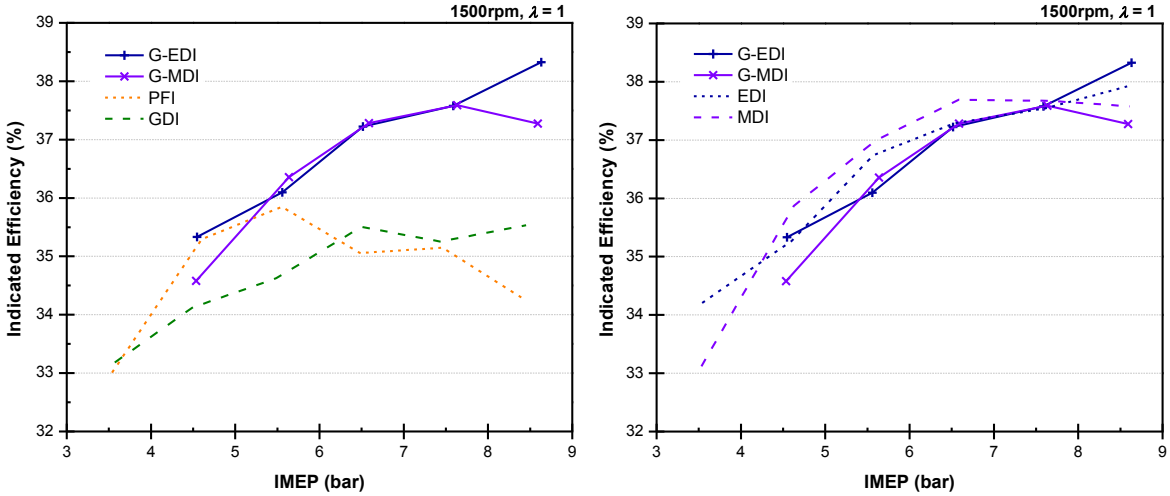

Figure 6.13 Indicated Efficiency compared to PFI and GDI (a) or EDI and MDI (b)

Although the results for G-EDI and G-MDI are comparable in Figure 6.13, there are subtle differences. For instance, up to 5.5bar IMEP, there is marginal change in indicated efficiency from PFI to G-EDI or G-MDI. However, above this load the indicated efficiency of the dual-injection cases increase similarly up to 7.5bar IMEP. At this point, the indicated efficiency of G-EDI begins to exceed that with G-MDI and reaches a maximum of 38.3% at 8.5bar IMEP, which is 1% higher than the maximum achieved with G-MDI (at 7.5bar IMEP). The decrease for G-MDI at 8.5bar IMEP may be due to the lower volume fraction of methanol compared to ethanol at this load (Figure 6.8a); the indicated efficiency of the gasoline that replaces the methanol would be lower. At this point, only 43% of methanol is required to reach MBT, whereas this increases to 51% with ethanol (Figure 6.8a). This is due to the greater charge-cooling with methanol; less fuel is required to suppress knock.

The effectiveness of G-EDI and G-MDI is better summarized by analysing the change in indicated efficiency from EDI and MDI shown in Figure 6.13b. For clarity, PFI and GDI are omitted. For the loads tested, G-EDI is closer to EDI than G-MDI is to MDI. For instance, at 4.5bar and 6.5bar IMEP, the indicated efficiency of G-EDI is equal to EDI. This is not true for methanol. At 4.5bar IMEP G-MDI is 1.3% lower than MDI and at 6.5bar IMEP it is 0.4% lower. In fact, throughout all loads, G-MDI never exceeds MDI but G-EDI exceeds EDI. For instance, at the highest load (8.5bar IMEP) G-EDI is 0.4% more than EDI, whereas the equivalent case for methanol is 0.3% less. This comparison shows how ethanol is more effective than methanol, in terms of indicated efficiency improvement.

The volumetric ISFC is shown in Figure 6.14a.

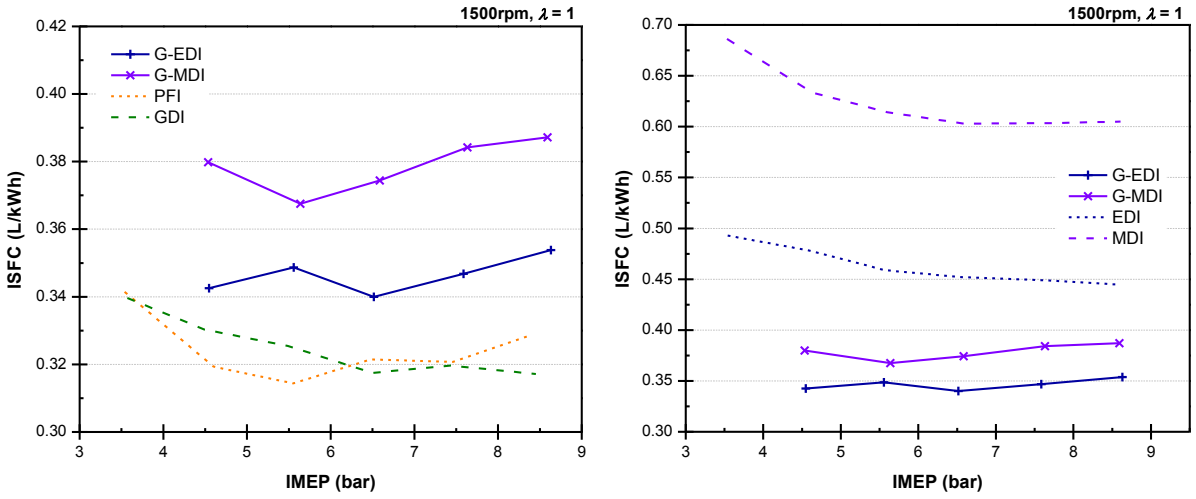

Figure 6.14 Volumetric ISFC compared to PFI and GDI (a) or EDI and MDI (b)

As the ethanol and methanol DI fractions (Figure 6.8a) and indicated efficiencies (Figure 6.13) are comparable, the difference in ISFC is due to the difference in LHV. For methanol, whose LHV is 26% lower than ethanol (Table 3.8), the ISFC increases above that with G-EDI by an average of 9.3% across the load range. At 8.5bar IMEP, the ISFC for G-EDI is

9.7% higher than GDI (the lowest for gasoline), whereas with G-MDI, this increase is over double (20.2%). Clearly, G-EDI would require less refuelling in a real-world situation than G-MDI. Although this is one measure of effectiveness, another approach is to compare the change in performance from EDI and MDI. This comparison is made in terms of volumetric ISFC in Figure 6.14b.

As opposed to the indicated efficiency, methanol is more effective than ethanol, as the decrease in ISFC is greater when switching from 100% DI to dual-injection. For instance, at 8.5bar IMEP, the ISFC with methanol decreases by 36% from MDI to G-MDI, compared to 20% with the ethanol equivalent. This larger drop in ISFC is due to the higher cooling with methanol. This is shown in Figure 6.15 using the pumping mean effective pressure (PMEP).

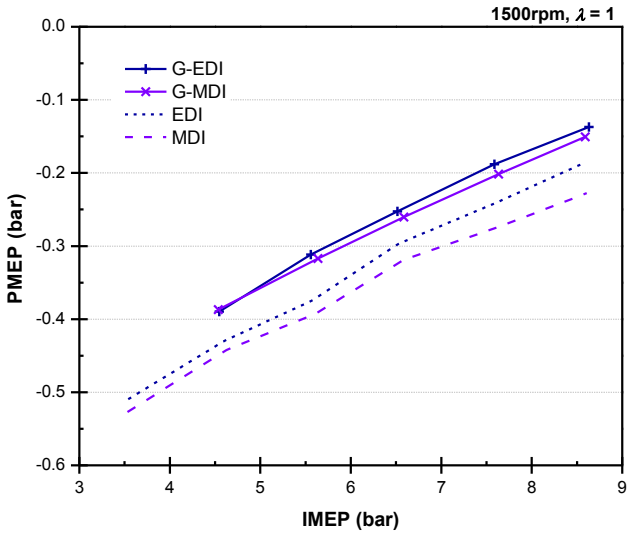

Figure 6.15 PMEP for G-EDI, G-MDI, EDI and MDI

Here, the PMEP changes more with methanol than ethanol when using dual-injection. This is due to the larger increase in AFR_{stoich} with G-MDI blends from MDI. For instance, at 8.5bar IMEP, the AFR_{stoich} of G-MDI blend is 10.9 which is 68% higher than the AFR_{stoich} of methanol (6.47). For G-EDI, the AFR_{stoich} is 11.6, only 29% higher than ethanol (8.95).

Clearly, the increase in AFR_{stoich} requires less throttling and therefore results in lower pumping losses.

6.4.3 Gaseous Emissions

The engine-out emissions of PFI and GDI are compared to G-EDI and G-MDI. This includes the regulated emissions (HC, NO_x and CO) and CO_2.

As shown in Figure 6.16, the isHC emissions for G-EDI and G-MDI are much lower than PFI and GDI.

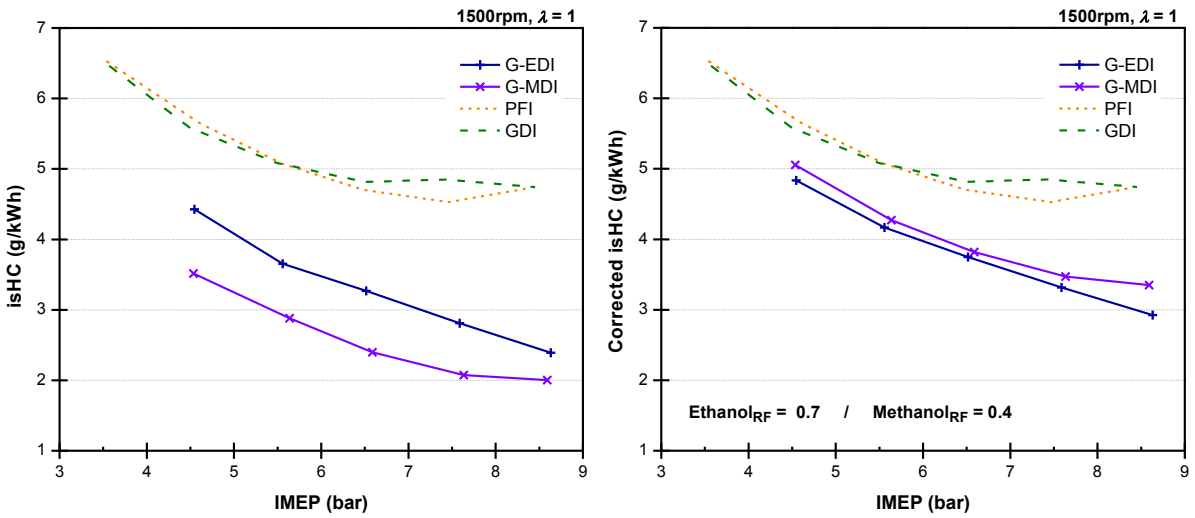

Figure 6.16 Uncorrected (a) and corrected (b) isHC for G-EDI, G-MDI, PFI and GDI

The impact on the isHC emissions when using G-MDI is, on average, 22% lower than with G-EDI, and 48% lower than PFI. The difference between G-EDI and G-MDI is due to the higher oxygen content of methanol (Table 3.8). This improves oxidation of unburned HCs becuase oxygen is more readily available. However, the reduced sensitivity of the FID analyser to oxygenated fuels suggests that the isHC emissions for G-EDI and G-MDI are higher than the FID states (Cheng, 1998, Wallner, 2008). Therefore, if the HC emissions

were assumed to be unburned fuel, FID response factors could be used to better approximate the isHC emissions of G-EDI and G-MDI. For ethanol and methanol, the typical FID response factors are 0.7 and 0.4 (Wallner, 2011, Grob, 1985). These factors have been applied to the results in Figure 6.16a and are shown as corrected isHC in Figure 6.16b.

On a corrected basis, the isHC emissions from G-EDI and G-MDI are more comparable but still offer a reduction from PFI and GDI. However, this is a simplified correction. This is because the HC emissions include various HCs, each with varying FID sensitivity. For instance, the dominant oxygenated HC from ethanol and methanol combustion is acetaldehyde and formaldehyde, respectively (Magnusson, 2011). Both these aldehydes produce a lower FID response factor than the fuel itself (Wallner, 2011), so would increase the FID value. In order to accurately quantify the isHCs, detailed speciation must be conducted.

The emissions of isNO_x, isCO and isCO_2 are shown in Figure 6.17. As mentioned, the formation of NO_x increases very strongly with combustion temperature (Stone, 1999). Therefore, the production of isNO_x increases with load (Figure 6.17a). The separation between G-EDI and G-MDI is due to higher combustion pressures with G-MDI (Figure 6.10), causing higher temperatures. For example, the isNO_x emissions for G-EDI and G-MDI are between 14-28% higher than PFI and GDI at 8.5bar IMEP. The higher combustion temperatures caused by the reduced charge-cooling of PFI and advanced spark timing when using lower alcohols both contribute to increasing isNO_x. However, the high conversion efficiency of TWCs (at λ=1) are able to dramatically reduce the NO_x emissions.

The dual-injection isCO emissions are always lower than GDI (Figure 6.17b). Compared to PFI, the isCO emissions are comparable up to 6.5bar IMEP. However, above this, the dual-

injection isCO emissions remain low. The improved oxidation is due to more advanced spark timing, which increases the combustion efficiency. The oxygen within the lower alcohols also promotes oxidation, as oxygen molecules are readily available. Also, the pre-mixed PFI component will be fully vaporized prior to ignition. Therefore, any localized fuel droplets from DI will benefit from the burning of PFI fuel vapour and further contribute to reduced isCO. Although primary use of PFI produces high isCO emissions at higher loads (due to spark retard), its use as a supplement to the DI fuel helps to reduce the isCO emissions.

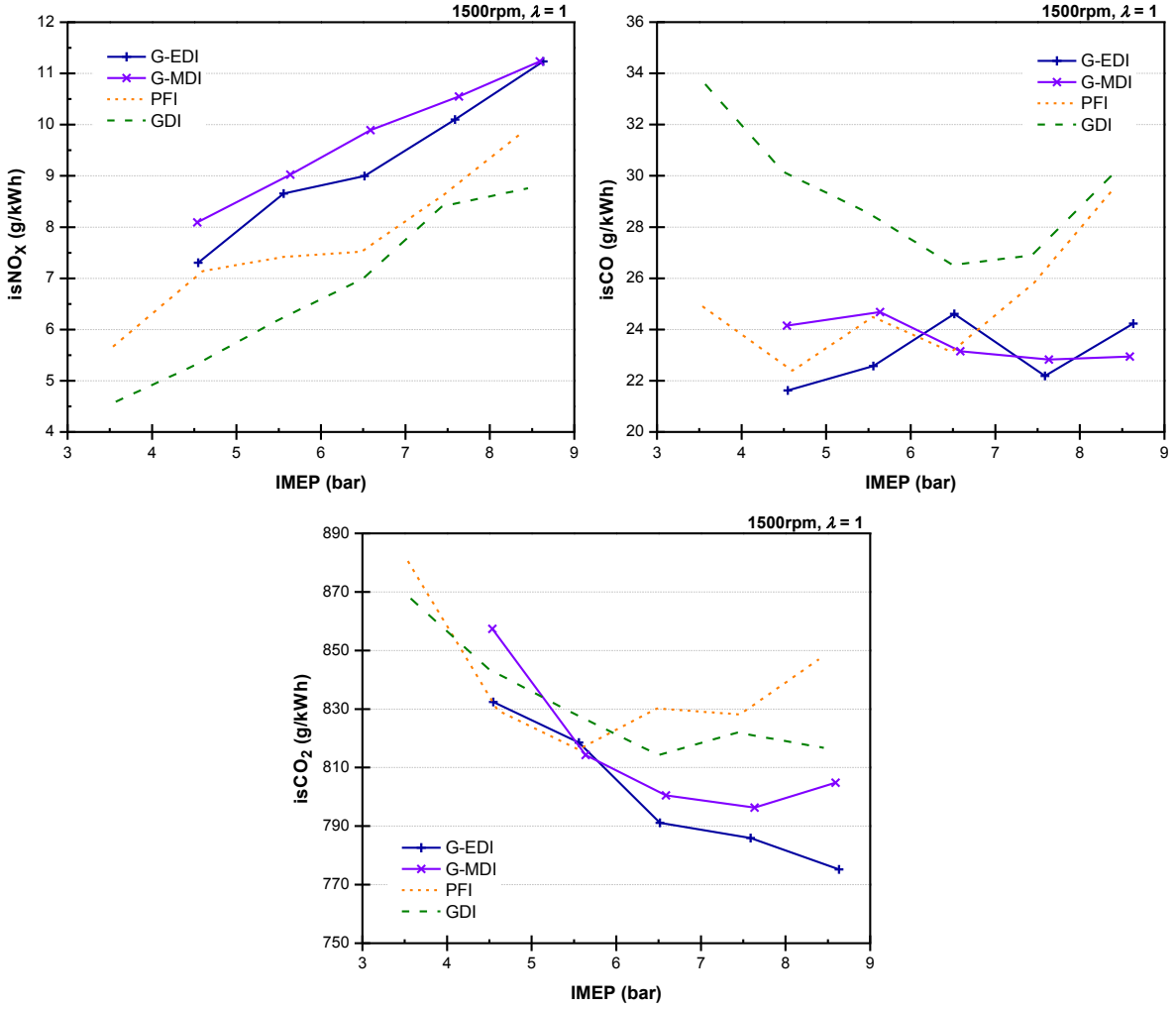

Figure 6.17 Effect of isNO$_x$ (a), isCO (b) & isCO$_2$ (c) for G-EDI, G-MDI, PFI and GDI

Finally, the isCO_2 production is shown in Figure 6.17c. The isCO_2 emissions reduce with dual-injection over GDI for almost every load. The critical load is 5.5bar IMEP. Above this, GDI emits lower isCO_2 emissions than PFI but dual-injection reduces this even further. At 8.5bar IMEP, the isCO_2 emission with G-EDI is 775g/kWh, which is 42g/kWh (5%) lower than GDI. This shows the ability of dual-injection to combat CO_2 emissions; the higher the alcohol content, the greater the CO_2 reduction, as shown by the reduced carbon intensity in Table 3.8. Furthermore, when taken from biomass, the production of ethanol and methanol will consume CO_2, making dual-injection even more favourable.

6.5 Summary

In summary, these experiments highlight the effectiveness of dual-injection to mitigate the knock with PFI. In particular, the minimum injection of ethanol or methanol in DI has been examined and compared against PFI and GDI.

The knock mitigation achieved with ethanol and methanol is due to their high ΔH_{vap} and OI. For instance, at 7.5bar IMEP, the high charge-cooling effect allows a spark advance (from PFI) between 11-12CAD despite a low DI volume fraction (41-43%). On an energy input basis, methanol is more effective. At 8.5bar IMEP, 14% less energy is required by methanol as a consequence of its higher OI and ΔH_{vap} due to its greater oxygen content.

The increased spark timing with dual-injection blends lowers CAD_{10-90} by up to 5CAD over GDI. However, due to the higher oxygen content of methanol, the CAD_{10-90} with G-MDI is up to 1.8CAD lower than with G-EDI. This has a direct influence on the indicated efficiency. Above 5.5bar IMEP, the indicated efficiency is higher with dual-injection than with PFI or GDI. Between 7.5-8.5bar IMEP, the indicated efficiency of G-EDI and G-MDI are at least 2% higher than GDI.

Reductions in HC, CO and CO_2 emissions are found at almost every load when using G-EDI and G-MDI, compared to PFI and GDI. At 8.5bar IMEP, the isCO_2 emissions are 5% lower with G-EDI, than with GDI. At 4.5bar IMEP, G-MDI produces 21% lower isHC emissions than G-EDI. Conversely, at the same load, G-EDI produces 2.9% lower isCO_2 emissions than G-MDI. However, the consequence of more advanced spark timing with dual-injection is higher combustion temperatures, which increases the NO_x emissions.

CHAPTER 7

DUAL-INJECTION BLENDS COMPARED TO DI BLENDS

This chapter compares the effectiveness of equivalent blends in dual-injection to DI. In particular, the effect on combustion performance and emissions is evaluated with DMF. However, three other oxygenated fuel blends have also been tested.

7.1 Introduction

Dual-injection is compared to DI using four oxygenated fuels to provide a balanced analysis. This includes ethanol, methanol, *n*-butanol and the new biofuel candidate DMF.

Engine load sweeps between 3.5-8.5bar IMEP, in 1bar increments, were performed using each neat fuel in DI (gasoline (also used in PFI), DMF, *n*-butanol, methanol and ethanol) as well as with gasoline-biofuel blends (25, 50 and 75%, by volume) in DI and dual-injection using optimised spark timings.

The effectiveness of each blend in dual-injection and DI was then examined. When using 25% blends of DMF or *n*-butanol with gasoline (D25 and B25, respectively), the ISFC falls below that of the equivalent blend in DI and even below that with GDI.

Compared to DI, dual-injection offers reduced CO and CO_2 emissions. However, the higher combustion temperatures due to the PFI component and advanced spark timings, results in an increase in NO_x emissions.

Overall, dual-injection is an effective method in utilising certain gasoline-biofuel blends. These results can also found in two journal publications (Daniel, 2012f, Daniel, 2012g).

7.2 Effect of 2,5-Dimethylfuran Blends

The indicated efficiency has been selected to highlight the varying influence of each element within the dual-injection and DI blends. This is followed by a direct comparison of D25 in DI (D_{25}DI) and dual-injection (G-D_{25}DI), in order to better highlight the differences.

The notation used to indicate the various fuel blends and injection modes is shown in Table 7.1 using D25 blends (25% DMF and 75% gasoline, by volume) as an example:

Table 7.1 Test Notation

PFI Fuel	DI Fuel	Notation
Gasoline		PFI
	Gasoline	GDI
	DMF	DDI
DI and Dual-Injection Blends		
	DMF/Gasoline	D_{25}DI
Gasoline	DMF	G-D_{25}DI

Following the indicated efficiency analysis, the impact on ISFC and VE is shown. The in-cylinder pressure and resulting MFB data is then analysed to better explain these trends in efficiency due to combustion.

7.2.1 Indicated Efficiency

The improvements in indicated efficiency when using DMF in DI (DDI) compared to gasoline in DI (GDI) are shown in Figure 7.1. This is due to greater spark advance because DMF has a higher OI and marginally higher charge-cooling effect (Table 3.8). This anti-knock quality is related to its compactness and the reduced branching of HCs (Hancock, 1985). Even though the two methyl groups are likely to first react during combustion, more

energy is required to break the five-ring compound structure of DMF due to the strong oxygen bond. Furthermore, the higher stoichiometric ΔH_{vap} of DMF (31kJ/kg_{air}) contributes to greater knock suppression compared to gasoline (25.8kJ/kg_{air}). However, the lower AFR_{stoich} of DMF (Table 3.8) suggests that the peak indicated efficiency of DDI is found at a higher IMEP than with GDI due to the greater throttling requirement and reduced volumetric efficiency with DDI. Nevertheless, this increase in indicated efficiency suggests that if DMF is used as the DI element in dual-injection, the indicated efficiency can be theoretically improved over the 'gasoline only' dual-injection strategy.

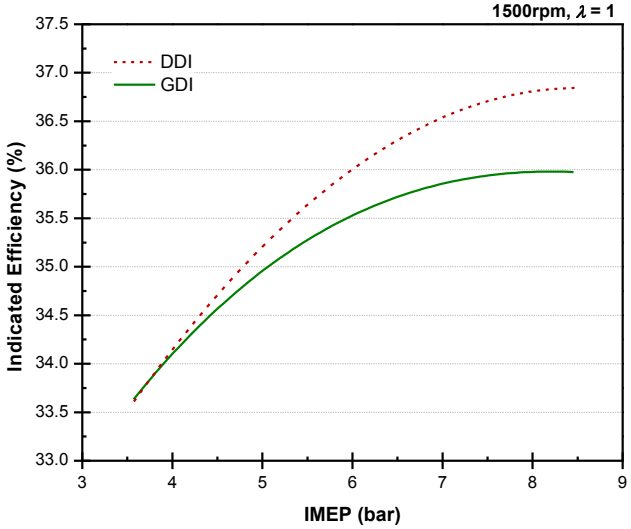

Figure 7.1 Indicated Efficiency using DDI and GDI

The indicated efficiency of G-D_{25}DI is compared to its elements (DDI and PFI) in Figure 7.2a. For most loads, the indicated efficiency of G-D_{25}DI consistently exceeds that with DDI and PFI. The peak indicated efficiency of 36.2% when using PFI is 0.7% higher (1.8% relatively) and occurs at a higher load when using G-D_{25}DI (7bar IMEP, as opposed to 5.7bar IMEP with PFI). Above 7.8bar IMEP, the indicated efficiency of G-D_{25}DI then decreases below that with DDI, because of the impact of the PFI element. The efficiency of

the PFI element is maintained at the lower loads (3.5-5.5bar IMEP) and is improved upon, by up to 1.7% (4.8% relatively), at the higher loads. The synergetic reaction of dual-injection has benefited CI engines (Reitz, 2011). The combustion benefits of in-cylinder blending, as discovered by Reitz, appear to be transferable to G-D_{25}DI in a modern DISI engine.

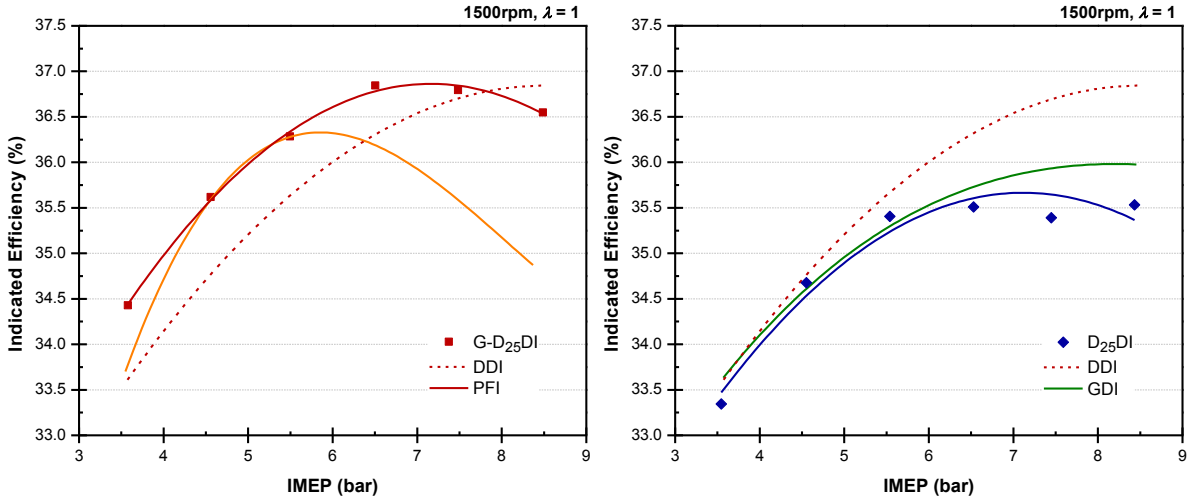

Figure 7.2 Indicated Efficiency using G-D_{25}DI (a) and D_{25}DI (b) and Constituents

In comparison to dual-injection, the results for the equivalent splash blends in DI (D_{25}DI) are presented in Figure 7.2b. The elements from Figure 7.1 are added to show the relationship with DMF addition to GDI. Conversely to the positive impact of G-D_{25}DI, the results for D_{25}DI are detrimental to performance compared to DDI and GDI. The indicated efficiency of D_{25}DI reaches a peak at 7bar IMEP, which is at least 0.3% and 0.8% lower than the peak with GDI and DDI, respectively. Although DMF is immiscible in water (Roman-Leshkov, 2007), its miscibility in gasoline is unknown. However, if like methanol, DMF requires blending additives to eliminate phase separation problems, the deterioration in performance could be due to the blend separating into DMF-rich and HC-rich (gasoline) phases (Hancock, 1985). Usually when this occurs, the combustion instability (COV of IMEP) increases.

Nevertheless, this non-linear behaviour when blending oxygenated fuels with gasoline has been seen in other research (Turner, 2011a, Kar, 2008).

The direct comparison between G-D_{25}DI and D_{25}DI is made in Figure 7.3.

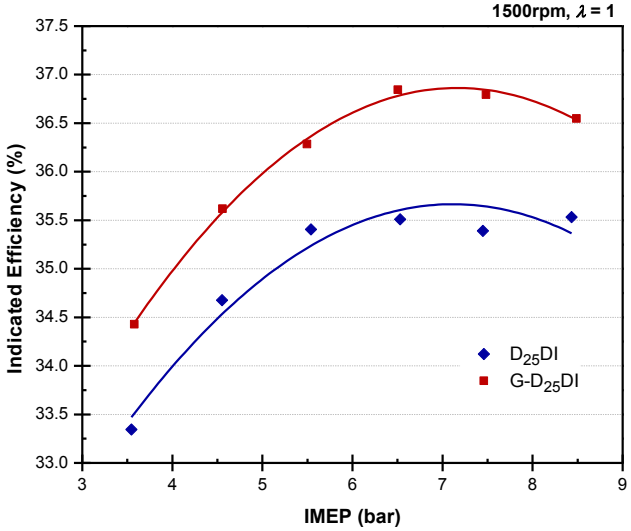

Figure 7.3 Indicated Efficiency using D_{25}DI and G-D_{25}DI

When using D25, the increase in indicated efficiency from D_{25}DI to G-D_{25}DI is between 0.9% and 1.4% for each load (up to 4% relative increase). Although both modes reach a peak indicated efficiency between 7-7.5bar IMEP, the efficiency at high loads using G-D_{25}DI is affected by the lower efficiency of the PFI component. The rise rate of efficiency from low load (3.5bar IMEP) to peak efficiency is higher with G-D_{25}DI. This reinforces the improved chemistry when using gasoline, a higher volatility fuel, to pre-mix the combustion chamber and promote the combustion of DMF. This may be either due to the inability of DMF to mix in gasoline, or the synergetic nature of the separate injections when in dual-injection. Nevertheless, thus far, dual-injection shows greater effectiveness in utilising D25. This proficiency is reiterated when comparing all blends in Figure 7.4.

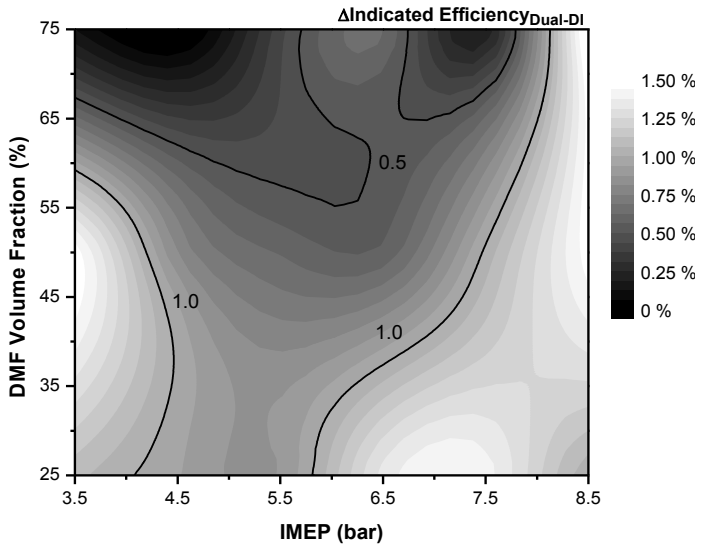

Figure 7.4 Indicated Efficiency Improvements using DMF Blends in Dual-Injection

The improvements in indicated efficiency when using dual-injection are consistent with higher blends of DMF (Figure 7.4). Although the greatest benefits of dual-injection arise with D25 blends, at 8.5bar IMEP, dual-injection consistently produces an increase in indicated efficiency of ≥1.5%. This is because the DI charge-cooling is more effective with DMF; more gas heat transfer occurs because the fuel impingement is reduced when the injection durations are lower than when using DI blends.

7.2.2 Indicated Specific Fuel Consumption

The improvements to indicated efficiency when using G-D_{25}DI, are more significant when analysing the effect on ISFC. In this case, the volumetric ISFC of D25 is presented in Figure 7.5 and for all DMF blends in dual-injection compared to GDI in Figure 7.6.

Immediately, there are two clear advantages with G-D_{25}DI. Firstly, the ISFC is reduced up to 3.2% (at 7.5bar IMEP) from the equivalent DI blends (D_{25}DI) and secondly, but also more significantly, the ISFC is reduced up to 1.2% (at 5.5bar IMEP) from homogeneous GDI. This

is a very promising result and counterintuitive because the marginally lower volumetric LHV of DMF is offset by improved efficiency. These results further highlight the synergy of dual-injection and the suitability to D25. Although the ISFC with PFI is lower below 6.7bar IMEP than with G-D_{25}DI, GDI is widely used in modern engines so provides the benchmark in this work. Nevertheless, above 7bar IMEP, G-D_{25}DI is up to 2.5% more efficient than PFI (at 8.5bar IMEP).

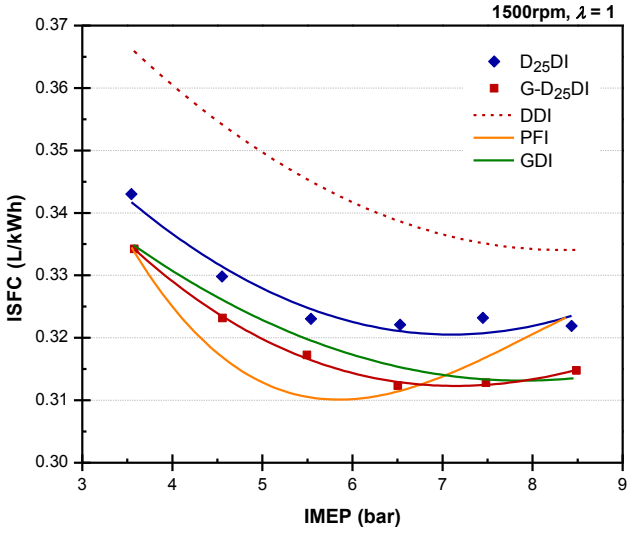

Figure 7.5 Volumetric ISFC using D_{25}DI, G-D_{25}DI, DDI, PFI and GDI

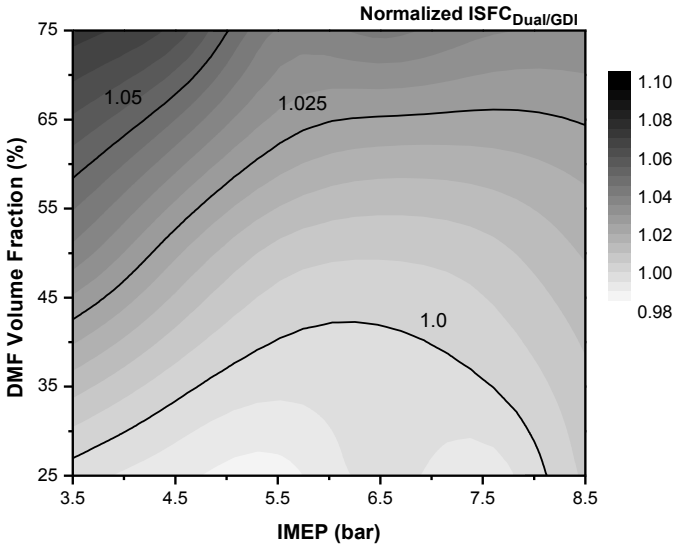

Figure 7.6 Normalized ISFC using DMF Blends in Dual-Injection compared to GDI

This low ISFC using dual-injection is consistent with high blends (G-D_{75}DI). As shown in Figure 7.6, the maximum fuel penalty is <10%.

The air flow characteristics and in-cylinder pressure data is examined in the next sections in order to find fundamental reasons for these increases in efficiency with dual-injection.

7.2.3 Volumetric Efficiency

The VE and intake manifold absolute pressure (MAP_i) is shown in Figure 7.7.

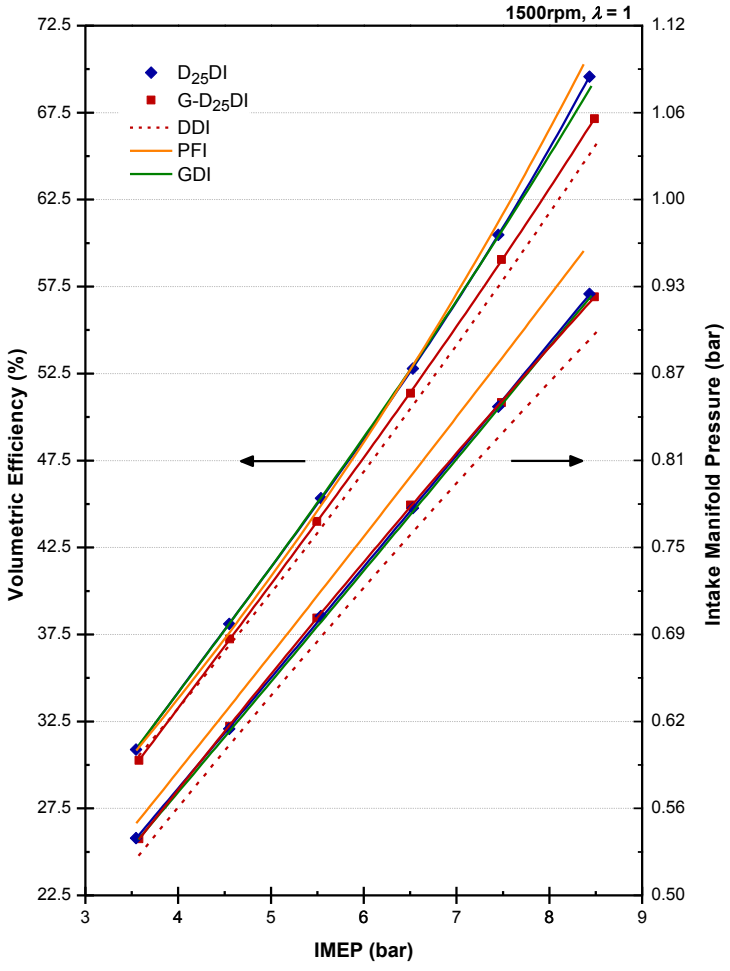

Figure 7.7 VE and MAP_i using D_{25}DI, G-D_{25}DI, DDI, PFI and GDI

The MAP_i is inversely proportional to the pumping work; as the throttle widens the pumping work is reduced and the MAP_i increases towards ambient pressure. Consistently with load, G-D_{25}DI produces lower VEs than D_{25}DI, despite the same AFR_{stoich}. At 8.5bar IMEP, the VE of G-D_{25}DI is 2.4% lower than D_{25}DI; less air is consumed because G-D_{25}DI is more effective at converting fuel energy into work, as shown with indicated efficiency (Figure 7.3). The reduced DI quantity of G-D_{25}DI reduces the charge-cooling and lowers VE.

The comparable MAP_i between the modes is surprising. This is because the PFI element in G-D_{25}DI reduces the partial pressure of the intake air. However, in this instance, the throttle demand is similar as the reduced partial pressure is overcome by the increased charge-cooling of DMF in DI with G-D_{25}DI. This is possibly due to reduced piston impingement of DI, which reduces heat transfer to the intake air (Fry, 1999). Although the overall charge-cooling impact is lower in G-D_{25}DI than in D_{25}DI, the fuel-specific effect is higher. This helps to raise the density of the intake air and partially offsets the need to open the throttle. The reduced piston impingement also explains the improvements in volumetric ISFC of G-D_{25}DI; impingement would compromise the mixture quality and reduce the combustion rate.

The benefits of reduced piston impingement with dual-injection are similar to the principle of double pulse or split-injection (Mittal, 2010, Yang, 1998). However, at WOT the overall charge-cooling with G-D_{25}DI would be lower, potentially reducing the maximum IMEP achievable (although greatly improved from PFI) compared to D_{25}DI. Therefore, the greatest benefits at WOT with dual-injection would be found when using fuels with a high ΔH_{vap} but low LHV (increased pulse-width), like ethanol and methanol (Daniel, 2012d).

7.2.4 In-Cylinder Pressure

By examining the in-cylinder pressure, the improvements in efficiency seen in Sections 7.2.1 and 7.2.2 are better explained. The maximum rate of in-cylinder pressure rise (RPR) and P_{max}, are shown in Figure 7.8a and Figure 7.8b, respectively.

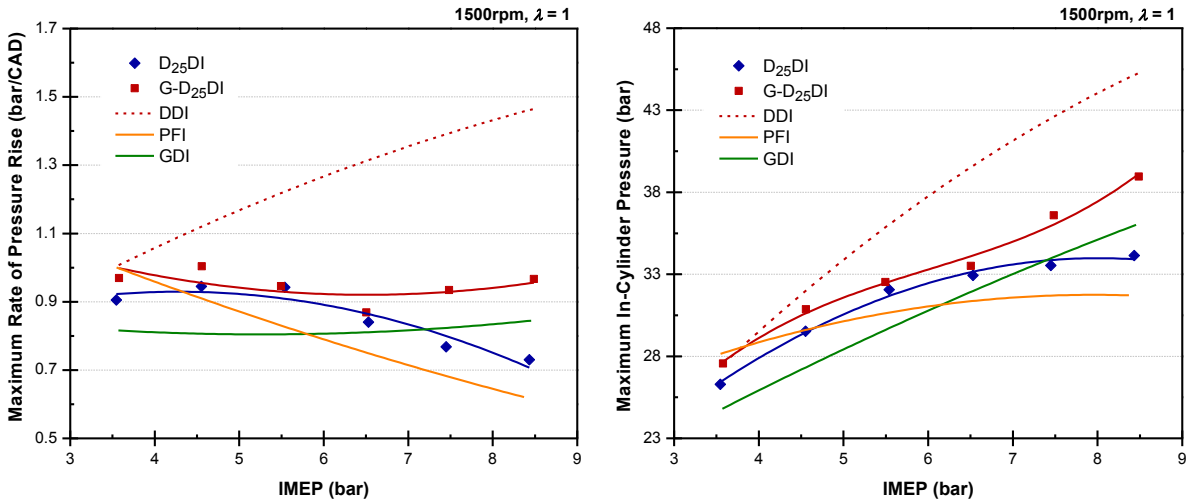

Figure 7.8 RPR (a) and P_{max} (b) using D_{25}DI, G-D_{25}DI, DDI, PFI and GDI

The combustion of G-D_{25}DI gives higher RPR and P_{max} than PFI, GDI and D_{25}DI. Although these values are lower than DDI, only 25% DMF is needed to dramatically improve the combustion of PFI. For all loads, the RPR remains high for G-D_{25}DI, helping to maintain its high efficiency (Figure 7.3). However, for D_{25}DI, the RPR decreases with loads above 4.5bar IMEP. At 8.5bar IMEP, the RPR of G-D_{25}DI is 0.97bar/CAD compared to 0.73bar/CAD with D_{25}DI (33% increase). This behaviour is due to the spark timing shown in Figure 7.9.

The spark timings between G-D_{25}DI and D_{25}DI are similar. This suggests that the higher RPR and P_{max} values result from higher combustion rates with G-D_{25}DI (similar to PFI and GDI below 6.5bar IMEP in Figure 6.2).

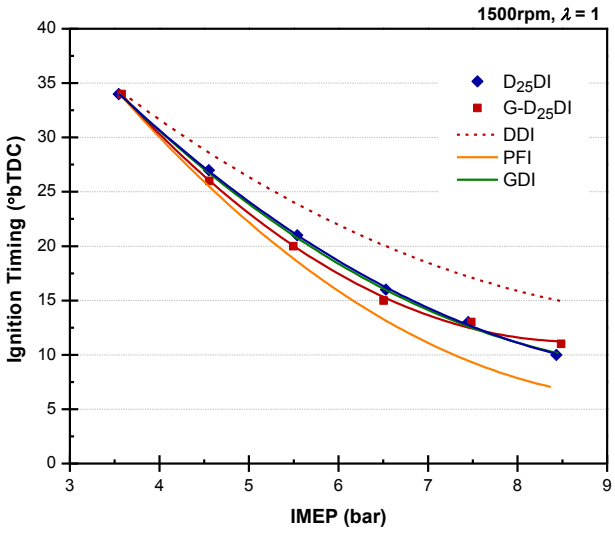

Figure 7.9 Ignition Timings using D_{25}DI, G-D_{25}DI, DDI, PFI and GDI

7.2.5 Mass Fraction Burned

The effect on $CAD_{10\text{-}90}$ is shown in Figure 7.10 and for all blends in Figure 7.11.

PFI is known to increase the air-fuel mixture homogeneity (Zhao, 2002). However, the reduced charge-cooling results in higher burning rates (lower $CAD_{10\text{-}90}$), which increases the combustion pressure and temperature (Figure 6.2). Although DMF, has a similar laminar velocity to gasoline (Tian, 2010a, Wu, 2011b, Wu, 2011c, Wu et al., 2009), the $CAD_{10\text{-}90}$ is lower (Figure 4.18). Therefore, the combination of PFI and DMF through dual-injection, results in lower $CAD_{10\text{-}90}$ than D_{25}DI with all loads. The largest difference is found at the highest load (8.5 bar IMEP). Here, the $CAD_{10\text{-}90}$ for G-D_{25}DI is 19.7CAD, 13% lower than D_{25}DI (22.8CAD) and 1.7CAD either side of GDI (21.4CAD) and DDI (18CAD). Clearly, the retarded spark timing between 4.5-6.5bar IMEP with G-D_{25}DI (Figure 7.9) does not impede the burning rate and the efficiency remains higher than D_{25}DI due to the low $CAD_{10\text{-}90}$. This trend is consistent with high DMF blends, although the advantage to dual-injection decreases due to the lower PFI fraction.

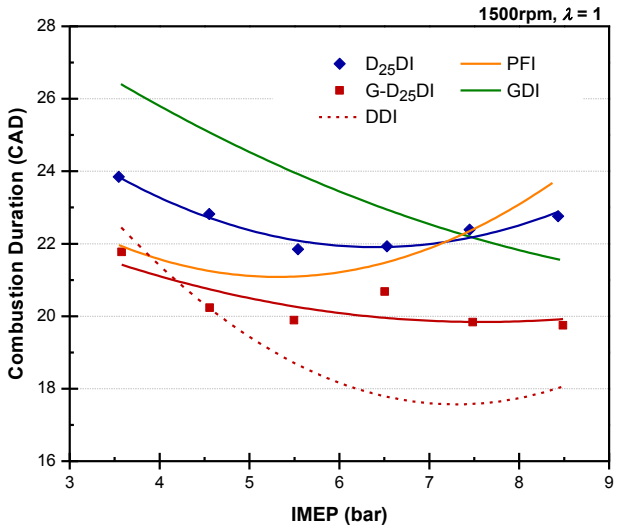

Figure 7.10 $CAD_{10\text{-}90}$ using $D_{25}DI$, G-$D_{25}DI$, DDI, PFI and GDI

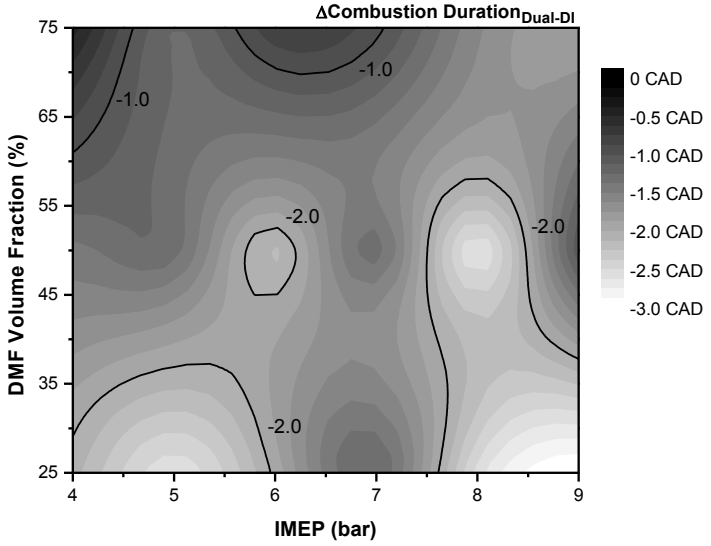

Figure 7.11 $CAD_{10\text{-}90}$ Improvements of DMF Blends in Dual-Injection

This independence of $CAD_{10\text{-}90}$ from ignition timing is also shown by CID in Figure 7.12.

Above 4.5bar IMEP, the CID of G-D_{25}DI is consistently lower than D_{25}DI (up to 10% at 8.5bar IMEP) and is comparable to PFI. Therefore, the improved homogeneity of PFI is negligibly affected by the addition of 25% DMF in DI. This helps to avoid the need for intake tumble flaps for improving mixture quality or the use of spark retard. In summary, dual-injection benefits from the high burning speeds of the individual elements.

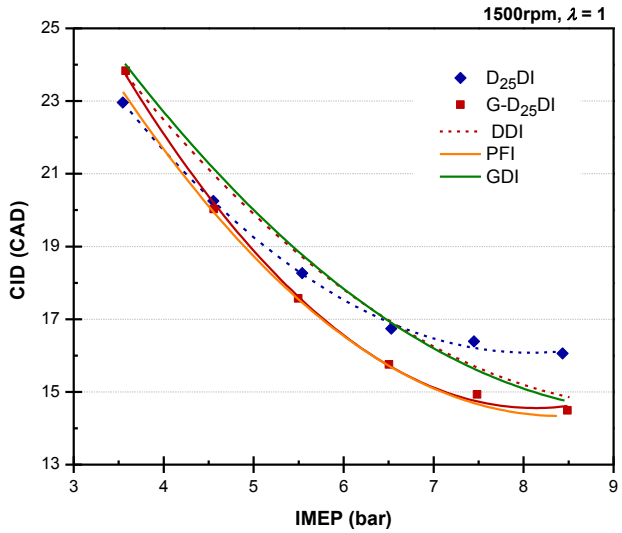

Figure 7.12 CID using D_{25}DI, G-D_{25}DI, DDI, PFI and GDI

7.2.6 Combustion Stability

The combustion stability (COV of IMEP) variation is shown in Figure 7.13.

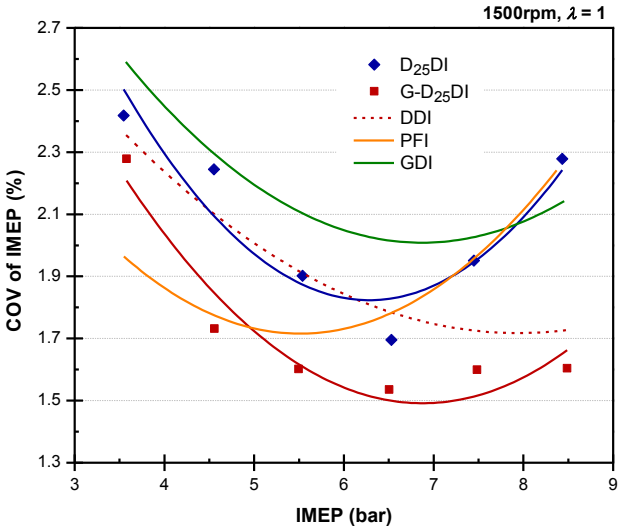

Figure 7.13 Combustion Stability using D_{25}DI, G-D_{25}DI, DDI, PFI and GDI

The overall trend between fuels is similar to the combustion rates in Figure 7.10 and Figure 7.12. Once again, at lower loads (<6.5bar IMEP) there is a large difference in COV of IMEP between G-D_{25}DI and D_{25}DI. The reduced $CAD_{10\text{-}90}$ and CID of G-D_{25}DI results in up to

20% (relatively) lower COV of IMEP. In fact, above 5bar IMEP, the COV of IMEP of G-D_{25}DI is the lowest between all combinations. Previously, it was suggested that DMF might be immiscible in gasoline as the indicated efficiency above 5.5bar IMEP was less than the constituent elements. Usually, when this occurs the COV of IMEP increases (Hancock, 1985). For D_{25}DI in Figure 7.13, the COV of IMEP increases above 6.5bar IMEP, which is more than with DDI and GDI. This further suggests that DMF is immiscible in gasoline.

7.2.7 Gaseous Emissions

The engine-out emissions for the various gasoline-biofuel blends using dual-injection and DI between 3.5-8.5bar IMEP are discussed. The regulated gaseous emissions are first evaluated (HC, CO and NO_x), which is then followed by an analysis of the CO_2 emissions.

7.2.7.1 Hydrocarbons

The isHC emissions are shown in Figure 7.14.

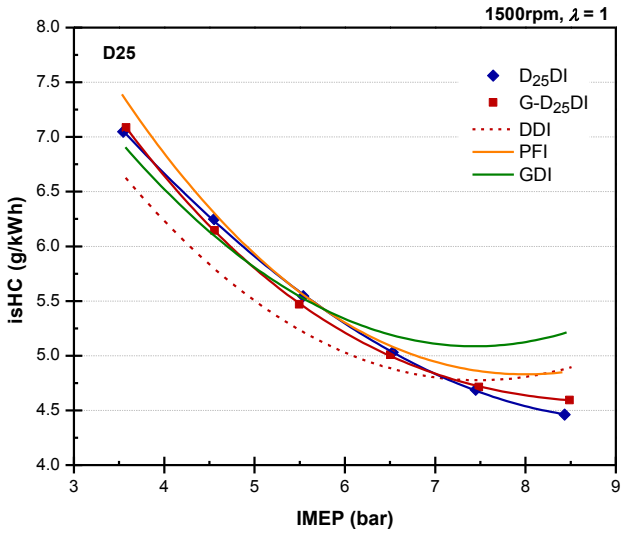

Figure 7.14 Effect of isHC using D_{25}DI, G-D_{25}DI, DDI, PFI and GDI

As discussed, FID analyzers are believed to have a reduced sensitivity to oxygenated HC fuels (Cheng, 1998, Wallner, 2008). Therefore, the results in Figure 7.14 provide a starting point for determining differences between the dual-injection and DI modes with D25. In previous work, the isHC emissions of DDI have been shown to be lower than GDI from 3.5bar to 8.5bar IMEP when using MBT timing (Figure 4.20b). This also extends to PFI, as shown in Figure 7.14. Therefore, the use of D_{25}DI and G-D_{25}DI shows an increase in isHC emissions from DDI, that is, up to loads of 7bar IMEP. The reduction in isHC emissions (increased oxidation of unburned fuel) at high loads is due to improved fuel vaporization. The oxygen molecule contained in the structure of DMF helps to increase the oxidation reaction as oxygen is readily available. Between D_{25}DI and G-D_{25}DI there is no discernible difference in isHC emissions. However, the rise in isHC emissions at low load for D_{25}DI above that with GDI is surprising as the DMF supplement contains oxygen.

Figure 7.15 shows the normalised isHCs between dual-injection and DI with higher blends.

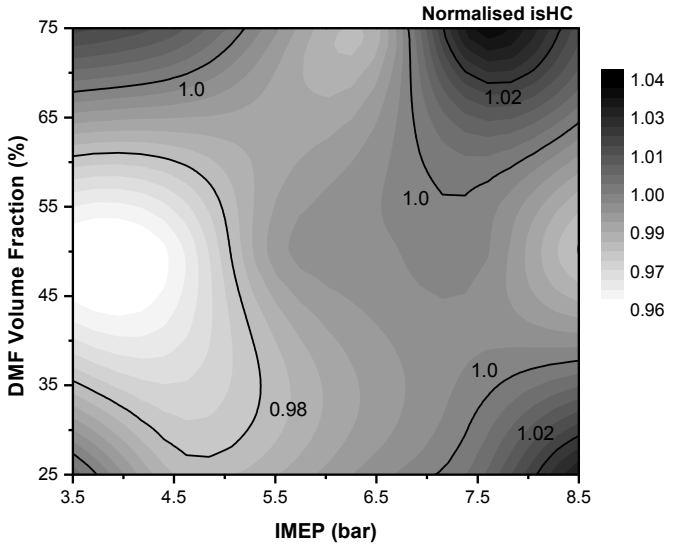

Figure 7.15 Normalized isHC Emissions for D_xDI and G-D_xDI

Although the difference in isHC emissions for all blends and loads is ±4%, the dual-injection mode offers more consistent reductions. For instance, the isHC emissions of D50 are consistently lower with dual-injection. The greatest difference is found at 3.5bar IMEP, where G-D_{50}DI is 4% lower (6.8g/kWh) than D_{50}DI (7.1g/kWh). However, at each corner of the emissions map, the isHC emissions are lower using DI. Clearly, as the load increases, the largest reductions in isHC emissions require modifications in blend ratio. This, however, is the advantage of dual-injection as the blend ratio can be varied instantaneously.

7.2.7.2 Nitrogen Oxides

The isNO_x emissions are shown in Figure 7.16 and show clear differences between modes.

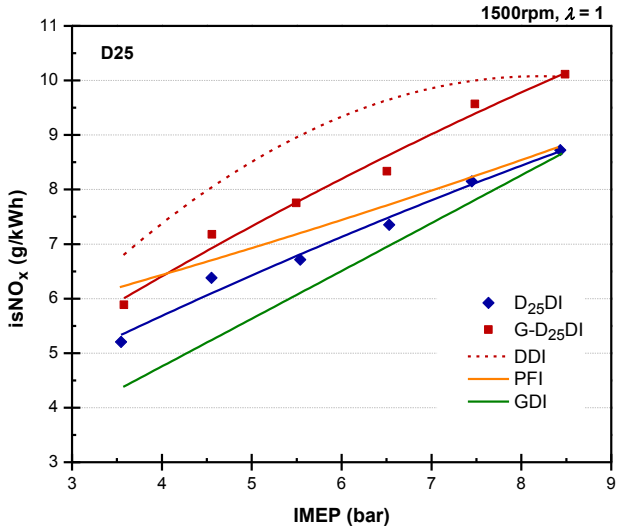

Figure 7.16 Effect of isNO_x emissions using D_{25}DI, G-D_{25}DI, DDI, PFI and GDI

The isNO_x emissions of G-D_{25}DI are between 13-16% higher than D_{25}DI as the load varies from 3.5-8.5bar IMEP. This is due to increased charge-cooling with GDI as opposed to PFI. At 8.5bar IMEP, the isNO_x emissions of D_{25}DI are comparable to PFI and GDI. The addition of 25% DMF has very little effect. However, the isNO_x emissions at this load are similar to

DDI when using G-D_{25}DI. The consequence of the PFI fraction with dual-injection is the increase in combustion temperature due reduced charge-cooling which occurs with GDI. This subsequently increases the isNO_x emissions (Stone, 1999), because the DMF component will also add to increased combustion temperatures (Daniel, 2011). PFI helps to improve vaporization but cannot reduce the charge temperature and suppress isNO_x.

The difference between all DMF blends in dual-injection and DI are shown in Figure 7.17.

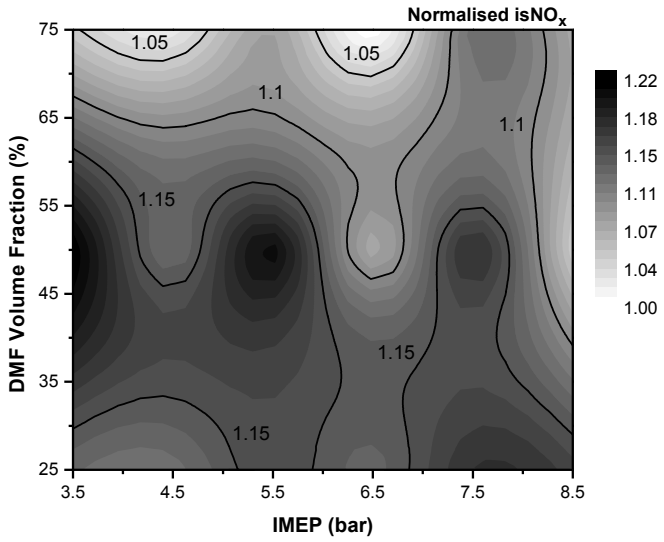

Figure 7.17 Normalized isNO_x Emissions for D_xDI and G-D_xDI

Here, the isNO_x emissions are consistently lower with DI blends. The largest increase in isNO_x occurs with G-D_{50}DI. At 5.5bar IMEP, the isNO_x emissions with G-D_{50}DI are 21% higher than D_{50}DI. However, as the DMF fraction increases the difference between the two modes decreases. For instance, the increase with G-D_{75}DI is less than 10% for all loads and at 6.5bar IMEP is equal to the result with D_{75}DI. This is mainly due to improved charge-cooling with D_{75}DI. As the fraction of gasoline reduces, so the combustion temperature increases which increases isNO_x emissions.

7.2.7.3 Carbon Monoxide

Conversely to the isNO_x emissions, the isCO emissions are consistently lower when using dual-injection, as shown in Figure 7.18. With G-D_{25}DI, the isCO is at least 11% lower than with D_{25}DI. The greatest decrease of 9.4g/kWh (31%) is seen at 5.5bar IMEP. Dual-injection also produces less isCO emissions than any other fuelling mode. For instance at 8.5bar IMEP, the isCO emissions when using G-D_{25}DI are at least 8g/kWh (28%) lower than PFI, GDI and DDI. Above 5.5bar IMEP, PFI results in increased isCO emissions due to the onset of knock and spark timing retard (Figure 6.3). However, the PFI fraction aids the atomization and resulting combustion of the biofuel fraction in DI. Such synergistic effects exist in CI engine research (Zhang, 2011). The PFI supplement aids the vaporization of the diesel fuel in DI and increases the combustion efficiency at low loads. Benefits have also been seen with diesel-gasoline splash blends but to a less extent (Turner, 2009, Zhong, 2005).

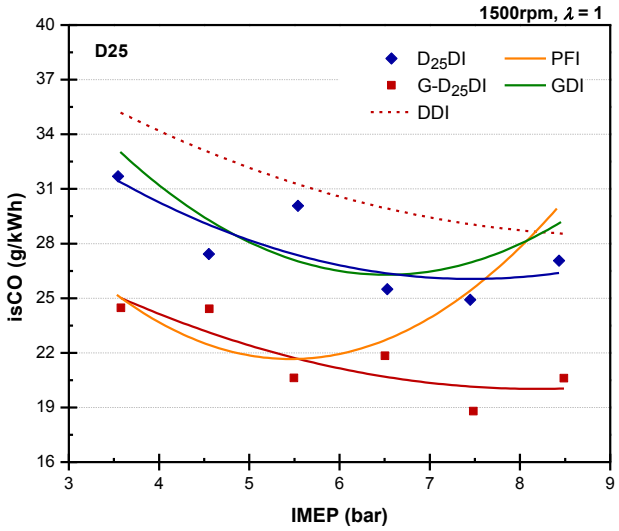

Figure 7.18 Effect of isCO emissions using D_{25}DI, G-D_{25}DI, DDI, PFI and GDI

The normalized isCO emissions for each blend and load is shown in Figure 7.19. An area of high efficiency (>20% decrease in isCO) exists for dual-injection fractions below D60 and

loads below 6bar IMEP. However, with higher blends, the difference in isCO emissions reduces. The PFI fraction helps to increase the reaction rate and the vaporized gasoline fuel burns quickly improving DMF combustion. Between 5.5-6.5bar IMEP, there is no advantage with G-D_{25}DI. The isCO emissions increase between 4-6%. However, reductions over 15% can be found with lower DMF fractions.

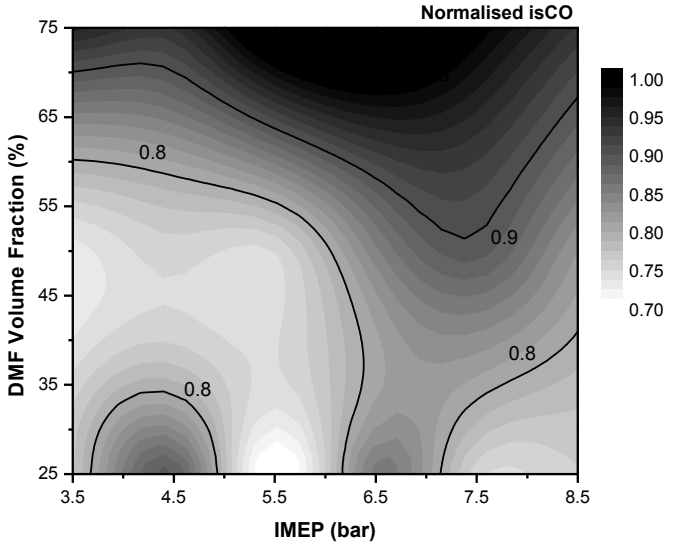

Figure 7.19 Normalized isCO Emissions for D_xDI and G-D_xDI

7.2.7.4 Carbon Dioxide

The isCO_2 production is compared between the fuels in Figure 7.20.

During complete combustion the carbon intensity of DMF is 83.6gCO_2/MJ, which is 12% higher gasoline (Table 3.8) and explains the increase in isCO_2 emissions with DDI over GDI. At 3.5bar IMEP, the isCO_2 emissions for DDI are 10% higher than for GDI. However, at 8.5bar IMEP, this is only 5%. This increase is due to the greater OI of DMF (Table 3.8), allowing greater spark advance.

At 3.5bar IMEP, the $isCO_2$ emissions are approximately ¼ higher than GDI which equates to the volume fraction of DMF. As the load increases, the increase in $isCO_2$ from GDI exceeds the fraction of DMF. At 8.5bar IMEP, the $isCO_2$ emission of $D_{25}DI$ is 4.5% higher than GDI and comparable to DDI. For dual-injection, however, the $isCO_2$ emissions increase from GDI is minimal but is reduced from DDI. Throughout the load range, the $isCO_2$ emissions of G-$D_{25}DI$ are consistently lower than $D_{25}DI$. This represents a similar improvement to that seen with isCO. The largest reductions with G-$D_{25}DI$ are found between 6.5-8.5bar IMEP. Within this region, the $isCO_2$ emissions are approximately 20g/kWh lower than $D_{25}DI$. Above 7bar IMEP, the synergistic effect of G-$D_{25}DI$ is shown by the improvement in $isCO_2$ over its constituent parts; G-$D_{25}DI$ produces less $isCO_2$ emissions than PFI or DDI. This highlights the synergetic nature of dual-injection for D25. The savings in ISFC (Figure 7.5) are translated to $isCO_2$ emissions reductions.

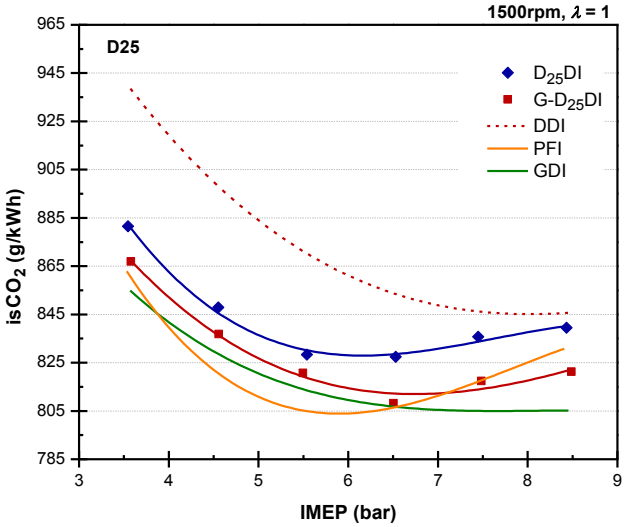

Figure 7.20 Effect of $isCO_2$ production using $D_{25}DI$, G-$D_{25}DI$, DDI, PFI and GDI

The normalized $isCO_2$ emissions are shown in Figure 7.21. As found with isCO (Figure 7.19), the $isCO_2$ emissions are lower when using dual-injection compared to DI for each

blend fraction and load combination. The lowest improvements are found between 4.5-5.5bar IMEP and the greatest improvements are found at loads above 5.5bar IMEP with any blend. The range of improvement is between 0.5% (D50 at 5.5bar) and 3.1% (D75 at 8.5bar).

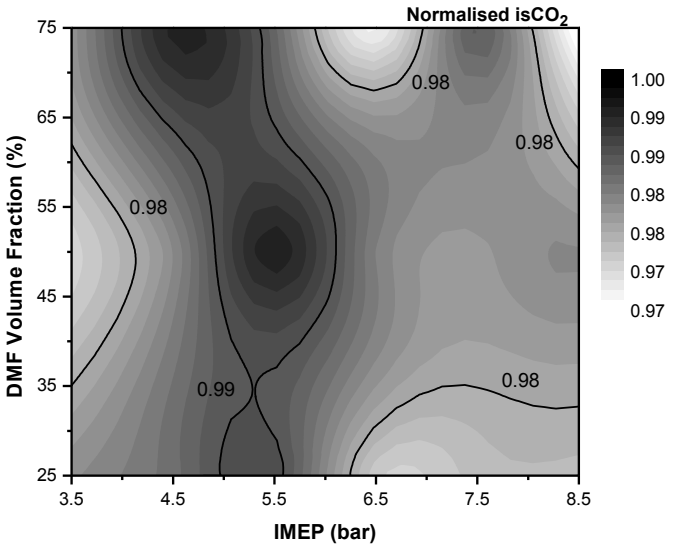

Figure 7.21 Normalized isCO_2 Emissions for DDI and G-DDI

7.2.8 Combustion Efficiency

The combustion efficiency of G-D_{25}DI and D_{25}DI are compared in Figure 7.22.

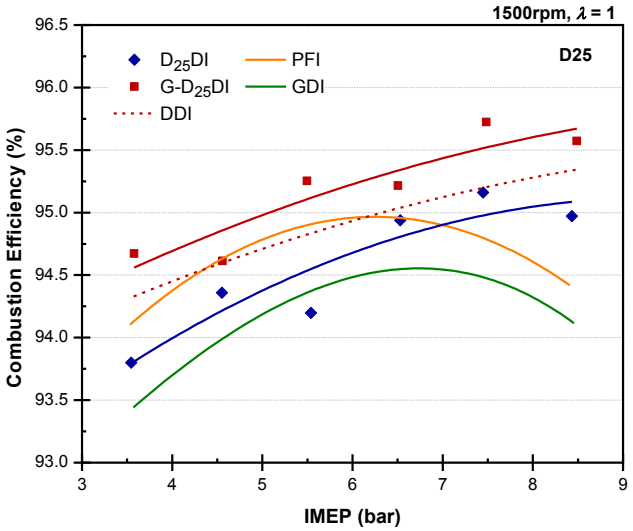

Figure 7.22 Combustion Efficiency using D_{25}DI, G-D_{25}DI, DDI, PFI and GDI

For most fuelling cases, the combustion efficiency increases with load, due to decreasing HC and CO emissions. The effect of DMF is to increase the high-load combustion efficiency. For D_{25}DI, the combustion efficiency reaches 95% at 8.5bar IMEP. This represents a relative increase of 0.8% over GDI. However, for G-D_{25}DI, the increase over GDI is much higher. At 8.5bar IMEP, the combustion efficiency with G-D_{25}DI reaches 95.6%, which is almost the relative increase of D_{25}DI over GDI (1.5%). This is due to the increased efficiency of the PFI component over GDI (0.5% higher at 8.5bar IMEP). However, the synergistic behaviour of PFI and DDI results in consistently higher combustion efficiencies for G-D_{25}DI than the constituent parts. This is possibly due to low isCO emissions when using G-D_{25}DI (Figure 7.18), which is caused by the improved mixture quality prior to combustion with G-D_{25}DI and the improved chemical reaction during the combustion process (Reitz, 2011).

7.3 Effect of *n*-Butanol Blends

The effectiveness of dual-injection blends compared to DI is briefly examined using other oxygenated fuels. The first is *n*-butanol. This higher alcohol is characterised by a high LHV (17% lower than gasoline, Table 3.8) but low ΔH_{vap} (≈50% lower than ethanol). These properties are similar to DMF, suggesting that *n*-butanol might produce competitive ISFC. The indicated efficiency comparison for B25 blends is shown in Figure 7.23.

The indicated efficiency of G-B_{25}DI is higher than B_{25}DI, PFI and GDI for all loads. The shape of the G-B_{25}DI curve is similar to PFI, which suggests that the behaviour is largely dominated by PFI. However, the higher efficiency of BDI raises the overall efficiency. This is also seen by the cross-over of indicated efficiency between BDI and G-B_{25}DI, which occurs at 6bar IMEP, 1.5bar IMEP lower than for the equivalent DMF case (Figure 7.2a).

The decline in efficiency at higher loads is due to the PFI component and partly BDI, which reaches a peak in indicated efficiency around 7.5bar IMEP, whereas no peak is seen with DDI (Figure 7.2a). Therefore, the overall trend with G-B_{25}DI is similar in curvature to PFI but is slightly raised in efficiency (consistently 1% higher between 6-8.5bar IMEP). As with D25 (Figure 7.2b), the indicated efficiency of B_{25}DI mirrors that with BDI.

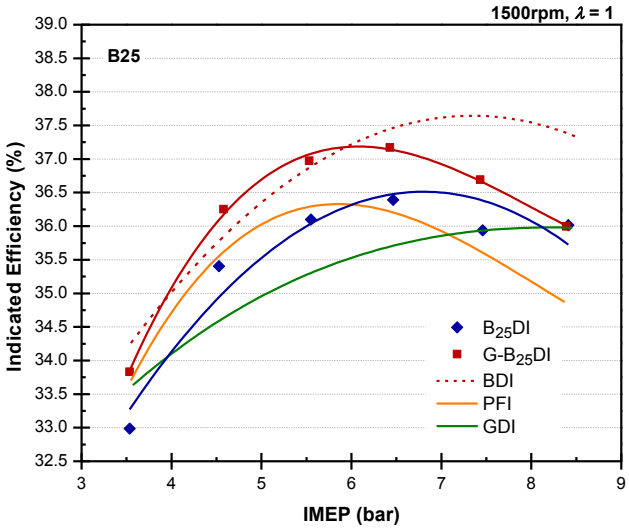

Figure 7.23 Indicated Efficiency using B_{25}DI, G-B_{25}DI, BDI, PFI and GDI

The indicated efficiency between G-BDI and BDI is made with higher blends in Figure 7.24.

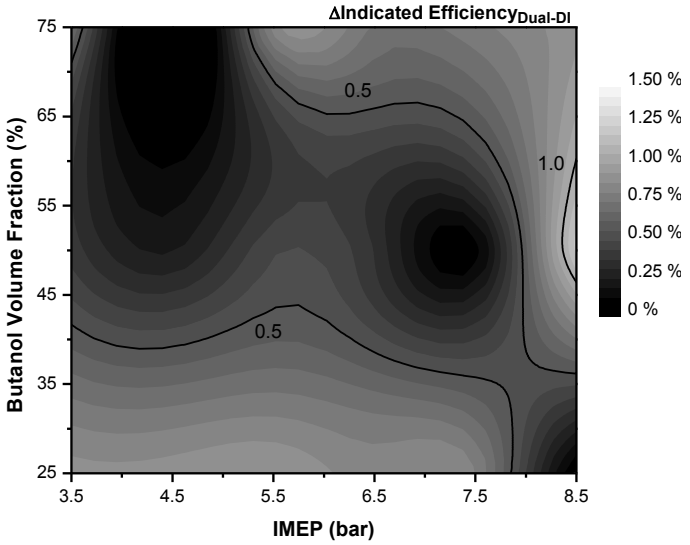

Figure 7.24 Indicated Efficiency Improvements using *n*-Butanol in Dual-Injection

The same z-axis scale (ΔIndicated Efficiency) as used for DMF in Figure 7.24 has been used. Clearly, the benefits of G-BDI are found using B25 blends and at 8.5bar IMEP with higher blends. The greater ratio of PFI with B25 helps to improved vaporization and the increased efficiency at 8.5bar IMEP with B50 and B75 may be due to reduced piston impingement (more effective charge-cooling).

Although the improvements with dual-injection are generally lower than that seen with DMF (Figure 7.4), improvements between 0.5-1% are seen ≤7.5bar IMEP with B25 blends. The higher efficiencies of G-B_{25}DI are likely to be due to the synergistic relationship between PFI and BDI rather than the spark timing advance shown in Figure 7.25. From 4.5-8.5bar IMEP, the spark timing of G-B_{25}DI is 3CAD more retarded than B_{25}DI despite a higher indicated efficiency. The cooling effect of BDI is not significant enough to make a difference to T_{ign}. The efficiency gains of G-B_{25}DI compared to B_{25}DI are therefore not obtained from advanced spark timing. The interaction between BDI and PFI components are important and the synergistic behaviour should be better understood.

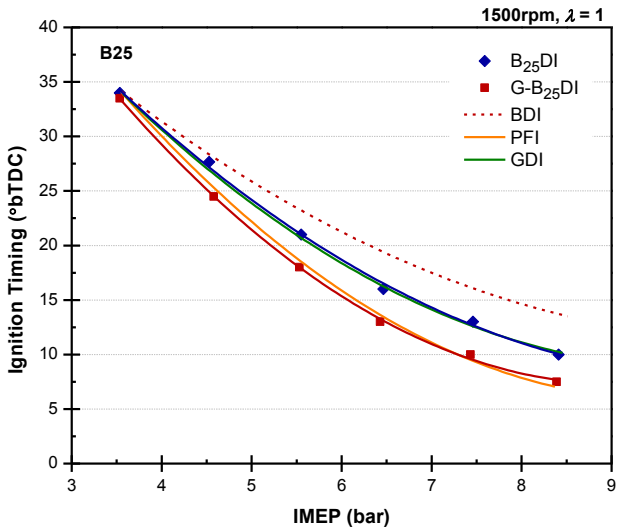

Figure 7.25 Ignition Timings using B_{25}DI, G-B_{25}DI, BDI, PFI and GDI

As with DMF, the PFI component improves the fuel-air mixture preparation and aids the combustion of the less volatile BDI component. This helps to improve combustion speed and is clearly shown when analysing the CID in Figure 7.26.

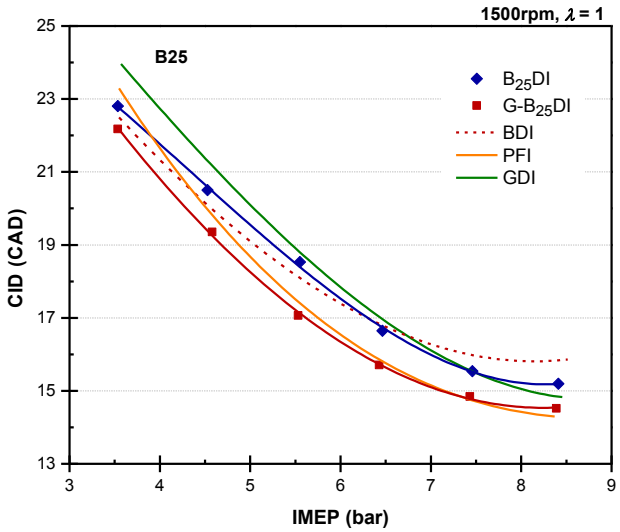

Figure 7.26 CID using B_{25}DI, G-B_{25}DI, BDI, PFI and GDI

The reduced CID of G-B_{25}DI provides the benefits usually achieved with spark advance. The CID is similar to PFI and consistently lower than B_{25}DI (≈1CAD). These differences in CID are similar to the differences in volumetric ISFC shown in Figure 7.27, however the ISFC of G-B_{25}DI is comparable to GDI at mid-loads.

The normalised increase in compared to GDI at all ratios and loads is shown in Figure 7.28. As expected with higher blend ratios, the ISFC increases due to the lower LHV of *n*-butanol compared to gasoline. However, for B25 and B50 blends, the ISFC increase is around 2.5% and 5% respectively. This highlights the benefits of dual-injection with *n*-butanol, even compared to GDI. This is a similar result to that seen with DMF (Figure 7.6).

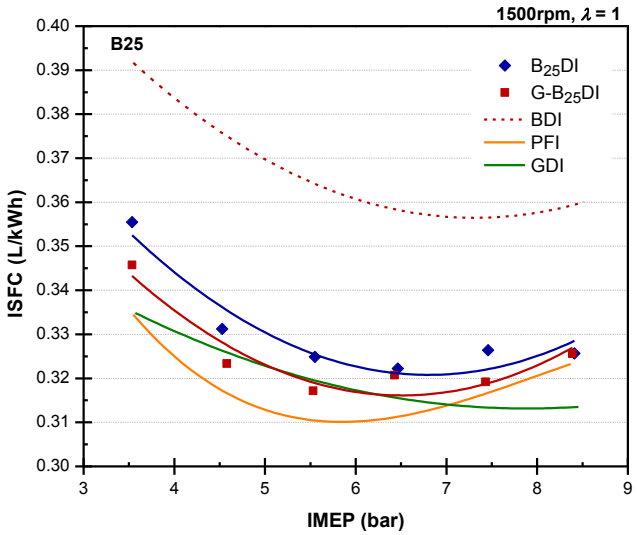

Figure 7.27 Effect of ISFC using B_{25}DI, G-B_{25}DI, BDI, PFI and GDI

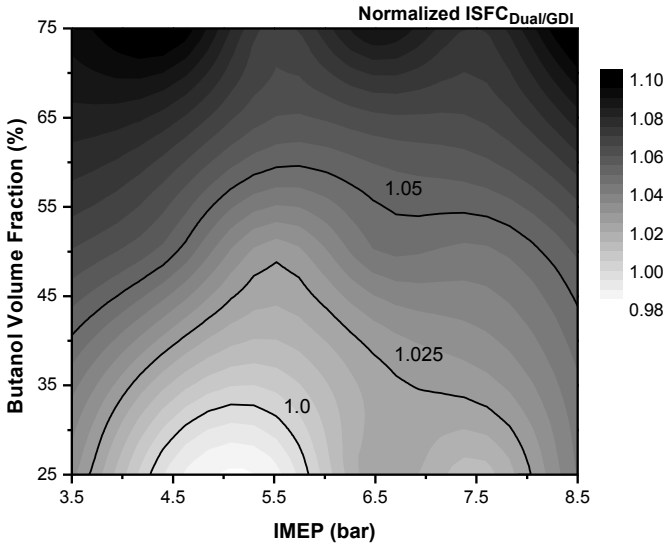

Figure 7.28 Normalized Volumetric ISFC using *n*-Butanol in Dual-Injection

7.4 Effect of Ethanol and Methanol Blends

The effectiveness of the lower alcohols (ethanol and methanol) blends using dual-injection compared to DI are briefly discussed. As with *n*-butanol blends, the combustion performance is only analysed and not the emissions.

Ethanol and methanol have been used in dual-injection to greatly advance the ignition timing, as shown in detail in Chapter 6. This is mainly due to their high ΔH_{vap} (Table 3.8), which increases charge-cooling, and OI. However, this section assesses the effectiveness of dual-injection to equivalent blends in DI. The comparison using ethanol is presented first.

The indicated efficiency comparison using E25 blends between dual-injection (G-E_{25}DI) and DI (E_{25}DI) is shown in Figure 7.29. Only results from 5.5bar IMEP using G-E_{25}DI are shown because E25 blends were not achievable at low loads due to the unobtainable DI durations.

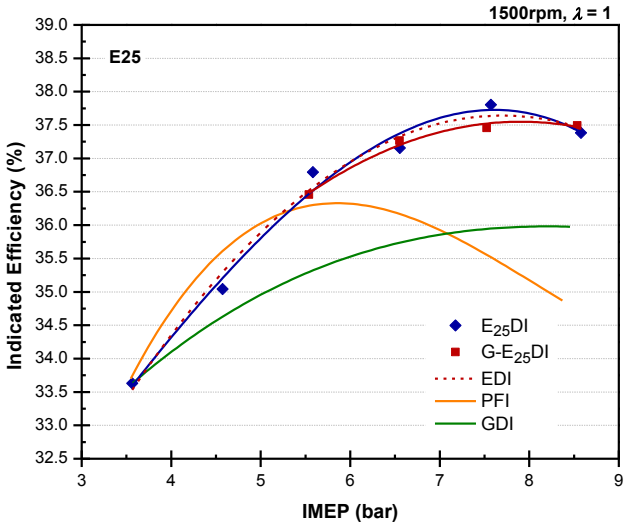

Figure 7.29 Indicated Efficiency using E_{25}DI, G-E_{25}DI, EDI, PFI and GDI

However, from 5.5bar IMEP, there is very little difference between the two combustion modes. This may be due to the comparable spark timings shown in Figure 7.30. Both modes are effective at permitting spark advance and the use of only 25% ethanol is effective at raising the spark timing from PFI even with G-E_{25}DI, which was shown to be less effective (Figure 7.25). The spark advance is due to charge-cooling and the chemical resistance of ethanol to pre-ignition, which is less evident when using DMF and *n*-butanol blends. This has a positive impact on the indicated efficiency.

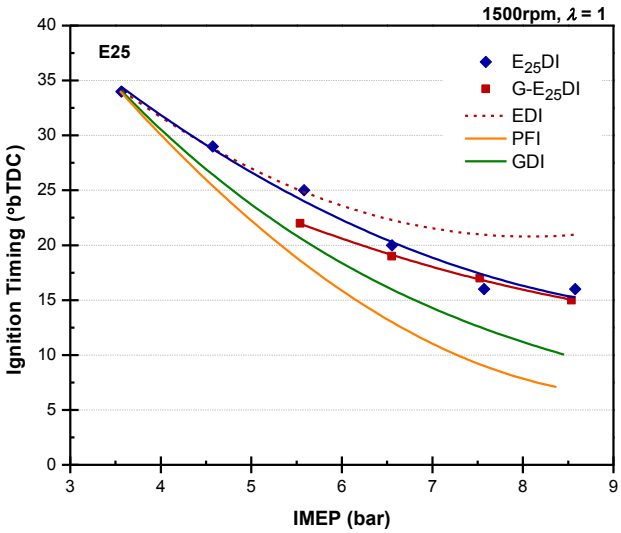

Figure 7.30 Ignition Timings using E_{25}DI, G-E_{25}DI, EDI, PFI and GDI

At 8.5bar IMEP, the spark timing is 5CAD retarded from EDI but the indicated efficiency is similar. For G-E_{25}DI, this can be explained by the consistently low $CAD_{10\text{-}90}$ shown in Figure 7.31a which is 1-2CAD lower than E_{25}DI. However, for E_{25}DI the high indicated efficiencies are more likely to be due to the lower ISFC, shown in Figure 7.31b (EDI is omitted).

The lower ISFC with E_{25}DI may be due to the slightly more advanced spark timings shown in Figure 7.30 which allows the combustion to take place at lower in-cylinder volumes.

The indicated efficiency comparison between methanol blends is made in Figure 7.32. Here, M25 blends are more effective in G-M_{25}DI than M_{25}DI. The high charge-cooling effect of methanol in DI allows the indicated efficiency of MDI to reach 38.4% at 8.5bar IMEP. This helps to increase the indicated efficiency of M_{25}DI with load. Nevertheless, when using G-M_{25}DI, the efficiency decreases >7.4bar IMEP due to the influence of PFI. This may be due to the immiscibility of methanol in gasoline. The blend may separate into methanol-rich and gasoline-rich phases, which would cause engine instability and directly impact the indicated

efficiency (Hancock, 1985).The behaviour with G-M_{25}DI follows the trend with MDI until 6bar IMEP. Above this load, the low efficiency of PFI reduces the overall efficiency.

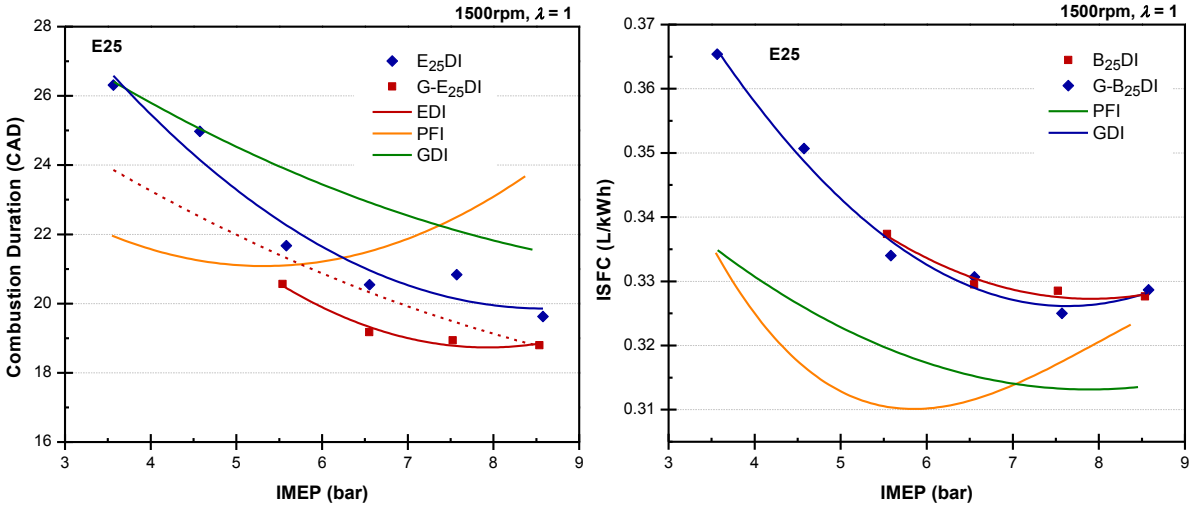

Figure 7.31 $CAD_{10\text{-}90}$ (a) and ISFC (b) using E_{25}DI, G-E_{25}DI, EDI, PFI and GDI

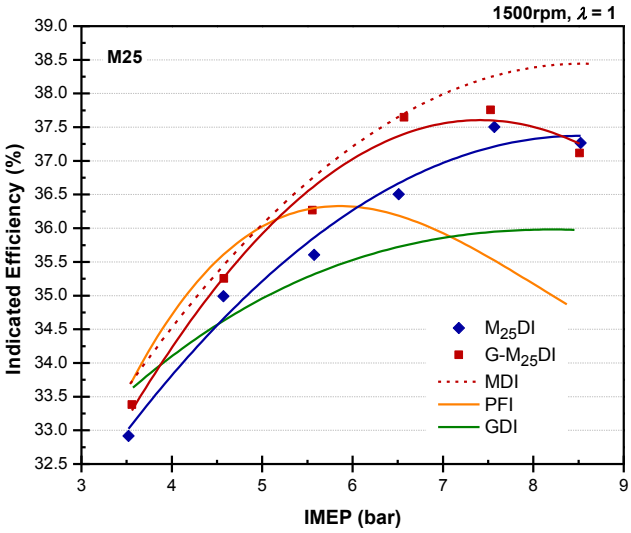

Figure 7.32 Indicated Efficiency using M_{25}DI, G-M_{25}DI, MDI, PFI and GDI

The higher indicated efficiencies with G-M_{25}DI are not due to more advanced spark timings despite the spark timing to be comparable to MDI, (Figure 7.33) because G-M_{25}DI is up to 4CAD more retarded than MDI. Therefore, the higher indicated efficiencies of G-M_{25}DI are

more likely to be due to improved combustion rates brought about by improved mixture preparation.

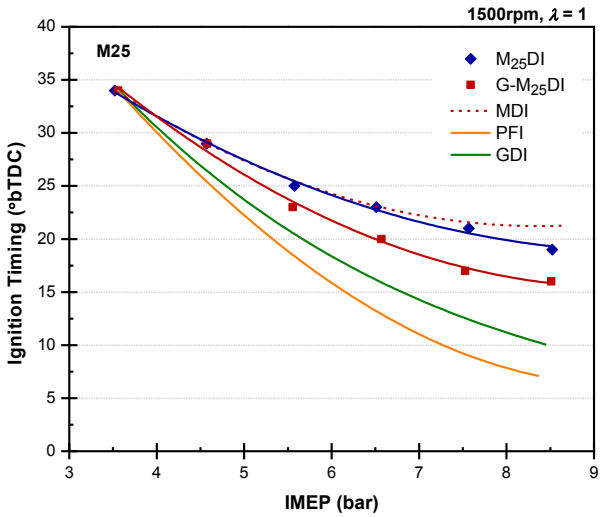

Figure 7.33 Ignition Timing using M_{25}DI, G-M_{25}DI, MDI, PFI and GDI

This is shown when analysing the CID and $CAD_{10\text{-}90}$ in Figure 7.34. The CID is consistently lower with G-M_{25}DI than M_{25}DI and both are similar to GDI despite more improved knock suppression. The advanced spark timings and improved mixture preparation are likely to cause the very low $CAD_{10\text{-}90}$, especially for G-M_{25}DI.

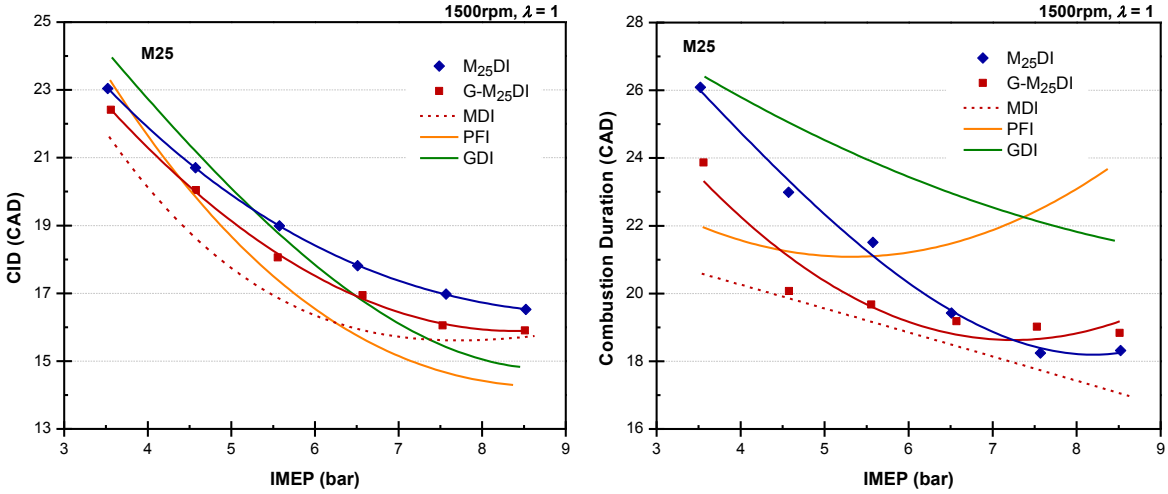

Figure 7.34 CID (a) and $CAD_{10\text{-}90}$ (b) using M_{25}DI, G-M_{25}DI, MDI, PFI and GDI

7.5 Summary

In this chapter, the performance and emissions of dual-injection has been studied in detail. The authors have compared the effectiveness to DI using various oxygenated fuel blends.

When using D25, the indicated efficiency in dual-injection (G-D_{25}DI) exceeds that of the individual components (PFI and DDI) up to 8bar IMEP. Between the two modes, G-D_{25}DI produces consistently higher indicated efficiencies than D_{25}DI (up to 4%; 36.8% at 7.5bar IMEP). This is reiterated with the volumetric ISFC. First, the ISFC is reduced, by up to 3.2% from D_{25}DI and second, this ISFC is up to 1.2% lower than GDI. The 8% lower LCV of DMF is offset by the higher efficiency of this combustion mode. This behaviour is possibly a result of improved mixing and lower wall wetting due to lower DI injection durations.

The improved efficiencies of dual-injection are correlated to higher P_{max} and RPR. At 8.5bar IMEP, P_{max} and RPR for G-D_{25}DI was 4.8bar and 0.24bar/CAD higher than D_{25}DI respectively. Therefore, CID and $CAD_{10\text{-}90}$ was up to 10% and 13% lower than D_{25}DI, respectively. These lower combustion durations produced higher combustion stabilities (lower COV of IMEP) than D_{25}DI. The lowest COV of IMEP was 1.5% at 6.5bar IMEP, which was lower than its individual components (PFI and DDI).

Ultimately, dual-injection is a very promising technique for optimising the combustion of low gasoline-DMF blends. This is also the case for *n*-butanol. The lower effect of charge cooling is overcome by the improved mixture quality. Methanol blends (M25) were also shown to be more effective in dual-injection but ethanol blends (E25) were comparable to DI_{hom}. However, in summary, dual-injection provides greater flexibility and lower ISFC than blends in DI, which is sometimes comparable to homogeneous GDI.

CHAPTER 8

HC SPECIATION AND PM EMISSIONS OF 2,5-DIMETHYLFURAN

This chapter examines the major HC species emitted from DMF combustion and compares their relative proportions. The effect of spark timing, engine load and dual-injection on PM emissions when using DMF and ethanol is also analysed.

8.1 Introduction

Hitherto, the emissions analysis of DMF has used traditional techniques. However, it is anticipated that the more harmful individual HCs will become regulated as the emissions legislations are tightened and new legislations are introduced. In the first instance, the automotive industry will inevitably see the tightening of PM emissions limits similar to that issued for CI engines. Secondly, the control of individual HCs, like that of formaldehyde currently in California, is likely to become more widespread leading to improved air quality and a focus on the reduction of carcinogenic emissions. These steps highlight the need to better understand the constituent HC emissions rather than the total HCs. This is particularly important when developing new fuels.

The speciated HC emissions are presented in this chapter using chromatographic techniques. The emissions from DMF are compared to ethanol and gasoline. Also, the effect of dual-injection on carbonyl emissions is compared to DI using DMF and ethanol blends.

Ethanol blends are then used to compare the PM emissions in dual-injection and DI. Although dual-injection produces high NO_x emissions, the PM mass is dramatically reduced due to the positive influence of gasoline in PFI.

8.2 Investigation of Hydrocarbon Species

Firstly, the analysis of DMF emissions using GC/FID and GC/MS is discussed. As the GC/FID is based on the retention time (t_R) the probable emissions products can be postulated (Grob, 1985). The GC/MS is then used to confirm the other peaks. Wherever possible, the formation pathways of the combustion products are explained. However, the author's speciality does not lie in Chemistry, so the chemical analysis is brief (support for the Chemical analysis was provided by Dr Lixia Wei, Tianjin University, China). The carbonyl emissions (Section 8.3) and PM emissions are then analysed (Section 8.4).

8.2.1 Light-Range Hydrocarbons using GC/FID

An important principle when qualitatively analysing chromatographic data is that the matched retention time of a known compound and an unknown does not necessarily prove that these compounds are identical. However, what can be said with certainty, is that if there is no discernible peak at the t_R of the known compound, then this compound is not present (Grob, 1985). Clearly, this process of probable identification and certain elimination of compounds requires knowledge of the likely compounds to start with. Therefore, in this work the common compounds eluted with gasoline are used as an indicator for the other fuels. The peaks were identified based on t_R matches with the standard (±0.1mins).

8.2.1.1 Gasoline

Of the 15 standard compounds (Table 3.6), 12 were identified from the gasoline emissions using t_R (Figure 8.1). The species not found were propane, *iso*-butane and 1,3-butadiene. Although only 0.2% of dienes are present in the gasoline (Table 3.9), a high concentration of

1,3-butadiene was expected. However because this compound is unstable in Tedlar bags, its emissions should be treated with caution.

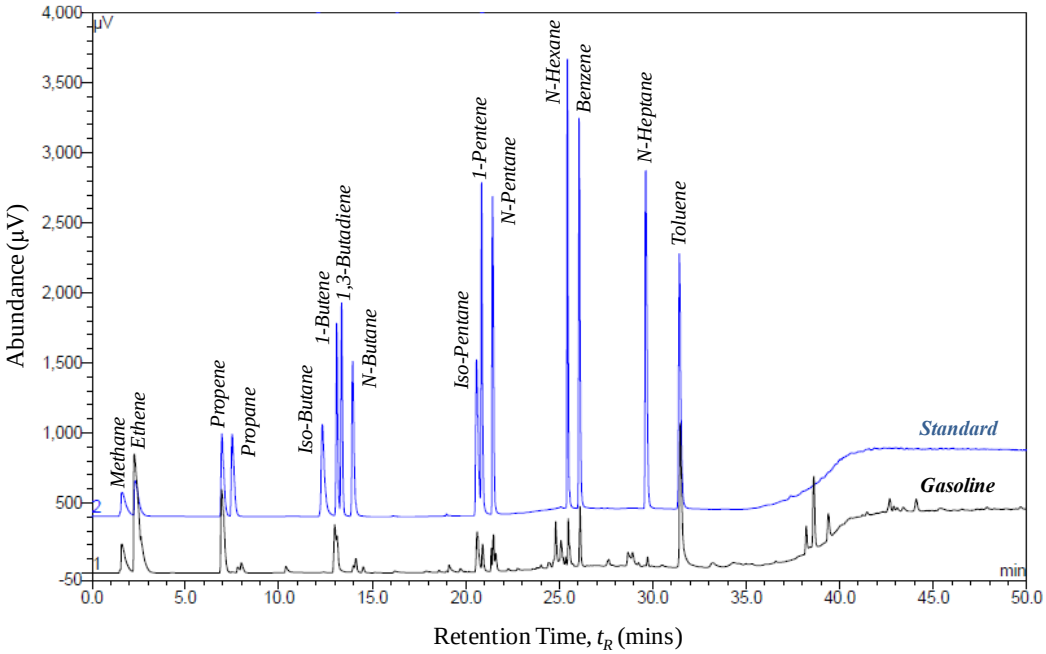

Figure 8.1 GC/FID Output of GDI Emissions compared to Standard

Table 8.1 Compounds identified from GC/FID when using GDI

	Compound	**Retention Time, t_R (mins)**	**Calibration Retention Time (mins)**
(1)	Methane (CH_4)	1.6	1.6
(2)	Ethene (C_2H_4)	2.28	2.31
(3)	Propene (C_3H_6)	6.94	6.95
(4)	1-Butene (C_4H_8)	13.11	13.09
(5)	*n*-Butane (C_4H_{10})	13.99	13.95
(6)	*iso*-Pentane (C_5H_{12})	20.61	20.58
(7)	1-Pentene (C_5H_{10})	20.9	20.85
(8)	*n*-Pentane (C_5H_{12})	21.48	21.44
(9)	*n*-Hexane (C_6H_{14})	25.52	25.44
(10)	Benzene (C_6H_6)	26.15	26.07
(11)	*n*-Heptane (C_7H_{16})	29.71	29.62
(12)	Toluene (C_7H_8)	31.60	31.42

Among the matched compounds, ethene (C_2H_4) was the most abundant species. In terms of chromatogram area, ethene is 1.9 and 2.6 times greater than toluene and propene on a C_1 basis, respectively. The response factors are determined from the calibration sample (0.72 and 0.69, respectively), as is normally required (Scanlan, 1985, Kállai, 2003, Kállai, 2002). Ethene is produced from the decomposition of carbonyls like *n*-propyl and *n*-butyl, which are produced directly from the fuel in either low or high temperature regions (Daniel, 2012e).

Ethene is then consumed through either oxygenation or H-abstraction reactions. However, since the C-H bond in ethene is stronger than in methane, it is more easily retained in the flame. Therefore, it is common to detect a higher concentration of ethene than methane in the emissions of gasoline (Kar, 2009).

8.2.1.2 DMF

The GC/FID results when using DMF are shown in Figure 8.2 and present a lower variation of species compared to gasoline in Figure 8.1. This is expected as gasoline is a combination of HC fractions and DMF is a single compound fuel. The low concentrations are due to the high dilution ratio. The large peak around t_R = 27.7mins, is likely to be unburned DMF. This is common for single component fuels. For example, the emissions of unburned Dimethyl ether (DME) are the most dominant HC; approximately 60% of the total HC (Zhu, 2011).

An expansion of the results in Figure 8.2 is given in Figure 8.3. The unmatched peaks (1-6) show that other compounds exist in this region, some of which are identified using GC/MS. The four peaks between 1,3-butadiene and *n*-hexane are likely to be determined by GC/MS.

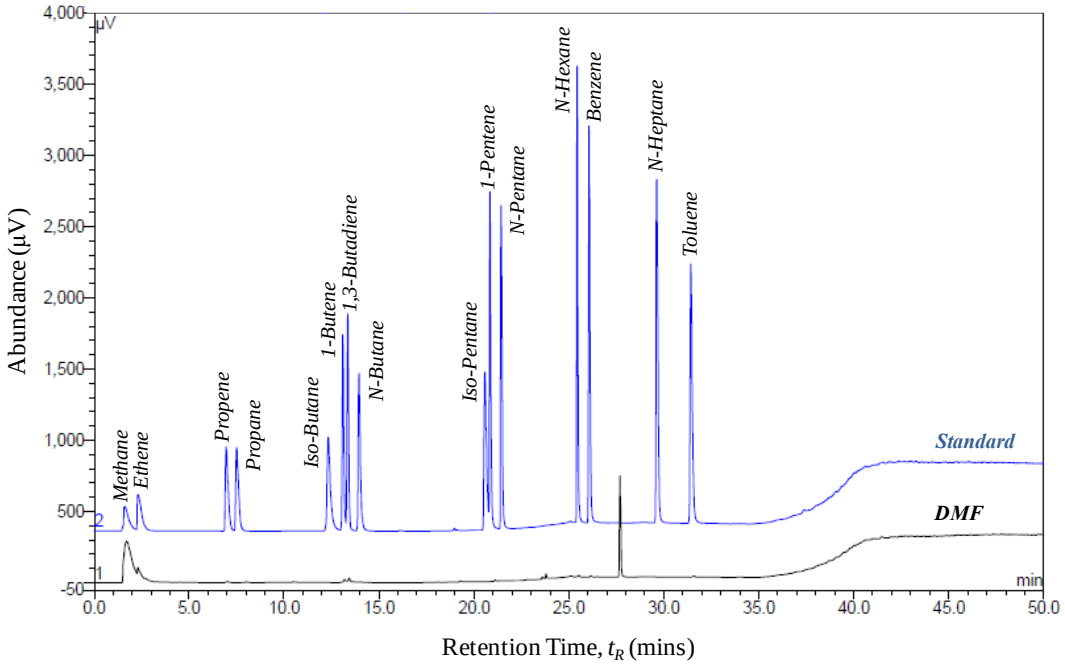

Figure 8.2 GC/FID Output of DMF Emissions compared to Standard

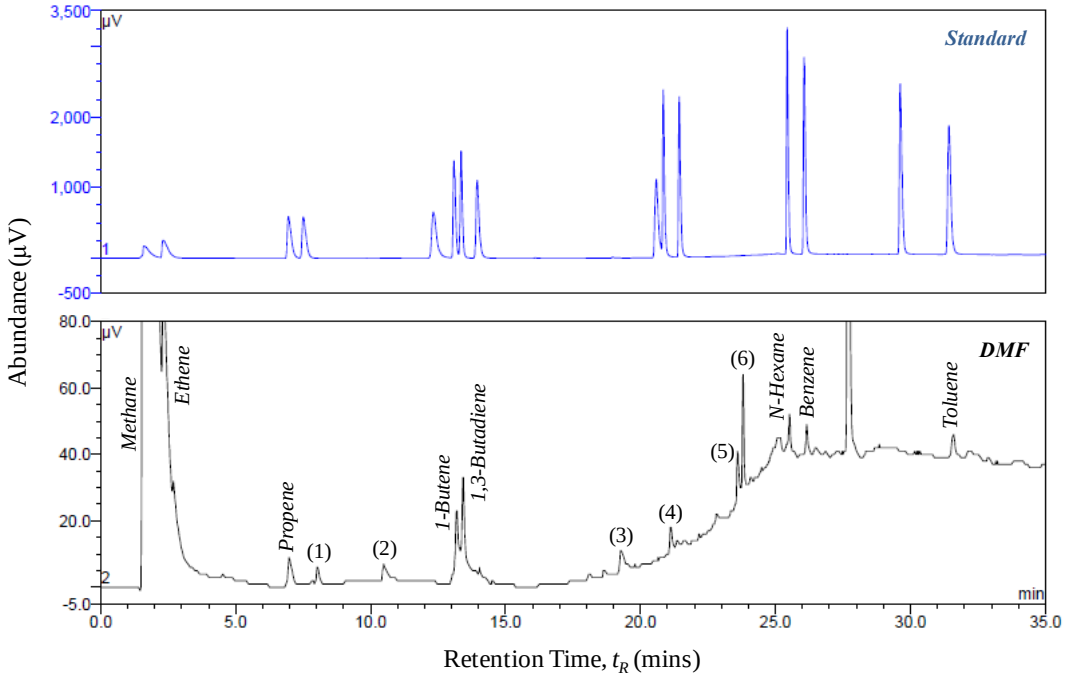

Figure 8.3 GC/FID Output (Expanded) of DMF Emissions compared to Standard

The matched compounds in the exhaust DMF of are summarized in Table 8.2.

Table 8.2 Compounds identified from GC/FID when using DMF in DI

Compound	Retention Time, t_R (mins)	Calibration Retention Time (mins)
Methane (CH_4)	1.7	1.6
Ethene (C_2H_4)	2.3	2.3
Propene (C_3H_6)	7.0	7.0
1-Butene (C_4H_8)	13.2	13.1
1,3-Butadiene (C_4H_6)	13.4	13.4
n-Hexane (C_6H_{14})	25.5	25.4
Benzene (C_6H_6)	26.2	26.1
Toluene (C_7H_8)	31.6	31.5

The low peak heights compared to the probable DMF peak suggest that the emissions of these other compounds are very low. Common compounds in the emissions of HC fuels, such as alkanes (methane, n-hexane), alkenes (ethane, propene, 1-butene), dienes (1,3-butadiene) and aromatics (benzene and toluene), have been observed in the exhaust of DMF.

The emission of methane is particularly high when using DMF, which is due to the two methyl groups (Daniel, 2012e). DME, which also has two methyl groups, produces high methane emissions in CI engines (Oguma, 2005). At medium loads, the total HCs when using DME comprise up to 20% of methane, whereas for diesel this is ≈5%. For gasoline and ethanol, the emissions of methane are typically between 8-9% of the total HCs (Kar, 2009).

In terms of area, the production of methane is three times higher than ethene on a C_1 basis (using the response factors from the standard sample of 1 and 0.63, respectively). This is because each reaction process produces lower concentrations of the next molecule. For instance, the order of concentration is usually: methane > ethane > ethyl > ethene. Therefore, the differences between the methane and ethene concentrations in the combustion of gasoline and DMF originate from the differences in their formation pathways (Daniel, 2012e).

As mentioned, the GC/FID process also allows the elimination of compounds when no peaks exist at the t_R of the standard. Therefore, the standard compounds which were not present in the DMF exhaust include: propane, *iso*-butane, *n*-butane, *iso*-pentane, *n*-pentane, 1-pentene and *n*-heptane. This is likely because straight-chain compounds are more difficult to form from benzene ring fuels.

8.2.1.3 Reliability of Identification using Retention Times

The GC/FID technique suffers from limitations. For example, *n*-hexane is matched in the GC/FID analysis but will be shown to be not present by GC/MS. This conflict suggests that *n*-hexane may not be produced by the combustion of DMF and the GC/FID results need to be treated with caution.

Although the t_R is reproducible if both the standard and sample are run under the same conditions shortly after each other, slight variations in temperature, carrier gas pressure, or delayed injection/acquisition can cause subtle changes in t_R. Therefore, the GC/FID method is a guide to the compounds emitted. Methods have been created to avoid these uncertainties such as the Kovats retention index (Kováts, 1958). However, an observation of Tedlar bag stability is made to analyse the HC concentration decay.

8.2.1.4 Effect of Species during Storage

The gasoline exhaust sample is relatively stable after 5 days, as shown in Figure 8.4 (<15% change in peak height). That is, apart from the unidentified compound that increases significantly in height at 24.9mins. Although this compound is not identified, its presence reinforces the need for immediate sample analysis.

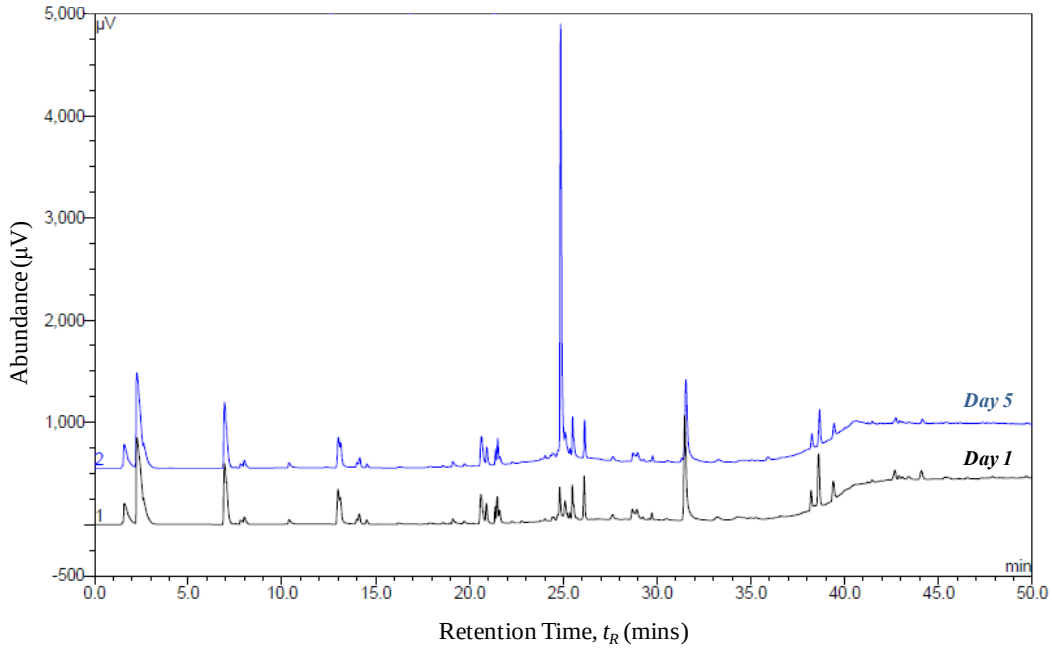

Figure 8.4 GC/FID Output of GDI Emissions (Day 1 and 5)

The stability of the DMF emissions sample is similarly shown in Figure 8.5 (over 7 days).

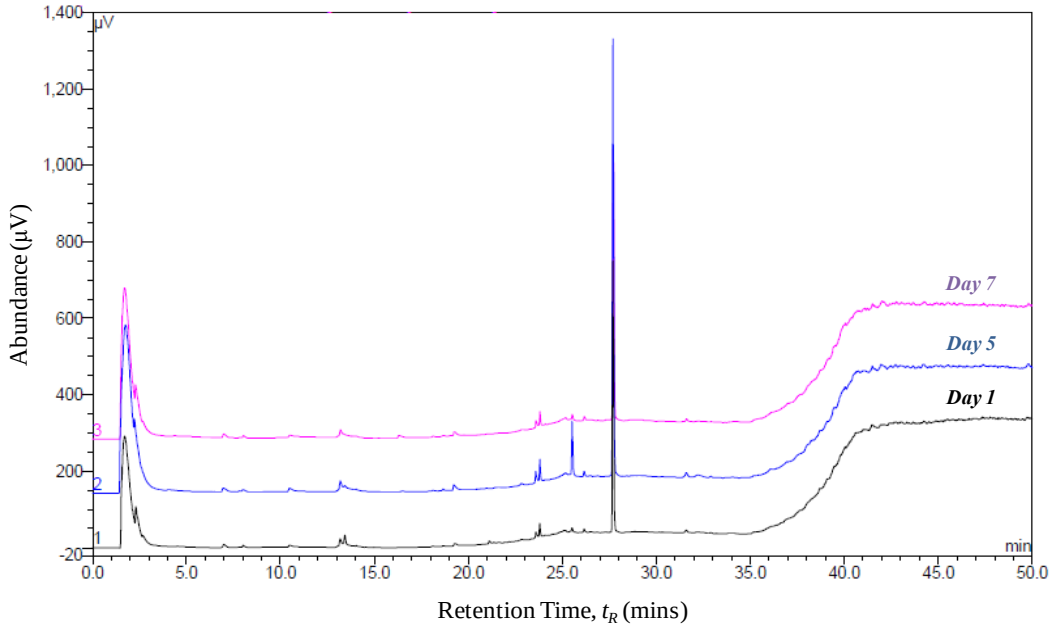

Figure 8.5 GC/FID Output of GDI Emissions (Day 1, 5 and 7)

The peak at 25.7mins, previously identified as *n*-hexane (Figure 8.2), increases at Day 5 and the peak at 13.2mins (1-butene) disappears. The areas of methane and ethane also vary. This suggests that chemical interactions do occur in the bag sample and it is important to analyse the sample immediately.

Nevertheless, the results from the Tedlar bag sample are relatively stable and it can be said with confidence that the detected compounds are likely to be present in the emissions of DMF. However these peaks are almost negligible compared to unburned DMF.

Furthermore, the low FID sensitivity for oxygenates suggests that a true emissions reading of DMF would eclipse the 'trace' peaks. The use of GC/MS gives a more definitive analysis.

8.2.2 Medium-Range Hydrocarbons using GC/MS

In this study, GC/MS is used to detect mid-range HCs. It helps to identify the unknown peaks found in the GC/FID work and any other significant HCs. However, the higher volatility compounds (from methane to 1,3-butadiene) cannot be detected with the column used, which suggests that compounds (1) and (2) in Figure 8.3 will not be identified. The chromatogram window starts from 2mins to avoid the large peak created by CO_2 (usually overcome by a solvent delay).

As suggested by the GC/FID work, the mid-range HCs are dominated by the emissions of unburned DMF, as shown in Figure 8.6. This mass spectrum of DMF is clearly shown in the inset graph, where the peak mass equates to the molecular mass (M_w=96 g/mol).

The spectral analysis was performed by comparing the experimental spectra with the reference in the library (95% match at 4.9mins).

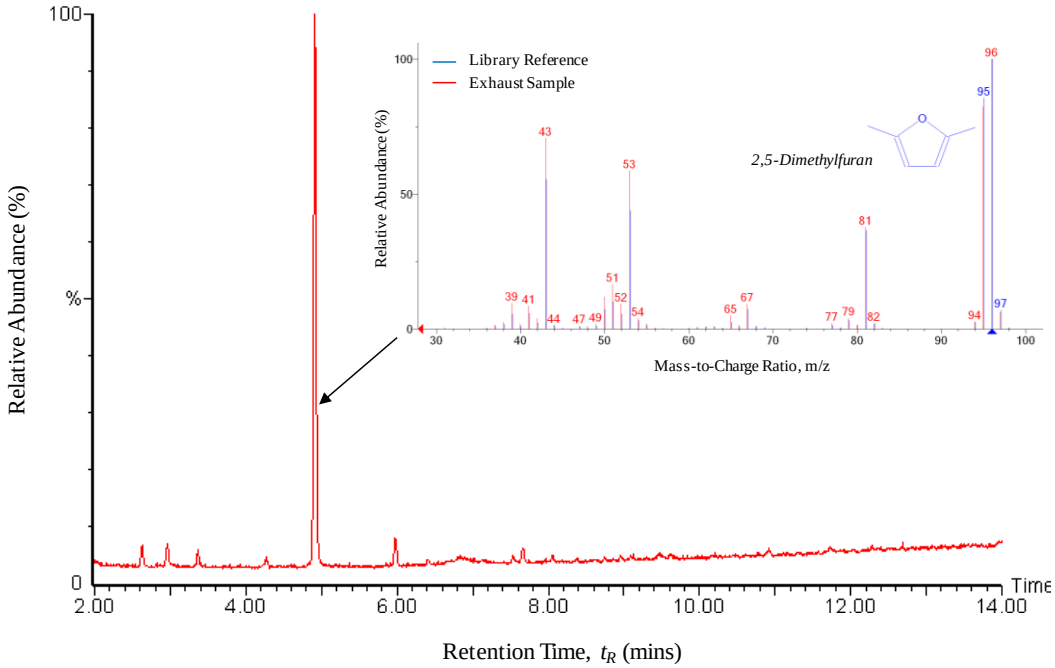

Figure 8.6 Mid-Range HC Emissions (C_5-C_{12}) from DMF Emissions

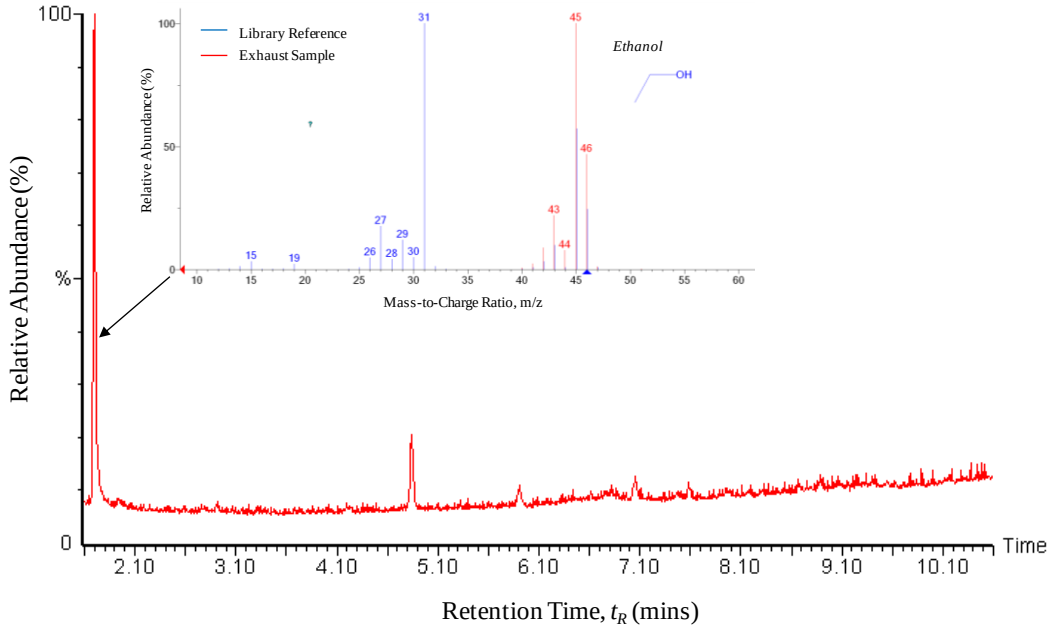

Figure 8.7 Mid-Range HC Emissions (C_5-C_{12}) from Ethanol Emissions

The high concentration of unburned DMF is common for pure component fuels (Kar, 2009, Zhu, 2011). This is shown by the domination of unburned fuel when using ethanol in Figure 8.7. This is a 60% library match as the lower masses (<35m/z) were not scanned (only 35-200m/z) unlike the work of others (Kar, 2011). The second largest peak at 4.7mins (90% match) is residual DMF within the fuel system.

The use of GC/MS allows the identification of additional HCs emitted during the combustion of DMF (expansion in Figure 8.8). This was obtained using the *combine spectra* function in the *TurboMass* software, which allows the subtraction of the background (helium and column material (fused silica) bleed) to obtain an accurate sample match to the library.

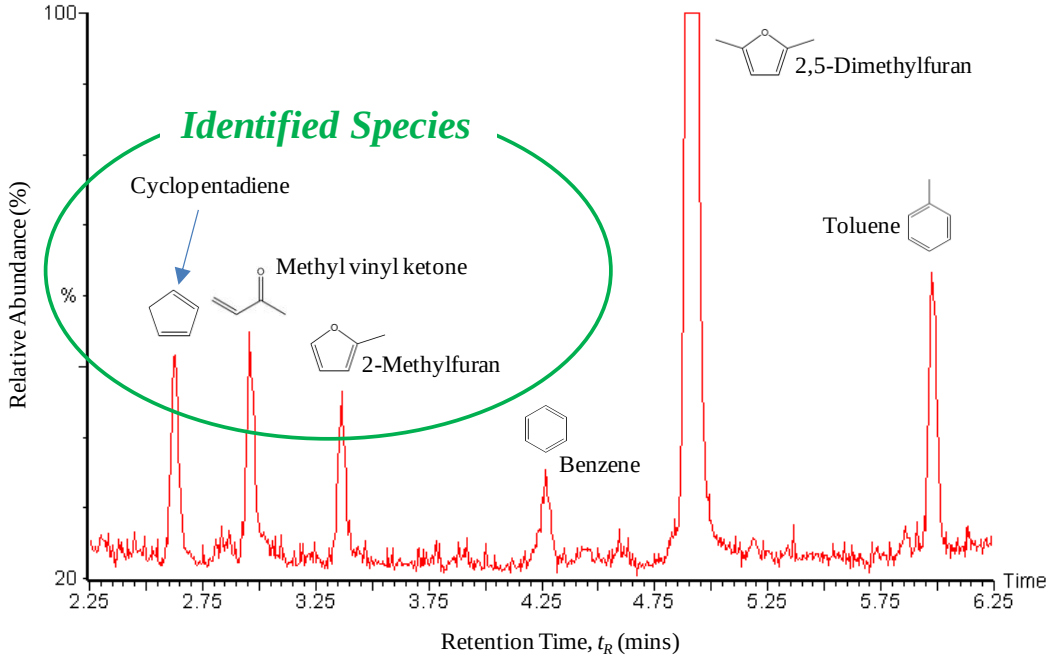

Figure 8.8 Chromatogram before DMF peak from DMF Emissions

The three HCs identified before the DMF peak are: cyclopentadiene, methylvinyl ketone (MVK) and 2-methylfuran (MF). The mass spectrums of each are shown in Figure 8.9.

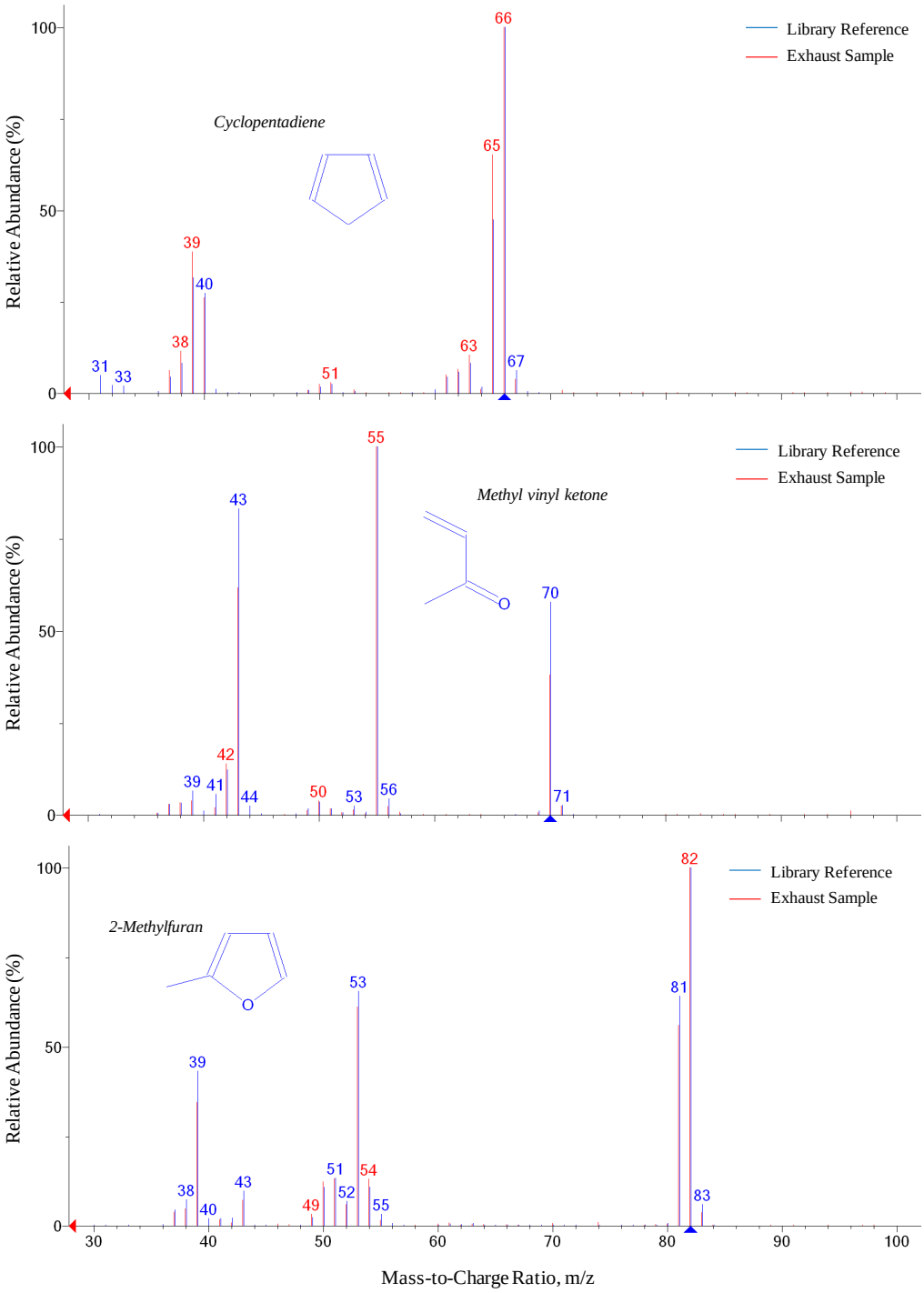

Figure 8.9 Mass Spectra for Cyclopentadiene (a), MVK (b) and MF (c)

The first two HCs identified (cyclopentadiene at t_R=2.6mins, 55% match and MVK at t_R=3mins, 90% match) are common in the emissions from gasoline (Westerholm, 1992). For

DMF, the reaction between various free radicals (R), common in hydrocarbon flames, could form MVK. For instance, the carbonyl radical formed from H-abstraction from acetaldehyde (C_2H_4O), C_2H_3O and the vinyl radical, C_2H_3 (produced from ethene (C_2H_4) consumption (Law, 2006)) is likely to form MVK, C_4H_6O:

(R1) $C_2H_3O + C_2H_3 \rightarrow C_4H_6O$

The third species detected is MF (t_R = 3.4mins, 75% match). This furan derivative is likely to be produced due to the reaction of DMF with a hydrogen atom and subsequent methyl elimination, as suggested by others (Simmie, 2011):

(R2) $C_6H_8O + H \rightarrow C_5H_6O + CH_3$

The analogous reaction of MF (C_5H_6O) would then result in the formation of furan (C_4H_4O) (Tian, 2011):

(R3) $C_4H_3OCH_3 + H \rightarrow C_4H_4O + CH_3$

However, the signal for furan was not clearly observed in the exhaust of DMF when using the GC/MS. This might be attributed to the low concentration of MF. The high concentration of DMF leads to a low signal of MF. Therefore, a similar decay would lead to a very low or possibly unobservable signal of furan, because they are formed in this order.

Nevertheless, when analysing the chromatogram for specific masses (39 and 68), a trace of furan is found. These masses represent the parent and fragmented (during the splitting of the furan ring) masses of furan, whose overall signal is negligible in the original chromatogram in Figure 8.6. The signal intensities are shown in Figure 8.10.

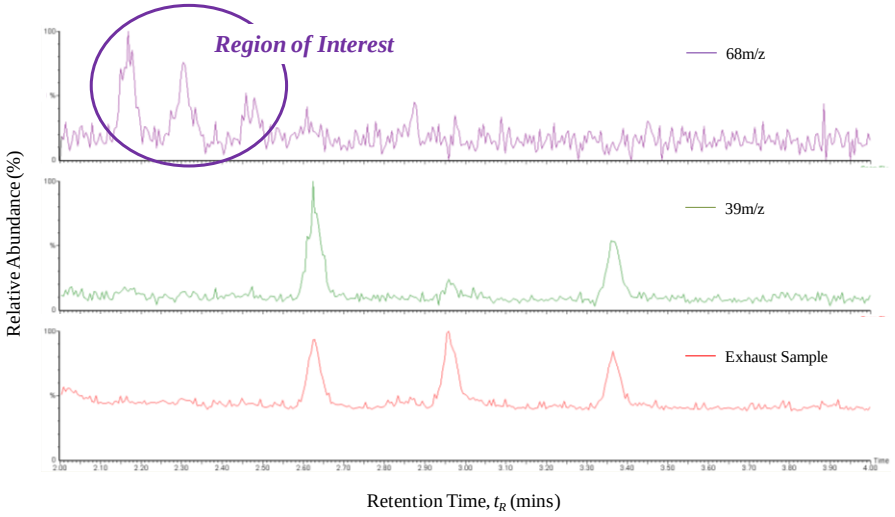

Figure 8.10 Chromatogram of 68m/z, 39m/z and DMF Emissions

When analysing the largest peak at mass 68 (2.2mins), the spectrum of furan is accurately matched with the library (70%), as shown in Figure 8.11.

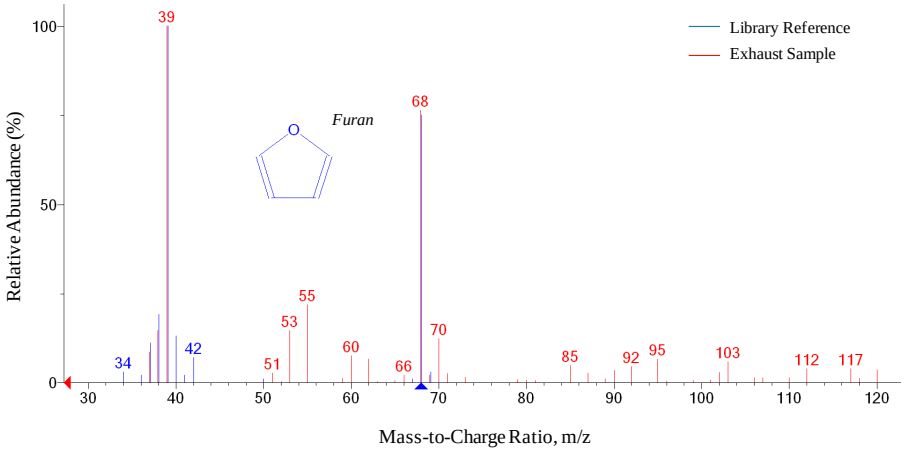

Figure 8.11 Mass Spectra for Furan (C_5H_6O)

Observations of the GC/MS analysis of Figure 8.6 at higher t_R leads to the detection of 2-ethyl-5-methylfuran (EMF), ethylbenzene, *p*-xylene and *o*-xylene (at 6.4, 7.5, 7.7 and 8.1mins, respectively with 60, 25, 30 and 30% matches), as indicated in Figure 8.12.

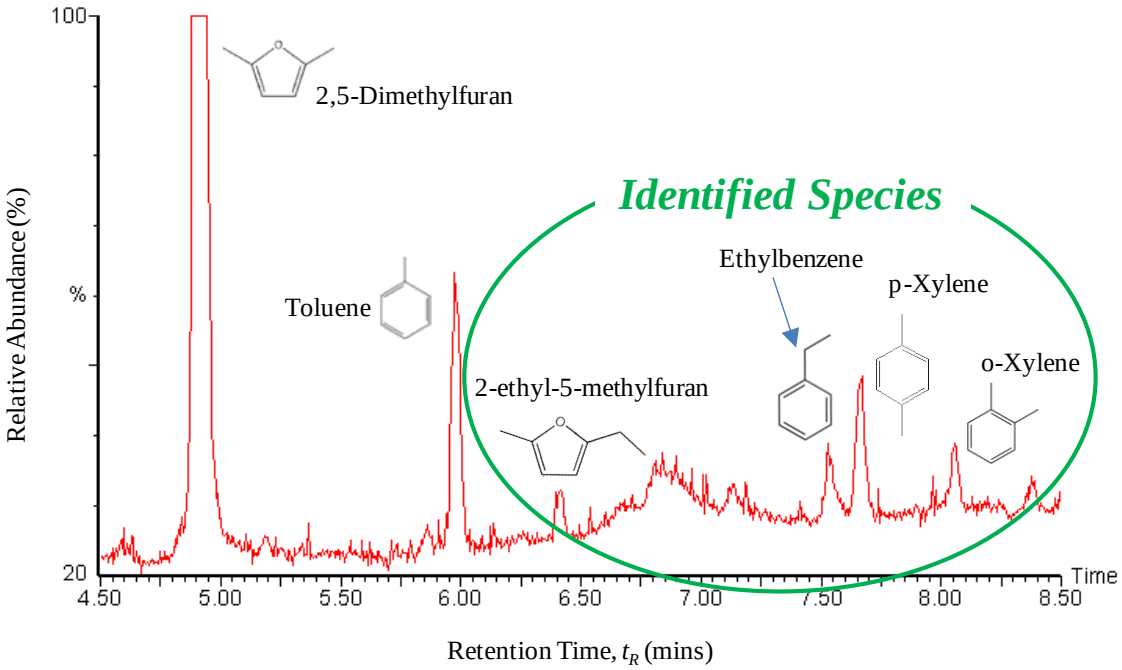

Figure 8.12 Chromatogram after DMF peak from DMF Emissions

EMF ($C_7H_{10}O$) is likely to be produced from the combination of methyl (CH_3) with 5-methylfuranylmethyl (C_6H_7O), which is easily produced by the H-abstraction reaction from a methyl chain of DMF by a radical, as shown in R4 and R5 (furan ring remains):

(R4) $C_6H_8O + R \rightarrow C_6H_7O + HR$ (R = OH, H, O, CH_3)

(R5) $C_6H_7O + CH_3 \rightarrow C_7H_{10}O$

The emissions of aromatics found in the GC/FID are re-iterated through the GC/MS analysis with benzene and toluene at 4.3mins (70% match) and 6mins (40% match), respectively. The formation of ethylbenzene (C_8H_{10}), *p*-xylene (*p*-C_8H_{10}) and *o*-xylene (*o*- C_8H_{10}) is a result of the presence of toluene (C_7H_8). These aromatics are formed in a similar manner to that of EMF (R4 and R5) and MF (R2) from DMF, respectively (Dagaut, 2002):

(R6) $C_7H_8 + R \rightarrow C_7H_7 + HR$ (R = OH, H, O, CH_3, etc)

(R7) $C_7H_7 + CH_3 \rightarrow C_8H_{10}$

(R8) $C_7H_8 + CH_3 \rightarrow p\text{-}\ C_8H_{10} + H$

(R9) $C_7H_8 + CH_3 \rightarrow o\text{-}\ C_8H_{10} + H$

Although *m*-xylene would be eluted at a similar time to *p*-xylene, it is unobservable from Figure 8.12. This is due to the selectivity of the benzene ring addition reaction. The isomers of dimethylbenzene produce three xylenes, which are determined by the arrangement of two methyl groups on the benzene ring carbon atoms. Methyl radicals are more likely to be first added to the *o*- or *p*- positions on the benzene ring in toluene, rather than the *m*-position, according to the rules of orientation on the benzene ring.

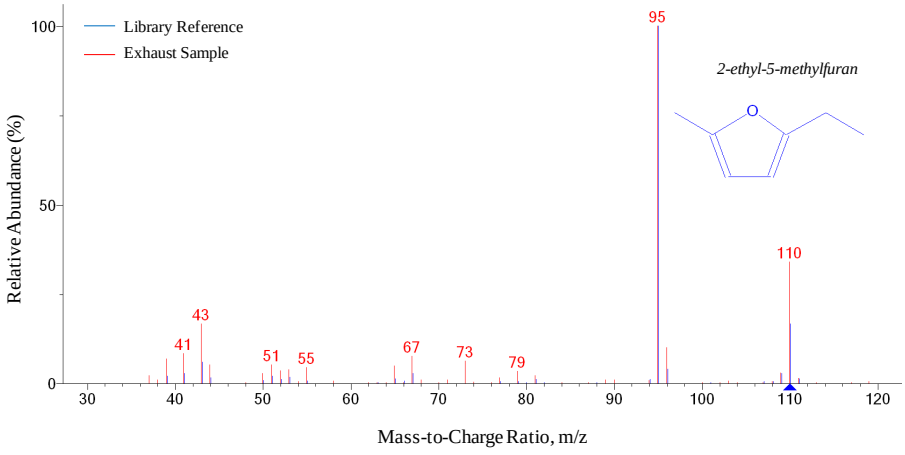

Figure 8.13 Mass Spectra for 2-Ethyl-5-Methylfuran ($C_7H_{10}O$)

In summary, the HC emissions detected from the combustion of DMF using GC/MS are individually ≤5% of the largest emissions (unburned DMF) as shown in Table 8.3. This includes four trace compounds (<1%) which were not identified in Figure 8.8 or Figure 8.12.

Table 8.3 Peak Chromatogram Areas from Engine-out Emissions when using DMF

	Major Compounds	Retention Time (mins)	Relative Area (%)
(1)	Cyclopentadiene	2.6	3.9
(2)	Methylvinyl Ketone	3.0	4.7
(3)	2-Methylfuran	3.4	3.2
(4)	Benzene	4.3	2.5
(5)	2,5-Dimethylfuran	4.9	100.0
(6)	Toluene	6.0	5.8
(7)	2-Ethyl-5-Methylfuran	6.4	0.9
(8)	Ethylbenzene	7.5	1.6
(9)	p-Xylene	7.7	3.0
(10)	o-Xylene	8.1	1.5
	Trace Compounds	**Retention Time (mins)**	**Relative Area (%)**
(1)	5-Methylfurfuraldehyde	8.8	0.6
(2)	Benzaldehyde	8.9	0.3
(3)	Phenol	9.0	0.8
(4)	1-Methylethylbenzene	9.1	0.5

8.3 Investigation of Carbonyl Emissions

In this section, a quantitative investigation of the carbonyl emissions is performed at a fixed engine load (5.5bar IMEP), speed (1500rpm) and relative AFR mixture (λ=1). The results using DI and dual-injection are discussed in turn.

8.3.1 HPLC

The reaction mechanism of the carbonyls absorbed in the DNPH solution is shown in Figure 8.14. The carbonyl derivatives are formed by the condensation reaction (loss of water, H_2O) and addition of -NH_2 to the C=O carbonyl group. In this form, the HPLC can be used to determine the concentration in the exhaust of DMF.

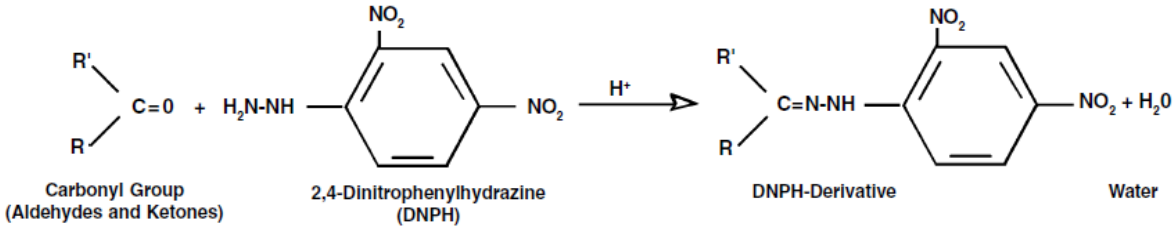

Figure 8.14 Reaction Mechanisms of Carbonyls with DNPH Solution (DeGraff, 1996)

The peak areas of each derivative are compared to the standard. The final concentration is then presented on a C_1 basis ppm (volume), equivalent to the concentration of formaldehyde (CH_2O), as shown using gasoline in Figure 8.15.

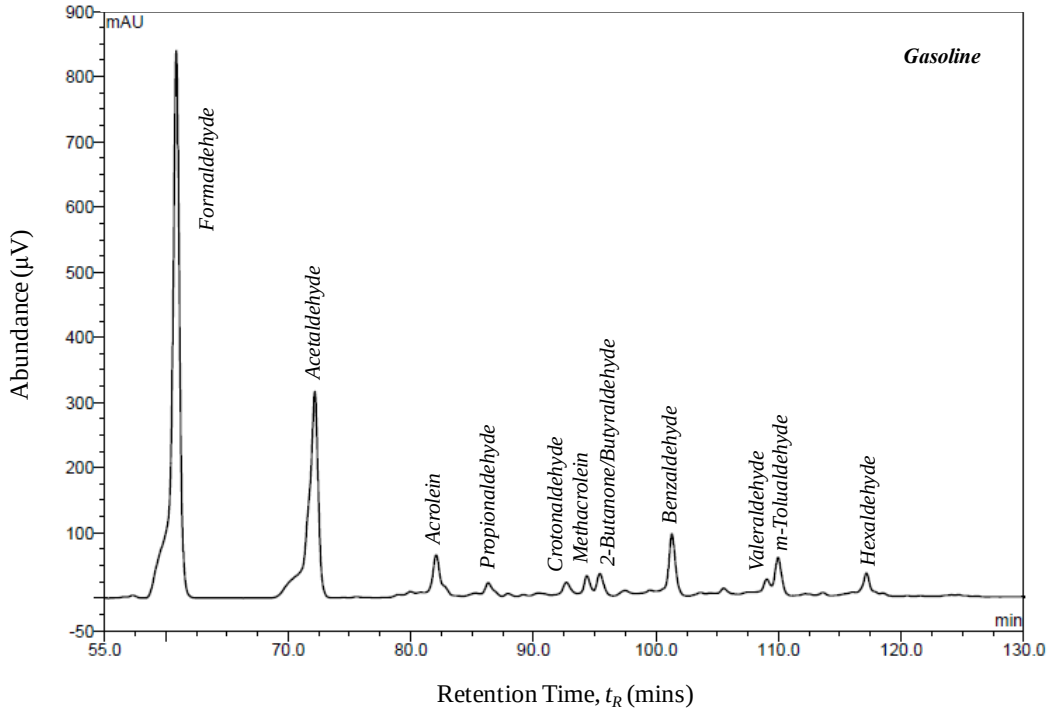

Figure 8.15 HPLC Output of GDI Emissions at 5.5bar IMEP

Firstly, the carbonyl emissions when using DMF are compared to ethanol and gasoline in DI.

8.3.2 DMF compared to Ethanol and Gasoline in DI

In the previous chapters, the total HC emissions produced from the combustion of ethanol, DMF and gasoline have been shown to increase in that order, regardless of the engine load. In comparison, the carbonyl emissions when using gasoline have been found to be approximately 5% of the total HC emissions (Elghawi, 2009, Zervas, 2002).

However, this comparison was made using an FID detector (Horiba MEXA-7100DEGR) which has been shown to be less sensitive to oxygenated compounds (Cheng, 1998, Wallner, 2008). Therefore, in order to reduce time and cost, the carbonyl emissions in this study are shown in ppm (volume). The indicated specific units (g/kWh) could not be calculated using the normal procedure (SAE, 1993) because the total HCs (including oxygenated compounds) was unreliable with an FID.

The emissions of the highest carbonyls when using gasoline (formaldehyde, acetaldehyde and benzaldehyde) are compared to ethanol and DMF in Figure 8.16.

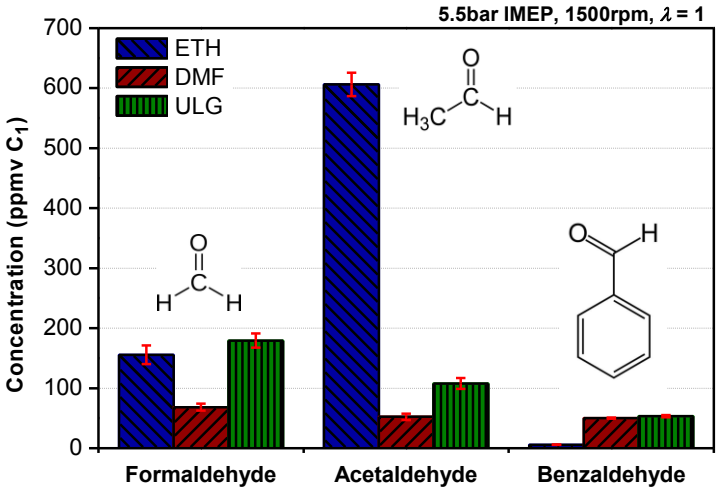

Figure 8.16 Formaldehyde, Acetaldehyde and Benzaldehyde Emissions

The high paraffin content in the gasoline (≈35%; Table 3.9) is responsible for producing the highest carbonyl emission of formaldehyde (Held, 1998). However, as the number of carbon atoms increases, the concentration decreases. This trend has been seen in other investigations (Magnusson, 2011). The formation of acetaldehyde when using ethanol is much higher than formaldehyde (by a factor of 4) and also much higher compared to DMF and gasoline. This high emission of formaldehyde has been seen in other work (Magnusson, 2011, Jacobson, 2007) and is closely related to the structure of the fuel. Ethanol (C_2H_6O) is mainly consumed in the following reaction:

(R10) $C_2H_6O + OH \rightarrow C_2H_5O + H_2O$

The radical formed in R10 mainly turns into acetaldehyde (C_2H_4O) leading to a high exhaust concentration (Knapp, 1998, Niven, 2005, Storey, 2010):

(R11) $C_2H_5O + M \rightarrow C_2H_4O + H + M$

The reaction of acetaldehyde then leads to the formation of methyl. Oxidation of methyl then forms formaldehyde:

(R12) $CH_3 + O_2 \rightarrow CH_2O + OH$

The dominance of R11 in the emissions of ethanol leads to a greater tendency for oxygenated HCs like formaldehyde to form. As a result, the concentration of acetaldehyde relative to formaldehyde is much higher than compared with DMF and gasoline. However, the emissions of formaldehyde when using ethanol are similar to gasoline, in agreement with the work of Magnusson (Magnusson, 2011).

When using DMF, the emissions of formaldehyde and acetaldehyde are lower than with gasoline and ethanol; decreases >50% are seen with DMF. Formaldehyde and acetaldehyde are formed during low temperature oxidation of HC fuels (Brackmann, 2003, Ogawa, 2011). However, DMF has been shown to burn with a high temperature (Daniel, 2011), which may help to inhibit the production of formaldehyde and acetaldehyde.

The low production of formaldehyde and acetaldehyde is due to DMF's chemical structure. Firstly, it is likely that the oxidation of each methyl group will form combustion radicals, such as ketenyl (HCCO) and propargyl (C_3H_3) (Wu, 2009b):

(R13) 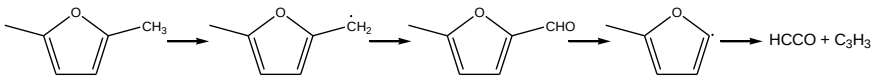

The reaction of ketenyl will lead to the products of complete combustion: CO_2 and H_2O. For propargyl, the first aromatic ring (benzene) is formed (Wu, 2009b):

(R14) $2C_3H_3 \rightarrow C_6H_6$

The reaction of benzene (C_6H_6) with a methyl radical (CH_3), will then lead to the formation of toluene (C_7H_8). Further oxidation of toluene will then lead to the formation of benzaldehyde:

(R15) 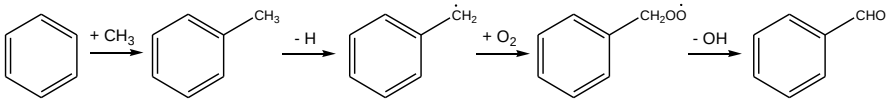

This reaction sequence (R3→R14→R15), competes with other reactions of DMF. As a result, the formation of formaldehyde and acetaldehyde is reduced. Since each reaction is

less likely and the radical combination reaction (R14) is unfavourable, the concentration of benzaldehyde is decreasingly lower than formaldehyde and acetaldehyde (Figure 8.16).

The remaining carbonyl emissions are shown in Figure 8.17. Apart from the common carbonyls (formaldehyde, acetaldehyde and benzaldehyde), the higher carbonyls shown in Figure 3.8 were detected in the emission of DMF. The total emissions concentration of these higher carbonyls between fuels is: gasoline > DMF > ethanol (115.5, 89.6 and 15.4ppm, respectively). Clearly, after acetaldehyde and then formaldehyde, the incomplete combustion of ethanol produces few higher carbonyls.

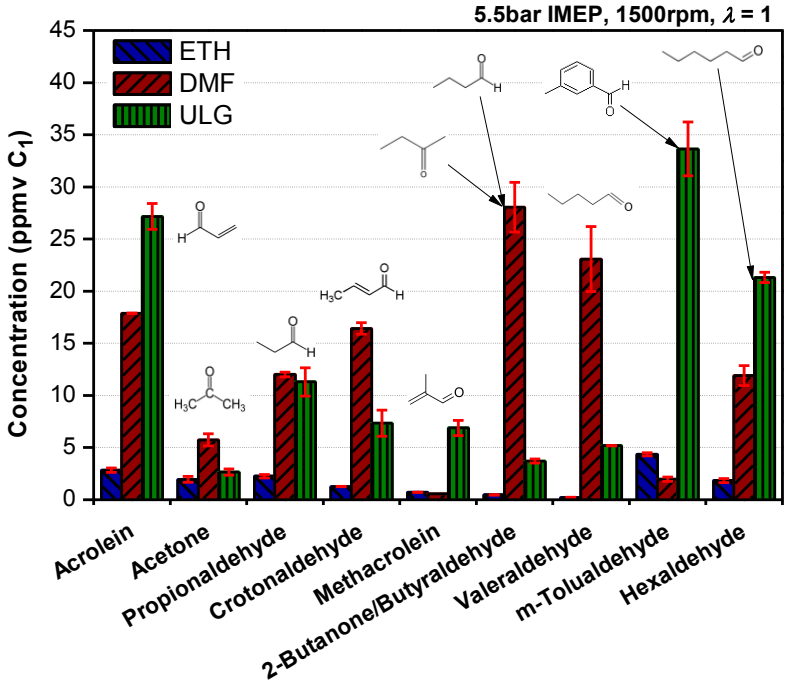

Figure 8.17 Higher Carbonyl Emissions

Although, the total carbonyl emission when using DMF is less than that with gasoline, there are four carbonyls which are greater (propionaldehyde, acetone, crotonaldehyde and valeraldehyde). The m-tolyualdehyde emissions are high when using gasoline due to the oxidation of toluene and *m*-, *o*- and *p*-xylene (Zervas, 2002); this is likely because the

gasoline used in this study contained 35% aromatics. Also, the high paraffin content in the gasoline contributes to high acrolein (Elghawi, 2009). The carbonyl breakdown is as follows:

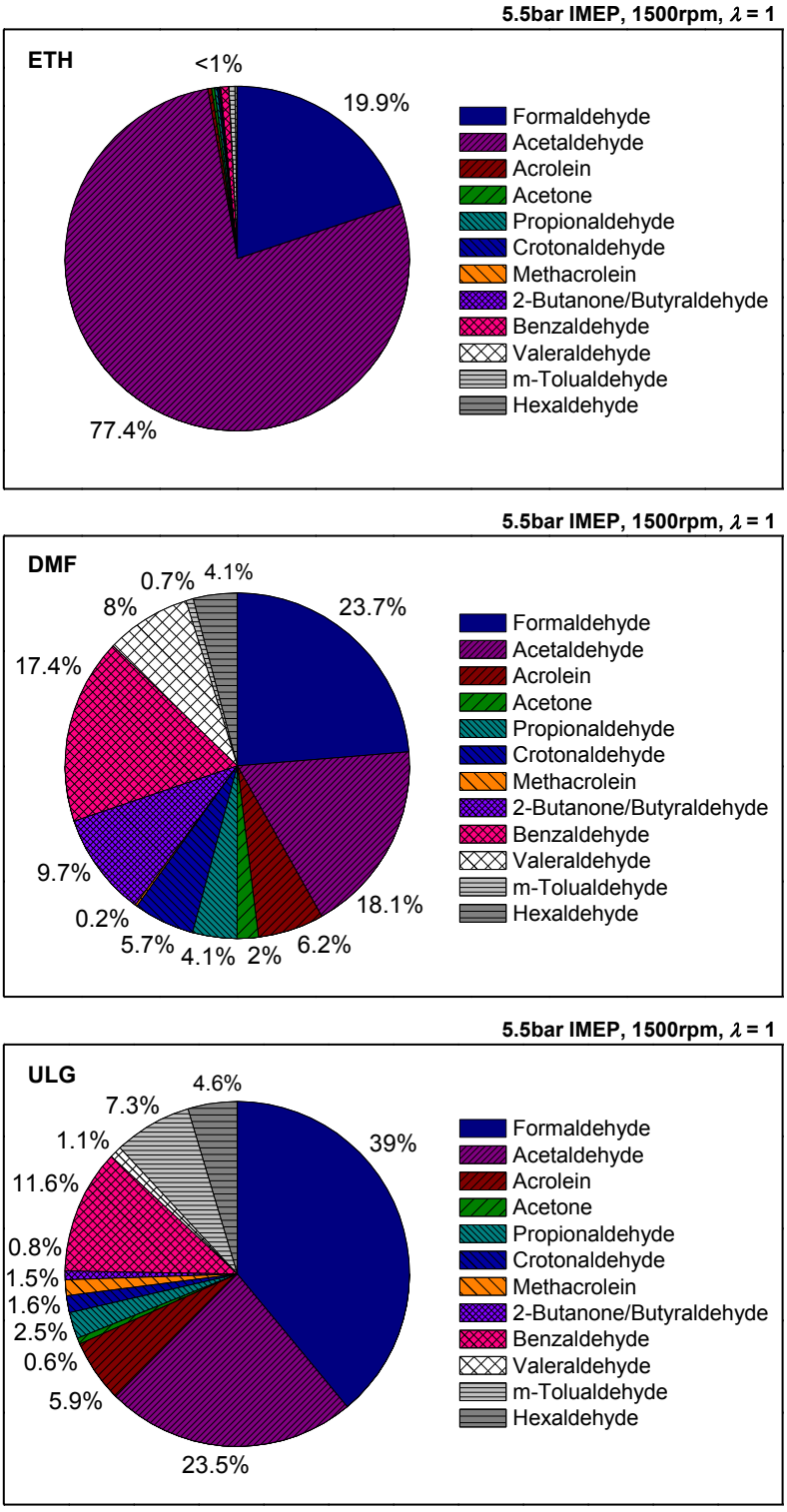

Figure 8.18 Carbonyl Emissions Variation with Ethanol (a), DMF (b) and Gasoline (c)

For gasoline, the proportion of carbonyls emitted (in Figure 8.18) decreases as the number of carbon atoms in each carbonyl increases. This is common in HC flames, since aldehydes with more carbon atoms have more hydrogen atoms are less likely to form ahead of aldehydes with fewer carbon and hydrogen atoms. This is because when stability is reached, more energy is required to form higher aldehydes and at the latter stages of combustion fewer free radicals exist. This behaviour is partially evident when using DMF. For ethanol, it is very clear that the abundance of acetaldehyde dominates the carbonyl formation, which is followed by formaldehyde (Magnusson, 2011).

8.3.3 DMF compared to other Oxygenated Fuels in DI

In this section, the carbonyl emissions of DMF are positioned amongst other oxygenated fuels (methanol and *n*-butanol). Between all fuels, DMF produces the lowest emissions of formaldehyde and acetaldehyde. In studies with ethanol, *n*-butanol and gasoline, these emissions are related to the oxygen content in the fuel (Wallner, 2010). However, the results in this section do not extend this relationship to methanol as shown in Figure 8.19.

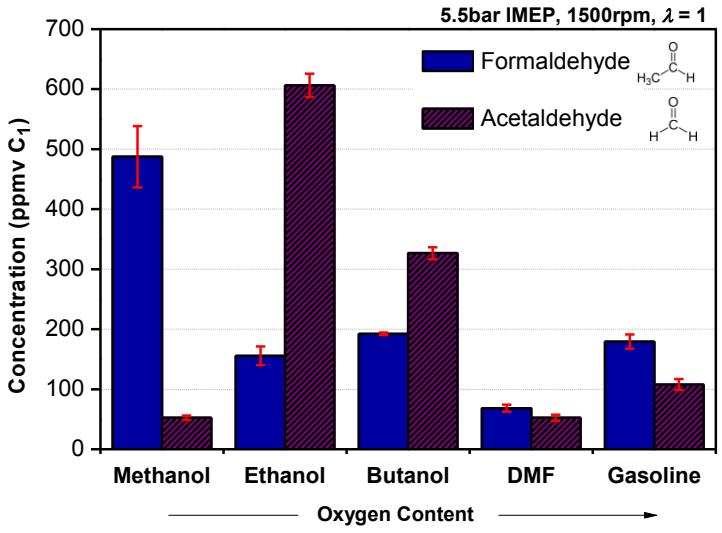

Figure 8.19 Formaldehyde and Acetaldehyde Emissions from Various Fuels

The direct comparison is made in Table 8.4. Magnusson and Nilsson showed that the total carbonyl emissions when using ethanol are higher than with methanol, whereby the main carbonyl emissions were acetaldehyde and formaldehyde, respectively (Magnusson, 2011). This behaviour is consistent with the results shown in this work (Table 8.4).

Table 8.4 Carbonyl Emissions Concentrations using Oxygenated Fuels and Gasoline

	Concentration ($ppmC_1$)				
Carbonyl	**Methanol**	**Ethanol**	***n*-Butanol**	**DMF**	**Gasoline**
Formaldehyde	487.5	155.7	192.2	68.4	179.4
Acetaldehyde	52.6	606.2	326.6	52.2	107.9
Acrolein	7.5	2.8	14.6	17.9	27.2
Acetone	2.5	2.0	9.2	5.7	2.7
Propionaldehyde	0.8	2.3	19.7	12.0	11.3
Crotonaldehyde	1.7	1.3	6.5	16.4	7.3
2-Butanone/ Butyraldehyde	0.6	0.5	151.2	28.0	3.7
Methacrolein	1.2	0.7	23.7	0.6	6.9
Benzaldehyde	9.3	5.7	7.0	50.2	53.6
Valeraldehyde	0.5	0.2	0.1	23.1	5.2
m-Tolualdehyde	6.6	4.3	4.1	2.0	33.6
Hexaldehyde	2.9	1.8	4.0	11.9	21.3
	573.7	783.5	758.9	288.4	460.1

Other research has also shown that the increasing methanol fraction in gasoline is directly related to the increasing formaldehyde emission concentrations (Wei, 2009, Zervas, 2002, Lipari, 1987, Williams, 1990). This is because during combustion, methanol oxidizes to form formaldehyde in the following reaction path (Held, 1998):

(R16) $2CH_3OH + O_2 \rightarrow 2CH_2O + 2H_2O$

The dominance of these carbonyl emissions is unsurprising as they are produced directly from the fuel, which is further reflected in the emissions of butanone/butyraldehyde during

the combustion of *n*-butanol (Wallner, 2010). The emissions of methacrolein is a major product in the oxidation of isobutene (Chen, 2000) which is likely to be high in the emission of *n*-butanol and gasoline.

The total carbonyl emissions also increase as the H/C ratio increases, when excluding methanol (ethanol > *n*-butanol > gasoline > DMF). This relationship was recognized by Zervas who drew a particular link to the emissions of formaldehyde, acetaldehyde, propionaldehyde and benzaldehyde (Zervas, 2002). This is because benzaldehyde is produced from low H/C ratio fuel components (largely fuel aromatics) whereas formaldehyde, acetaldehyde and to a lesser extent, propionaldehyde, are all formed from high H/C ratio fuel components. Zervas also noticed the inverse relationship of these carbonyl emissions with exhaust temperature (except for benzaldehyde).

This relationship extends to the combustion of DMF (H/C = 1.333: Table 3.8), as shown in Figure 8.20 (the results for methanol have been included, despite the aforementioned disagreement).

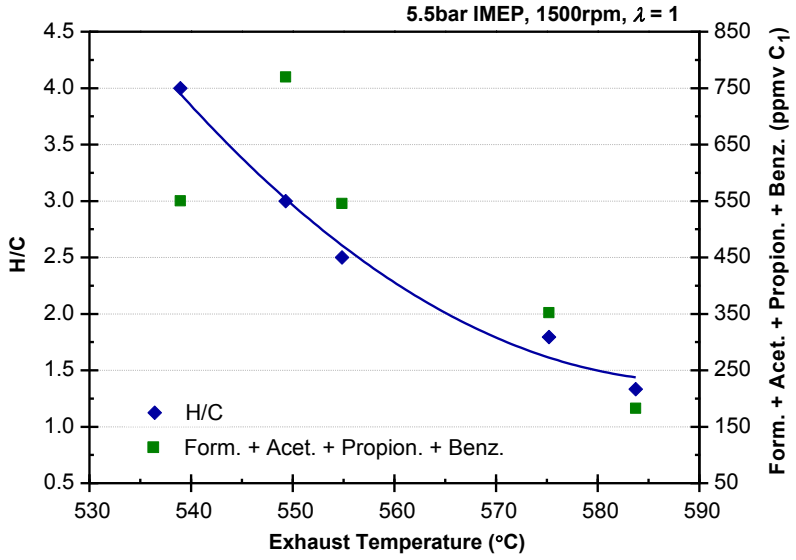

Figure 8.20 H/C Ratio and Combined Carbonyl Emissions with Exhaust Temperature

8.3.4 Dual-Injection Blends

The carbonyl emissions between direct- and dual-injection blends are discussed in this section. Firstly, the comparison between GDI and PFI are examined in order to appreciate the effect of fuel delivery on the emissions of carbonyls.

8.3.4.1 Gasoline

The individual concentrations of the three largest carbonyl emissions in GDI and PFI are shown in Figure 8.21.

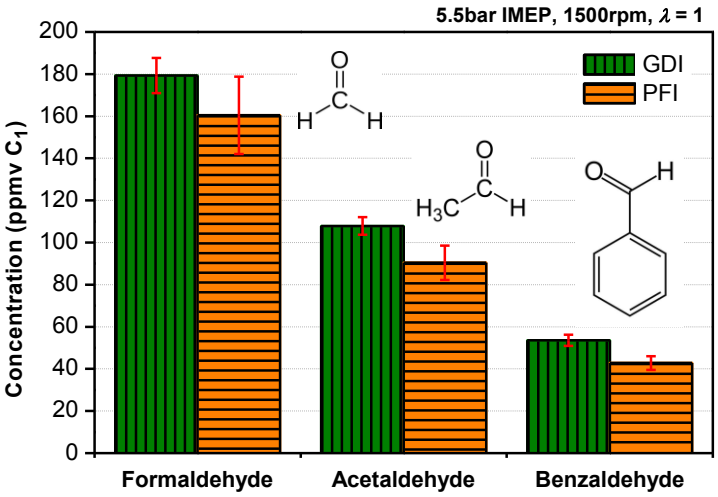

Figure 8.21 Formaldehyde, Acetaldehyde and Benzaldehyde for GDI and PFI

When in GDI, the combustion of gasoline produces 16% more emissions of each carbonyl than PFI. Formaldehyde and acetaldehyde are formed at low temperatures (Brackmann, 2003, Ogawa, 2011), which is more likely to occur in GDI due to the charge-cooling effect. The exhaust temperature when using PFI is also higher than with GDI (≈5%) largely because of greater spark retard (Figure 6.3). This helps to reduce the occurrence of formaldehyde and acetaldehyde. Benzladehyde, on the other hand is produced at higher temperatures, which

suggests that it is more likely to occur with PFI. However, combustion is more complete when using PFI which reduces the likeliness of benzaldehyde formation. This is because the mixture is more homogeneous due to increased fuel vaporisation time.

The remaining carbonyl emissions, when using GDI and PFI, are shown in Figure 8.22.

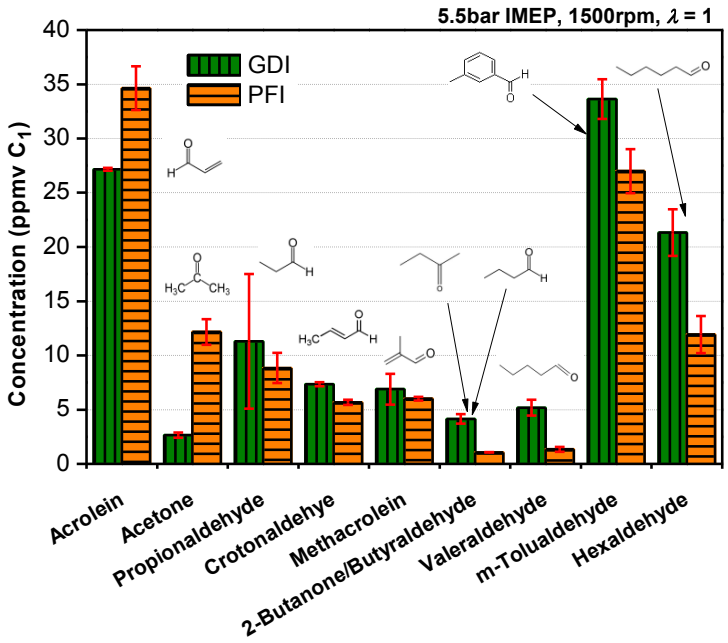

Figure 8.22 Higher Carbonyl Emissions for GDI and PFI

The sum of the carbonyls in Figure 8.22 is marginally higher in GDI (115.5ppm) than PFI (107.6ppm). PFI has been shown to produce marginally lower total HC emissions when using an FID (≈40ppm), as shown in this study (Figure 7.14) and that by others (Cole, 1998). Therefore, it is reasonable that the carbonyl species are proportionately lower. Nevertheless, there are clear increases of acrolein and acetone with PFI over GDI, which has been seen in other research (Graham, 2008). The pathways for its formation are more favourable in PFI. With the exception of 2-butanone/butyraldehyde and valeraldehyde (74% decrease), the

individual carbonyl emissions decrease from GDI to PFI, is between 10-45%. However, the overall carbonyl emissions decrease with PFI is 11%.

The difference in mixture preparation between GDI and PFI helps to explain the behaviour when using various blends in dual-injection. A summary of the emissions of formaldehyde, acetaldehyde and benzaldehyde are shown in Figure 8.23.

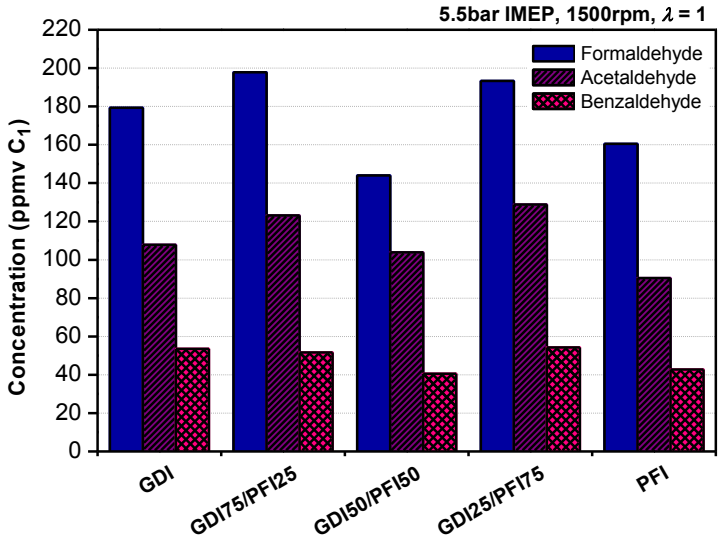

Figure 8.23 Formaldehyde, Acetaldehyde and Benzaldehyde for ULG Dual-Injection

Although the differences are marginal and there is no obvious relationship with varying dual-injection fractions (GDI75/PFI25 and GDI25/PFI75 blends are higher than GDI or PFI), the results for equal fuelling (GDI50/PFI50) show lower emissions of all three carbonyls (the total is also 1.7% less than in PFI).

The results for each carbonyl is summarised in Table 8.5. Except acetaldehyde, valeraldehyde and hexaldehyde, the emissions are lower with a GDI50/PFI50 blend than in PFI. This suggests that combustion is more complete as less fuel is unburned. The total carbonyl emission for a GDI50/PFI50 blend is 7.4% (29.6ppm) lower than PFI and 18.6%

(84.7ppm) lower than GDI. Although the other blends in dual-injection (GDI75/PFI25 and GDI25/PFI75) show increased formaldehyde/acetaldehyde emissions over GDI50/PFI50, when excluding these aldehydes, the total emissions is similar (GDI75/PFI25 = 170ppm), if not lower (GDI25/PFI75 = 162ppm) than the total for GDI (169ppm).

Table 8.5 Carbonyl Emissions Concentrations using ULG Dual-injection

	Concentration ($ppmC_1$)				
Carbonyl	**GDI**	**GDI75/PFI25**	**GDI50/PFI50**	**GDI25/PFI75**	**PFI**
Formaldehyde	179.4	197.8	144.0	193.3	160.4
Acetaldehyde	107.9	123.1	103.9	128.8	90.4
Acrolein	27.2	30.5	24.7	30.7	34.7
Acetone	2.7	3.1	1.4	2.7	12.2
Propionaldehyde	11.3	4.8	3.9	10.1	8.8
Crotonaldehyde	7.3	6.6	3.8	5.9	5.7
Methacrolein	6.9	7.8	4.9	7.1	6.0
2-Butanone/ Butyraldehyde	4.1	2.8	2.5	3.0	1.1
Benzaldehyde	53.6	51.6	40.6	54.3	42.8
Valeraldehyde	5.2	4.0	2.2	2.7	1.3
m-Tolualdehyde	33.6	31.5	24.4	31.0	27.0
Hexaldehyde	21.3	22.3	17.7	25.5	11.9
	456.3	483.1	371.6	492.3	401.2

These results suggest that varying the fuel delivery can help to reduce the emissions of carbonyls. In order to find out if this is transferable to oxygenated fuels, an analysis of ethanol and DMF dual-injection has been carried out. The results are shown in the next section.

8.3.4.2 Ethanol and DMF

As discussed in Section 6.4 dual-injection offers an alternative method of supplying biofuels blends to DI.

In terms of emissions, improvements were shown when using dual-injection for unburned HCs (Figure 7.15), CO (Figure 7.19) and CO_2 (Figure 7.21). Although the improvements with HCs were more marginal than the other two emissions, this section analyses the effect on carbonyls when using dual-injection compared to DI, with ethanol and DMF blends.

The comparison of formaldehyde is made in Figure 8.24. The improved mixture formation and higher combustion temperatures with the PFI component in dual-injection helps to decrease the formaldehyde emissions, by up to 29% when using ethanol (E25 and E50) and DMF (D25 and D75).

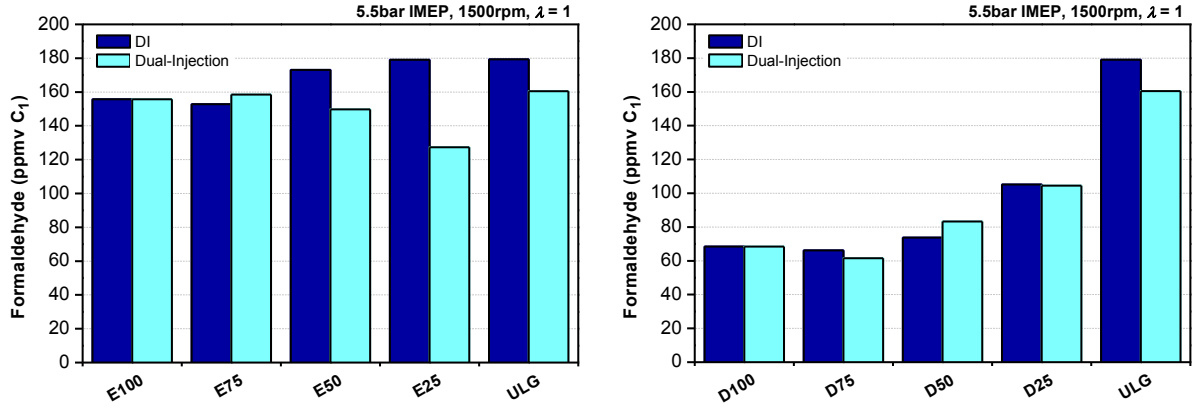

Figure 8.24 Formaldehyde Emissions using ETH (a) & DMF (b) in DI & Dual-Injection

As shown in Figure 8.25, the combustion of DMF and gasoline results in the production of lower acetaldehyde emissions than with ethanol.

Therefore, this directly effects the acetaldehyde emissions in dual-injection and DI, as shown in Figure 8.25. Between the two modes, there seems to be little difference when using DMF compared to ethanol blends. The increased combustion temperature of dual-injection helps to reduce the formation of acetaldehyde and incomplete combustion.

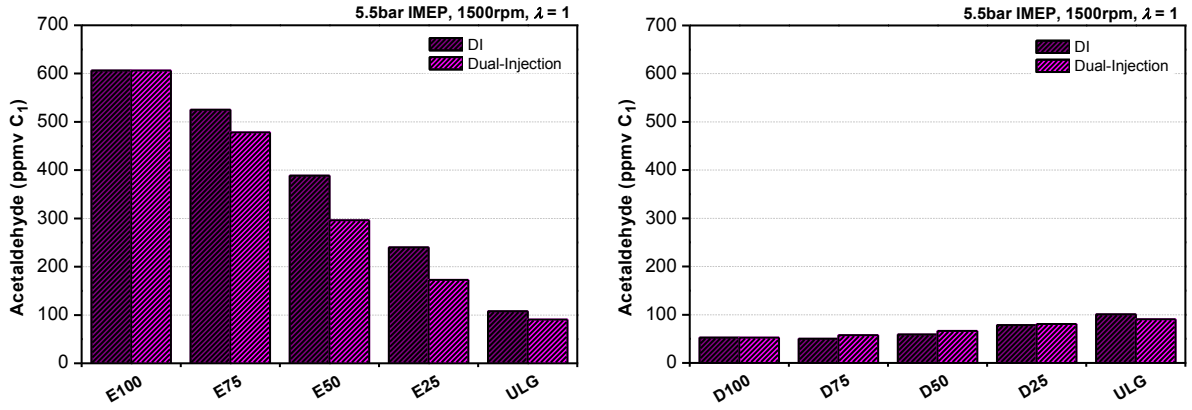

Figure 8.25 Acetaldehyde Emissions using ETH (a) & DMF (b) in DI & Dual-Injection

The lower emissions of benzaldehyde with dual-injection for ethanol and D25, shown in Figure 8.26, are due to more complete combustion, which helps to reduce the unburned fuel. However, for D50 and D75, the dual-injection mode produces higher emissions than in DI.

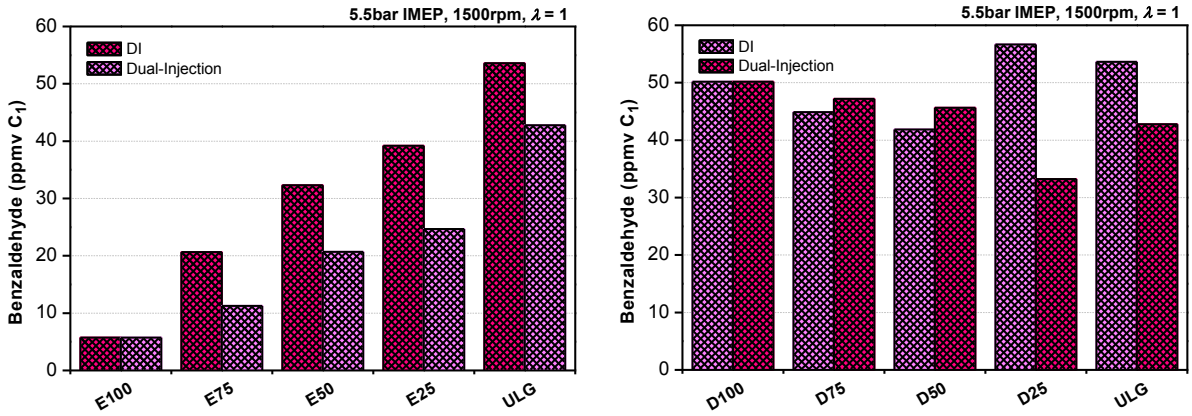

Figure 8.26 Benzaldehyde Emissions using ETH (a) & DMF (b) in DI & Dual-Injection

The change in individual and total carbonyl emissions when using ethanol blends in dual-injection and DI are shown in Table 8.6 (negative numbers indicate reduced emissions with dual-injection). For any ethanol blend, the dual-injection carbonyl emissions are consistently lower than in DI, highlighted by the decrease in acetaldehyde. This is due to the increased combustion temperatures with dual-injection as the charge-cooling effect is reduced. The E25 blend in dual-injection shows the greatest decrease in total carbonyl emissions; 16.9ppm

and 100.5ppm less than E50 and E75, respectively. Clearly, the reductions are directly proportional to the PFI fraction.

Table 8.6 Carbonyl Emissions Improvement with Ethanol Blends in Dual-Injection

	$\Delta_{(Dual-DI)}$ Concentration ($ppmC_1$)		
Carbonyl	**E75**	**E50**	**E25**
Formaldehyde	5.6	-23.4	-51.8
Acetaldehyde	-46.5	-92.4	-67.4
Acrolein	-0.9	1.5	0.8
Acetone	-3.4	-2.5	-1.9
Propionaldehyde	-1.3	-2.6	-4.4
Crotonaldehyde	-1.5	-2.1	-3.3
Methacrolein	-1.2	-1.9	-2.4
2-Butanone/ Butyraldehyde	-0.8	-1.2	-1.8
Benzaldehyde	-9.4	-11.6	-14.6
Valeraldehyde	0.1	0.3	-2.0
m-Tolualdehyde	-6.6	-10.9	-12.7
Hexaldehyde	-1.8	-3.7	-6.8
	-67.6	-150.6	-168.1

For DMF, the change in carbonyls between dual-injection and DI are shown in Table 8.7.

Unlike with ethanol, the benefits with dual-injection are less apparent. Both D50 and D75 show increases in the total emissions with dual-injection largely due to the increases in acetaldehyde and valeraldehyde. However, D25 produces 49.4ppm less total emissions in dual-injection than in DI. This is because the increase in acetaldehyde and valeraldehyde seen with D50 and D75 are suppressed and benzaldehyde emissions are dramatically reduced. Again, the higher weighting of the gasoline fraction in PFI provides an improved fuel-air mixture and reduces the amount of unburned fuel which can be oxidised to form benzaldehyde or other carbonyls.

Table 8.7 Carbonyl Emissions Improvement with DMF Blends in Dual-Injection

Carbonyl	Δ (Dual-DI) Concentration (ppmC1)		
	D75	D50	D25
Formaldehyde	-4.5	9.6	-0.6
Acetaldehyde	7.5	7.6	2.3
Acrolein	-2.5	-2.2	-4.6
Acetone	-0.5	0.6	-3.9
Propionaldehyde	2.9	1.2	-2.5
Crotonaldehyde	-0.3	0.1	-4.3
Methacrolein	0.3	1.0	3.1
2-Butanone/ Butyraldehyde	-0.7	-5.3	-0.1
Benzaldehyde	2.3	3.8	-23.4
Valeraldehyde	11.2	10.4	1.1
m-Tolualdehyde	-0.4	-0.1	-7.7
Hexaldehyde	-0.9	-1.3	-8.8
	14.5	25.3	-49.4

Although the greatest reductions in carbonyl emissions are found with ethanol, the total concentration is higher than with DMF, as shown in Figure 8.27.

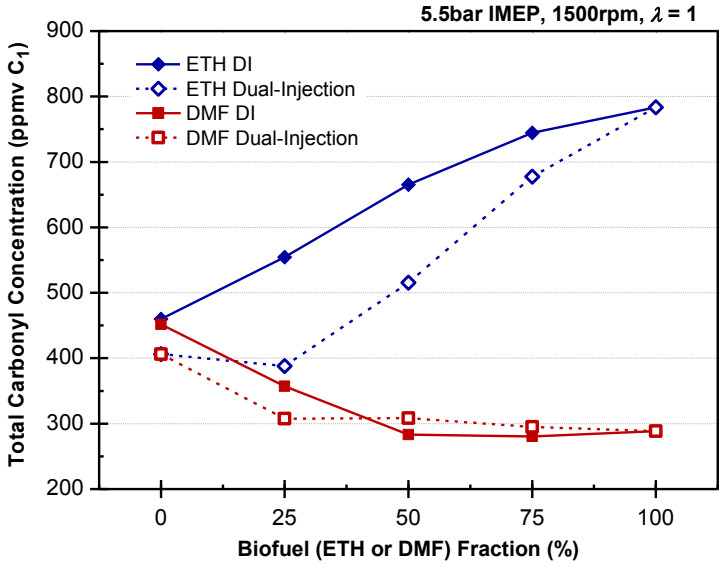

Figure 8.27 Total Carbonyls using ETH and DMF in DI & Dual-Injection

Using 25% blends, both biofuels in dual-injection produce lower total carbonyls than GDI and PFI. This is significant as low fractions are likely to become commercialised in the near-term. Furthermore, the use of dual-injection helps to reduce the total carbonyl emissions when using high ethanol blends.

8.3.5 Discolouration of DNPH

During the HPLC testing, the acidified solution of DNPH was discoloured due to the reaction with the carbonyls as shown in Figure 8.28.

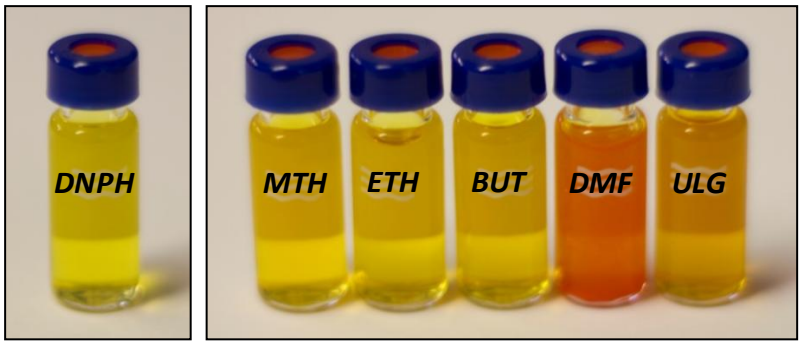

Figure 8.28 DNPH Solution and Emissions Samples in DNPH using DI

This discolouration provides further information on the dominant carbonyl emissions and indicates the dominance of either aromatic (conjugated; e.g. acrolein, benzaldehyde) or aliphatic (unconjugated; e.g. acetaldehyde, formaldehyde) carbonyl compounds. In each case the DNPH solution changes to a red-orange or yellow colour, respectively (Pavia, 2004).

The pale yellow colour of the DNPH emissions sample when using methanol, ethanol and *n*-butanol is because these fuels are largely dominated by the aliphatic carbonyl compounds (Table 8.4). However, the high proportion of aromatic carbonyls with gasoline and DMF (Figure 8.18) results in a darker DNPH emissions sample. DMF also emits a high

concentration of NO_x which potentially increases the concentration of NO_2. NO_2 is a red-brown coloured gas so may further darken the DNPH emissions sample.

8.4 Investigation of Particulate Matter

This section analyses the effect of DMF and ethanol on PM emissions. The sensitivity of PM emissions to load, spark timing and dual-injection (with ethanol blends only) is examined.

8.4.1 Effect of Load

The PM size distributions for the three fuels at 3.5bar IMEP using gasoline MBT timing (34ºbTDC), are shown in Figure 8.29a. Typically, the PM size distribution consists of two modes: the accumulation and nucleation modes. The former consists of solid carbonaceous species usually greater than 50nm in diameter, whereas the latter consists of liquid particles usually less than 50nm in diameter (Rönkkö, 2007). The separation between the modes is shown by the peak in the size distributions around 50nm in Figure 8.29a. At this low load, the size distribution shows marginally more accumulation mode particles than nucleation ones. For gasoline, 62.1% of the total particles are accumulation particles, whereas for DMF and ethanol, this rises to 64.4 and 67.1%, respectively. The difference between DMF and ethanol is 21,805 particles/cm^3. This might be caused by DMF's lower viscosity and surface tension, which leads to smaller injected fuel particles (Tian, 2010b). Also, the in-cylinder temperature when using ethanol (Figure 4.15b) is much lower than for DMF. This is caused by the greater charge-cooling effect when using ethanol, which counteracts the benefit that the higher oxygen content (Table 3.8) would have in helping to lower the PM emissions.

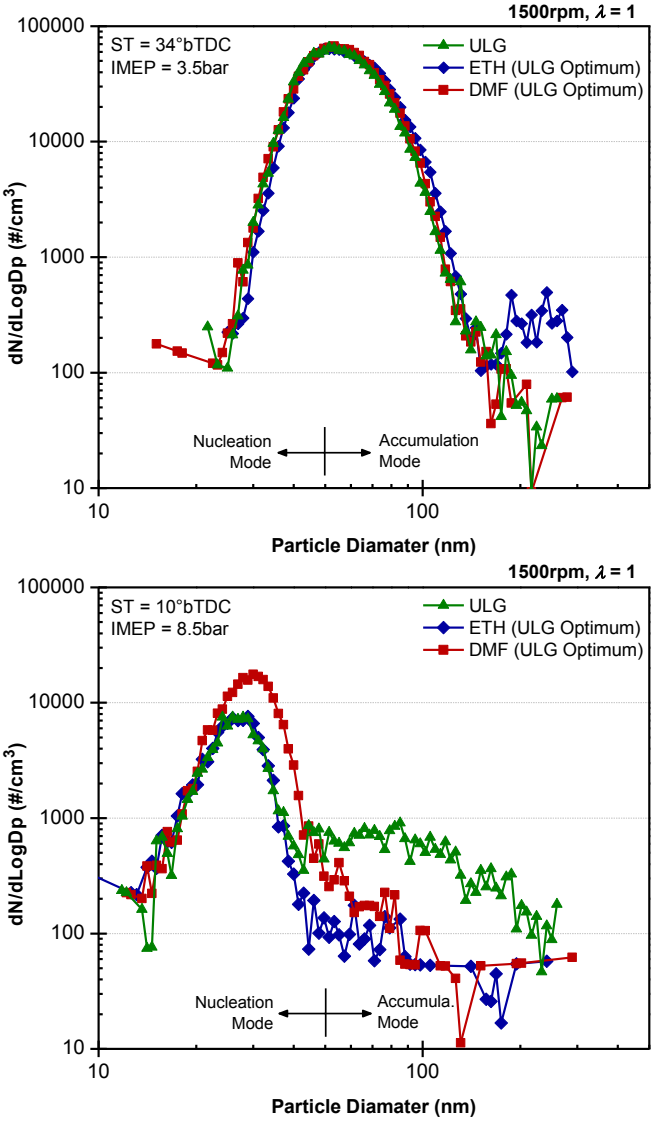

Figure 8.29 PM Size Distributions at 3.5bar (a) and 8.5bar (b) IMEP at ULG MBT

The PM size distributions are also compared at 8.5bar IMEP using gasoline KLSA timing (10ºbTDC). This is shown in Figure 8.29b. Evidently, the effect of load has a significant impact on the PM emissions. The separation between the nucleation and accumulation modes is shown clearly by the inflection in the size distributions around 50nm in Figure 8.29b. Here, the nucleation mode particles dominate the particle size distribution for each fuel, with peaks between 25-30nm.

For ethanol and DMF, the accumulation mode now only represents 2.1 and 1.7%, of the total particle concentrations, respectively. However, for gasoline, the proportion of accumulation mode particles is much higher (18.3%).

In absolute terms, gasoline combustion produces more accumulation mode particles than when fuelled with biofuels; both biofuels produce less than 4,000 particles/cm^3, whereas gasoline produces almost 21,000 particles/cm^3. This is likely to be caused by the higher droplet velocity of gasoline and relatively high mean droplet diameter (Tian, 2010b). This could increase the piston impingement, which would explain why the relatively lower combustion efficiency is seen in Figure 4.14. At this load, the biofuels also burn at higher pressures (Figure 4.15a), which helps to promote pyrolysis and further reduce the solid carbonaceous emissions.

The opposite is true, however, for gasoline when analysing the nucleation concentration at 8.5bar IMEP. Now, gasoline combustion produces a similar amount of particles to that of ethanol, and DMF is the worst offender; almost 122,000 particles/cm^3, or 30% more particles are produced when using DMF. This relative increase in nucleation mode particles for DMF has been seen by others (Zhong, 2010) and might be caused by the incomplete combustion of the ring structure of DMF, which is a known soot precursor (Takatori, 1998, Tosaka, 1989).

8.4.2 Effect of Ignition Timing

In addition to the CO_2 emissions, the monitoring of PM number emissions from gasoline engines is set to be enforced. Currently, PM number emissions do not form part of the emissions legislations for gasoline SI engines in Europe or the US. However, control of these emissions is expected to commence in European regulation in 2014

(Regulation(EC)No(715/2007), 2007). This will require not only the monitoring of PM, but also the PM number for all light-duty vehicles. Therefore, an understanding of these emissions will become much more important, especially when using biofuels.

In this section, the PM emissions between the three primary fuels only are studied at MBT and SR10 at the highest target load (8.5bar IMEP). The PM size distributions are shown in Figure 8.30. Typically, the PM size distribution is bimodal and consists of a nucleation and an accumulation mode. The former constitutes liquid particles, whereas the latter constitutes solid carbonaceous species. Although the separation between these two modes is ill-defined (Kittelson, 1998), in this study, a particle diameter of 50nm has been applied to separate the nucleation (<50nm) and accumulation modes (>50nm) as used in publications by the author's group (Zhong, 2010, Daniel, 2011).

The separation between the nucleation and accumulation modes is shown clearly by the inflection in size distributions around 50nm for all fuels in Figure 8.30.

Clearly, the nucleation mode is the dominant mode for all three fuels. The total concentration of this mode is higher when using the two biofuels, compared to gasoline but the accumulation mode is much smaller, similarly found by others (Price, 2007). The PM emissions variation with spark retard appears to be the most sensitive when using ethanol, whereas with DMF, it is the least. At SR10, the peak number concentration using ethanol is 359,614 particles/cm^3, with a particle diameter of 38.5nm, which is 46% and 33% more than at MBT, respectively. However, with DMF the increase in particle concentration and diameter is less than half of this (20% and 15%, respectively).

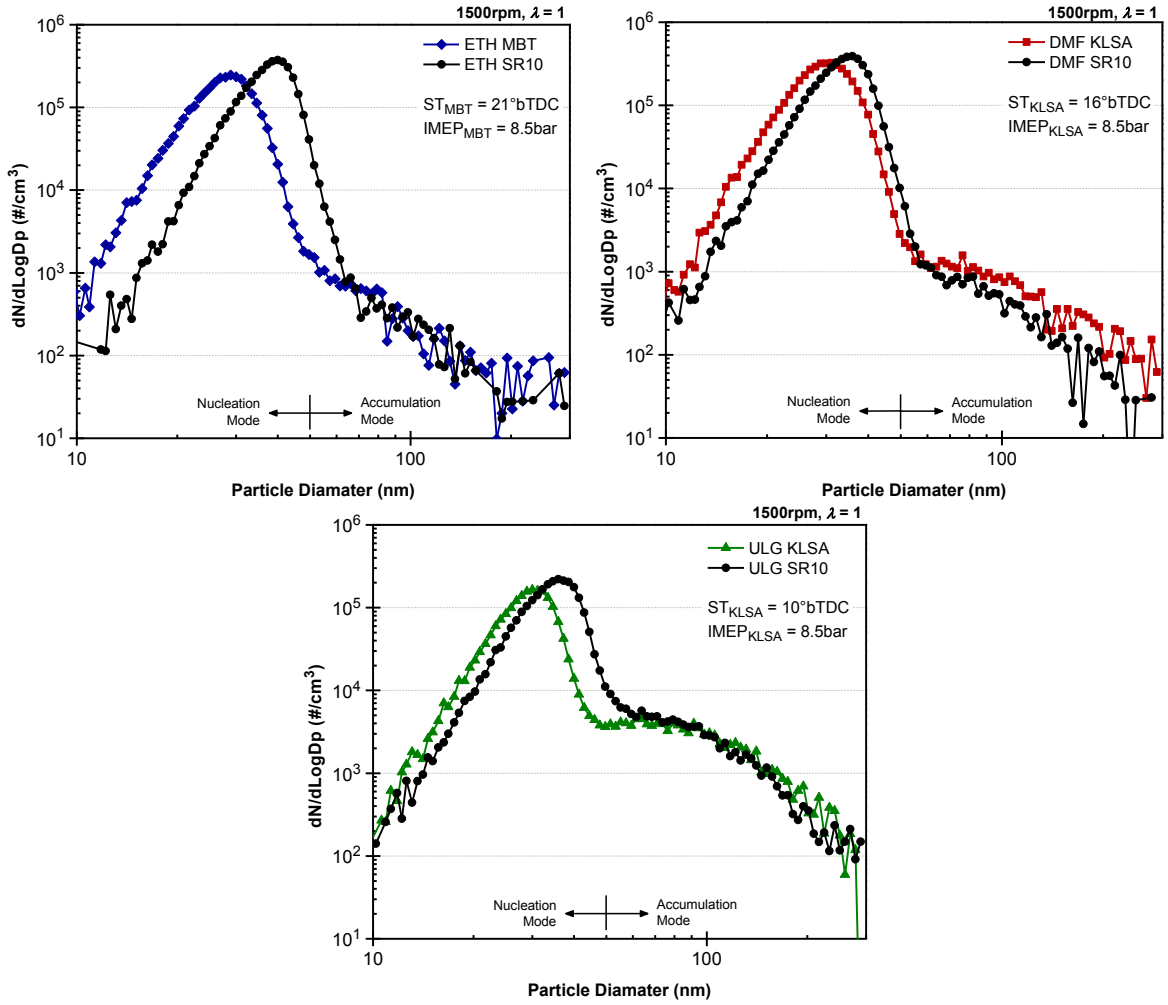

Figure 8.30 Effect of SR10 on PM Size Distribution for ETH (a) DMF (b) and ULG (c)

This trend might be a function of the in-cylinder temperature, whereby its change using ethanol at SR10, is greater than that with DMF (surmised from the NO_x emissions in Figure 4.5b). Although this helps to reduce the isNO_x emissions, it conversely affects the PM nucleation mode with little effect on the accumulation mode. Overall, spark retard at SR10 largely affects the nucleation mode and not the accumulation mode distribution.

Figure 8.31a shows the total PM concentration for the three fuels at the highest initial load.

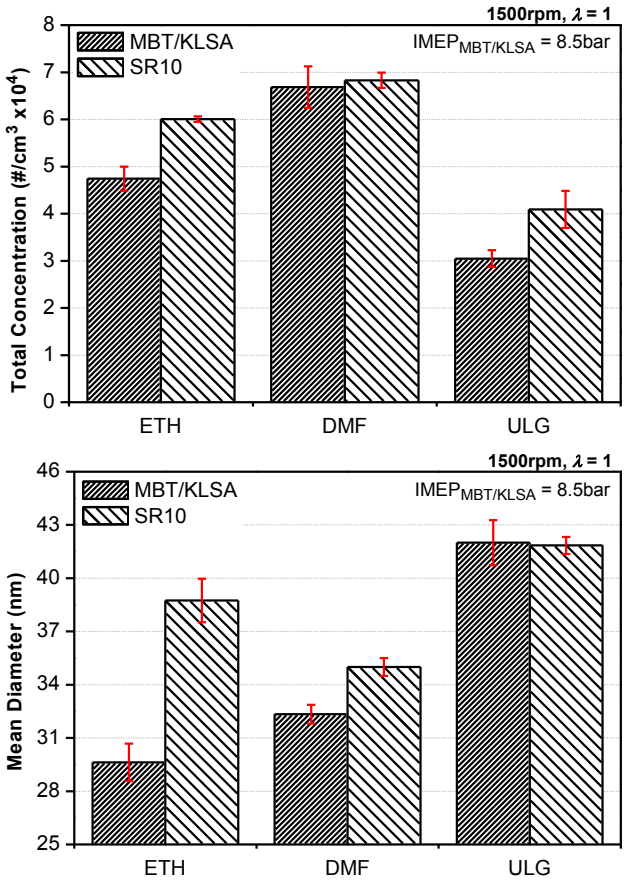

Figure 8.31 Effect of SR10 on PM Total (a) & Mean Diameters (b) at High Load

At SR10, the total PM concentration and particle diameter increases in almost every case. As shown with the size distributions (Figure 8.30), the change in total concentration when using DMF is the lowest, albeit at a greater absolute value. For instance, from KLSA to SR10 timing, the total PM concentration with DMF increases by 1,429 particles/cm^3 (2.1%), whereas with ethanol this is 12,620 particles/cm^3 (26.6%). However, the two biofuels have larger total concentrations compared to gasoline due to the dominant nucleation mode.

Nevertheless, the two biofuels produce a lower mean particle diameter than with gasoline, as shown in Figure 8.31b. Ethanol shows the greatest sensitivity to spark retard. For instance,

the mean diameter increases rapidly to 38.7nm at SR10 from 29.6nm at MBT timing. However, for gasoline the mean diameter is consistently 42nm.

8.4.3 Effect of Dual-Injection

In this section, the PM emissions results are discussed for ethanol blends only at 5.5bar IMEP using dual-injection and DI. Due to stratification of DISI engines, the PM emissions can be much higher than in PFI (Xu, 2011). Therefore, dual-injection can help to obtain PFI level PM emissions with DISI performance. Ethanol has been used because it is the most widely used commercial biofuel and is commonly used with gasoline and has attracted attention in dual-injection (Cohn et al., 2010, Cohn et al., 2005, Stein et al., 2009).

8.4.3.1 Particulate Matter Mass Distribution

Figure 8.32a shows the shift in PM mass distribution from a unimodal distribution with EDI, to a bimodal distribution with GDI and various distributions of the blends in between (E_{25}DI, E_{50}DI and E_{75}DI). As the ethanol fraction decreases, the height of the nucleation mode decreases and accumulation mode appears. Therefore, the effect of the oxygen content in ethanol is to reduce the large soot particles but consequently increase the nucleation mode. Although the first peak with E_{25}DI is positioned as expected (in blend order), the second peak exceeds that with GDI, which is unexpected. This highlights the non-linear relationship with blend ratio in the accumulation mode.

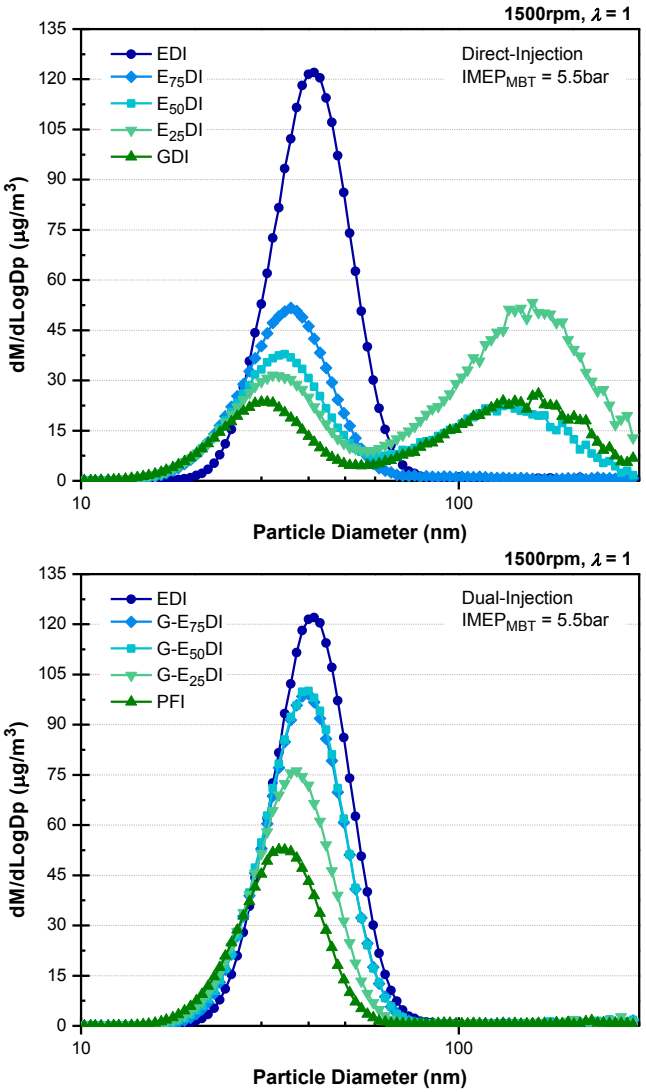

Figure 8.32 PM Mass Distribution for E_xDI (a) and G-E_xDI (b)

In comparison to DI, the equivalent dual-injection PM data in Figure 8.32b results in a unimodal distribution, where the larger accumulation mode particles present in DI are removed. Nevertheless, the consequence is a higher nucleation peak. At this load (5.5bar IMEP), dual-injection results in higher combustion temperatures (as surmised from the increase of isNO_x in Figure 7.16 and Figure 7.17). This encourages fuel vaporization and prevents the accumulation of particles, which ensures that fuel droplets are burned fully and soot formation is suppressed. The greater the PFI volume fraction, the lower the peak particle

mass becomes. This is due to increased mixture preparation time and reduced wetting of the piston and cylinder walls with DI. Similarly, to DI blends, the decreasing ethanol fraction in dual-injection largely results in proportional decreases in the nucleation mode.

The vaporization and breakup of large ethanol fuel droplets is evidently less proficient than with gasoline, which has been shown in previous work (Tian, 2010b). However, the distribution for G-E_{75}DI and G-E_{50}DI are inseparable and so the relationship of the PM mass emissions with blend ratio is not strictly linear. Further testing would have to be conducted to confirm this disparity. The injection timing using DI is early and represents a homogeneous mode. If stratification was employed, in the absence of EGR, the particulate emissions would increase due to decreased fuel evaporation time and the potential for greater wall wetting.

A statistical summary of the PM size distributions is shown in Figure 8.33.

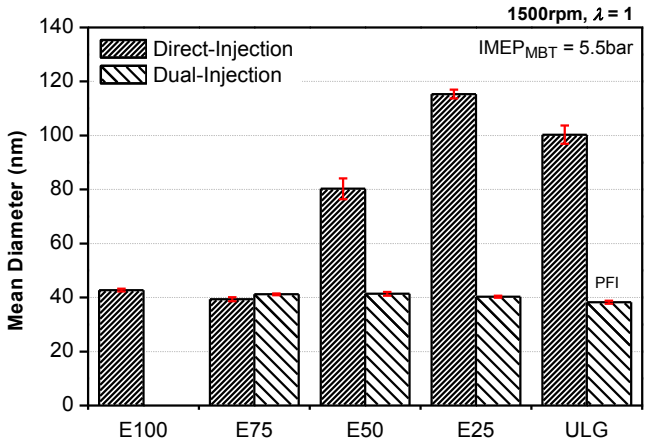

Figure 8.33 PM Mean Diameters for E_xDI and G-E_xDI

The mean PM diameters for dual-injection blends are consistently lower than in DI. Despite the negligible difference between E_{75}DI and G-E_{75}DI blends, decreases in ethanol content results in clear differences and a large increase in mean diameter with DI towards GDI. As shown previously (Figure 8.32b), dual-injection consistently results in low mean diameter

particles, which are similar to PFI. For instance, the mean diameter with E_{25}DI (115.3nm) is 75nm larger than G- E_{25}DI (40.3nm) and even greater than GDI (100.3nm). This quantifies the trends seen in Figure 8.32 where the PFI component is critical in PM mass reduction.

8.4.3.2 Particulate Matter Number Distribution

The PM number distribution also reveals differences between the two injection modes and is shown in Figure 8.34.

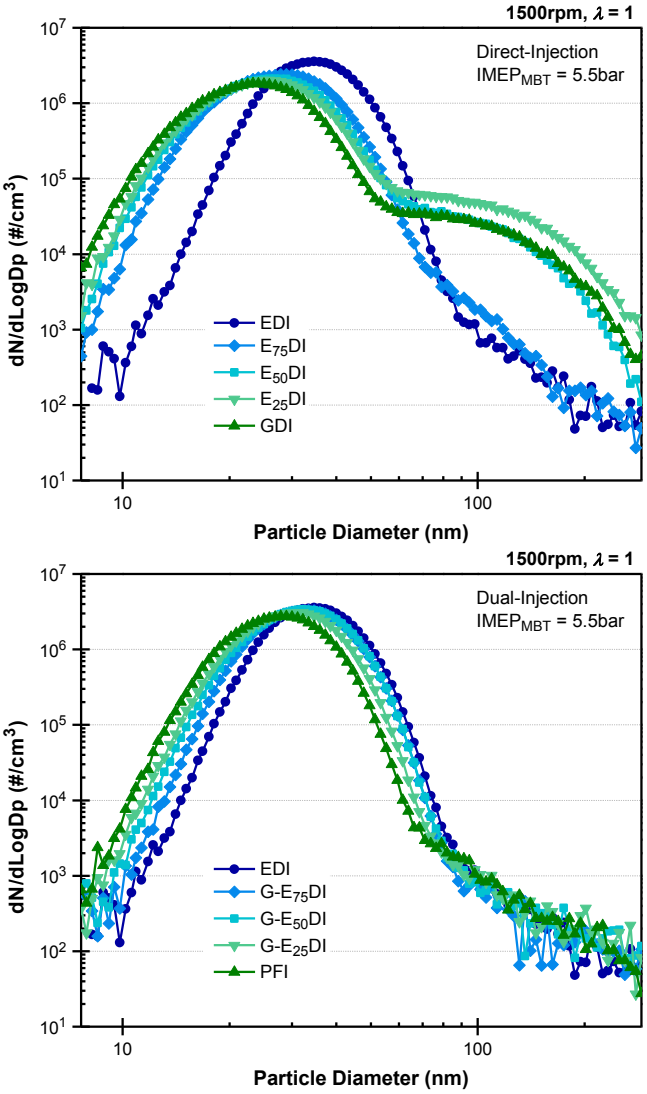

Figure 8.34 PM Number Distribution for E_xDI (a) and G-E_xDI (b)

The number distribution using blends in DI in Figure 8.34a shows a high number concentration of accumulation mode particles (>50nm), which is not seen with the dual-injection blends in Figure 8.34b. This trend is clearly shown when shifting from GDI (Figure 8.34a) to PFI (Figure 8.34b). For instance, the vaporization of fuel droplets is improved due to the increased mixing time and combustion temperatures. This results in more complete combustion and reduces the tendency of particles to accumulate. Furthermore, this tendency occurs with increasing ethanol fractions in DI. However, the ethanol content helps to prevent soot formation due to the oxygen molecule inherent in its chemical structure. Therefore, the dual-injection mode is more effective at reducing the large accumulation particles compared to equivalent gasoline-ethanol blends in DI. The statistical summary of the PM number distributions is shown in Figure 8.35, including error bars to highlight the repeatability.

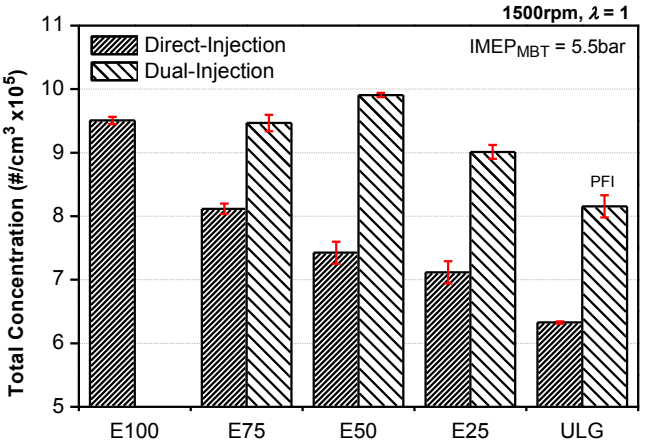

Figure 8.35 PM Total Number for E_xDI and G-E_xDI

Here, it is DI which produces the lowest total PM numbers compared to dual-injection. The decrease in is linear from E100 to GDI. However, with dual-injection, the concentration is always >230,000/cm^3 compared to the equivalent DI blend. Although dual-injection helps to lower the mean particle diameter and reduce the soot concentration, it conversely increases

the total number concentration compared to gasoline-ethanol blends in DI, due to the increase in the volatile component (nucleation mode particles). The summary of the two PM number modes - nucleation and accumulation - is shown in Figure 8.36, respectively.

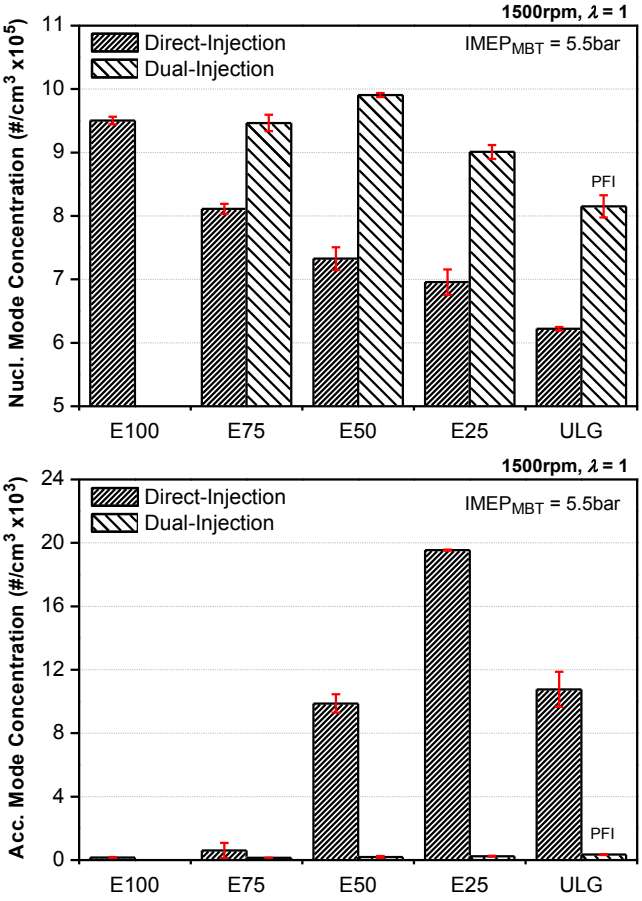

Figure 8.36 Nucleation (a) & Accumulation (b) PM Numbers for E_xDI and G-E_xDI

The separation of the two modes is based on the point of inflection (rather than a fixed diameter), which is clear in Figure 8.34. The nucleation mode represents >98% of the total PM with GDI, so is similar to the overall (Figure 8.35). It is therefore easier to appreciate the differences between the modes when analysing the accumulation summary in Figure 8.36b. As shown with the mean diameter (Figure 8.33), PFI dramatically reduces the accumulation particles. Although the ethanol fraction decreases in dual-injection, the accumulation

particles remain <350/cm^3. However, with DI, the accumulation particles rise to 19,550/cm^3 at E_{25}DI, approximately 80 times higher than with G-E_{25}DI. This is primarily due to the poorer vaporization of fuel particles in DI reducing droplet breakup and oxidation.

8.5 Summary

In summary, the HC emissions of DMF are dominated by unburned fuel as seen with other single component fuels. However, other HCs have been identified by GC/MS. The HCs that were ≤5% of unburned DMF include: cyclopentadiene, MVK, MF, benzene, toluene, EMF, ethylbenzene and *p*- and *o*-xylene.

In total, 12 carbonyls were identified in the exhaust. The emissions of formaldehyde, acetaldehyde and benzaldehyde were lower than with gasoline. DMF produces the lowest total carbonyl emissions and more significantly, the lowest emissions of formaldehyde and acetaldehyde between the oxygenated HCs and gasoline.

This speciation technique helps to develop a method for FTIR analysis, which provides greater flexibility in emissions measurements. Even though there was no discernible peak in the chromatogram for furan, it was detected by searching for its parent mass (molecular weight).

In terms of PM emissions, DMF helps to lower accumulation particles, as does ethanol. The PM emissions increase with spark retard when using both DMF and ethanol, where the latter is the most sensitive.

In dual-injection, ethanol results in a unimodal mass distribution; the larger, accumulation mode particles are removed and the mean PM diameter is lowered from 115.3nm with E_{25}DI to 40.3nm with G-E_{25}DI. This is due to higher combustion temperatures with dual-injection, which ensures the fuel droplets are more completely burned suppressing the formation of soot. The increased mixture preparation time also helps to reduce wall wetting.

CHAPTER 9

SUMMARY, CONCLUSIONS AND FURTHER WORK

The main aim of this thesis was to explore the combustion and emissions of oxygenated fuels in modern SI engines. In particular the characteristics of DMF were studied and the results and discussion from this work are shown in the preceding chapters. The similarities of DMF to gasoline allow the relative ease of implementation into current engine technology. However, in order to maximise performance, the differences in vaporisation, burning characteristics and products of combustion should be observed. The main conclusions from this work are presented in this chapter, which is followed by suggestions for further work.

9.1 Summary and Conclusions

This thesis contains a multitude of results from five experimental chapters. However, the most significant findings are presented below in the order that the chapters appear.

Combustion Behaviour and Emissions of 2,5-Dimethylfuran

The oxygenated fuels and gasoline have increasing spark sensitivities with respect to engine load. Between the fuels, the order of spark sensitivity is: methanol < ethanol < DMF < *n*-butanol < gasoline due to the chemical (OI) and physical (ΔH_{vap} and O_2 content) properties. When using gasoline spark timings, the combustion rate using DMF is faster than with ethanol, but both fuels have a lower CID and $CAD_{10\text{-}90}$ than gasoline, especially with advanced spark timing. The volumetric ISFC when using DMF is similar to that with gasoline. Also, with the exception of NO_x, the engine-out emissions of DMF are similar, if

not lower, than with gasoline. The higher NO_x emissions can be explained by the higher combustion temperatures. Ethanol showed the least sensitivity to AFR and intake/exhaust valve timing, which allowed the lean limit to be extended and the indicated efficiency to be maximised, respectively.

Overall, the reduced parameter sensitivity of the oxygenated fuels permits a wider window for emissions optimisation compared to gasoline largely due to improved antiknock qualities.

Modern GDI Combustion Modes using DMF and Ethanol

The single-pulse SOI timing sensitivities of DMF and ethanol at WOT were compared to gasoline. The order of descending peak IMEP was: ethanol (10.58bar) > DMF (10.27bar) > gasoline (9.36bar). This was due to the varying knock resistance and charge-cooling effect, which greatly affects the VE. When fuelled with ethanol, the VE was symmetrical either side of the optimum at 270°bTDC$_{comb}$. However, for DMF and gasoline, the trend was asymmetric about the respective peaks with opposing peak locations. When using split-injection with DMF and ethanol, the increase in IMEP (over the single-pulse injection case) was more sensitive to SOI_2 timing than with gasoline. However, increases of up to 2.3% were seen at early SOI_2 timings due to improve vaporisation and reduced piston wetting. Later SOI_2 timings saw a decrease in CAD_{10-90} which compromised performance.

In summary, split-injection strategies at WOT can help to raise the VE and therefore maximum IMEP when using ETH and DMF. However, earlier injections with a greater split ratio are favourable.

Dual-Injection as a Knock Mitigation Method

Dual-injection using gasoline only was shown to improve part-load efficiency by up to 1% by decreasing CAD_{10-90} due to improved mixture formation. For significant knock mitigation means, ethanol and methanol have been successfully used for gasoline in PFI. This is due to the high latent heat of vaporization and octane number which allows the spark timing to be advanced. At 7.5bar IMEP, approximately 40% of these lower alcohols raise the KLSA to over 10CAD from PFI and reduce CAD_{10-90} by up to 5CAD over GDI. Due to the greater knock resistance of methanol, the energy fractions required are lower than with ethanol. Nevertheless, the spark advance with G-EDI allows the indicated efficiency to exceed 38%, similar to the case of neat ethanol. In terms of emissions, reductions in HC, CO and CO_2 are seen at almost every load over PFI and GDI. However, due to the increase in combustion pressure, the NO_x emissions are up to 14% higher than in PFI, and almost double this compared to GDI.

Overall, these results show the effectiveness of ethanol and methanol as knock mitigation fuels. Although methanol is more effective on an energy basis, ethanol reduces the overall ISFC.

Dual-Injection Blends compared to DI Blends

Dual-injection was a more effective method to utilise oxygenated fuel blends than in DI only. The indicated efficiency of D25 in dual-injection mode (G-D_{25}DI) exceeds that of its individual components up to 8bar IMEP and produces consistently higher indicated efficiencies than D_{25}DI (up to 4%; 36.8% at 7.5bar IMEP). The volumetric ISFC with G-D_{25}DI is reduced by up to 3.2% from D_{25}DI and 1.2% compared to homoenegous GDI. This

behaviour is possibly due to improved mixing and lower wall wetting as a result of shorter DI injection durations (as found with *n*-butanol). The peak combustion pressure is also 4.8bar higher with G-D_{25}DI than with D_{25}DI at 8.5bar IMEP due to 13% lower $CAD_{10\text{-}90}$, despite similar spark timings. The CO and CO_2 emissions with G-D_{25}DI are dramatically reduced. However, as seen with other work on dual-injection, the NO_x emissions increase.

Ultimately, dual-injection is a promising technique for optimising the combustion of low DMF (and *n*-butanol) blends with gasoline. As well as providing greater flexibility and efficiency over external blends using DI only, dual-injection produces lower CO_2 emissions.

HC Speciation and PM Emissions of 2,5-Dimethylfuran

When fuelled with single component fuels like DMF and ethanol, the major HC emitted is unburned fuel. For DMF, the remaining HCs are less than 5% of unburned fuel (in terms of chromatrogram area), including (in descending order): toluene, MVK, cyclopentadeine, MF and benzene. MF is likely formed during the reaction of DMF with a hydrogen atom and subsequent methyl elimination. Although within the detection limit of the GC/MS, the emissions of furan are negligible.

In total, 12 carbonyls were identified in the DMF exhaust. The emissions of formaldehyde, acetaldehyde and benzaldehyde were lower than with gasoline (decreases of 62%, 52% and 6%, respectively). The emission of DMF also produced the lowest total carbonyl emissions and more significantly, the lowest emissions of formaldehyde and acetaldehyde.

The PM emissions for DMF are comparable to gasoline at low load (3.5 bar IMEP) but include higher nucleation mode particles at high load (8.5 bar IMEP). Dual-injection dramatically reduces PM emissions and produces a unimodal mass distribution when using

ethanol blends. This is due to the increased mixture preparation time of PFI and reduced wall wetting of DI. In terms of PM number concentration, the accumulation mode particles are almost eliminated with dual-injection despite an increase in nucleation mode particles.

Overall, these findings present the major HCs emitted by DMF and compare the carbonyls to other oxygenated fuels and gasoline. The effect of spark timing and load on PM has been quantified as well as the comparison between dual-injection and DI blends using ethanol.

9.2 Further Work

This study has explored a wide variety of combustion and emission aspects of oxygenated fuels, in particular DMF. However, before these approaches can be commercialised, research is required to better understand the behaviour and tackle the main challenges. The author has outlined some outstanding issues below to serve as recommendations for future work.

9.2.1 DMF Performance and Emissions

The NO_x emissions from DMF combustion are much higher than with ethanol or gasoline. Therefore, an in-depth analysis of EGR on NO_x reduction would be worthwhile. It would then be important to understand the trade-off between the NO_x and PM emissions and the effect of EGR on combustion stability when using DMF.

The high knock resistance of DMF allows the use of high compression ratios or turbo-charging. The benefits of these ‘downsizing’ techniques could be compared to that with other oxygenated fuels. The performance of DMF during cold engine starts has also not yet been investigated. This is important if the use of DMF was to be extended to cold climates and not limited geographically like high blends of ethanol.

9.2.2 Other Furan Derivatives

Although this study briefly discusses the current investigations using MF as an alternative to DMF, the volatility of MF is closer to gasoline (Table 3.8) so could be more tolerant to cold engine starts. However, similarly to DMF, the result of high combustion pressures with MF is high NO_x emissions. Furthermore, the current studies on MF do not include an in-depth unregulated emission analysis despite the disclosure of formaldehyde, acetaldehyde and benzaldehyde emissions (Wang, 2012). Therefore, this could be considered in future work.

9.2.3 Dual-Injection

The reduction in volumetric ISFC was seen with D25 and B25 in dual-injection compared to GDI. However, the fuel consumption rate was interpreted from the DI calibration curves, VAF meter and cross-over of the CO and O_2 concentrations. Therefore, an accurate fuel flow meter, such as a coriolis mass flow meter would prove more accurate. Optical investigations would also help to confirm the improved mixture quality of the dual-injection blends. Some work has already been published in this area, however, the authors stated that this was only preliminary (Jiang, 2012). Another area is to understand the effect of DI injection timing on dual-injection. This could extend to stratified DI combustion or even increasing the number of DI injections. Other work could include interchanging the fuels. For instance, if DMF was used as the PFI fuel in dual-injection, the vaporisation rate of DMF would improve.

9.2.4 Unregulated and PM Emissions

A final area which requires further understanding is the unregulated emissions. This study did not quantify the light to mid-range hydrocarbons. The comparison should also be made

to ethanol and to gasoline. With an exhaustive list of HC emissions, the accurate use of FTIR could then be performed. This would increase the flexibility of testing. For instance, the observation of aldehydes during cold starts and transient conditions could be observed. In terms of PM emissions, the use of a thermodenuder would help to remove the volatile PM with the soot remaining. The soot emissions of DMF and other oxygenated fuel blends in dual-injection could be then compared to the equivalent blends in DI. Finally, the life cycle CO_2 emissions of DMF could be compared to other fuels. However, this work depends on the manufacturing methods and raw materials so would be difficult to quantify.

APPENDIX A

Table A.1 Toxicity Ratings of various HC species (IARC, 2011, NTP, 2011)

Compound	IARC	NTP
1,3-Butadiene	1	A
Benzene	1	A
Formaldehyde	1	A
Acetaldehyde	2B	B
Ethylbenzene	2B	-
Furan	2B	B
Naphthalene	2B	B

IARC Classifications	Group 1	Carcinogenic to humans
	Group 2A	Probably carcinogenic to humans
	Group 2B	Possibly carcinogenic to humans
NTP Classifications	Part A	Known to be human carcinogens
	Part B	Reasonably anticipated to be human carcinogens

Table A.2 MIR Values (g ozone/g HC) of various HC species (CARB, 2010)

Compound	MIR	Compound	MIR	Compound	MIR
1,3-Butadiene	12.61	Propionaldehyde	7.08	2-Butanone	1.48
1,3,5-Trimethylbenzene	11.76	Cyclopentadiene	6.98	*iso*-Pentane	1.45
Propene	11.66	3-Methylfuran	6.90	*n*-Pentane	1.31
m-Xylene	9.75	Acetaldehyde	6.54	*n*-Hexane	1.24
1-Butene	9.73	*iso*-butene	6.29	*iso*-Butane	1.23
Methylvinylketone	9.65	Methacrolein	6.01	*n*-Butane	1.15
Formaldehyde	9.46	Butyraldehyde	5.97	*n*-Heptane	1.07
Crotonaldehyde	9.39	*p*-Xylene	5.84	Benzene	0.72
Furan	9.15	1-Hexene	5.49	**Methanol**	**0.67**
Ethene	9.00	Valeraldehyde	5.08	Propane	0.49
2-Methylfuran	8.30	Hexaldehyde	4.35	Acetone	0.36
2,5-Dimethylfuran	**7.88**	Toluene	4.00	Methane	0.01
o-Xylene	7.64	Naphthalene	3.34	Benzaldehyde	0.00
Acrolein	7.45	Ethylbenzene	3.04	*m*-Tolualdehyde	0.00
1-Pentene	7.21	**Ethanol**	**1.53**		

APPENDIX B

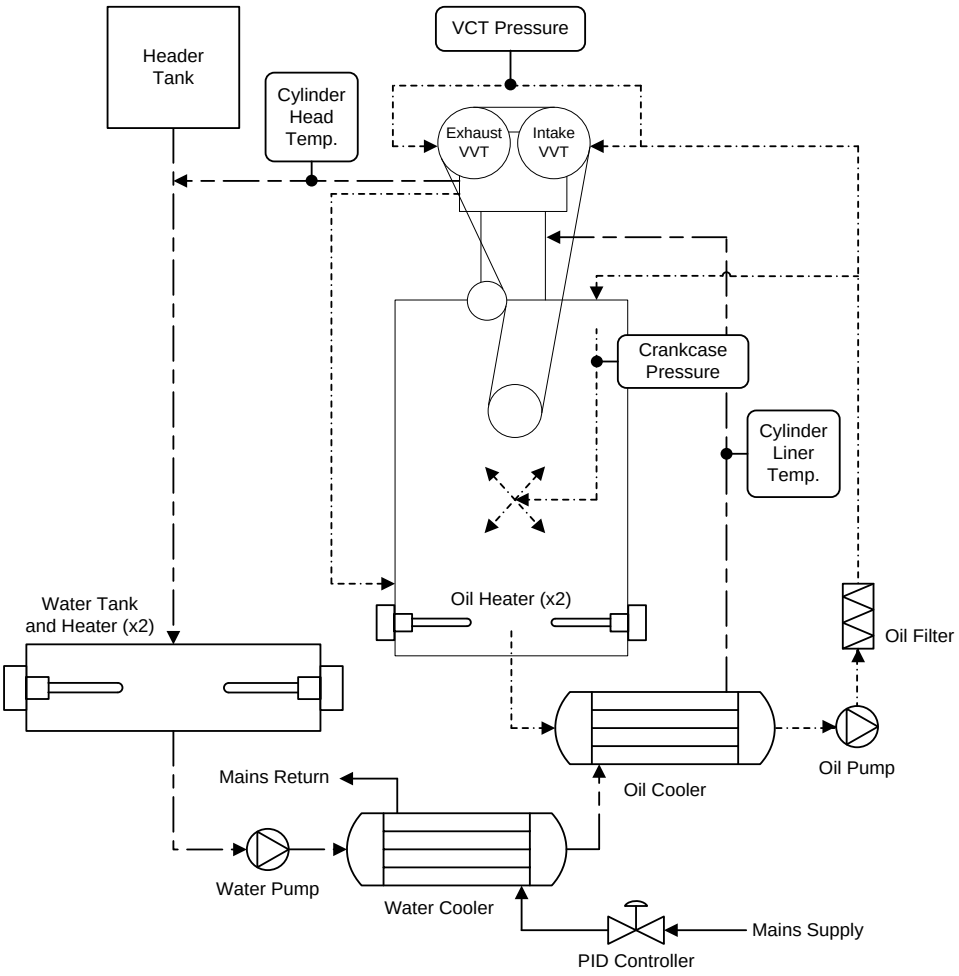

Figure B.1 Schematic of Water Cooling and Engine Oil Lubricating Circuits

LIST OF REFERENCES

ADOMEIT, P., LANG, O., PISCHINGER, S., AYMANNS, R., GRAF, M. AND STAPF, G. 2007. Analysis of Cyclic Fluctuations of Charge Motion and Mixture Formation in a DISI Engine in Stratified Operation. SAE 2007-01-1412.

AGARWAL, A. K. 2007. Biofuels (alcohols and biodiesel) applications as fuels for internal combustion engines. Progress in Energy and Combustion Science, 33, 233-271.

AICHE 2007. BP, ABF and DuPont Unveil Plans for Grassroots Biofuels Plant. Chemical Engineering Progress. New York: American Institute of Chemical Engineers (AIChE).

AKIYAMA, K. AND NAKAYAMA, A. 2005. Analysis of Low Concentration Aldehyde and Ketone Compounds in Automotive Exhaust Gas by New Collection Reagent. SAE 2005-01-2152.

ALEIFERIS, P. G., MALCOLM, J.S., TODD, A.R., CAIRNS, A. AND HOFFMANN, H. 2008. An Optical Study of Spray Development and Combustion of Ethanol, Iso-Octane and Gasoline Blends in a DISI Engine. SAE 2008-01-0073.

ALKIDAS, A., DREWS, R. AND MILLER, W. 1995. Effects of Piston Crevice Geometry on the Steady-State Engine-Out Hydrocarbons Emissions of a S.I. Engine. SAE 952537.

ALKIDAS, A. C. AND EL TAHRY, S.H. 2003. Contributors to the Fuel Economy Advantage of DISI Engines Over PFI Engines. SAE 2003-01-3101.

ALLEN, M., FRAME, D., FRIELER, K., HARE, W., HUNTINGFORD, C., JONES, C., KNUTTI, R., LOWE, J., MEINSHAUSEN, M., MEINSHAUSEN, N. AND RAPER, S. 2009. The exit strategy. In: REPORTS, N. (ed.) Climate Change.

ANDERSSON, J., PRESTON, H., WARRENS, C. AND BRETT, P. 2004. Fuel and Lubricant Effects on Nucleation Mode Particle Emissions From a Euro III Light Duty Diesel Vehicle. SAE 2004-01-1989.

AYALA, F. A., GERTY, M.D. AND HEYWOOD, J.B. 2006. Effects of Combustion Phasing, Relative Air-fuel Ratio, Compression Ratio, and Load on SI Engine Efficiency. SAE 2006-01-0229.

AYERS, A. L. AND SCOTT, C.R. 1951. Substituted Furans as Hypergolic Fuels. US patent application.

BAI, Y., WANG, Z. AND WANG, J. 2010. Knocking Suppression using Stratified Stoichiometric Mixture in a DISI Engine. SAE 2010-01-0597.

BARLOW, M. T., SMITH, D.J.H. AND STEWART, D.G. 1982. Fuel Composition. GB patent application 82306744.2.

BARLOW, M. T., SMITH, D.J.H. AND STEWART, D.G. 1981. Fuel Composition. GB patent application.

BECK, C., STEVENSON, P. AND ZIMAN, P. 2006. The Impact of Gasoline Octane on Fuel Economy in Modern Vehicles. SAE 2006-01-3407.

BEECKMANN, J., RÖHL, O. AND PETERS, N. 2009. Experimental and Numerical Investigation of Iso-Octane, Methanol and Ethanol Regarding Laminar Burning Velocity at Elevated Pressure and Temperature. SAE 2009-01-1774.

BEHAM, M. AND YU, D.L. 2004. Modelling a variable valve timing spark ignition engine using different neural networks. IMechE, 218, 1159-1171.

BERCKMÜLLER, M., ROTTENGRUBER, H., EDER, A., BREHM, N., ELSÄSSER, G., MÜLLER-ALANDER, G. AND SCHWARZ, C. 2003. Potentials of a Charged SI-Hydrogen Engine. SAE 2003-01-3210.

BERNTSSON, A., JOSEFSSON, G., EKDAHL, R., OGINK, R. AND GRANDIN, B. 2011. The Effect of Tumble Flow on Efficiency for a Direct Injected Turbocharged Downsized Gasoline Engine. SAE 2011-24-0054.

BINDER, J. B. AND RAINES, R.T. 2009. Simple Chemical Transformation of Lignocellulosic Biomass into Furans for Fuels and Chemicals. Journal of the American Chemical Society, 131, 1979-1985.

BLUMBERG, P. N., BROMBERG, L, KANG, H. AND TAI, C. 2008. Simulation of High Efficiency Heavy Duty SI Engines Using Direct Injection of Alcohol for Knock Avoidance. SAE 2008-01-2447.

BOSCH, R. 2006. Gasoline-Engine Management, Chichester, John Wiley and Sons, Ltd.

BRACKMANN, C., NYGREN, J., BAI, X., LI, Z. BLADH, H., AXELSSON, B., DENBRATT, I., KOOPMANS, L., BENGTSSON, P. AND ALDÉN, M. 2003. Laser-Induced Fluorescence of Formaldehyde in Combustion using Third Harmonic Nd:YAG Laser Excitation. Spectrochimica Acta Part A, 59, 3347-3356.

BRADLEY, D., SHEPPARD, C.G.W., BURLUKA, A.A., SHARPE G. AND KALGHATGI, G.T. 2011. Influence of Pressure on Burning Velocity, Flame Instabiliteis and Auto-ignition. In: SAUDI-ARAMCO, U. O. L. A. (ed.) Engine Downsizing. London: IMechE Seminar Proceedings

BRAISHER, M., STONE, R. AND PRICE, P. 2010. Particle Number Emissions from a Range of European Vehicles. SAE 2010-01-0786.

BREHOB, D. D., FLEMING, J.E., HAGHGOOIE, M. AND STEIN, R.A. 1998. Stratified-Charge Engine Fuel Economy and Emission Characteristics. SAE 982704.

BREVITT, B. 2002. Alternative Vehicle Fuels. In: ENVIRONMENT, S. A. (ed.). London: House of Commons Library.

BROMBERG, L., COHN, D. R. & HEYWOOD, J. B. 2010. Water Based Systems for Direct Injection Knock Prevention in Spark Ignition Engines. United States patent application 20100121559.

BROMBERG, L. AND COHN, D. 2010. Alcohol Fueled Heavy Duty Vehicles Using Clean, High Efficiency Engines. SAE 2010-01-2199.

BRYNER, M. 2008. BP and DuPont Expand Biofuels Pact. Chemical Week. New York: IHS Inc.

CAIRNS, A., STANSFIELD, P., FRASER, N. AND BLAXILL, H. 2009. A Study of Gasoline-Alcohol Blended Fuels in an Advanced Turbocharged DISI Engine. SAE 2009-01-0138.

CARB 2010. Tables of Maximum Incremental Reactivity (MIR) Values. In: REGULATIONS, C. C. O. (ed.). California Air Resources Board.

CARTER, W. P. L. 2010. Updated Maximum Incremental Reactivity Scale and Hydrocarbon Bin Rreactivities for Regulatory Applications. In: BOARD, C. A. R. (ed.).

CELIK, M. B. AND OZDALYAN, B. 2010. Gasoline Direct Injection. In: SIANO, D. (ed.) Fuel Injection. InTech.

CHADWELL, C. J. AND WALLS, M. 2010. Analysis of a SuperTurbocharged Downsized Engine Using 1-D CFD Simulation. SAE 2010-01-1231.

CHEN, C. J. AND BOZZELLI, J.W. 2000. Thermochemical Property, Pathway and Kinetic Analysis on the Reactions of Allylic Isobutenyl Radical with O2: an Elementary Reaction Mechanism for Isobutene Oxidation. Journal of Physical Chemistry, 104, 9715-9732.

CHEN, L., BRAISHER, M., CROSSLEY, A., STONE, R. AND RICHARDSON, D. 2010. The Influence of Ethanol Blends on Particulate Matter Emissions from Gasoline Direct Injection Engines. SAE 2010-01-0793.

CHENG, W., HAMRIN, D., HEYWOOD, J., HOCHGREB, S., MIN, K. AND NORRIS, M. 1993. An Overview of Hydrocarbon Emissions Mechanisms in Spark-Ignition Engines. SAE 932708.

CHENG, W. K., SUMMER, T AND COLLINGS, N. 1998. The Fast-response Flame Ionization Detector. Progress in Energy and Combustion Science, 24, 89-124.

CHRISTENSEN, E., YANOWITZ, J., RATCLIFF, M. AND MCCORMICK, R.L. 2011. Renewable Oxygenate Blending Effects on Gasoline Properties. Energy and Fuels, 25, 4723-4733.

CHRISTENSEN, M. AND JOHANSSON, B. 2000. Supercharged Homogeneous Charge Compression Ignition (HCCI) with Exhaust Gas Recirculation and Pilot Fuel. SAE 2000-01-1835.

CHUNG, M. Y., MARIS, C., KRISCHKE, U., MELLER, R. AND PAULSON, S.E. 2003. An Investigation of the Relationship between Total Non-Methane Organic Carbon and the Sum of Speciated Hydrocarbons and Carbonyls Measured by Standard GC/FID: Measurements in the Los Angeles Air Basin. Atmospheric Environment, 37, 159-170.

COHN, D. R., BROMBERG, L. & HEYWOOD, J. B. 2005. Direct Injection Ethanol Boosted Gasoline Engines: Biofuel Leveraging For Cost Effective Reduction of Oil Dependence and CO2 Emissions. Cambridge, MA 02139: Massachusetts Institute of Technology.

COHN, D. R., BROMBERG, L. & HEYWOOD, J. B. 2010. Fuel Management System for Variable Ethanol Octane Enhancement of Gasoline Engines. United States patent application 7640915.

COLE, R. L. POOLA, R.B. AND SEKAR, R. 1998. Exhaust Emissions of a Vehicle with a Gasoline Direct-Injection Engine. SAE 982605.

COUTRIM, M. X., NAKAMURA, L.A. AND COLLINS, C.H. 1993. Quantification of 2,4-Dinitrophenyl-Hydrazones of Low Molecular Mass Aldehydes and Ketones using HPLC Chromatographia, 37, 185-190.

CURTIS, B. 2008. U.S. Ethanol Industry: The Next Inflection Point. In: ENERGY, U. S. D. O. (ed.). Washington DC: BCurtis Energies and Resource Group.

DAGAUT, P., PENGLOAN, G. AND RISTORI, A. 2002. Oxidation, Ignition and Combustion of Toluene: Experimental and Detailed Chemical Kinetic Modeling Physical Chemistry Chemical Physics, 4, 1846-1854.

DANIEL, R., BROOKS, T. AND PATES, D. 2009. Analysis of US and EU Drive Styles to Improve Understanding of Market Usage and the Effects on OBD Monitor IUMPR. SAE 2009-01-0236.

DANIEL, R., TIAN, G., XU, H. AND SHUAI, S. 2012a. Ignition Timing Sensitivities of Oxygenated Biofuels Compared to Gasoline in a Direct-Injection SI Engine. Fuel. In Press.

DANIEL, R., TIAN, G., XU, H., WYSZYNSKI, M.L., WU, X. AND HUANG, Z. 2011. Effect of spark timing and load on a DISI engine fuelled with 2,5-dimethylfuran. Fuel, 90, 449-458.

DANIEL, R., WANG, C., TIAN, G. AND XU, H. 2012b. Effects of Combustion Phasing, Injection Timing, Relative Air-Fuel Ratio and Variable Valve Timing on SI Engine Performance and Emissions using 2,5-Dimethylfuran SAE 2012-01-1285.

DANIEL, R., WANG, C., TIAN, G. AND XU, H. 2012c. Split-Injection Strategies at Wide-Open Throttle using Gasoline, Ethanol and 2,5-Dimethylfuran in a Direct-Injection SI Engine. SAE 2012-01-0403.

DANIEL, R., WANG, C., TIAN, G., XU, H. AND RICHARDSON, D. 2012d. Dual-Injection as a Knock Mitigation Strategy using Ethanol and Methanol. SAE 2012-01-1152.

DANIEL, R., WEI, L., WANG, C., XU, H. AND WYSZYNSKI, M.L. 2012e. Hydrocarbon and Carbonyl Emissions Speciation of 2,5-Dimethylfuran in a DISI Engine. Energy and Fuels. In Review.

DANIEL, R., XU, H., WANG, C. AND RICHARDSON, D. 2012f. Combustion Performance of 2,5-Dimethylfuran blends using Dual-Injection compared to Direct-Injection in a SI Engine. Applied Energy. In Press.

DANIEL, R., XU, H., WANG, C. AND RICHARDSON, D. 2012g. Gaseous and Particulate Matter Emissions of Biofuel Blends in Dual-Injection compared to Direct-Injection. Applied Energy. In Review.

DEGRAFF, I. D., NOLAN, L., WOOLLEY, C. AND FIORANTE, A. 1996. Analysis of Formaldehyde-DNPH and Other Carbonyl-DNPH Derivatives by Capillary Gas Chromatography.

DELPHI 2012. Worldwide Emissions Standards - Passenger Cars and Light Duty Vehicles.

DEMIRBAS, A. 2007. Progress and recent trends in biofuels. Progress in Energy and Combustion Science, 33, 1-18.

DEMIRBAS, A. 2011. Competitive liquid biofuels from biomass. Applied Energy, 88, 17-28.

DIESEL, R. 1895. Method of and Apparatus for Converting Heat into Work. US patent application US 542846.

DIRECTIVE(70/156/EC) 1970. On the Approximation of the Laws of the Member States Relating to the Type-Approval of Motor Vehicles and their Trailers. Official Journal of the European Union.

DIRECTIVE(78/611/EC) 1978. On a Limit Value for Lead in the Air Official Journal of the European Union.

DIRECTIVE(2009/28/EC) 2009. On the Promotion of the use of Energy from Renewable Sources. Official Journal of the European Union, 47.

DOLAN, G. 2008. China Takes Gold in Methanol Fuel. Journal of Energy Security.

DUMESIC, J. A., ROMAN-LESHKOV, Y. AND CHHEDA, J.N. 2007. Catalytic Process for Producing Furan Derivatives from Carbohydrates in a Biphasic Reactor. US patent application.

DUNN-RANKIN, D. 2007. Lean Combustion: Fundamentals, Applications, and Prospects. In: ELSEVIER (ed.) Combustion Treatise Series.

EASTOP, T. D. AND MCCONKEY, A. 1993. Applied Thermodynamics for Engineering Technologists, Prentice Hall.

ELGHAWI, U. 2009. Speciation and Quantification of Individual Hydrcarbons during Fuel Reforming and in Exhaust Emissions from a Gasoline (SI/HCCI) Engine. PhD Thesis, University of Birmingham.

ENGLER-PINTO, C. M. AND NADAI, L.D. 2008. Volumetric Efficiency and Air-Fuel Ratio Analysis For Flex Fuel Engines. SAE 2008-36-0223.

EPA 1970. Clean Air Act Amendments of 1970. In: AGENCY, U. E. P. (ed.). Public Law Number 91-604.

FATIH DEMIRBAS, M. 2009. Biorefineries for biofuel upgrading: A critical review. Applied Energy, 86, S151-S161.

FELIX-MOORE, A. 2009. Gasoline Compositions. GB patent application.

FERGUSON, C. R. AND KIRKPATRICK., A.T. 2001. Internal Combustion Engines: Applied Thermosciences, John Wiley and Sons, Inc.

FRASER, N., BLAXILL, H., LUMSDEN, G. AND BASSETT, M. 2009. Challenges for Increased Efficiency through Gasoline Engine Downsizing. SAE 2009-01-1053.

FRASER, N. AND BASSETT, M. 2011. Extreme Engine Downsizing with a Single Turbocharger - 100kW/L and 30bar BMEP. In: MAHLE POWERTRAIN, U. (ed.) Engine Downsizing. London: IMechE Seminar Proceedings

FROMOWITZ, M., SHUGA, J., WLASSOWSKY, A.Y., ZHANG, L. AND SMITH, M.T. 2010. Studies on the Genotoxicity of 2,5-Dimethylfuran, a Potential Biofuel. 49th Annual Meeting of the Society of Toxicology (SOT). Salt Lake City, UT.

FRY, M., KING, J. AND WHITE C. 1999. A Comparison of Gasoline Direct Injection Systems and Discussion of Development Techniques. SAE 1999-01-0171.

GANDHI, A. H. AND MEINHART, M. 2009. Fuel Injector Flow Rate Analysis for the Duratec 35 EcoBoost Engine. SAE 2009-01-1505.

GASMET 2009. Calcmet for Windows: User's Guide and Reference Manual.

GAUTAM, M. AND MARTIN, D.W. 2000. Combustion characteristics of higher-alcohol/gasoline blends. IMechE, 214, 497-511.

GIECHASKIEL, B., CARRIERO, M., MARTINI, G. AND ANDERSSON, J. 2009. Heavy Duty Particle Measurement Programme (PMP): Exploratory Work for the Definition of the Test Protocol. SAE 2009-01-1767.

GOLDEMBERG, J. 2008. The challenge of biofuels. Energy & Environmental Science, 1, 523-525.

GORSKI, W. 2011. Possibilities for Production of 2,5-Dimethylfuran as a Motor Fuel Component in Poland. Przemysł Chemiczny, 90, 66-68.

GRAHAM, L. A., BELISLE, S.L. AND BAAS, C.L. 2008. Emissions from Light Duty Gasoline Vehicles operating on Low Blend Ethanol Gasoline and E85. Atmospheric Environment, 42, 4498-4516.

GRASKOW, B. R., KITTELSON, D.B., AHMADI, M.R. AND MORRIS, J.E. 1999. Exhaust Particulate Emissions from a Direct Injection Spark Ignition Engine. SAE 1999-01-1145.

GROB, R. L. 1985. Modern Practice of Gas Chromatography, John Wiley and Sons, Inc.

GRUTER, G. AND JONG, E.D. 2009. Furanics: Novel Fuel Options from Carbohydrates. Biofuels Technology, 11-17.

GUERRIER, M. AND CAWSEY, P. 2004. The Development of Model Based Methodologies for Gasoline IC Engine Calibration. SAE 2004-01-1466.

GÜLDER, O. L. 1982. Laminar Burning Velocities of Methanol, Ethanol and Isooctane-Air Mixtures. The Combustion Institute, Laminar Flames II, 275-281.

GUZMAN, D. D. 2010. Biobutanol fuel Prepares for Launch. ICIS Chemical Business, 278, 20-21.

HANCOCK, E. G. 1985. Technology of Gasoline, Blackwell Scientific Publications.

HARRINGTON, J. A. AND SHISHU, R.C. 1973. A Single-Cylinder Engine Study of the Effects of Fuel Type, Fuel Stoichiometry, and Hydrogen-to-Carbon Ratio and CO, NO, and HC Exhaust Emissions. SAE 730476.

HELD, T. J. AND DRYER, F.L. 1998. A Comprehensive Mechanism for Methanol Oxidation. International Journal of Chemical Kinetics, 30, 805-830.

HENNESSEY, R., FUENTES, A. AND WICKER, R. 2001. Effect of Injection Timing on Piston Surface Fuel Impingement and Vaporization in Direct Injection, Spark Ignition Engines. SAE 2001-01-2025.

HEYWOOD, J. B. 1988. Internal Combustion Engine Fundamentals, McGraw-Hill.

HEYWOOD, J. B. AND WELLING, O.Z. 2009. Trends in Performance Characteristics of Modern Automobile SI and Diesel Engines. SAE 2009-01-1892.

HOEKMAN, S. K. 1993. Improved Gas Chromatography Procedure for Speciated Hydrocarbon Measurements of Vehicle Emissions. Journal of Chromatography, 639, 239-253.

HOLLIDAY, T., LAWRANCE, A.J. AND DAVIS, T.P. 1998. Engine-Mapping Experiments: A Two-Stage Regression Approach. Technometrics, 40.

HONDA, T., KAWAMOTO, M., KATASHIBA, H., SUMIDA, M., FUKUTOMI, N. AND KAWAJIRI, K. 2004. A Study of Mixture Formation and Combustion for Spray Guided DISI. SAE 2004-01-0046.

HU, L., SUN, Y. AND LIN, L. 2011. Pathways and Mechanisms of Liquid Fuel 2,5-Dimethylfuran from Biomass. Progress in Chemistry, 23, 2079-2084.

IARC 2011. Agents Classified by the IARC Monographs.

IKOMA, T., ABE, S, SONODA, Y. AND SUZUKI, H. 2006. Development of V-6 3.5-liter Engine Adopting New Direct Injection System. SAE 2006-01-1259.

IWACHIDO, K., ONODERA T., WATANABE, T., KOYAMA, M., OKUMURA A. AND HORI, M. 2009. NOx Trap Catalyst Technologies to Attain 99.5% NOx Reduction Efficiency for Lean Burn Gasoline Engine Application. SAE 2009-01-1077.

JACOBSON, M. Z. 2007. Effects of Ethanol (E85) versus Gasoline Vehicles on Cancer and Mortality in the United States Environmental Science and Technology, 41, 4150-4157.

JEMMA, C. A., SHORE, P.R. AND WIDDICOMBE, K.A. 1995. Analysis of C1-C16 HCs Using Dual-Column Capillary GC: Application to Exhaust Emissions from Passenger Car and Motorcycle Engines. Journal of Chromatographic Science, 33, 34-48.

JIANG, C., MA, X., XU, H. AND RICHARDSON, S. 2012. An Optical Study of DMF and Ethanol Combustion under Dual-Injection Strategy. SAE 2012-01-1237.

JOHNSON, T. V. 2010. Review of CO2 Emissions and Technologies in the Road Transportation Sector. SAE 2010-01-1276.

JONG, E. D. AND GRUTER, G. 2009. Furanics: A Novel Diesel Fuel with Superior Characteristics. SAE 2009-01-2767.

KAISER, E., SIEGL, W., LAWSON, G., CONNOLLY, F., CARMER, C.F., DOBBINS, K.L., ROTH, P.W. AND SMOKOVITZ, M. 1996. Effect of Fuel Preparation on Cold-Start Hydrocarbon Emissions from a Spark-Ignited Engine. SAE 961957.

KAISER, E. W., SIEGL, W.O., COTTON, D.F. AND ANDERSON, R.W. 1992. Effect of Fuel Structure on Emission from a Spark-Ignited Engine. 2. Naphthene and Aromatic Fuels. Environmental Science and Technology, 26, 1581-1586.

KAISER, E. W. AND SIEGL, W.O. 1994. High Resolution GC Determination of the Atmospheric Reactivity of Engine-out HC Emissions from SI Engine. Journal of High Resolution Chromatography, 17, 264-270.

KALGHATGI, G. T. 2001a. Fuel Anti-Knock Quality - Part I. Engine Studies. SAE 2001-01-3584.

KALGHATGI, G. T. 2001b. Fuel Anti-Knock Quality – Part 2, Vehicle Studies—How Relevant is Motor Octane Number (MON) in Modern Engines. SAE 2001-01-3585.

KÁLLAI, M. AND BALLA, J. 2002. The Effect of Molecular Structure upon the Response of the Flame Ionization Detector. Chromatographia, 56, 357-360.

KÁLLAI, M. AND. BALLA, J. 2003. Effects of Experimental Conditions on the Determination of the Effective Carbon Number. Chromatographia, 57, 639-644.

KAPUS, P. E., FUERHAPTER, A., FUCHS, H. AND FRAIDL, G.K. 2007. Ethanol Direct Injection on Turbocharged SI Engines – Potential and Challenges. SAE 2007-01-1408.

KAR, K., CHENG, W. 2009. Speciated Engine-Out Organic Emissions from PFI-SI Engine Operating on Ethanol/Gasoline Mixtures. SAE 2009-01-2673.

KAR, K., CHENG, W. 2011. Using Mass Spectrometry to Detect Ethanol and Acetaldehyde Emissions from a Direct Injection Spark Ignition Engine Operating on Ethanol/Gasoline Blends. SAE 2011-01-1159.

KAR, K., LAST, T., HAYWOOD, C. AND RAINE, R. 2008. Measurement of Vapor Pressures and Enthalpies of Vaporization of Gasoline and Ethanol Blends and Their Effects on Mixture Preparation in an SI Engine. SAE 2008-01-0317.

KASTNER, L. J. 1947. The Airbox Method of Measuring Air Consumption. Proceedings of the IMechE, 157.

KAZI, F. K., PATEL, A.D., SERRANO-RUIZ, L.C., DUMESIC, J.A. AND ANEX, R.P. 2011. Techno-economic analysis of dimethylfuran (DMF) and hydroxymethylfurfural (HMF) production from pure fructose in catalytic processes. Chemical Engineering Journal, 169, 329-338.

KELLY, K. J., BAILEY, B.K., COBURN, T., CLARK, W. AND LISSIUK, P. 1996. Federal Test Procedure Emissions Test Results from Ethanol Variable-Fuel Vehicle Chevrolet Luminas. SAE 961092.

KIENCKE, U. AND NIELSEN, L. 2000. Automotive Control Systems: For Engine, Driveline, and Vehicle, Springer.

KING, J. 2011. Application of Synergistic Technologies to Achieve High Levels of Gasoline Engine Downsizing. In: RICARDO, U. (ed.) Engine Downsizing. London: IMechE Seminar Proceedings

KITTELSON, D. B. 1998. Engines and Nanoparticles: A Review. Journal of Aerosol Science, 29, 14.

KNAPP, K. T., STUMP, F.D AND TEJADA, S.B. 1998. The Effect of Ethanol Fuel on the Emissions of Vehicles over a Wide Range of Temperatures. Journal of the Air & Waste Management Association, 48, 646-653.

KOVÁTS, E. 1958. Retentionsindices aliphatischer Halogenide, Alkohole, Aldehyde und Ketone. Helvetica Chimica Acta, 41, 1915-1932.

KOWALEWICZ, A. 1993. Methanol as a Fuel for Spark Ignition Engines: a Review and Analysis. Proceedings of the IMechE, 207, 43-52.

KÜSELL, M., MOSER, W. AND PHILIPP, M. 1999. Motronic MED7 for Gasoline Direct Injection Engines: Engine Management System and Calibration Procedures. SAE 1999-01-1284.

LAKE, T., STOKES, J., MURPHY, R., OSBORNE, R. AND SCHAMEL, A. 2004. Turbocharging Concepts for Downsized DI Gasoline Engines. SAE 2004-01-0036.

LAW, C. K. 2006. Combustion Physics, Cambridge University Press.

LEERMAKERS, C., VAN DEN BERGE, B., LUIJTEN, C., SOMERS, L., GOEY, L.P.H. AND ALBRECHT, B.A. 2011. Gasoline-Diesel Dual Fuel: Effect of Injection Timing and Fuel Balance. SAE 2011-01-2437.

LI, T., NISHIDA, K., ZHANG, Y., ONOE, T. AND HIROYAU, H. 2005. Enhancement of Stratified Charge for DISI Engines through Split Injection. JSME International Journal, 48, 687-694.

LIPARI, F. AND COLDEN, F.L. 1987. Aldehyde and unburned fuel emissions from development methanol-fueled 2.5L vehicles. SAE 872051.

LIPARI, F. AND SWARIN, S. 1982. Determination of Formaldehyde and other Aldehydes in Automobile Exhaust with an Improved 2,4-Dinitrophenyle-hydrazine Method. Journal of Chromatography, 247, 297-306.

LIU, S., CLEMENTE, E.R.C., HU. T. AND WEI, Y. 2007. Study of Spark Ignition Engine Fueled with Methanol/Gasoline Fuel Blends. Applied Thermal Engineering, 27, 1904-1910.

LLOYD, J. E., POTTER, E.B.V. AND RIDLEY, K.F. 1956. Motor Fuel Composition. GB patent application.

LUPESCU, J. A., CHANKO, T.B., RICHERT, J.F. AND DEVRIES, J.E. 2009. Treatment of Vehicle Emissions from the Combustion of E85 and Gasoline with Catalyzed Hydrocarbon Traps. SAE 2009-01-1080.

LUQUE, R., HERRERO-DAVILA, L., CAMPELO, J.M., CLARK, J.H, HIDALGO, J.M., LUNA, D., MARINASA, J.M. AND ROMEROA, A.A. 2008. Biofuels: a Technological Perspective. Energy and Environmental Science, 1, 513-593.

LUSZCZ, P. M. 2009. Combustion Diagnostics in Homogeneous Charge Compression Ignition Optical and Thermal Single Cylinder Engines. PhD Thesis, University of Birmingham.

MAGNUSSON, R., NILSSON, C. AND ANDERSSON, B. 2002. Emissions of Aldehydes and Ketones from a Two-Stroke Engine Using Ethanol and Ethanol-Blended Gasoline as Fuel. Environmental Science and Technology, 36, 1656-1664.

MAGNUSSON, R. AND NILSSON, C. 2011. The Influence of Oxygenated Fuels on Emissions of Aldehydes and Ketones from a Two-Stroke Spark Ignition Engine. Fuel, 90, 1145-1154.

MASCAL, M. 2009. High-Yield Conversion of Cellulosic Biomass into Furanic Biofuels and Value-Added Products. US patent application.

MASCAL, M. AND NIKITIN, E.B. 2008. Direct, High-Yield Conversion of Cellulose into Biofuel. Angewandte Chemie Internation Edition, 47, 7924-7926.

MCAULAY, J. AND HEYWOOD, J.B. 2010. Coordinated Strategies for Ethanol and Flex Fuel Vehicle Deployment: A Quantitative Assessment of the Feasibility of Biofuel Targets. SAE 2010-01-0735.

MCCARRICK, A. 2000. Long Term Storage of Air Samples - A Study of Two Bag Materials. SAE 2000-01-2502.

MCNAIR, H. M. AND MILLER, J.M. 1997. Basic Gas Chromatography - Techniques in Analytical Chemistry, Basingstoke, John Wiley and Sons, Inc.

MEIER, D. 2007. Downsizing – the Specification and New Trend of the Motor Industry on Example of 1.4L 125KW/170HP Engine of the Golf GT. Journal of KONES Powertrain and Transport, 13.

MEROLA, S., TORNATORE, C., VALENTINO, G., MARCHITTO, L. AND CORCIONE, F. 2011. Optical Investigation of the Effect on the Combustion Process of Butanol-Gasoline Blend in a PFI SI Boosted Engine. SAE 2011-24-0057.

MILPIED, J., JEULAND, N., PLASSAT, G., GUICHAOUS, S., DIOC, N., MARCHAL, A. AND SCHMELZLE, P. 2009. Impact of Fuel Properties on the Performances and Knock Behaviour of a Downsized Turbocharged DI SI Engine – Focus on Octane Numbers and Latent Heat of Vaporization. SAE 2009-01-0324.

MITTAL, M., HUNG, D.L.S., ZHU, G. AND SCHOCK, H. 2010. A Study of Fuel Impingement Analysis on In-Cylinder Surfaces in a Direct-Injection Spark-Ignition Engine with Gasoline and Ethanol-Gasoline Blended Fuels. SAE 2010-01-2153.

MITTAL, V. AND HEYWOOD, J.B. 2008. The Relevance of Fuel RON and MON to Knock Onset in Modern SI Engines. SAE 2008-01-2414.

MITTAL, V. AND HEYWOOD, J.B. 2009. The Shift in Relevance of Fuel RON and MON to Knock Onset in Modern SI Engines Over the Last 70 Years. SAE 2009-01-2622.

MORRIS, G., CRIDDLE, M., DOWSETT, M., HEASON, T., KAPUS, P. AND NEUBAUER, M. 2010. A New Engine Boosting Concept with Energy Recuperation

for Micro/Mild Hybrid Applications. 22nd International AVL Conference “Engine & Environment”. Graz, Austria.

MORTON, T. M. AND KNOTT, S. 2002. Radial basis functions for engine modelling. SAE 2002-04-0079.

MOTTLAU, A. Y. AND MILLER, P. 1943. Motor Fuel. US patent application.

MOUSDALE, D. M. 2008. Bio-ethanol as a Fuel: Biotechnology, Biochemical Engineering and Sustainable Development, Boca Raton, CRC Press.

NAKAJIMA, S., SAIKI, R., AND GORYOZONO, Y. 2007. Development of an Engine for Flexible Fuel Vehicles (FFV). SAE 2007-01-3616.

NAKAMA, K., KUSAKA, J. AND DAISHO, Y. 2008. Effect of Ethanol on Knock in Spark Ignition Gasoline Engines. SAE 2008-32-0020.

NAKATA, K., UCHIDA, D., OTA, A., UTSUMI, S. AND KAWATAKE, K., 2007. The Impact of RON on SI Engine Thermal Efficiency. SAE 2007-01-2007.

NATKIN, R., TANG, X., BOYER, B., OLTMANS, B., DENLINGER, A. AND HEFFEL, J.W. 2003. Hydrogen IC Engine Boosting Performance and NOx Study. SAE 2003-01-0631.

NIASS, T., AMER, A., XU, W., VOGEL, S., KREBBER-HORTMANN, K., ADOMEIT, P. AND BRASSAT, A. 2011. Butanol Blending - a Promising Approach to Enhance the Thermodynamic Potential of Gasoline - Part 1. SAE 2011-01-1990.

NISBET, H. B. 1946. The Blending Octane Numbers of 2,5-dimethylfuran. Journal of the Institute of Pertroleum, 32, 162-166.

NISHINO, T., SENBA, H. AND MURAKAMI, N. 2004. Study of Engine Cooling Technologies for Knock Suppression in Spark Ignition Engines. Mitsubish Motors Technical Review.

NIVEN, R. K. 2005. Ethanol in Gasoline: Environmental Impacts and Sustainability Review Article. Renewable and Sustainable Energy Reviews, 9, 535-555.

NTP 2011. Report on Carcinogens. In: SERVICES, U. S. D. O. H. A. H. (ed.) Twelth Edition ed.: National Toxicology Program.

OECD 2008. Biofuel Support Policies: An Economic Assessment. Paris.

OGAWA, H. AND LI, T. 2011. Volatile Organic Compounds in Exhaust Gas from Diesel Engines under Various Operating Conditions. International Journal of Engine Research, 12, 30-40.

OGUMA, M., SHIOTANI, H., GOTO, S. AND SUZUKI, S. 2005. Measurement of Trace Levels of Harmful Substances Emitted from a DME DI Diesel Engine. SAE 2005-01-2202.

OHTOMO, M., NISHIKAWA, K., SUZUOKI, T., MIYAGAWA, H. AND KOIKE, M. 2011. Auto-ignition Characteristics of Biofuel Blends for SI Engines. SAE 2011-01-1989.

OTTO, N. A. 1887. Gas Motor Engine. US patent application US 365701.

OWEN, K. AND COLEY, T. 1995. Automotive Fuels Reference Book, Warrendale, Society of Automotive Engineers.

PAVIA, D. L. 2004. Introduction to Organic Laboratory Techniques: A Small-Scale Approach, Brooks/Cole.

PECKHAM, M., FINCH, A., CAMPBELL, B., PRICE, P. AND DAVIES, M.T. 2011. Study of Particle Number Emissions from a Turbocharged Gasoline Direct Injection (GDI) Engine Including Data from a Fast-Response Particle Size Spectrometer. SAE 2011-01-1224.

PIOCK, W. F., WEYAND, P., WOLF, E. AND HEISE, V. 2010. Ignition Systems for Spray-Guided Stratified Combustion. SAE 2010-01-0598.

PLINT, M. AND MARTYR., A. 1999. Engine Testing: Theory and Practice, Butterworth-Heinemann.

POULOPOULOS, S. G., SAMARAS, D.P. AND PHILIPPOPOULOS, C.J. 2001. Regulated and Unregulated Emissions from an Internal Combustion Engine Operating on Ethanol-Containing Fuels. Atmospheric Environment, 35, 4399-4406.

POURKHESALIAN, A. M., SHAMEKHI, A.H. AND SALIMI, F. 2009. Performance and Emission Comparison and Investigation of Alternative Fuels in SI Engines. SAE 2009-01-0936.

PRICE, P., TWINEY, B., STONE, R., KAR, K. AND WALMSLEY, H. 2007. Particulate and Hydrocarbon Emissions from a Spray Guided Direct Injection Spark Ignition Engine with Oxygenate Fuel Blends. SAE 2007-01-0472.

PRICE, P. AND STONE, R. 2006. Particulate Matter and Hydrocarbon Emissions Measurements: Comparing First and Second Generation DISI with PFI in Single Cylinder Optical Engines. SAE 2006-01-1263.

REGULATION(EC)NO(715/2007) 2007. On Type Approval of Motor Vehicles with Respect to Emissions from Light Passenger and Commercial Vehicles (Euro 5 and Euro 6) and on Access to Vehicle Repair and Maintenance Information. Official Journal of the European Union, 16.

REITZ, R. D., HANSON, R.M., SPLITTER, D.A. AND KOKJOHN, S.L. 2011. Engine Combustion Control via Fuel Reactivity Stratification.

RICHARDSON, M. AND GANGOLLI, S. 1994. The Dictionary of Substances and Their Effects, Royal Society of Chemistry.

ROEPKE, K., ROSENEK, A. AND FISCHER, M. 2002. Practical Application of DoE Methods in the Development of Production Internal Combustion Engines. SAE 2002-04-0083.

ROMAN-LESHKOV, R., BARRETT, C.J., LIU, Z.Y. AND DUMESIC, J.A. 2007. Production of dimethylfuran for liquid fuels from biomass-derived carbohydrates. Nature, 447, 982-986.

RÖNKKÖ, T., VIRTANEN, A., KANNOSTO, J., KESKINEN, J., LAPPI, M. AND PIRJOLA, L. 2007. Nucleation Mode Particles with a Nonvolatile Core in the Exhaust of a Heavy Duty Diesel Vehicle. Environ. Sci. Technol., 41, 6384-6389.

ROUNCE, P. L. 2011. Engine Performance and Particulate Matter Speciation for Compression Ignition Engines Powered by a Range of Fossil and Biofuels. PhD Thesis, University of Birmingham.

SAE 1993. Standard J1088: Test Procedure for the Measurement of Gaseous Exhaust Emissions from Small Utility Engines. In: COMMITTEE, S. E. A. P. E. (ed.) SAE 1993-02-01.

SANDFORD, M., PAGE, G. AND CRAWFORD, P. 2009. The All New AJV8. SAE 2009-01-1060.

SCANLAN, J. T. AND WILLIS, D.E. 1985. Calculation of flame ionisation detector relative response factors using the effective carbon number concept. Journal of Chromatographic Science, 23, 333-340.

SCHMIDT, L., SEABROOK, J., STOKES, J., ZUHDI, M.F.A., BEGG, S., HEIKEL, M. AND KING, J. 2011. Multiple Injection Strategies for Improved Combustion Stability under Stratified Part Load Conditions in a Spray Guided Gasoline Direct Injection (SGDI) Engine. SAE 2011-01-1228.

SERRAS-PEREIRA, J., ALEIFERIS, P.G., RICHARDSON, D. AND WALLACE, S. 2007a. Mixture Preparation and Combustion Variability in a Spray-Guided DISI Engine. SAE 2007-01-4033.

SERRAS-PEREIRA, J., ALEIFERIS, P.G., RICHARDSON, D. AND WALLACE, S. 2007b. Spray Development in a Direct-Injection Spark-Ignition Engine. SAE 2007-01-2712.

SERRAS-PEREIRA, J., ALEIFERIS, P.G., RICHARDSON, D. AND WALLACE, S. 2008. Characteristics of Ethanol, Butanol, Iso-Octane and Gasoline Sprays and Combustion from a Multi-Hole Injector in a DISI Engine. SAE 2008-01-1591.

SHAYLER, P. J., JONES, S.T. AND HORN, G. 2001a. Characterisation of DISI Emissions and Fuel Economy in Homogeneous and Stratified Charge Modes of Operation. SAE 2001-01-3671.

SHAYLER, P. J., JONES, S.T., HORN, G. AND EADE, D. 2001b. DISI Engine Spark and Fuel Injection Timings. Effects, Compromise and Robustness. SAE 2001-01-3672.

SHELL 2011. Shell Energy Scenarios to 2050. Signals and Signposts. The Hague: Shell International BV.

SIMMIE, J. M. AND METCALFE, W.K. 2011. Ab Initio Study of the Decomposition of 2,5-Dimethylfuran. Journal of Physical Chemistry, 115, 8877-8888.

SMITH, J. D. AND SICK, V. 2007. The Prospects of Using Alcohol-Based Fuels in Stratified-Charge Spark-Ignition Engines. SAE 2007-01-4034.

SODRÉ, J. R. 2003. Chromatograph Determination of Total and Speciated Hydrocarbons in the Exhaust of a Spark Ignition Engine. IMechE, 217, 8.

SPARTZ, M. 2008. Infrared Analysis of E85 Engines. Automotive Testing Technology International.

STEIN, R. A., HOUSE, C. J. & LEONE, T. G. 2009. Optimal Use of E85 in a Turbocharged Direct Injection Engine. SAE TECHNICAL PAPER SERIES, 2009-01-1490.

STEIN, R. A., HOUSE, C.J. AND LEONE, T.G. 2009. Optimal Use of E85 in a Turbocharged Direct Injection Engine. SAE 2009-01-1490.

STEPANEK, J., KOCI, P., MAREK, M., MAUNULA, T. AND KINNUNEN, T. 2010. Effects of Biofuel Blends on Performance of Exhaust Gas Catalyst: Ethanol and Acetaldehyde Reactions. SAE 2010-01-0894.

STONE, R. 1999. Introduction to Internal Combustion Engines, Basingstoke, Macmillan Press Ltd.

STOREY, J. M. E., BARONE, T.L., NORMAN, K.M. AND LEWIS, S.A. 2010. Ethanol Blend Effects On Direct Injection Spark-Ignition Gasoline Vehicle Particulate Matter Emissions. SAE 2010-01-2129.

STUHLER, H., KRUSE, T., STUBER, A., GSCHWEITL, K., PIOCK, W., PFLUEGL, H. AND LICK, P. 2002. Automated Model-Based GDI Engine Calibration Adaptive Online DoE Approach. SAE 2002-01-0708.

SUZUKI, K. AND NEMOTO, M. 2009. A Model-Based Technique for Spark Timing Control in an SI Engine Using Polynomial Regression Analysis. SAE 2009-01-0933.

SZEKELY, G. A. AND ALKIDAS, A.C. 2005. Combustion Characteristics of a Spray-Guided Direct-Injection Stratified-Charge Engine with a High-Squish Piston. SAE 2005-01-1937.

SZENGEL, R., MIDDENDORF, H., POTT, E., THEOBALD, J., ETZRODT, T. AND KREBS, R. 2007. The TSI with 90 kW – the Expansion of the Volkswagen Family of Fuel Efficient Gasoline Engines. 28. Internationales Wiener Motorensymposium.

TAKATORI, Y., MANDOKORO, Y., AKIHAMA, K., NAKAKITA, K., TSUKASAKI, Y., IGUCHI, S., YEH, L.I. AND DEAN, A.M. 1998. Effect of Hydrocarbon Molecular Structure on Diesel Exhaust Emissions Part 2: Effect of Branched and Ring Structures of Paraffins on Benzene and Soot Formation. SAE 982495.

TAYLOR, J., FRASER, N., DINGELSTADT, R. AND HOFFMANN, H. 2011. Benefits of Late Inlet Valve Timing Strategies Afforded Through the Use of Intake Cam In Cam Applied to a Gasoline Turbocharged Downsized Engine. SAE 2011-01-0360.

THANANATTHANACHON, T. AND RAUCHFUSS, T. B. 2010. Efficient Production of the Liquid Fuel 2,5-Dimethylfuran from Fructose Using Formic Acid as a Reagent. Angewandte Chemie Internation Edition, 49, 6616-6618.

THEWES, M., MUETHER, M., PISCHINGER, S., BUDDE, M., BRUNN, A., SEHER, A., ADOMEIT, P. AND KLANKERMAYER, J. 2011a. Analysis of the Impact of 2-Methylfuran on Mixture Formation and Combustion in a Direct-Injection Spark-Ignition Engine. Energy and Fuels, 25, 5549-5561.

THEWES, M., MÜTHER, M., BRASSAT, A., PISCHINGER, S. AND SEHR, A. 2011b. Analysis of the Effect of Bio-Fuels on the Combustion in a Downsized DI SI Engine. SAE 2011-01-1991.

TIAN, G., DANIEL, R., LI, H., XU, H., SHUAI, S. AND RICHARDS, P. 2010a. Laminar Burning Velocities of 2,5-Dimethylfuran compared with Ethanol and Gasoline. Energy and Fuels, 27, 3898-3905.

TIAN, G., LI, H, XU, H., LI, Y, AND SATISH M.R. 2010b. Spray Characteristics Study of DMF Using Phase Doppler Particle Analyzer. SAE 2010-01-1505.

TIAN, Z., YUAN, T., FOURNET, R., GLAUDE, P.A., SIRJEAN, B., BATTIN-LECLERC, F., ZHANG, K. AND QI, F. 2011. An Experimental and Kinetic Investigation of Premixed Furan/Oxygen/Argon Flames. Combustion and Flame, 158, 756-773.

TONG, X., MA, Y. AND LI, Y. 2010. Biomass into Chemicals: Conversion of Sugars to Furan Derivatives by Catalytic Processes. Applied Catalysis A: General, 385, 1-13.

TOSAKA, S., FUJIWARA, Y. AND MURAYAMA, T. 1989. The Effect of Fuel Properties on Particulate Formation (The Effect of Molecular Structure and Carbon Number). SAE 891881.

TOULSON, E., SCHOCK, H.J. AND ATTARD, W.P. 2010. A Review of Pre-Chamber Initiated Jet Ignition Combustion Systems. SAE 2010-01-2263.

TURNER, D. 2010. The Combustion and Emissions Performance of Fuel Blends in Modern Combustion Systems. PhD Thesis, University of Birmingham.

TURNER, D., XU. H., CRACKNELL, R.F., NATARAJAN, V. AND CHEN, X. 2011a. Combustion Performance of Bio-ethanol at Various Blend Ratios in a Gasoline Direct Injection Engine. Fuel, 90, 1999-2006.

TURNER, J. W. G., PEARSON, R. AND LUARD, N. 2011b. Investigation of Appropriate Technologies for a Highly-Downsized DISI Engine. In: ENGINEERING, L. (ed.) Engine Downsizing. London: IMechE Seminar Proceedings

TURNER, T., TIAN, G., XU, H., WYSZYNSKI, M.L. AND THEODORIDIS, E. 2009. An Experimental Study of Dieseline Combustion in a Direct Injection Engine. SAE 2009-01-1101.

VANCOILLIE, J., VERHELST, S. DEMUYNCK, J. 2011. Laminar Burning Velocity Correlations for Methanol-Air and Ethanol-Air Mixtures Valid at SI Engine Conditions. SAE 2011-01-0846.

VANDYNE, E. A. AND RILEY, M.B. 2008. An advanced Turbocharging System for Improved Fuel Efficiency. 2007 Fall Technical Conference of the ASME Internal Combustion Engine Division. American Society of Mechanical Engineers.

WAGNER, T. AND WYSZYNSKI, M. L. 1996. Aldehydes and Ketones in Engine Exhaust Emissions - a Review. Journal of Automobile Engineering Part D, 210, 109-122.

WALLNER, T. 2011. Correlation Between Speciated Hydrocarbon Emissions and Flame Ionization Detector Response for Gasoline/Alcohol Blends. Journal of Engineering for Gas Turbines and Power, 133, 8.

WALLNER, T. A. F., R. 2010. Study of Regulated and Non-Regulated Emissions from Combustion of Gasoline, Alcohol Fuels and their Blends in a DI-SI Engine. SAE 2010-01-1571.

WALLNER, T. AND MIERS, S.A 2008. Combustion Behavior of Gasoline and Gasoline/Ethanol Blends in a Modern Direct-Injection 4-Cylinder Engine. SAE 2008-01-0077.

WANG, C., XU, H., DANIEL, R., GHAFOURI, A., HERREROS, J.M. SHUI, S. AND MA, X. 2012. Combustion and Emissions of 2-Methylfuran in a DISI Engine. Fuel. In Review.

WANG, Q. AND TIAN, Z. 2011. Biofuels and the Policy Implications for China. Asian-Pacific Economic Literature, 25, 161-168.

WEI, Y., LIU, S., LI, H., YANG, R., LIU, J. AND WANG, Y. 2008. Effects of Methanol/Gasoline Blends on a Spark Ignition Engine Performance and Emissions. Energy and Fuels, 22, 1254-1259.

WEI, Y., LIU,S., LIU, F., LIU, J., ZHU, Z. AND LI, G. 2009. Formaldehyde and Methanol Emissions from a Methanol/Gasoline-Fueled Spark-Ignition (SI) Engine. Energy and Fuels, 23, 3313-3318.

WESTERHOLM, R., ALMÉN, J. AND LI, H. 1992. Exhaust Emissions from Gasoline-Fuelled Light Duty Vehicles Operated in Different Driving Conditions: A Chemical and Biological Characterization. Atmospheric Environment, 26, 79-90.

WHITE, T. L. 1902. Alcohol as a Fuel for the Automobile Motor. SAE 070002.

WIGG, B., COVERDILL, R., LEE, C. AND KYRITSIS, D. 2011. Emissions Characteristics of Neat Butanol Fuel Using a Port Fuel-Injected, Spark-Ignition Engine. SAE 2011-01-0902.

WILLIAMS, R. L., LIPARI, F. AND POTTER, R.A. 1990. Formaldehyde, methanol and hydrocarbon emissions from methanol-fueled cars. Journal of Air and Waster Management Association, 40, 747-756.

WU, X., DANIEL, R., TIAN, G., XU, H., HUANG, Z. AND RICHARDSON, D. 2011a. Dual-Injection: the Flexible Bi-Fuel Concept for Spark-Ignition Engines Fuelled with Various Gasoline and Biofuel Blends. Applied Energy, 88, 2305-2314.

WU, X., HUANG, Z., JIN, C., WANG, X., ZHENG, B., ZHANG, Y. & WEI, L. 2009. Measurements of Laminar Burning Velocities and Markstein Lengths of 2,5-Dimethylfuran-air-diluent Premixed Flames. Energy & Fuels, 23, 4355-4362.

WU, X., HUANG, Z., JIN, C., WANG, X. AND WEI, L. 2011b. Laminar Burning Velocities and Markstein Lengths of 2,5-Dimethylfuran-Air Premixed Flames at Elevated Temperatures. Combustion Science and Technology, 158, 220-237.

WU, X., HUANG, Z., JIN, C., WANG, X., ZHENG, B., ZHANG, Y. AND WEI, L. 2009a. Measurements of Laminar Burning Velocities and Markstein Lengths of 2,5-Dimethylfuran-Air-Diluent Premixed Flames. Energy and Fuels, 23, 4355-4362.

WU, X., HUANG, Z., WANG, X., JIN, C., TANG, C., WEI, L., LAW, C.K. 2011c. Laminar Burning Velocities and Flame Instabilities of 2,5-Dimethylfuran-Air Mixtures at Elevated Pressures. Combustion and Flame, 158, 539-546.

WU, X., HUANG, Z., YUAN, T., ZHANG, K. AND WEI, L. 2009b. Identification of Combustion Intermediates in a Low-Pressure Premixed Laminar 2,5-Dimethylfuran/Oxygen/Argon Flame with Tunable Synchrotron Photoionization. Combustion and Flame, 156, 1365-1376.

WU, X., LIA, Q., FUA, J., TANG, C.,HUANG, Z., DANIEL, R., TIAN, R. AND XU, H. 2012. Laminar Burning Characteristics of 2,5-Dimethylfuran and Iso-octane Blend at Elevated Temperatures and Pressures. Fuel, 95, 234-240.

WURMS, R., JUNG, M., ADAM, S., DENGLER, S., HEIDUK, T. AND EISER, A. 2011. Innovative Technologies in Current and Future TFSI Engines from Audi. 20th Aachen Colloquium Automobile and Engine Technology 2011.

WYSZYNSKI, L. P., STONE, R.C. AND KALGHATGI, G.T. 2002. The Volumetric Efficiency of Direct and Port Injection Gasoline Engines with Different Fuels. SAE 2002-01-0839.

XU, F., CHEN, L. AND STONE, R. 2011. Effects of a Catalytic Volatile Particle Remover (VPR) on the Particulate Matter Emissions from a Direct Injection Spark Ignition Engine. Environmental Science and Technology, 45, 9036-9043.

YACOUB, Y. 1999. Method Procedures for Sampling Aldehyde and Ketone using 2,4-Dinitrophenylhydrazine - a Review. Journal of Automobile Engineering Part D, 213, 503-517.

YANG, J. AND ANDERSON, R.W. 1998. Fuel Injection Strategies to Increase Full-Load Torque Output of a Direct-Injection SI Engine. SAE 980495.

YANG, J. AND KENNEY, T. 2002. Some Concepts of DISI Engine for High Fuel Efficiency and Low Emissions. SAE 2002-01-2747.

YELIANA, C., C., WORM, J. AND NABER, J.D. 2008. The Calculation of Mass Fraction Burn of Ethanol-Gasoline Blended Fuels Using Single and Two-Zone Models. SAE 2008-01-0320.

YOON, S. H., HA, S.H., ROH, H.G. AND LEE, C.S. 2009. Effect of bioethanol as an alternative fuel on the emissions reduction characteristics and combustion stability in a spark ignition engine. IMechE, 223.

ZERVAS, E., MONTAGNE, X. AND LAHAYE, J. 2002. Emission of Alcohols and Carbonyl Compounds from a Spark Ignition Engine. Influence of Fuel and Air/Fuel Equivalence Ratio. Environmental Science and Technology, 36, 2414-2421.

ZHANG, F., SHUAI, S., WANG, J. AND WANG, Z. 2009. Influence of Methanol Gasoline Blend Fuel on Engine and Catalyst Performance. SAE 2009-01-1182.

ZHANG, F., XU, H. ZHANG, J., TIAN, G. AND KALGHATGI, G. 2011. Investigation into Light Duty Dieseline Fuelled Partially-Premixed Compression Ignition Engine. SAE 2011-01-1411.

ZHANG, F., ZHANG, X., SHUAI, S., XIAO, J. AND WANG, J. 2010. Unregulated Emissions and Combustion Characteristics of Low-Content Methanol-Gasoline Blended Fuels. Energy and Fuels, 24, 1283-1292.

ZHAO, F., HARRINGTON, D.L. AND LAI, M.C. 2002. Automotive Gasoline Direct-Injection Engines, Warrendale, SAE Publications.

ZHAO, H., HOLLADAY, J.E., BROWN, H. AND ZHANG, Z.C. 2007. Metal Chlorides in Ionic Liquid Solvents Convert Sugars to 5-Hydroxymethylfurfural. Science, 316, 1597-1600.

ZHONG, S., DANIEL, R., XU, H., ZHANG, J., TURNER, D., WYSZYNSKI, M.L. AND RICHARDS, P. 2010. Combustion and Emissions of 2,5-Dimethylfuran in a Direct-Injection Spark-Ignition Engine. Energy and Fuels, 24, 2891–2899.

ZHONG, S., WYSZYNSKI, M.L., MEGARITIS, A.,YAP, D. AND XU, H. 2005. Experimental Investigation into HCCI Combustion Using Gasoline and Diesel Blended Fuels. SAE 2005-01-3733.

ZHU, G. G., HASKARA, I. AND WINKELMAN, J. 2007. Closed-Loop Ignition Timing Control for SI Engines Using Ionization Current Feedback. IEEE Transactions on Control Systems Technology, 15, 12.

ZHU, Z., LI, D.K., LIU, J., WEI, Y.J. AND LIU, S.H. 2011. Investigation on the regulated and unregulated emissions of a DME engine under different injection timing. Applied Thermal Engineering.